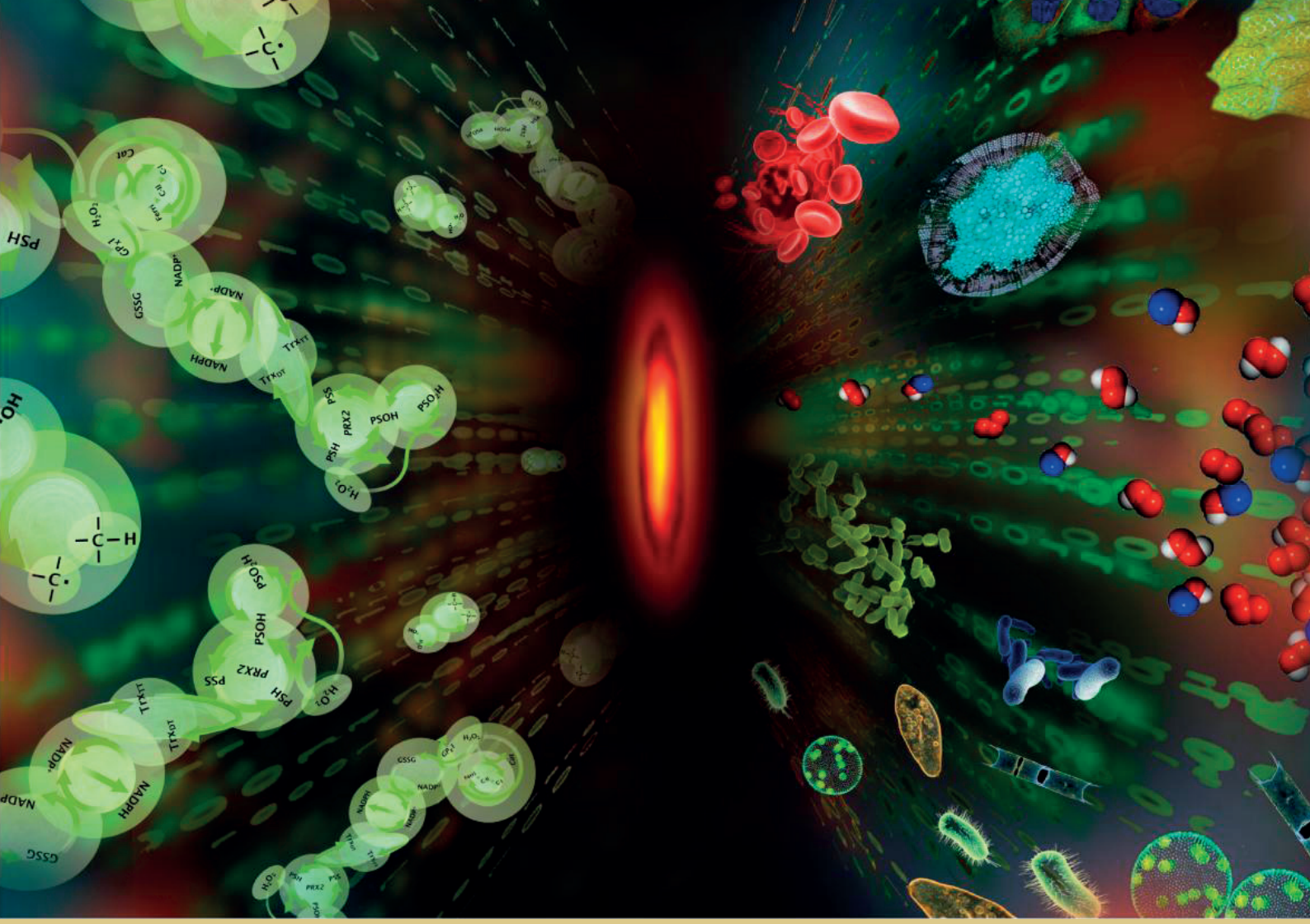

Rui Manuel Vicente Benfeitas

ACTIVE AND PASSIVE DEFENSES AGAINST OXIDATIVE STRESS: A COMPUTATIONAL STUDY

Tese de doutoramento em Biologia Experimental e Biomedicina, Ramo de Biologia Molecular, Celular e do Desenvolvimento orientada pelo Dr. Armindo Salvador e apresentada ao Instituto de Investigação Interdisciplinar da Universidade de Coimbra

Março de 2016

· U C ·

Universidade de Coimbra

INSTITUTO DE INVESTIGAÇÃO INTERDISCIPLINAR (III-UC)

Active and passive defenses against oxidative stress: a computational study

Tese de Doutoramento em Biologia Experimental e Biomedicina,

Ramo de Biologia Molecular, Celular e do Desenvolvimento

Rui Manuel Vicente Benfeitas

Março 2016

Tese apresentada à Universidade de Coimbra (III-UC) para prestação de provas de Doutoramento em Biologia Experimental e Biomedicina, Ramo de Biologia Molecular, Celular e do Desenvolvimento. Este trabalho foi realizado no Centro de Neurociências e Biologia Celular (CNC) da Universidade de Coimbra sob orientação do Doutor Armindo José Alves da Silva Salvador. O trabalho foi efectuado ao abrigo de uma bolsa de doutoramento atribuída pelo programa doutoral em Biologia Experimental e Biomedicina do Centro de Neurociências e Biologia Celular da Universidade de Coimbra, financiada pela Fundação para a Ciência e Tecnologia (SFRH / BD / 51199 / 2010).

À Teresita e à minha mãe,
as minhas duas forças.

Acknowledgments

A todos os meus amigos,

Gostaria de agradecer-vos pela força e palavras de encorajamento que sempre me deram.

Aos meus orientadores Armindo Salvador e Rui Alves. Ao Armindo, porque foi tão meu amigo ao longo de todos estes anos. Logo desde aquele dia em que lhe bati à porta do gabinete mostrou-se paciente com aquele rapaz verdinho de apenas 19 anos. Pelos valores que me transmitiu, por tudo o que me ensinou e por ter acreditado em mim desde tão cedo. Ao Rui, por tudo o que aprendi com ele. Por me mostrar que apesar de a Ciência ser muito séria, há sempre espaço para *sillyness* no laboratório. E que bom que era! Pela grande ajuda que sempre me deu. Pela amizade de irmão que teve para comigo, fazendo-me sentir como se tivesse uma segunda família quando estava tão longe da minha.

À minha família. À Teresita, por aturar tantos dos meus devaneios de cabeça cansada ao final do dia. Por me encorajar sempre, por me animar quando tudo parecia tão difícil, perto e longe de mim. Pelo amor e amizade. Por isto e por tanto mais. À minha mãe, pelo seu terno carinho. Por toda a força que sempre me deu. Pela ajuda incondicional, das palavras amigas, e do amor terno que só esta mãe podia dar. Ao meu irmão, por aquelas palavras de ânimo e pelas cervejas na varanda, por ser um bom amigo. Pelas noites em sua casa e pelas jantaradas. Ao meu pai, pelo seu apoio e encorajamento.

To my friends at the laboratory in Coimbra. The *fighettas* Alessandro and Gianlu, my dearest friends whom I've missed so much already. You have been amazing friends all these years, and every time I am with you I feel as if we've never been away. I take with me many good memories of our times. To my friend David. For all your counsel, friendship and help. For all the talks we had on those early mornings where I promised to start working earlier. For the great apple pie and for always having a good word to cheer me up. To Pedro Coelho, for so many things that I cannot write down. For all the help and support you gave me, in so many ways. To Patrícia, for being such a dear friend, always. To my friends Hugo, Renato, Filipe, Pedro Branco and Inês, always close to me and ready to listen and give a kind word, and to bear all my frequente idiocy. …sorry and thank you.

To my friends at the laboratory in Lleida. To Ester, for being such a great friend that I treasure so much. For making me feel part of your family. For all those weekends and all those things we did together with Rui and your kids. Miss you all! To Jorge, for being such a fun pain in the ass and for all the geekiness in the lab. And for making fun of my 2-week unwashed coffee cup (it adds flavor!). To Zé and Liliana, for the friendship, for showing me so many cool places in Lleida. For teaching me what and where to eat. Also, for teaching me what brochetta means in Catalan. To the Montses, Baldiri and Vero for being so nice all the times! Moltes gracies a tots!

Aos meus amigos de Coimbra. Ao pessoal do Mines. À Joana por todos os conselhos e palavras amigas. À Ana Sofia, iAna, Angela e João, Catarina e Sérgio, Soeiro e Ana. Pela vossa amizade e companhia. Por todos aqueles "só mais um fino" no trops. Ao Pedro e à Sónia, pelos jantares em vossa casa, pelas nossas noites de parvoíce e cumplicidade. Por serem tão meus amigos, sempre! Pela fantástica imagem de capa! Por tudo o resto… e pelo *jogo*. Ao Ber e à Dani, por serem grandes amigos de há tantos anos, que sempre irei acarinhar. À Carolina, amiga de sempre! De copos e alegrias, em todo o nosso tempo em Coimbra e antes. Ao amigo Pedro Gouveia, pelo carinho e amizade de família.

Aos meus amigos João, Teresa e Patrícia Alves. Por todo o carinho e ajuda que me deram, em especial no último ano. Por me fazerem sempre sentir tão bem-vindo e parte da família. Estou-vos profundamente grato por tudo. Mesmo.

A todos vocês, por isto e por tanto mais que fica por dizer. Gostava de vos dizer tanto mais mas correria o risco de que os agradecimentos ficassem maiores do que o trabalho que aqui apresento. Sei que poderei contar sempre convosco.

Trazer-vos-ei no meu coração, sempre. Obrigado!

Agradeço ainda ao CNC pela possibilidade que me deu para trabalhar neste projecto, à Universidade de Lleida e ao Institut de Recerca Biomèdica onde parte do trabalho foi desenvolvido, e à FCT pelo financiamento (bolsa SFRH/BD/51199/2010).

Publications and Presentations

Articles

•Benfeitas, R., Selvaggio, G., Antunes, F., Coelho, P.M.B.M., Salvador, A. "Hydrogen peroxide metabolism and sensing in human erythrocytes: a validated kinetic model and reappraisal of the role of peroxiredoxin II." Free Radic. Biol. Med. 74:35-49. 2014

•Benfeitas, R.; Moura, A.; Alves, R., Salvador, A. “The imprint of aerotolerance on protein amino acid composition”. [In preparation]

Conference and seminar presentations

•Benfeitas, R., Selvaggio G., Antunes F., Coelho, P.M.B.M., Salvador, A. (2014) Is peroxiredoxin II’s peroxidase activity strongly inhibited in human erythrocytes?. Meeting of the European Society for Free Radical Research - Free radicals. Paris, France. Poster

•Benfeitas, R., Selvaggio G., Antunes F., Coelho, P.M.B.M., Salvador, A. (2014) Is the peroxiredoxin 2/thioredoxin/thioredoxin reductase system in human erythrocytes designed for redox signaling?. Meeting of the European Society for Free Radical Research. Paris, France. Poster

•Benfeitas, R., Antunes, F., Salvador, A. (2013) What is the role of Peroxiredoxin 2 in H2O2 metabolism in human erythrocytes?. Annual meeting of the Center for Neuroscience and Cell Biology, Coimbra, Portugal. Oral communication.

•Benfeitas, R., Antunes, F., Salvador, A. (2013) Understanding the role of peroxiredoxin 2 in antioxidant defense in human erythrocytes. Center for Neuroscience and Cell Biology, Coimbra, Portugal. Seminar

•Benfeitas, R., Antunes, F., Salvador, A. (2013) Peroxiredoxin 2 in hydrogen peroxide metabolism: how can an idle weapon help against a threat?. International Conference Frontiers in Systems and Synthetic Biology, Atlanta, United States of America. Poster

•Benfeitas, R., Antunes, F., Salvador, A. (2012) Are Peroxiredoxin 2 and Catalase redundant defenses against H2O2 in human erythrocytes?. International Conference of Systems Biology, Toronto, Canada. Poster

•Benfeitas, R., Antunes, F., Salvador, A. (2012) Why do cells rely on both peroxidases and catalases for protection against hydrogen peroxide? The case of human erythrocytes. IV Spanish and Portuguese Meeting on Free Radicals, Valencia, Spain. Poster

•Benfeitas, R., Antunes, F., Salvador, A. (2012) Connecting function and design in cellular protection against hydrogen peroxide. Bioinformatics Open Days, Braga, Portugal. Oral communication

•Benfeitas, R., Antunes, F., Salvador, A. (2011) Are the defenses of human erythrocytes against hydrogen peroxide functionally redundant?. International Congress on Molecular Systems Biology 2011, Lleida, Spain. Oral communication

•Benfeitas, R., Antunes, F., Salvador, A. (2011) The Role of Peroxiredoxin 2 in Protecting Human Erythrocytes Against Hydrogen Peroxide: A Kinetic Analysis. International Congress on Molecular Systems Biology, Lleida, Spain. Poster

Table of contents

Abbreviations

$^{\bullet}OH$	Hydroxyl Radical
AA	Amino acid (abbreviations at bottom)
AAC	Amino acid composition
Aerotol	Aerotolerance
AI	Aerointolerant (Microaerofilic and Anaerobes)
AT	Aerotolerant (Aerobes and Facultative Aerobes)
ATP	Adenosine Triphosphate
Cat	Catalase
cDNA	Coding DNA
C-I	Catalase compound I
C-II	Catalase compound II
CO_2	Carbon dioxide
CPTTRS	Cat/Prx2/Trx1/TrxR system
Cysp (Cp)	Peroxidatic cysteine
Cysr (Cr)	Resolving cysteine
Ferri	Ferricatalase
G+C	Genomic G+C content
GPx	Glutathione peroxidase
GSH	Glutathione
GSR	Glutathione Reductase
GSSG	Glutathione Disulfide
H_2O_2	Hydrogen Peroxide
KM,E,S	Michaelis-Menten constant of enzyme E for substrate S
MW	Molecular Weight
nAA	Number of amino acids
NADH	Nicotinamide adenine dinucleotide
NADPH	Nicotinamide adenine dinucleotide phosphate
nProts	Number of proteins
Prx	Peroxiredoxin
Prx2	Peroxiredoxin II
PSH	Prx2 monomer with peroxidatic Cys in thiol form
PSize	Protein size
PSO2H	Prx2 monomer with peroxidatic Cys in sulfinic form
PSOH	Prx2 monomer with peroxidatic Cys in sulfenic form
PSS	Prx2 monomer with peroxidatic Cys in disulfide form
PTP	Protein Tyrosine Phosphatase
q	Average protein •OH-reactivity per residue
r	Average protein •OH-reactivity per residue, weighted by amino acid exposure to solvent
ROS	Reactive Oxygen Species
RSH	Thiol
RSO_2H	Sulfinic acid
RSO_3H	Sulfonic acid
RSOH	Sulfenic acid
RT	Plasma recirculation time
SOD	Superoxide Dismutase
Srx	Sulfiredoxin

t_c	Erythrocyte transit time through an inflammation focus
Therm	Thermophily
Tpx	Thiol peroxidase
t_r	Mean recurrence period between successive crossing of inflammation foci by erythrocytes
Trx	Thioredoxin
Trx1	Thioredoxin 1
Trx1$_{xy}$	Trx1 with active site dithiol in state x and regulatory dithiol in state y (T, thiol D, disulfide)
TrxR	Thioredoxin reductase
TrxR	Thioredoxin Reductase
TrxSH	Trx1 with active site dithiol in reduced form
v_{sup}	Rate of H_2O_2 supply

Amino acid abbreviations

Ala (A)	Alanine
Arg (R)	Arginine
Asn (N)	Asparagine
Asp (D)	Aspartate
Cys (C)	Cysteine
Gln (Q)	Glutamine
Glu (E)	Glutamate
Gly (G)	Glycine
His (H)	Histidine
Ile (I)	Isoleucine
Leu (L)	Leucine
Lys (K)	Lysine
Met (M)	Methionine
Phe (F)	Phenilalanine
Pro (P)	Proline
Ser (S)	Serine
Thr (T)	Threonine
Trp (W)	Triptophane
Tyr (Y)	Tyrosine
Val (V)	Valine

List of figures

List of tables

Resumo

Esta tese analisa dois modos complementares de defesa antioxidante – ativo e passivo.

Primeiro, analisámos o papel da peroxiredoxina 2 (Prx2) – uma defesa *ativa* – no metabolismo de peróxido de hidrogénio (H_2O_2). As peroxiredoxinas são importantes na proteção antioxidante e sinalização redox em muitas células, mas a sua contribuição para o consumo de H_2O_2 e os seus mecanismos de sinalização não são claros. Como ponto de partida para clarificar estas questões revimos a informação disponível sobre o metabolismo de H_2O_2 em eritrócitos humanos, as células onde este processo foi mais estudado. Isto permitiu-nos contruir um modelo matemático que representa o conhecimento atual sobre este processo. A comparação das previsões deste modelo com observações experimentais em eritrócitos humanos permitiu identificar uma discrepância importante: os parâmetros cinéticos determinados para a Prx2 purificada de eritrócitos humanos implicam que esta proteína consumiria >99% do H_2O_2 nestas células, mas experiências com eritrócitos intactos indicam uma contribuição muito menor. No entanto, a Prx2 é rápida e substancialmente oxidada quando eritrócitos são expostos a pulsos de H_2O_2. Uma avaliação computacional de possíveis explicações desta discrepância demonstra que modelos onde se assume que a concentração de Prx2 foi sobrestimada são inconsistentes com as observações experimentais. Por outro lado, é conseguida uma concordância quantitativa com as observações quando se considera que a atividade *efetiva* de peroxidase da Prx2 é ≈1% da estimada para a proteína purificada, devido a uma inibição rapidamente reversível ou à sobrestimativa da reatividade da Prx2 purificada. A segunda destas possibilidades é improvável, pois metodologias distintas originaram resultados mutuamente consistentes. A inibição da Prx2 por modificação covalente é excluída por considerações energéticas e porque a Prx2 purificada não se encontra modificada. O hipotético inibidor terá pois de ser suficientemente abundante para titular a Prx2, que é a terceira proteína mais abundante em eritrócitos humanos (≈0.6 mM). Isto deixa como candidatos: apenas duas proteínas e poucos metabolitos, a maioria dos quais são abundantes também noutras células. Portanto, é provável que a atividade de peroxidase da Prx2 esteja também inibida noutras células.

Os resultados acima indicam que minimizar a concentração de H_2O_2 não é a razão para a grande abundância da Prx2 em eritrócitos humanos. Que vantagens poderão conferir uma elevada concentração e inibição rapidamente reversível da atividade de peroxidase da Prx2? Para clarificar esta questão avaliámos a fisiologia e dinâmica de exposição de eritrócitos a H_2O_2 *in vivo*, e utilizámos um modelo matemático para prever as respostas do sistema Prx2 / tioredoxina 1 / tioredoxina reductase a estímulos fisiológicos de H_2O_2. Estas análises indicam que a baixa atividade de peroxidase da Prx2 *in vivo* melhora várias propriedades de sinalização do sistema e poupa NADPH. Finalmente, com base nos resultados computacionais e nas interações da Prx2 com outras proteínas propomos um modelo conceptual da ativação da Prx2 por recrutamento regulado.

A segunda parte do trabalho foca-se em mecanismos *passivos* de defesa. Nomeadamente, analisámos se a adaptação evolutiva de microrganismos a ambientes ricos em O_2 afeta a composição relativa de aminoácidos (AAC), diminuindo a reatividade de proteínas com o radical hidroxilo (•OH). Este trabalho foi baseado na comparação de genomas e proteomas de 1099 organismos aerotolerantes (AT; aeróbios e facultativos) e aerointolerantes (AI; microaerófilos e anaeróbios), dos três domínios filogenéticos.

Em todos os filos examinados, a reatividade média com •OH por resíduo (q) é menor em proteínas de AT do que em AI. Esta diferença é fundamentalmente devida à menor utilização de tirosina, cisteína e metionina, os resíduos com maior contribuição para a reatividade de proteínas com •OH. No entanto, as proteínas de AT são enriquecidas em triptofano, histidina e arginina – resíduos muito reativos com •OH – e empobrecidas em lisina – resíduo pouco reativo com •OH. Este empobrecimento poderá ser devido à grande reatividade da lisina com produtos de autoxidação. Curiosamente, o triptofano, histidina e arginina são resíduos substituintes de tirosina e lisina, evolutivamente favorecidos devido às propriedades físico-químicas semelhantes com estes últimos.

Modelos estatísticos que consideram os efeitos da aerotolerância, conteúdo G+C da sequência codificante, termofilia, tamanho de proteína, e filogenia indicam que a aerotolerância é o principal fator explicativo da variabilidade nos valores de *q* e de frequência de cisteína. A aerotolerância é também um fator importante

para explicar a variabilidade das frequências da maioria dos aminoácidos. Finalmente, demonstramos que custos diferenciais de biossíntese de aminoácidos em condições de fermentação *vs* respiração não explicam os padrões de AAC observados.

Abstract

This thesis addresses two complementary means of defense against oxidative stress — active and passive.

First, we aimed to clarify the role of peroxiredoxin 2 (Prx2) – an *active* defense – in hydrogen peroxide (H_2O_2) metabolism. Peroxiredoxins play key roles in antioxidant protection and redox signaling in most cells, but their quantitative contribution to H_2O_2 clearance and signaling mechanisms are unclear. As a starting point to clarify these issues we thoroughly surveyed the available data about H_2O_2 metabolism in human erythrocytes, the cells for which this process has been most scrutinized. We then set up a mathematical model that accurately represents the present understanding of this process. Comparing model predictions to experimental observations of the behavior of intact erythrocytes we flagged a strong and hitherto unappreciated discrepancy. Namely, whereas the kinetic parameters determined for Prx2 purified from human erythrocytes imply that this protein should clear >99% of the H_2O_2, experiments show that it has a much lower contribution to H_2O_2 clearance. Nevertheless, Prx2 is quickly and quantitatively oxidized when erythrocytes are exposed to H_2O_2 boluses. A computational assessment of alternative explanations showed that models considering that the cellular concentration of Prx2 had been overestimated were inconsistent with the experimental observations. In contrast, quantitative agreement was achieved by considering an *effective* peroxidase activity of Prx2 ~1% of that determined for the purified protein, either due to a quickly reversible inhibition or to overestimation of Prx2's intrinsic activity. The latter possibility is unlikely, because distinct methods yielded consistent determinations. Inhibition by covalent modification is excluded by energetic considerations and because purified Prx2 is not extensively modified. Further, the hypothetical inhibitor must virtually titrate Prx2, which is the third most abundant protein in human erythrocytes (~0.6 mM). This leaves few candidates: two proteins and a few metabolites, most of which also abundant in other cells. It is thus likely that Prx2's peroxidase activity is also inhibited in other cells.

The results above indicate that Prx2 is abundant in human erythrocytes for reasons other than minimizing H_2O_2 concentrations. And they raise the question

of what advantages could a high Prx2 concentration combined with a strong quickly reversible inhibition of its peroxidase activity have. Seeking to clarify this question, we surveyed the available information about the physiology and dynamics of erythrocyte's exposure to H_2O_2 *in vivo*. We then used the refined mathematical model to predict the responses of the Prx2 / thioredoxin 1 / thioredoxin reductase to physiologically plausible H_2O_2 stimuli. These analyses indicate that the low effective peroxidase activity of Prx2 *in vivo* endows this system with desirable redox signaling properties and spares NADPH. Finally, based on our results and in face of the interactions of Prx2 with many other proteins we proposed a conceptual model of Prx2 activation by regulated recruitment.

The second part of the work focused on passive antioxidant defense. Namely, we analyzed if evolutionary adaptation of microorganisms to O_2-rich environments modulated relative aminoacyl compositions (AAC) so as to decrease proteins' reactivity with the hydroxyl radical ($^{\bullet}OH$). The work was based on comparisons of aerotolerant (AT; aerobic or facultative aerobic) to aerointolerant (AI; microaerophilic or anaerobic) organisms across 1099 genomes and proteomes of unicellulars from the three phylogenetic domains.

In all phyla examined, the mean $^{\bullet}OH$-reactivity per aminoacyl residue (*q*) is lower for the proteins from AT organisms than for those from AI organisms. The lower *q* values in AT organisms are mainly due to a rarefaction of tyrosine, cysteine and methionine residues, which contribute majorly for proteins' $^{\bullet}OH$-reactivity. However, the very $^{\bullet}OH$-reactive tryptophan, histidine and arginine residues are enriched, and the relatively $^{\bullet}OH$-unreactive lysine residues are consistently and substantially rarefied in the proteins from AT organisms. This rarefaction may be due to lysine's high reactivity with electrophilic autoxidation products. Interestingly, tryptophan, histidine and arginine are among the most selectively favored substituents for tyrosine and lysine residues, due to their similar physical-chemical properties.

Statistical models accounting for the effects of aerotolerance, coding sequence G+C content, thermophily, protein size, and phylogeny highlight that aerotolerance is the main factor explaining variability in *q* values and cysteinyl

frequency, and an important explanatory factor for the variability in most residues' frequencies. Finally, we showed that the cost differentials in synthesizing the aminoacids in fermentative *vs.* respiratory conditions cannot explain the observed variation in AAC.

CHAPTER 1 – GENERAL INTRODUCTION

1. General Introduction

1.1 Hydrogen peroxide and hydroxyl radical as important ROS

Oxidative stress is defined as the "imbalance between oxidants and antioxidants in favor of the oxidants, leading to a disruption of redox signaling and control and/or molecular damage" [1]. Oxidative stress arises as a consequence of the reactions involving reactive oxygen species (ROS), oxygen-derived species that are produced both intracellularly [2-6] and extracellularly [7-9]. Exposure to extracellular ROS is potentially very toxic for cells because these species quickly permeate the cell membrane [6] and oxidize cellular components (reviewed by [10-14]).

Among all ROS one may distinguish between two classes: radicals, which have unpaired electrons (e.g. hydroxyl radical •OH), and non-radicals, which do not (e.g. hydrogen peroxide H_2O_2). Within these two classes of ROS some species are more reactive than others. The oxidizing strength of radical ROS may be ranked based on their one-electron reduction potential, whereas that of non-radicals also requires that one takes into consideration kinetic properties such as the activation energy [15]. These different physicochemical properties of ROS result in different reactivities with the different cellular compounds.

H_2O_2 reacts slowly with most biological compounds, but shows very high reactivities with some thiolates depending on their chemical environment (see Section 1.2.2.2). For instance, it reacts very quickly with peroxiredoxin thiolates ($k \approx 10^5 – 10^8$ $M^{-1}s^{-1}$ [16-18]). H_2O_2 is an important compound for cell physiology. Not only do cells have a widespread array of H_2O_2 scavengers such as peroxidases, catalases and peroxiredoxins (e.g. [19, 20]), they also have many transcription factors [21-23] and other thiol proteins [24-29] that are directly or indirectly regulated by H_2O_2. Furthermore, H_2O_2 is catalytically produced by specific enzymes (e.g. [30-33]). H_2O_2 is involved in many processes including cell proliferation, migration and death [34-37].

In turn, •OH is very reactive with many compounds, oxidizing nucleic acids [38, 39], lipids [40] and proteins [41-43]. Protein oxidation by •OH may lead to carbonylation and backbone breaks [41-43]. No viable cellular •OH scavengers

are known because •OH reacts with biological compounds with diffusion-limited rate constants. This results in •OH being potentially very toxic for cells, having been implied in many pathologies [44-48]. Part of the toxicity of H_2O_2 is due to it being a •OH precursor [12, 49, 50].

Other ROS (Table 1.1), reactive nitrogen species (reviewed by [51]), reactive chlorine species (reviewed by [52]) and other reactive species [53], also have important pathophysiological roles, but are usually less abundant than H_2O_2 and less reactive than •OH.

Table 1.1 – Examples of radical and non-radical ROS, reactive nitrogen species (RNS), reactive chlorine species. Adapted from [53].

	Radicals	**Non-radicals**
Reactive oxygen species	Superoxide ($O_2^{\bullet-}$)	Hydrogen peroxide (H_2O_2)
	Hydroxyl (•OH)	Ozone (O_3)
	Hydroperoxyl ($HO_2^{\bullet}$)	Organic peroxides (ROOH)
	Peroxyl ($RO_2^{\bullet}$)	
	Alkoxyl ($RO^{\bullet}$)	
Reactive nitrogen species	Nitric oxide ($NO^{\bullet}$)	Peroxynitrite ($ONOO^-$)
	Nitrogen dioxide ($NO_2^{\bullet}$)	Peroxynitrate (O_2NOO^-)
Reactive chlorine species	Atomic chlorine ($Cl^{\bullet}$)	Hypochlorous acid (HOCl)
		Nitryl chloride (NO_2Cl)
		Chloramines

Below we discuss the main features of H_2O_2 and •OH metabolism (Sections 1.2 and 1.3, respectively). We discuss their main mechanisms of generation *in vivo* and their reactions with biological components, with a focus on protein oxidation. We then briefly overview some of the main defense mechanisms against H_2O_2 (Section 1.4).

1.2 Intracellular H_2O_2 metabolism

1.2.1 What are the main sources of H_2O_2?

A wide number of processes produce H_2O_2 or produce superoxide which is then dismutated to H_2O_2 [54, 55]. H_2O_2 is produced at the mitochondria [56, 57], at the

cytosol [58-62], in membranes and extracellularly [54, 63-66], in peroxisomes [5, 6, 67], and in the endoplasmic reticulum [68, 69]. This discussion will now focus on the contributions of these sources of H_2O_2 production. Other minor sources include lipoxygenase and prostaglandin endoperoxide synthase [70, 71], monoamine oxidase in brain tissues [72], cytochrome P450 [73, 74], and menaquinone autoxidation in *E. coli*'s periplasm [75], or NADH dehydrogenases [76], and are not discussed here. Importantly, the work presented in Chapter 2 considers the cytoplasmic production of H_2O_2 through hemoglobin and glutathione autoxidation, the main sources of intracellular ROS in human erythrocytes, and are discussed in Section 2.10.2.

1.2.1.1 Mitochondria

Mitochondria are often considered the main source of intracellular H_2O_2. The estimated mitochondrial steady state concentrations amount to 0.08 – 0.2 nM $O_2^{\bullet-}$ and ≈5 nM H_2O_2 in rat and pigeon heart and liver [77]. *In vitro* experiments suggested that up to 4% [78] of the total O_2 consumed by bovine heart mitochondria leaks to $O_2^{\bullet-}$ under normoxic conditions ([O_2] = 200 μM). This would correspond to a H_2O_2 production of <8.3 nM $H_2O_2.s^{-1}$ assuming that all $O_2^{\bullet-}$ is dismutated to H_2O_2, and considering the respiration rates in the fmole $O_2.min^{-1}.cell^{-1}$ range for human adipocytes and lymphoid cells in culture [79], and a spherical eukaryotic cell of volume ≈10^{-14} m^3 [80]. Similar 3% is observed *in vitro* in pigeon heart mitochondria [81] and a 1-2% estimated *in vitro* [82].

However, these H_2O_2 fluxes may substantially overestimate the rates *in vivo* for the following three reasons. First, not all the $O_2^{\bullet-}$ produced is dismutated to H_2O_2. Some of it reacts with nitric oxide to form peroxynitrite [83, 84]. This reaction occurs very quickly (k ≈ 10^{10} $M^{-1}s^{-1}$ [85]) and may compete with the dismutation of $O_2^{\bullet-}$ under upper physiological levels of nitric oxide [83, 85]. Second, the above rates of $O_2^{\bullet-}$ dismutation were determined using non-physiological substrates for mitochondrial culture (succinate). The *in vitro* substrate used greatly affects ROS release by mitochondria, with succinate being usually associated with the highest yields [86].

Third, the *in vivo* production of $O_2^{\bullet-}$ from O_2 likely is much lower owing to the lower partial oxygen pressures that the tissues are subjected [82]. The oxygen

concentration used to determine the rates of $O_2^{\bullet-}$ production above was 7- 70 fold [82] higher than that found under physiological conditions. Determinations under more physiological conditions [87] yield 0.1 – 0.2% H_2O_2 produced per $O_2^{\bullet-}$ consumed. Unlike the experiments in ref. [5] where the rates were determined under mitochondrial State 4, those in ref. [87] considered State 3, a mitochondrial respiratory state and intermembrane potential that should be closer to the physiological conditions.

It should also be noted that H_2O_2 production by mitochondria is tightly controlled by a number of processes (see [88] for reviews) greatly varies with tissues, cell types [87] and organisms, and is affected by various factors such as mitochondrial membrane potential [89].

1.2.1.2 Membranes and extracellular

NADPH oxidases are membrane proteins found in plasma membranes and subcellular compartments such as the endoplasmic reticulum [90], nucleus [91] and mitochondria [92], and are found in many different tissues [55, 93-96]. NADPH oxidases were the first group of enzymes recognized to have ROS production as their main role [54, 55]. These proteins differ in structural organization, but all produce superoxide or H_2O_2 at the membrane side opposed to where their NADPH binding site is located [31]. Superoxide is released not only to the extracellular side but also to the lumen of intracellular vesicles which therefore promotes cytosolic H_2O_2 production. To our knowledge, a quantitative comparison of their contribution for intracellular H_2O_2 production was not performed. However, extensive evidence indicates that through this family of enzymes, particularly NOX2 in leukocytes and Duox1/2/NOX4 in some tissues, massive fluxes of H_2O_2 production are observed in various tissues [97]. The H_2O_2 production, cellular regulation and biological role of NADPH oxidases is reviewed by [30-33, 98].

Some crosstalk exists between these sources of H_2O_2. For instance, it was observed that mitochondrial ROS activate $O_2^{\bullet-}$ (and H_2O_2) production by NADPH oxidases, which in turn stimulate production of mitochondrial ROS [99]. This positive feedback may be important for the activation of phagocytic NADPH oxidase by superoxide [100].

1.2.1.3 Peroxisomes

Peroxisomes are among the main cellular sources of H_2O_2. This organelle produces H_2O_2 through respiratory pathways not linked with oxidative phosphorylation [101]. The β-oxidation of fatty acids by Acyl-CoA oxidases is the main source of H_2O_2 in peroxisomes [102, 103], but a wide number of other enzymes (e.g. urate oxidases, D-amino acid oxidase, D-aspartate oxidase) produce H_2O_2 in this organelle. About 18% of all O_2 consumed by peroxisomes yields H_2O_2, but a substantial fraction (60 – 80%) is consumed by the antioxidant enzymes in this organelle [5]. Because of this, only 20 – 40% of H_2O_2 effluxes from the peroxisome, as determined in isolated organelles [5]. Overall, an upper estimate for the contribution of peroxisomes indicates that it may account for the generation of 35% H_2O_2 in rat liver [6]. H_2O_2 production by peroxisomes is reviewed in more detail by refs. [102-104].

1.2.1.4 Endoplasmic reticulum

The endoplasmic reticulum produces H_2O_2 through two processes. First, a thioredoxin protein disulfide isomerase [68] catalyzes oxidative protein folding. The mechanism of oxidative folding is initiated by the thiol oxidase, which introduces disulfide bonds into target proteins and uses O_2 as two-electron acceptor to form one H_2O_2 molecule per disulfide bond catalyzed [68]. Second, H_2O_2 is generated by two-electron reduction of O_2 by a membrane-located NADPH oxidase [90, 105]. Although the mechanisms of H_2O_2 production and contribution of the endoplasmic reticulum for this process are not fully clear, observations in microsomes consisting mostly of endoplasmic reticulum membranes indicate that these vesicles account for 45% of H_2O_2 production [6] in rat liver. A recent study also observed that mitochondrial dysfunction, typically associated with higher ROS levels [56, 106], leads to increased cellular levels of H_2O_2 mostly produced by the endoplasmic reticulum in yeast [105]. These observations indicate a potentially important role of this organelle for H_2O_2 homeostasis.

1.2.2 Reactions with biomolecules and consequences

H_2O_2 regulates many cellular processes. From the production of antioxidant and repair proteins in unicellular [107-109] and multicellular [110, 111] organisms, to

inducing cell proliferation [34, 35, 112], differentiation [113, 114], and migration [34, 36, 115-118].

Redox regulation of cell migration occurs by H_2O_2-mediated oxidation of the phosphatase Slingshot-1L [115], or through c-Src tyrosine kinase-induction [117]. In zebrafish, leukocytes are recruited across hundreds of micrometers to wound locations by H_2O_2 [116]. The shuttling of histone deacetylase HDAC4 between the nucleus and cytoplasm is controlled by a thioredoxin 1-dependent disulfide bond formation by H_2O_2 and used to control cardiac hypertrophy [119]. Stem cell proliferation and neurogenesis is also controlled by NADPH-oxidase-generated H_2O_2 in order to maintain normal stem cell population sizes and neurogenesis [120, 121]. NADPH oxidase-produced H_2O_2 also reacts with phosphatases, kinases and transcription factors that control the propagation of survival signaling (see [33] and references therein).

Exposure to H_2O_2 also elicits some pathological cell responses. H_2O_2's toxicity is owed to its involvement in the production of •OH and consequent protein carbonylation [122, 123] (Section 1.3.1.1). The protein radicals formed upon reaction with •OH often propagate to other sites [124] (Section 1.3.2). This is prevented in the presence of H_2O_2-scavenging enzymes [125, 126]. H_2O_2 also oxidizes iron sulfur clusters, with concomitant enzyme inactivation, though this process occurs mostly through superoxide [127, 128]. More importantly, most of the toxic and physiological roles of H_2O_2 involve thiols (Section 1.2.2). Often, the outcome of H_2O_2 toxicity is apoptosis [37, 129, 130].

1.2.2.1 Genetic sensing

H_2O_2 is sensed by transcription factors such as OxyR in *E. coli* [21], Yap1 in yeast [22], and FoxO4 in mammals [23]. Sensing occurs by direct reaction with H_2O_2 [131], or indirectly through a response to the redox status of the cell, such as accumulation of cysteine sulfinic acids [131]. For instance, transcription factors such as Yap1 and Pap1 rely on upstream activators to sense oxidative stress [132-134]. Interestingly, both upstream activators of Yap1 and Pap1 are H_2O_2 scavengers: glutathione peroxidase 3 and the peroxiredoxin Tpx1, respectively [132-134]. Additionally, other mechanisms of H_2O_2 sensing by transcription

factors depend on metal-catalyzed generation of •OH and oxidation of His [109]. For reviews of H_2O_2 sensing mechanisms see [135-137].

1.2.2.2 Reaction with sulfur compounds

The reaction of H_2O_2 with sulfur compounds such as cellular thiols is thermodynamically favored, owing to the very negative reduction potentials of thiol compounds and positive potential of H_2O_2 (Table 1.2). Among these reactions, those with Cys (Figure 1.1) are among the most studied and recognized protein post-translational modifications. Cys thiols play a crucial role in protein structure and function [138]. Various chemical features of the reaction of H_2O_2 with thiols were reviewed by [139].

Table 1.2 – Reduction potentials of H_2O_2 and selected thiol compounds, determined in vitro.

	E (mV)	Reference
H_2O_2	+1350	[140]
Protein disulfide isomerase DsbA	-89	[141]
Thioredoxin 1	-280	(Chapter 2)
Poplar peroxiredoxin Q	-325	[142]
Gluthathione	-360	(Chapter 2)

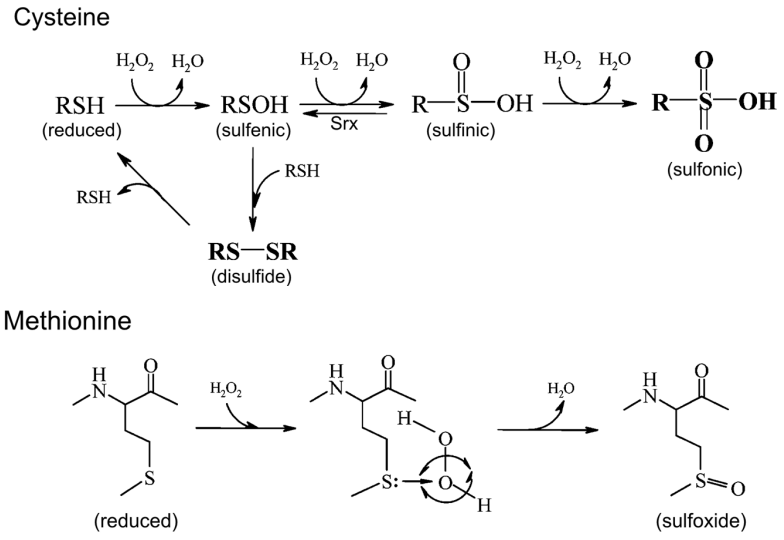

Figure 1.1 – Reactions between H_2O_2 and sulfur-bearing amino acids. The reactions of H_2O_2 with Cys (top) leads to the formation of sulfenic, sulfinic and sulfonic acid, or of disulfides by reaction with other thiols. The sulfinic acid may be reduced to sulfenic acid by sulfiredoxin (Srx) at expense of ATP [143]. The reaction of Met with H_2O_2 (bottom) and subsequent electron rearrangement lead to the formation of Met sulfoxides. Adapted from [144].

Met, also a sulfur-bearing amino acid, is oxidized by H_2O_2 relatively slowly ($k \approx 10 – 120\ M^{-1}s^{-1}$ pH 7 [145]) compared to Cys oxidation ($k \approx 10^8\ M^{-1}s^{-1}$ in some proteins [18]).

Glutathione, one of the most abundant low molecular weight thiol compounds in cells, also reacts with protein sulfenic acids thereby glutathionylating the protein [146]. Additionally, sulfenic acids may be further oxidized by H_2O_2 to sulfinic and sulfonic acids. These higher oxidized forms may be reduced to sulfenic acid by sulfiredoxins at the expense of ATP [143, 147].

Various properties of proteins influence the reactivity of their sulfhydryl groups with H_2O_2. Thiolate availability and enhanced acidity influence reactivity with H_2O_2 [139]. Charge and dipole distribution in the thiol environment are known to influence its reactivity with H_2O_2, with His [148-152], Arg [153, 154], and Lys [145, 155, 156] lowering the pK_as of nearby Cys thereby increasing their reactivity with H_2O_2. Anionic residues in the environment of protein thiols have the opposite effect [157-159]. Other effects such as α-helix dipoles following the redox motifs [160-162] and hydrogen bonds stabilization of thiolates [159, 163] also influence thiol reactivity with H_2O_2. Additionally, it is hypothesized that desolvation of the active site also affects the reactivity with H_2O_2. Based on structures deposited at the Protein Data Bank, Ferrer-Sueta and colleagues [139] observed that 20 peroxiredoxins have no water molecules near (<4.5 Å) the peroxidatic Cys sulfur atom, and only 6 structures have at most one water molecule at <4.5 Å [139]. This desolvation is hypothesized to enhance electrostatic interactions such as ion-dipole interactions with nearby residues and basicity of the thiolate increases.

1.2.2.3 The outcome of protein thiol oxidation depends on H_2O_2 levels

The reaction of H_2O_2 with proteins regulates the activity of important signaling mechanisms. Protein tyrosine phosphatases undergo reversible Cys oxidation with concomitant inactivation thereby affecting numerous signaling pathways [164-167]. Their inactivation occurs by formation of intermolecular disulfides [168] or sulfonamides [169], which enhances forward kinase signaling for various receptor-ligand interactions. Prx1 protects against PTEN oxidation [170], which leads to PTEN's transient inactivation [168]. Prx1 also regulates MAPK

phosphatases in a H_2O_2-dose dependent manner, where the sulfonylation of Prx1 induced at high H_2O_2 levels leads to dissociation of Prx1-MKP-1 and inactivation of MKP-1 (thus maintaining p38MAPK active) [171]. In turn, the Prx1-MKP-5 complex does not dissociate upon Prx1 sulfonylation which results in MKP-5 inhibiting p38MAPK [171]. This process is discussed in more detail in Section 1.4.1.2.

H_2O_2 also promotes tyrosine phosphorylation through activation of protein tyrosine kinases. For instance, this occurs during the activation of the tyrosine kinase Src due to H_2O_2 oxidation of two Cys residues [172]. Additionally, thiol peroxidases are intermediate H_2O_2 sensors in protein tyrosine phosphatase regulation [173], with the active-site cysteine of PTPs being oxidized by peroxiredoxin sulfenic acid. The interaction of peroxiredoxins and phosphatases has been suggested to provide selectivity for the signaling process [27].

Peroxiredoxins also interact with kinases, which is the case of MST1 kinase activation by H_2O_2 which requires interaction with peroxiredoxin 1 and this mediates p53 activation and apoptosis [174]. Additionally, it is hypothesized [27] that downstream proteins responsible for recycling an H_2O_2 sensor (e.g. thioredoxins and glutathione) could transmit the signal to other proteins. There is some experimental support for this mechanism. The apoptosis signaling kinase ASK1 is activated by oxidized thioredoxins [175], and are possibly oxidized by peroxiredoxin. It was also shown that Prx2 interacts with the ASK1/reduced thioredoxin complex in neurons, where Prx2 overoxidation prevented the oxidation and dissociation of Trx1-ASK1 complex therefore preventing apoptosis [176]. Peroxiredoxin oxidation is also hypothesized as a critical element during apoptosis and that sulfinylated peroxiredoxin can be used as biomarker for initiation and progression of cell death [177][1].

Interestingly, some cell responses to H_2O_2 are not obvious. For instance, exposure of hepatocytes to high H_2O_2 concentrations results in reduced insulin-stimulated Akt phosphorylation and increased JNK/c-Jun phosphorylation

[1] Sulfinylated peroxiredoxin is an *hyperoxidized* and peroxidatically inactive form of peroxiredoxin attained under high oxidative stress. The catalytic cycle of peroxiredoxins is more extensively discussed in Section 1.4.1.2.

whereas low H_2O_2 concentrations enhance insulin-stimulated Akt phosphorylation [178]. Similarly, low steady state H_2O_2 concentrations lead to increased fatty acid synthase activity and *FAS1* mRNA levels in *S. cerevisae*, whereas high concentrations lead to the opposite outcome [179]. In *S. pombe*, low to moderate H_2O_2 concentrations activate Pap1 [180], a transcription factor responsible for expression of many genes involved in antioxidant defense and drug resistance [181, 182]. In turn, higher H_2O_2 concentrations trigger the general stress response MAP kinase pathway through Yap1 activation [183]. For other examples see reviews by [135-137, 184-187].

The H_2O_2 concentrations that produce physiological responses or lead to toxic outcomes are widely different between different organisms and tissues. For instance, *E. coli* cells display intracellular [H_2O_2] ≈ 0.2 µM, but H_2O_2 becomes toxic at concentrations >0.5 µM [188]. Comparable concentrations are estimated in plant cells [189]. In jurkat T cells, extracellular > 5 µM H_2O_2 is sufficient to lead to cell apoptosis [190], and nonpathological concentrations reported may vary between 0.001 and 0.7 µM [191]. Concentrations as low as 60 µM extracellular H_2O_2 lead to significant DNA damage in HeLa cells [192]. Overall, *in vivo* concentrations ranges <0.1 µM H_2O_2 have physiological properties, 0.1 – 10 µM lead to growth arrest, and higher concentrations lead to apoptosis [185].

1.2.2.4 How are reactions between H_2O_2 and various proteins discriminated?

The observations above indicate that H_2O_2 modulates the activity of a wide variety of proteins, eliciting miscellaneous cell responses, often in the same cell types. But what permits discriminating the reactions of H_2O_2 with so many proteins? Four points may help us answer this question.

1. Thiol compounds and proteins have widely different cellular abundances and reactivities with H_2O_2;
2. Sulfhydryl groups may be oxidized to various redox states (e.g. sulfenic and sulfinic acids, intra- and intermolecular disulfides) each with different properties such as reactivity with H_2O_2 and other thiols;

3. There can be high intracellular concentration gradients and H_2O_2 is often generated near its target sites of activity;
4. Cellular membrane compartmentalization affects H_2O_2 diffusion.

Cellular thiols have widely different abundances and reactivities with H_2O_2

The widely different reactivities of cellular thiols with H_2O_2 are greatly affected by the local protein environment where the thiol is inserted. For instance, the reaction of Prx2 with H_2O_2 is facilitated by steric factors [193] and H-bonds [194] in the microenvironment of the catalytic Cys (we discuss this in more detail in Section 1.4.1.2). The microenvironment near Cys of protein tyrosine phosphatases also facilitates its reaction with H_2O_2 through a conserved motif [165]. These interactions result in the widely different reactivities of H_2O_2 with thiols (Table 1.3). For instance, peroxiredoxin 2's is seven orders of magnitude higher than that of protein tyrosine phosphatase type 1B. [193]

These different reactivities yield different responses to H_2O_2, with more abundant and reactive thiols reacting faster. For instance, *in silico* estimates for the reaction of H_2O_2 with phosphatases vs antioxidant defenses [136, 195] indicate that H_2O_2 would react very quickly with cellular defenses (peroxiredoxins and glutathione peroxidase 1) but slowly with phosphatases owing to the much higher abundances and reactivities of the defenses, in an homogenous system. One other example is observed in our estimates in Chapter 2 as follows. In human erythrocytes, despite glutathione's much higher abundance (3 mM [196]) than Peroxiredoxin 2 (≈0.3 mM Chapter 2), most H_2O_2 reacts with Prx2 rather than with glutathione owing to Prx2's higher H_2O_2-reactivity. This is observed in the much higher pseudo-first order of Prx2 (k_{Prx2} ≈ 57 000 s^{-1}, Chapter 2) vs that of GPx1 (k_{GPx1} ≈ 25 s^{-1}, Chapter 2)[2]. These differences yield distinct responses upon erythrocyte expose to a H_2O_2 pulse (Chapter 2), with oxidized Prx2 accumulating faster and more extensively than oxidized GSH. We have also shown that the peroxiredoxin 2/thioredoxin/catalase system in human erythrocytes displays

[2] It should be noted that this reaction is catalyzed by Glutathione Peroxidase 1 because if we were considering the non-catalyzed reaction of GSH with H_2O_2 it would go even slower.

desirable signaling properties for the transduction of H_2O_2-mediated signaling, despite peroxiredoxin 2 not being the main H_2O_2 sink.

The observation that some antioxidant defenses are much more reactive with H_2O_2 than some hypothetical H_2O_2 sensors raises questions about the roles of thiols (and H_2O_2 *per se*) in redox signaling. Using kinetic modelling, others have showed that $<10^{-4}$ % H_2O_2 would be consumed by PTP1B and other phosphatases in homogeneous systems, with the bulk of H_2O_2 being consumed mostly by the antioxidant defenses [28, 195]. However, a system with a highly reactive/abundant defense would nevertheless permit H_2O_2-mediated signaling through a phosphatase [136]: an antioxidant defense 9 orders of magnitude more reactive with H_2O_2 (pseudo-first order $k \approx 120\ s^{-1}$) than PTP1B (pseudo-first order $k \approx 10^{-7}\ s^{-1}$) permits a half-life of oxidized PTP1B of about 6 minutes. This is the time scale of a typical signaling response. However, the authors estimate a (H_2O_2) ≈ 100 μM [136], far from the physiologically postulated concentrations. It is nevertheless possible that such high concentrations are locally achieved for instance if the PTP1B co-localizes with the sources of H_2O_2 (see below).

For H_2O_2 to act as a signaling messenger for the phosphatases above, their reactivity would have to approach that of the defenses [27], or require the localized inactivation of the H_2O_2 sinks (e.g. peroxiredoxin sulfinylation in the "floodgate model" [197], discussed below). One other possible mechanism of H_2O_2-mediated signaling uses the peroxiredoxins as redox relays owing to their high abundance/reactivity [27, 28, 198].

Sulfhydryl groups are oxidized to various redox states

A second layer of control of thiol- and H_2O_2-mediated signaling is related with the various redox states of sulfhydryl groups (sulfenic, disulfide, sulfinic) and how they may carry signaling messages.

Widespread sulfenic acids are observed in cells exposed to H_2O_2 concentrations as low as 10 μM [199], or to growth factors that promote H_2O_2 generation (e.g. TNF-α and EGF) [199-202], though short-lived (e.g. [203, 204]). For instance, as others [205, 206] have observed in human erythrocytes, extracellular [H_2O_2] = 5 μM quickly but transiently oxidizes peroxiredoxin 2 and thioredoxin 1. Our estimates indicate that some forms such as sulfenic acid Prx2 have a half-life of

less than 2 minutes, whereas disulfide and sulfinic Prx2 may range many minutes to hours, depending on the H_2O_2 pulse (Chapter 2). The activity of thiols as signaling transducers was experimentally observed [24, 25] and their role as regulatory switches for activation and inactivation of tyrosine phosphatases is well known [169, 207].

Peroxiredoxins and thioredoxins may therefore function as redox transducers to downstream proteins [26-29]. Examples of this are the regulation of nucleo-cytoplasmic shuttling of histone deacetylase HDAC4, a process that is controlled by Trx1-dependent disulfide bond formation mediated by H_2O_2 during cardiac hypertrophy [119]. One other example of peroxiredoxins as H_2O_2 sensors and transducers was observed in yeast in the oxidation of Orp1 to sulfenic acid which then forms a disulfide bond with the transcription factor Yap1 [134] triggering antioxidant gene responses. Cells lacking peroxiredoxins and glutathione peroxidases are unable to regulate the gene response to H_2O_2, suggesting that these thiol proteins are responsible for sensing and transducing oxidative signals whereas a direct reaction of H_2O_2 with other redox proteins plays secondary roles [208].

Nevertheless, long-lived sulfenic acids have been observed in various proteins [209-212] where they are possibly stabilized from condensation to disulfide bonds by steric hindrance and H-bonding [213, 214].

Protein disulfides are relatively stable compounds with potentially important properties in protein structure[3] and dynamics of reaction with H_2O_2, and may form intra- or inter-molecularly. For instance, erythrocytes exposed to H_2O_2 accumulate disulfide peroxiredoxin 2 for several minutes [205], which hinders peroxiredoxin 2-mediated H_2O_2 consumption (Chapter 2). Thioredoxins and glutaredoxins, together with thioredoxin and glutaredoxin reductases, regulate the intracellular disulfide content of cells [216-218]. This is observed in the mechanism of peroxiredoxin 2 reduction through the thioredoxin/thioredoxin reductase cycle for instance [219].

[3] Protein folding and oxidation in the endoplasmic reticulum is controlled by protein disulfide isomerases through their intramolecular Cys-Cys disulfide bonds, as reviewed by [215].

Table 1.3 – Reactivities of H_2O_2 with selected thiol compounds and proteins. Values determined at pH 7.4 – 7.6, 37 ºC unless otherwise stated. Adapted from [28, 136, 195].

Compound	***k* ($M^{-1}s^{-1}$)**	**Reference**
Glutathione	0.87	[220]
Cysteine (free)	2.9	[220, 221]
Thioredoxin (Bacterial)	1.1	[222]
Phosphatases		
PTP1B* (Rat, Human)	9 – 43	[223-225]
SHP-2** (Human)	9 - 60	[226-228]
Cdc25B (Human)	160	[229]
Methionine sulfoxide reductase A (mouse)	32 (pH 8)	[230]
KEAP1# (Human)	140	[136]
GAPD (Rabbit)	200	[231]
Transcription factors		
OxyR† (Bacterial)	2×10^5	[131]
NADH peroxidase (Bacterial)	2×10^6 (25ºC, pH 7)	[232]
Peroxiredoxins		
DJ-1	0.56 (pH 7)	[233]
Prx5 (Human)	3×10^5 (25ºC)	[17]
Prx6## (Rat)	3.4×10^7	[234]
Tsa1 (Yeast)	10^7 (25ºC)	[235]
AhpC (Bacterial)	3.9×10^7 (25ºC)	[236]
Prx2 (Human)	10^8 (25ºC)	[18]

* Values are: 9 $M^{-1}s^{-1}$ (human, pH 7, 25 ºC) [225]; 20 $M^{-1}s^{-1}$ (rat, pH 7.4 37ºC) [223]; 43 $M^{-1}s^{-1}$ (human, pH 7 25 ºC) [224].

** Estimates based on mathematical modelling in cells indicate slightly higher values ($k \approx$ 57-60 $M^{-1}s^{-1}$ [228]) than the experimentally determined *in vitro* (9-15 $M^{-1}s^{-1}$ [226, 227]).

Estimated from [237].

Determined at room temperature.

† Determined at room temperature, pH 7.

One other process to selectively control reactivity with cellular thiols is through their inactivation. Sulfinic acids do not react with other thiols, and represent a small fraction of cellular thiols: an estimated 5% of thiol content in sulfinic form in rat liver homogenates [238]. We also estimate very small fractions of sulfinylated proteins in human erythrocytes[4]. The inactivation of peroxiredoxins to sulfinylated state [239, 240] is reversed through sulfiredoxin activity [143, 147]. Sulfiredoxin activity therefore represents an additional step in redox regulation of peroxiredoxin activity [241]. The formation of H_2O_2 at specific locations is thought to locally lead to the inactivation of Prx2, thereby permitting a buildup of the redox signal in that location of the cell (see below). This is called the "floodgate" hypothesis and is theorized to selectively control localized H_2O_2 fluxes [240, 242]. This hypothesis gets some support on the observation that peroxiredoxin sulfinylation is present in cells exposed to relatively low H_2O_2 levels [239, 243, 244]. Peroxiredoxins are additionally inactivated through phosphorylation. This is the case of Peroxiredoxin 1 [245] where its inactivation by phosphorylation permits localized accumulation of H_2O_2 required for cell signaling [25].

While both peroxiredoxin sulfinylation and phosphorylation are reversible processes, oxidation to sulfonic acid irreversibly inhibits H_2O_2 consumption by the peroxiredoxin. Sulfonic acid peroxiredoxins may have some biologically significance since they exhibit chaperone activity [246] and are markers for ubiquitin-dependent proteolysis [247]. Other post-translational regulation mechanisms of peroxiredoxins such as nitrosilation, glutathionylation, acetylation or phosphorylation are reviewed by [28].

---

[4] In human erythrocytes, we roughly estimate that $<10^{-4}$% of cellular thiols are in sulfinylated form under basal oxidative conditions as follows. As per our estimates, 10^{-3} % Prx2 in sulfinylated form (Chapter 2), and this is the 3rd most abundant protein in those cells. Together with GSH, they comprise ≈3.5 mM of cellular thiols [196] (and Chapter 2), yielding

$$10^{-5}\times(0.29\text{ mM (Prx2)})/((0.29\text{ mM (Prx2)})+(3.2\text{ mM (GSH)})) \approx 10^{-6}\text{ M sulfinylated thiols}$$

Glutathione is either in reduced or disulfide state (and only accumulates significantly in oxidized form under very high H_2O_2 doses) so the estimate above is robust to changes in redox state of glutathione. Nevertheless, it is possible that a significant fraction of other cellular thiols (e.g. peroxiredoxins 1 and 6) is sulfinylated, though they represent a much smaller protein fraction (concentrations of Prx1 and 6 are <2% of that of Prx2).

1. General Introduction

Co-localization of H_2O_2 sources and targets

Most estimates comparing relative consumption of H_2O_2 by antioxidant defenses and signaling targets [27, 136] assume a homogeneous cellular distribution of H_2O_2. However this molecule is often produced in specific locations where it may co-localize with its targets [248]. For instance, NADPH oxidases are colocalized with physiological targets such as phosphatases and kinases, which may affect the activity of the latter enzymes while preventing oxidation of pathological targets that are confined to other parts of the cell [249, 250]. This is the case of NADPH oxidase 4 and its target the phosphatase PTP1B which colocalized in the endoplasmic reticulum [251].

Lipid peroxidation and the formation of reactive lipid species is initiated by H_2O_2 which is produced in specific membrane compartments, and is also hypothesized to have signaling roles in cells [252]. This colocalization is important because although H_2O_2 is very diffusible (1.4×10^{-9} m^2/s [253]), the presence of highly reactive H_2O_2 sinks (e.g. Prx2 or GSH+GPx1) severely decreases the diffusion distance of H_2O_2. For instance, the H_2O_2 diffusion distance in the presence of Prx2 is <20 µm, smaller than the diameter of a typical cell [15]. On the other hand, less reactive proteins (e.g. PTP1B) permit H_2O_2 diffusion outside the cell (up to 1.5 mm) before a significant fraction of the target proteins may react with H_2O_2 [15, 28]. This suggests that the generation of H_2O_2 does not necessarily imply that H_2O_2 will act with nearby targets unless highly H_2O_2-reactive compounds are nearby.

Cellular membranes affect H_2O_2 diffusion

H_2O_2 has been involved not only to be involved in intracellular signaling but also in intercellular signaling between cultured human epidermal keratinocytes and neighboring melanocytes [254] and myofibroblasts and lung epithelial cells [255] for instance. Membranes may confine H_2O_2 to particular cell locations (e.g. peroxisomes) where antioxidant defenses prevent their diffusion [188, 256, 257]. Membrane composition affects H_2O_2 transmembrane diffusion and adapt to growth conditions, particularly to exogenous H_2O_2 levels [258]. For instance, mechanical changes imposed by osmotic stretching of lipid bilayers affect H_2O_2 permeation [259]. But given the observation that protein and lipid composition of

membranes change transmembrane diffusion [260, 261] it is also possible that H_2O_2 permeation is also affected by these factors. This is observed in yeast mutants of the ergosterol biosynthesis pathway which show decreased membrane H_2O_2 permeability (vs wild type) in stationary phase, and increased H_2O_2 permeability under exponential growth [258]. Membrane-limited H_2O_2 diffusion was observed in liposomes [262], horse [263] and human erythrocytes [264], spinach thylakoids [265], *E. coli* [188], and *S. cerevisiae* [266] for instance.

However, cell membranes are permeable to H_2O_2 through anionic channels [267] and aquaporins [268-270]. The observation that aquaporins facilitate H_2O_2 permeation [269] raises the possibility that aquaporins may be important for regulating potential signaling roles of H_2O_2 [271]. This is supported by the observation that some aquaporins are involved in intracellular H_2O_2 signaling processes [272], for instance in the induction of T-cell migration by H_2O_2 [273].

1.3 Cellular production and reactions of hydroxyl radical with biomolecules

The hydroxyl radical is one of the most toxic ROS species due to its high reactivity with biomolecules, often reaching diffusion limited rate constants [274]. Because of this, it is estimated that the diffusion distance of •OH is roughly the size of a small protein (≈80 Å [275]). It is therefore very likely that once formed it will lead to localized oxidation of nearby biomolecules. Furthermore, due to its high reactivity with many cellular compounds, it is not possible to get effective cellular scavengers of •OH.

It is currently thought that the main source of cellular •OH is the metal-catalyzed Fenton reaction [122, 123]. This radical may also be produced through water photolysis in a process that requires only water radiated with photons [276]. This process possibly occurs *in vivo* because it only requires water and solar UV radiation [276], which is known to penetrate living matter and to react with tissues [277].

•OH is involved in various cellular disorders such as inflammation [44], embryo teratogenesis [45], cell death [46], Alzheimer's [47] and Parkinson's [48] disease, and pathogen defense [278]. The involvement of H_2O_2, $O_2^{\bullet-}$, and metals in other

diseases such as diabetes and atherosclerosis [279] suggest that •OH may also be involved in those diseases.

1.3.1 Production

1.3.1.1 The Fenton/Haber-Weiss reactions

The hydroxyl radical is produced by reaction of $O_2^{\bullet-}$ with H_2O_2 through the Haber-Weiss reaction [122, 280] with overall reaction:

$$O_2^{\bullet-} + H_2O_2 \xrightarrow{Fe} \bullet OH + OH^- + O_2 \qquad \textit{Reaction 1.1}$$

Although this reaction is thermodynamically favored (ΔG ≈ -46 kJ/mol at pH 7 [281], estimated from [282]), it occurs very slowly, with bimolecular rate constants of the order of <2 $M^{-1}s^{-1}$ [283-285]. The mechanism of reaction was later clarified [122], where the first catalytic step is the oxidation of iron by H_2O_2 through the Fenton reaction [280][5]:

$$Fe^{2+} + H_2O_2 \rightarrow Fe^{3+} + \bullet OH + OH^- \qquad \textit{Reaction 1.2}$$

It was observed that the reaction above is not only catalyzed by free iron but also by heme peroxidases [288].

Fe^{3+} can then be reduced by reaction with superoxide anion

$$Fe^{3+} + O_2^{\bullet-} \rightarrow Fe^{2+} + O_2 \qquad \textit{Reaction 1.3}$$

Although Fe^{3+} reduction (Reaction 1.3) occurs by reaction with $O_2^{\bullet-}$ *in vitro*, it is still unclear whether this radical is the main biological reductant *in vivo* [289-291]. Despite the high reactivity of $O_2^{\bullet-}$ and Fe^{3+} ($k \approx 10^4$ $M^{-1}s^{-1}$ for reaction with Fe^{3+} heme, pH = 9.7 [292, 293]), the intracellular concentration of $O_2^{\bullet-}$ is very low (≈10^{-10} $M^{-1}s^{-1}$ in *E. coli* [294]) and translates into a very slow Fe^{3+} reduction ($k \approx 10^{-6}$ s^{-1} yields $t_{1/2}$ > 100 hours). Other possible Fe^{3+} reductants are glutathione, L-cysteine, NAD(P)H and $FADH_2$ [289], though NAD(P)H [295] and glutathione [296] are far more abundant but less reactive with free iron than $O_2^{\bullet-}$. One other compound that may also play a role as iron reducing agent is ascorbic acid, which

[5] Reviewed by [286]. The secondary reactions of Fenton-generated hydroxyl radicals were discussed by [287].

may replace superoxide in •OH-generating systems with iron and copper *in vitro* [297].

Other metals such as chromium, cobalt, vanadium, and nickel, also catalyze the reactions above *in vitro* [298][6], raising the possibility that some of these metals may also catalyze •OH-production *in vivo*. Under pH 7 it was observed that copper, chromium, and cobalt catalyze the Fenton reaction at faster rates than iron, whereas nickel shows slower-Fenton chemistry than iron [298]. However, many factors such as pH and relative reduction potential affect the rates of the reactions above, making it a fairly complicated task to demonstrate that these reactions also occur *in vivo*.

Nevertheless, both iron and copper [300] are known catalysts of these reactions *in vivo* when bound to proteins. For instance, horseradish peroxidase-bound [288] and chromatin-complexed [301] iron catalyze the Fenton production of •OH. The contribution of copper is questioned due to its low intracellular concentration (≈1 atom per cell, [302]). Interestingly, copper protects *E. coli* against H_2O_2-mediated DNA damage [300] and most copper-catalyzed production of •OH in this bacteria is localized in the periplasmic space [300]. In turn, $FADH_2$ [303] and cysteine [304] are very reactive with free iron *in vitro*. The observations that both NAD(P)H and thiol compounds lead to increased •OH production *in vitro* [296], and increased oxidative DNA damage susceptibility in *E. coli* [303, 304] suggest that these compounds may also play a role in •OH production *in vivo* [305].

The metal catalyzed Fenton reaction is now thought to be the main process by which •OH is produced *in vivo* [291]. Others have estimated that the Fenton chemistry would generate only one •OH molecule per minute in *E. coli* [289], considering an intracellular 20 nM H_2O_2 [188], the rate constant for the Fenton reaction $k \approx 76\ M^{-1}s^{-1}$ [289, 306] and an intracellular free iron concentration of 20 µM [303, 307]. A rate of 1 •OH molecule/min suggests that •OH-generation in *E. coli* would be a negligible process. However, the following evidences indicate that the rate of •OH production by the Fenton reaction is much higher *in vivo* [289]. First, the Fenton reaction is greatly accelerated when iron is bound to nucleotides

[6] Reviewed by [291, 299].

and DNA for instance, reaching rate constants of 6000 - 7000 $M^{-1}s^{-1}$ (pH 7.2 – 7.8) [308]. Second, H_2O_2 quickly permeates cellular membranes [188], and increased oxidative damage to DNA is observed upon cell exposure to H_2O_2 [289]. This H_2O_2 toxicity is associated with •OH production: *E. coli* exposure to H_2O_2 leads to higher free iron concentrations released from storage proteins and enzymatic iron-sulfur clusters, and concomitantly higher spontaneous mutagenesis rates and DNA damage [307]. Further, *E. coli* cells where peroxidases [309] or catalases were mutated displayed higher •OH production by the Fenton reaction [310] and higher mutagenesis rates [309, 310]. It remains to explain whether the toxic effects from increased H_2O_2 concentrations are mostly owed to toxic effects of H_2O_2 itself, to those of increased •OH generation, or a combination of both. Nevertheless, due to the association between iron/copper-catalyzed •OH production and H_2O_2 derived reactions it is not surprising that redox-sensitive transcription factors not only regulate ROS-detoxification but also metal homeostasis [311].

1.3.1.2 Water photolysis

The photolysis of pure water by UV light leads to the formation of •OH radicals [276] in a reaction that takes only a few picoseconds [312]:

$$H_2O \xrightarrow{h\nu} \bullet OH + H^+ + e^- \qquad \textit{Reaction 1.4}$$

Numerous other radicals are produced due to reaction of intermediate excited water-derived molecules [313] (e.g. $H^{\bullet}$, $HO_2^{\bullet}$) with different yields [314] per 100 eV of energy:

$$4.14\ H_2O \xrightarrow{100\text{eV}} 2.87\ HO^{\bullet} + 2.7e^-_{aq} + 0.61H^{\bullet} + 0.03HO_2^{\bullet} + 0.61H_2O_2 + 0.43H_2 + 2.7H^+$$

Reaction 1.5

In absence of other reactants, these radicals may quench at diffusion-limited rates [312]. This process is frequently used to produce •OH and other radicals under moderately dilute solutions [274] for various assays and through different techniques [144, 315].

The fluxes of *in vivo* •OH production through water photolysis are currently unknown. An experimental determination of these fluxes is pinned with various technical difficulties. First, the radical species formed are often very reactive with

many molecules, as is the case[7] of •OH, and therefore technically difficult to quantify especially in an *in vivo* setting. Second, because many of the products of water photolysis are also formed by other processes, some of which of endogenous origin (e.g. H_2O_2), discriminating the production by water photolysis from other sources is problematic. To our knowledge, no studies have tackled these problems.

Nevertheless, it is clear that the products of UV radiation have damaging and lethal effects for cells, with observations indicating that •OH is the most toxic species formed by UV-induced water photolysis [316]. Because UV light penetrates living matter, radical production by water photolysis possibly occurs intracellularly in all sunlight-exposed unicellular organisms, and in the superficial tissues in multicellular organisms. Further studies clarifying the extent of •OH production in cells by water photolysis are required.

1.3.2 Reactions with biomolecules and consequences

In its reactions with organic molecules •OH behaves as an electrophile, reacting quickly and non-selectively with most electron-rich sites of organic molecules [317]. These reactions occur by hydrogen abstraction (Reaction 1.6) from C-H, N-H or O-H groups [318, 319], or hydroxyl addition to unsaturated carbons, e.g. carbon double/triple bonds (Reaction 1.7), aromatic rings (Reaction 1.8) and sulfhydryl groups (Reaction 1.9) [274, 320].

$$\bullet OH + R - H \longrightarrow H_2O + R^{\bullet} \qquad \textit{Reaction 1.6}$$

$$\bullet OH + C = C \longrightarrow HO - C - C^{\bullet} \qquad \textit{Reaction 1.7}$$

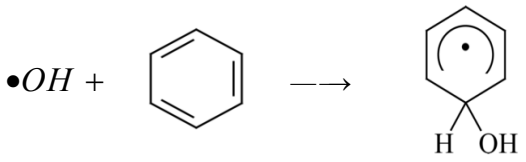

Reaction 1.8

$$\bullet OH + RSH \longrightarrow H_2O + RS^{\bullet} \qquad \textit{Reaction 1.9}$$

[7] An extensive list of reactivities of •OH and other radicals was compiled by [274].

Carbon centered radicals may also be formed from reactions with alkoxyl- (Reaction 1.10) [321, 322], peroxyl- (Reaction 1.11) [323, 324], nitrogen-centered (Reaction 1.12) [325], and aromatic ring (Reaction 1.13) [326] radicals (adapted from [124]).

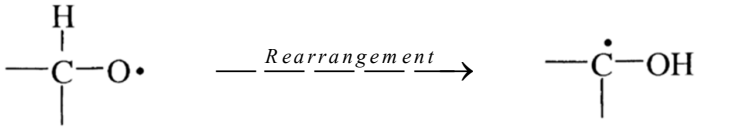

Reaction 1.10

$$ROO\bullet + R'H \longrightarrow ROOH + R'\bullet$$

Reaction 1.11

Reaction 1.12

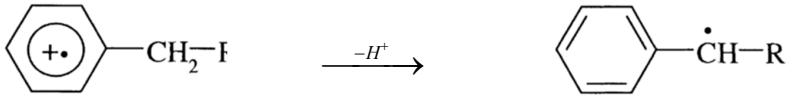

Reaction 1.13

The reactions between •OH and biological compounds are usually very fast, ranging from reactivities of 10^7 $M^{-1}s^{-1}$ to diffusion-limited reactions (>10^{10} $M^{-1}s^{-1}$) (Table 1.4)[8].

Table 1.4 – Rate constants for the reaction of •OH with selected cellular compounds. All rate constants measured at pH ≈ 7. Rate constants taken from [274] and [332] unless otherwise stated. An extensive list of rate constants for reaction of •OH with organic and inorganic compounds was curated by [274].

Cellular compound	Rate constant ($M^{-1}s^{-1}$)	Reference
DNA	10^8 -10^9	
RNA	10^9	
Lipids (linoleic acid)	10^{10}	[334]
Free amino acids	10^7 - 10^{10}	[335]
Small peptides	10^8	
Proteins	>10^9	

All of the product radicals may react with other compounds, thereby propagating radical formation and damage through various chain reactions. This is the case of lipid peroxidation and protein oxidation by •OH as we will see in the next

[8] Due to this high reactivity, •OH is frequently used as probe to assess solvent accessible area in proteins [144, 327-333].

sections. We will now briefly overview the reactions between •OH and nucleic acids, lipids and proteins.

1.3.2.1 Reactions with DNA and lipids

The reaction between •OH and nucleotides is potentially very toxic. •OH is very reactive [274] with both the ribose phosphate moiety ($k \approx 10^9$ $M^{-1}s^{-1}$, pH 7), and also purine- and pyrimidine-moieties (>10^8 $M^{-1}s^{-1}$, pH 7). •OH damages [38] and breaks [39] DNA chains (reviewed by [336, 337]). Many observations show that iron- [338], but not copper- [300], catalyzed Fenton chemistry leads to genotoxicity *in vivo*. In *E. coli*, mutations disrupting iron homeostasis increase Fenton-active iron (Fe^{2+}, Reaction 1.2), accelerate DNA damage [307] and lead to cell death [339]. Iron-mediated oxidative damage to DNA by •OH seems to be the primary cause of ROS-induced cell death in *E. coli* [300], and higher eukaryotes [340].

•OH also reacts with membrane lipids [40]. •OH reacts with lipids by abstracting hydrogen atoms and forming a lipidic carbon centered radical which may react with O_2 and form peroxyl radicals, and subsequently alkoxyl radicals [341]. Both peroxyl and alkoxyl radicals stimulate the chain reaction of lipid peroxidation by abstracting additional hydrogen atoms [342]. This propagates the formation of radicals and other cytotoxic products [343]. The peroxidation of lipids may disturb membrane assembly, changing fluidity and permeability, ion transport and inhibition of metabolic processes [344]. Lipid peroxidation in mitochondrial membranes may lead to additional ROS production [345]. Lipid peroxidation is one of the main outcomes of oxidative stress in mammalians [289].

1.3.2.2 Reactions with amino acids and proteins

The reaction between hydroxyl radicals and proteins and peptides form a wide array of products (Table 1.5) which may lead to loss of catalytic activity and even proteolysis [41-43]. Due to its electrophilic nature, •OH preferably oxidizes electron-rich sites [43], with reactivities ranging from 10^7 $M^{-1}s^{-1}$ (Gly) to 10^{10} $M^{-1}s^{-1}$ (for Trp and Cys) [274, 335] in free amino acids, and frequently 10^8 – 10^{10} $M^{-1}s^{-1}$ in peptides [346-349] and proteins [274, 350]. The location of an amino acid in a peptide sequence also influences the proportions of the formation of different oxidation products, particularly in aliphatic residues (Gly, Ala, Val and Pro) [351].

Further, because the overall yields of products of peptide oxidation by •OH are higher than those of •OH generation, it is suggested that secondary chain reactions lead to significant peptide oxidation [351].

Table 1.5 – Amino acid reactivity with •OH and products of reaction. Reactivities of free amino acids in solution as per [335].

Amino acid	k ($M^{-1}s^{-1}$)	Product	Reference
Cys	4×10^{10}	Cys-Cys crosslinks (intra- or intermolecular); Sulfenic-, Sulfinic-, Sulfonic- acids, Serine	[352-356]
Tyr	1×10^{10}	Tyr-Tyr crosslinks; Dihydroxyphenylalanine	[357, 358]
Trp	1×10^{10}	Hydroxy Trp; N-formylkynurenine	[359, 360]
Met	9×10^{10}	Met sulfoxide, Met sulfone	[361, 362]
His	6×10^{10}	Asn, Asp, Hydroperoxides, Hydroxylated products	[363-365]
Pro	5×10^{10}	Pyroglutamic acid, Glutamylsemialdehyde	[366, 367]

The reactions between •OH and proteins are influenced by intrinsic reactivity and solvent accessibility [144, 368]. •OH attacks avoid α-carbons due to the protonated nature of amino groups, and occur mostly on amino acid side chains [43, 369] especially in free amino acids [124]. However, α-carbon attacks nevertheless occur [43, 370].

Direct backbone attack by •OH

Direct attack of •OH on α-carbons leads to hydrogen abstraction and formation of a peroxyl radical on the α-carbon after the carbon-centered radical reacts with O_2 (Figure 1.2) [371]. The existence of bulky amino acid side chains sterically shields the main chains from direct α-carbon oxidation by •OH [369]. Together with steric effects of the side chains, electron delocalization to amino or carbonyl groups and secondary protein structure [372] highly influence the stability of these carbon centered radicals and differently favor α-carbon attacks by •OH. For instance, as a result of the very small side chains of Gly and Ala (-H and $–CH_3$, respectively), these amino acids favor α-carbon radical formation with respect to side chain radicals [43]. Due to these observations, oxidation of surface-exposed Gly and Ala α-carbon is hypothesized to be responsible for significant protein backbone cleavage [43]. Presumably, smaller peptides with larger solvent-exposure surfaces should also be prone to backbone cleavage owing to a facilitated formation of α-carbon radicals. In larger proteins, residue side chains

will hide most of the protein backbone from radicals in solution therefore blocking direct attack on protein backbone. Indeed, side chain rather than backbone reactions predominate in larger peptides [43, 373, 374].

Carbon-centered radicals are particularly stable as result of electron delocalization to the amino or carbonyl groups [372], and their stability is highly influenced by secondary [372], and possibly tertiary, protein structure.

Carbon-centered radicals may react with other residues in the same or different proteins to form other carbon-centered radicals. These reactions lead to the formation of protein-protein crosslinks [375, 376]. In the presence of O_2, the carbon–centered radicals further react with ROS, iron or copper and may lead to protein cleavage [14, 375-377]. Oxidation of carbon-centered radicals by O_2 occurs at diffusion-limited rates ($k > 10^9$ $M^{-1}s^{-1}$, [376]) whereas formation of crosslinks is a slower process ($k \approx 10^5 – 10^7$ $M^{-1}s^{-1}$).

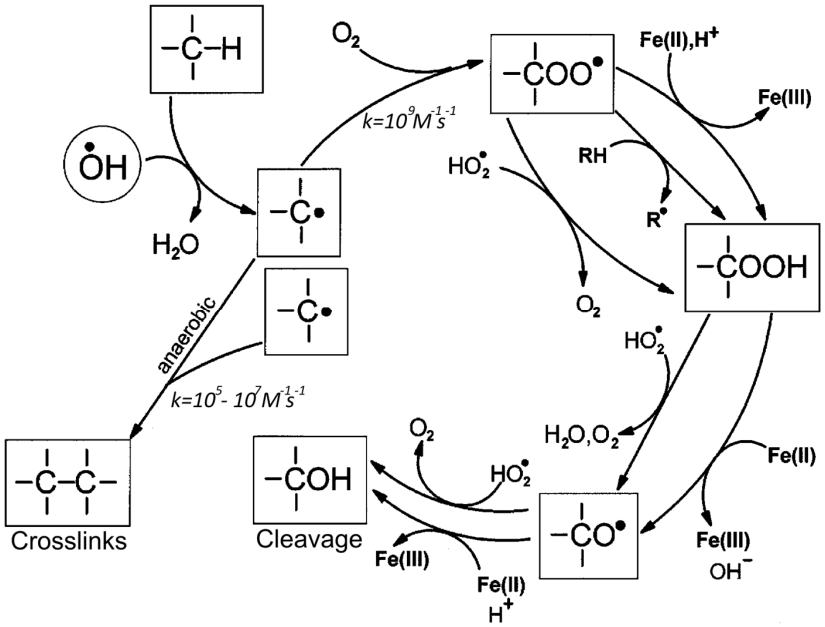

Figure 1.2 – Hydroxyl radicals oxidize proteins and lead to the formation of protein-protein crosslinks and backbone cleavage. The reaction of •OH with an α-carbon forms a peroxyl radical. This radical may then form protein-protein crosslinks in the absence of O_2 or progress through O_2-dependent reactions that eventually lead to protein backbone cleavage. Adapted from [378]. References for rate constants indicated in main text.

Oxidation of residue side chains

The oxidation of protein side chains occurs either by direct attack at the side chains, or by reactions with backbone (α-, β- and γ-carbon) radicals [379]. All amino acids side chains are prone to oxidation by •OH, though attack on α-carbons is favored in Gly and Ala. Side chain reactivity with •OH tends to increase with the number of C-H bonds and length of the hydrocarbon side chain [43].

Numerous products[9] result from side chain oxidation, usually following similar reactions as those in Figure 1.2. Because carbon-centered radicals usually exist in low concentrations, the reactions with O_2 tend to predominate under aerobic environment. An exception to this is Tyr, whose carbon-centered aromatic ring radicals tend to dimerize irrespective of O_2 concentration [380, 381]. Under low O_2 concentrations, carbon-centered radicals undergo slow unimolecular elimination reactions [382]. Many of the products of side chain oxidation give rise to other radicals such as hydroperoxides, hydroxides, carbonyl, and alkoxyl radicals [383], which may lead to backbone oxidation and cleavage [41, 42] (Figure 1.3).

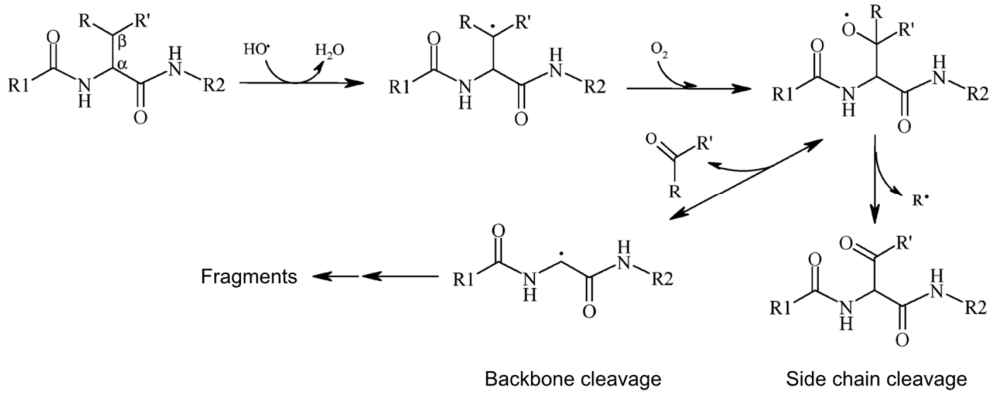

Figure 1.3 – Backbone cleavage by radical transfer from β-carbon radicals at side chains. The reaction of •OH with β-carbons and formation of peroxyl radicals may undergo multiple electron transfer processes, leading to the formation of a backbone-centered radical and backbone or side chain cleavage. This process may also occur by radical transfer from γ-carbon radical transfer of side chains [41, 42]. R1 and R2 are N- and C-terminal sides of protein, R and R' – side chain substituents. Adapted from [144].

[9] Reaction schemes for the radical formation and products of side chain oxidation in the various groups of amino acids are reviewed by [14, 144].

For the sake of brevity, and because others have already reviewed the consequences of individual amino acid and protein oxidation by •OH [14, 144, 378], we are only going to discuss the reactions with Cys, Tyr, Trp, Met and Pro in here. These amino acids either exhibit a very high reactivity with •OH and form toxic radicals, or there is significant evidence that their oxidation leads to protein cleavage.

Cys oxidation

The sulfur containing amino acids Cys and Met tend to be buried within protein cores, hidden from solvent exposure and potential radical attacks. Both residues are easily oxidized by •OH [384, 385], and the primary •OH attack occurs on sulfur [386]. In the mechanism[10] of Cys oxidation by •OH (Figure 1.4), the reaction of •OH with the thiol group leads to the formation of a thiyl radical ($RS^{\bullet}$) which may then form an intra- or intermolecular disulfide bond with other $RS^{\bullet}$ group in the absence of O_2 [353]. In the presence of O_2, the thiyl radical is quickly ($k \approx 10^8 – 10^{10}$ $M^{-1}s^{-1}$ [387]) oxidized by O_2 and, through subsequent reactions with other thiols, O_2 or water it forms sulfenic (RSOH) [352, 356], sulfinic (RSO_2H), sulfonic (RSO_3H) acids [355] or is converted to serine [354]. O_2 competes with thiolate anions (RS^-) for thiyl radicals under physiological pH [388]. In the absence of oxygen the sulfinic acid is produced in moderate yields whereas disulfides are produced in high yields [389]. Additional thiyl radicals may be formed by attack of disulfide bonds by •OH [389, 390]. These reactions are important because the redox state of Cys and protein thiols regulates various functions in the cell (e.g. [391-394]).

Many *in vitro* studies suggest that thiol-mediated reduction of some metal species, such as those potentially involved in Fenton chemistry Fe^{2+} and Cu^+ (Reaction 1.2, Section 1.3.1.1), may lead to ROS generation by intermediate thiyl radical chemistry [290, 395, 396], though it is unclear whether these radicals are implicated in ROS formation *in vivo*.

[10] The full mechanism of Cys oxidation is not completely understood, but was more thoroughly reviewed by [354, 386].

Met oxidation

Met oxidation by •OH (Figure 1.5) leads to the formation of Met sulfoxide, Met sulfone as well as radical products [361, 362, 386], with methionine sulfoxide being the main product [361]. Met oxidation occurs mostly through •OH addition to the sulfur moiety though hydrogen abstraction may also occur [362]. It was also observed that Met peptides oxidized by •OH form α-carbon centered radicals on the peptide backbones only when electron rich amino acids were in the neighboring chains [397], and under particular conditions (such as in pH = 3 solutions) [398]. The oxidation to Met sulfoxide is important because this oxidized compound leads to protein inactivation [399-402], though surface-exposed Met may act as antioxidant [401] and specific Met sulfoxide reductases reverse Met oxidation [403, 404]. It was also observed that when other amino acids with higher reactivity than Met were present neighboring this residue, the Met oxidation was not observed [397, 405].

Tyr oxidation

Tyr oxidation also starts with •OH addition, forming adduct radicals which can react further to produce 3,4-dihydroxyphenylalanine (DOPA) [358]. This compound is used as marker of tyrosine and protein oxidation [406], and leads to DNA damage [407]. Phenoxyl radicals, the products of reaction between Tyr and •OH, may quickly form ($k \approx 10^9$ $M^{-1}s^{-1}$) protein-protein crosslinks [357]. Although these radicals may react with O_2 (not shown), this is a slow process ($k < 10^3$ $M^{-1}s^{-1}$) which does not significantly affect Tyr-Tyr dimerization and forms DOPA at much lower yields [408]. Phenoxyl radicals have been implied in oxidation of many cellular targets, including amino acids, proteins [409, 410] and lipoproteins [411].

Trp oxidation

The oxidation of Trp follows a similar pattern to that of Tyr, starting with •OH addition [359, 412] and produces a number of radicals through a mechanism that is not completely known. Both hydroxylated compounds and N-formylkynurenine, products of Trp oxidation by •OH [359, 360], have been implied in the oxidation of various biological targets [410, 413]. Together with the loss of Trp fluorescence

they have been employed as markers of Trp oxidation (reviewed by [406]), and to examine protein structure [414].

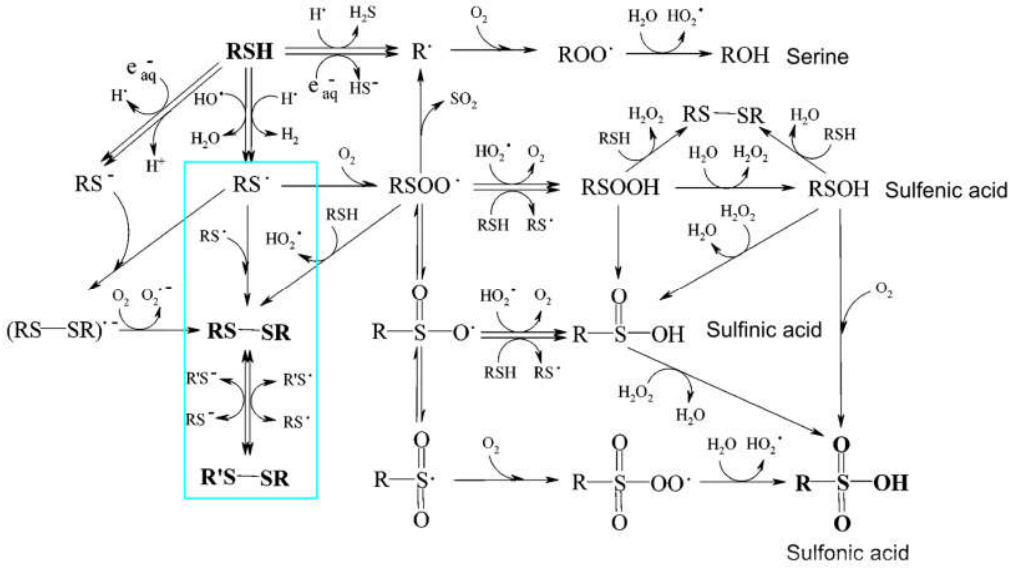

Figure 1.4 – Oxidation of protein sulfhydryls by •OH. Thyil radical formation by thiol oxidation and subsequent reactions in the absence (blue square) or presence of O_2. R – non-thiol part of Cys. Adapted from [386].

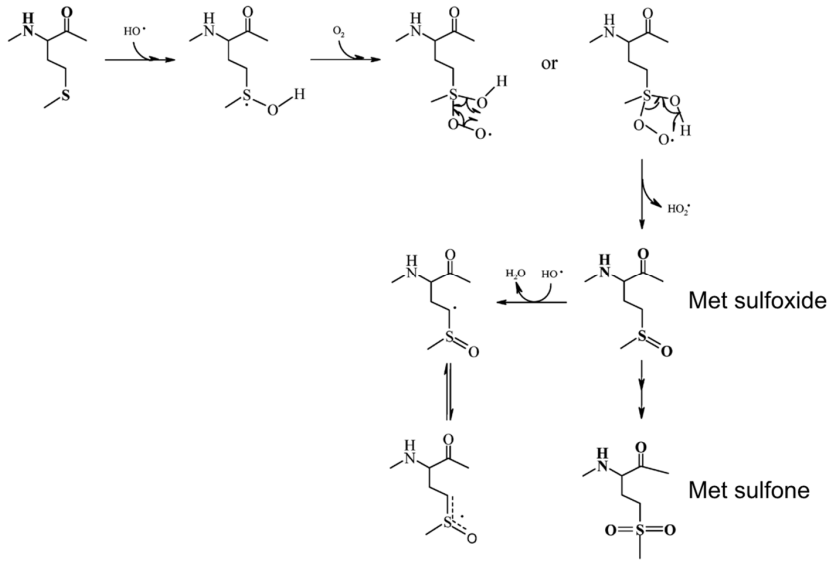

Figure 1.5 – Mechanism of Met oxidation by •OH. This mechanism starts with hydrogen abstraction (not shown) or •OH addition to the sulfur group, followed by oxidation by O_2 in solution. Through radical rearrangement Met sulfoxide, Met sulfone and other radicals may be formed. Adapted from [405].

His oxidation

The reactions of •OH with His also occur by hydroxyl addition in various positions in the imidazole ring [415, 416]. Though not all the products of this oxidation are known [124], peroxyl radicals are formed from O_2 incorporation after His oxidation by •OH [363]. These radicals may lead to the production of Asn, Asp, hydroperoxides and hydroxylated products [364, 365] depending on many conditions including the neighboring amino acid sequence [363, 366, 417].

Pro oxidation

Pro is an amino acid implied in protein cleavage by radical attack. The cyclic structure of its side chain usually puts it in bend and loop regions of proteins [418, 419] which may imply that it is particularly exposed to solvent – and thereby prone to radical attacks – in relatively small proteins. Oxidation of Pro side chains is linked with protein backbone oxidation and may also lead to protein cleavage [363]. Interestingly, the number of peptide fragments produced by protein radiolysis correlates with the number of Pro in the protein [366, 375]. This may also be related to the localization of Pro in protein bends, where the protein backbone is more exposed. Nevertheless, Pro side chain oxidation propagates to the protein backbone and leads to protein cleavage [363]. This is also observed in •OH-mediated oxidation of γ- [41] and β-carbon radicals [420] in side chains, where the radicals are transferred to the backbone in the presence of O_2.

1.4 Mechanisms of protection against H_2O_2 and •OH

Several levels of defense exist for protection against H_2O_2 and •OH (Table 1.6). A first level is given by *passive* mechanisms of defense and comprises cell compartmentalization and protein sequence/structure. Cell membranes decrease H_2O_2 permeation across compartments, and the structural and chemical configuration of proteins may prevent oxidation of aminoacyl residues by either utilizing less reactive residues or burying them away from exposure to H_2O_2 and •OH in the solvent. Metal chelation also represents a passive mechanism of protection, where iron and copper ions are bound to proteins (e.g. desferrioxamine) and prevent the initiation of radical-generating reactions [421].

In turn, *active* mechanisms of defense include proteins that prevent the formation of toxic compounds, repair or degrade them. This is the case of the three following levels of defense. At a second level antioxidant defenses (e.g. peroxidases and catalases) decompose H_2O_2 to less reactive compounds thereby preventing their cellular accumulation. This defense is not possible in the case of •OH because this oxidant reacts with biomolecules with diffusion-limited rate constants (Section 1.3.2). On a third level, protein oxidation is repaired by specific proteins (e.g. thioredoxins, peroxiredoxins, sulfiredoxins) that reduce the oxidized protein groups thereby preventing potentially deleterious outcomes of protein oxidation. Lastly, the proteolysis of oxidized proteins prevents potentially toxic effects that may result from the reaction of those proteins with other compounds.

Table 1.6 – Cellular mechanisms of protection against H_2O_2 and •OH.

		Defense mechanisms	**Role**
Passive	Primary	Cell membranes	Limit H_2O_2 permeation across compartments
		Protein sequence/structure	Structural and compositional properties of proteins preventing residue oxidation by H_2O_2 and •OH.
		Metal chelation	Iron and copper sequestration prevents generation of potentially toxic radicals (e.g. Fenton reactions)
Active	Secondary	Antioxidant defenses	Prevent potentially toxic H_2O_2 accumulation
	Tertiary	Redox repair enzymes	Repair oxidative damage to proteins
	Quaternary	Proteasome	Copes with oxidative damage to proteins

These different levels of defense carry different costs for the cell. For instance, antioxidant defenses carry the cost of synthesizing them (i.e. *deployment* cost) and that of their activity (*operating* cost). The deployment cost may be very high for the cell, depending on size and abundance of the enzyme, because it involves synthesizing all protein residues which not only uses resources for amino acid biosynthesis and peptide assembly, it also occupies the cell machinery with the biosynthesis of those compounds. These costs are lower for non-protein defenses (e.g. ascorbate), but these are much less efficient at removing H_2O_2

compared to the enzymatic processes. Second, the activity of some defenses such as peroxidases carries an operating cost because it is coupled with the oxidation of reducing equivalents. This is observed for instance in glutathione peroxidase and peroxiredoxin/thioredoxin activity where the oxidized glutathione and thioredoxin must then be reduced at expense of NADPH. The oxidative repair of proteins through thioredoxins also carries an operating cost because the oxidized thioredoxins must then be reduced. To this extent, catalase and superoxide dismutase activities are much cheaper because they are not stoichiometrically coupled with the oxidation of reducing equivalents. Finally, proteasomal degradation should occur as a last measure of cell defense because it implies *de novo* protein synthesis of the damaged protein.

Ideally protection against ROS would occur by completely preventing their permeation across cell membranes. However, not only are membranes partially permeable to ROS, but these oxidants are also endogenously produced and necessary for various cellular processes (e.g. H_2O_2, Section 1.3.2.2, Figure 1.2).

Considering the work presented in Chapters 2 and 3, it is now appropriate to discuss some of these defenses in depth. In Chapter 2 we aim to clarify the role of Peroxiredoxin 2 in H_2O_2 metabolism in human erythrocytes (secondary defense in Table 1.6) considering the H_2O_2 exposure regimes that these cells face while in circulation. We will now briefly review some of the properties of the main antioxidant defenses against H_2O_2 in cells focusing on peroxiredoxins because these are central players in our work. We have already briefly discussed how cell membranes and localized H_2O_2 production hinder the accumulation of H_2O_2 albeit limitedly (Section 1.2.2.3). We will not address the role of proteolysis because this process has been thoroughly discussed elsewhere [422] and is out of our scope. In turn, whether proteins are designed to minimize oxidative damage by •OH (primary level of protection in Table 1.6) is the focus of our work in Chapter 3.

1.4.1 Antioxidant scavengers

The decomposition of H_2O_2 by antioxidant defenses occurs with the help of electron donors. These are usually found in metal-based (e.g. heme/manganese catalases) or thiol-based (e.g. cysteine/selenocysteine peroxidases) antioxidant

defenses. Overall, H_2O_2 decomposition occurs through two main mechanisms: dismutation (Reaction 1.14) and reduction (Reaction 1.15)[11]. The former is catalyzed by catalases whereas the latter is catalyzed by peroxidases and peroxiredoxins.

$$2H_2O_2 \xrightarrow{Cat} O_2 + 2H_2O \qquad \textit{Reaction 1.14}$$

$$H_2O_2 + 2H^+ + 2e^- \xrightarrow{Per} 2H_2O \qquad \textit{Reaction 1.15}$$

There is some apparent overlap in the utilization of multiple defenses within the same cell. For instance, the OxyR transcription factor induces the translation of various catalases and peroxidases in *E. coli* upon exposure to H_2O_2 [423]. This was also observed in the PerR-regulated transcription activation of peroxidases and catalases in *Bacillus subtilis* [424], and in the simultaneous presence of catalase [425], glutathione peroxidase [426] and peroxiredoxin 2 [427, 428] in human erythrocytes. What could explain why various H_2O_2 scavengers are present in the same cell? Five non-mutually exclusive hypotheses may explain this [27, 429, 430]. First, in eukaryotic cells it may be important to have different isoforms in different cellular compartments. Second, cells may require that multiple defenses exist based on their different substrate specificities, despite their possible overlap. For instance, in human erythrocytes though both glutathione peroxidase 1 and catalase scavenge H_2O_2, glutathione peroxidase is mostly responsible for scavenging organic hydroperoxides [431, 432]. This substrate specificity may also be important to respond to different levels of H_2O_2. In *E. coli* peroxiredoxins are mostly used as scavengers of low H_2O_2 concentrations whereas catalases are the main defenses against high concentrations [433, 434]. Third, the utilization of different defenses may be necessary under different energetic conditions, prioritizing the utilization of defenses that do not couple H_2O_2 scavenging to oxidation of reducing equivalents (catalases) over defenses where this coupling occurs (peroxidases). Under high H_2O_2 concentrations the limited availability of NADPH may lead to slow thioredoxin and peroxiredoxin recycling, or peroxiredoxins may be inactivated by

[11] Henceforth *H_2O_2 reduction* is referred as the “peroxidase activity”, and *H_2O_2 dismutation* will refer to the “catalase activity” typically referred in the literature. This because some catalases also display peroxidase activity as we see below.

sulfinylation. Fourth, the utilization of enzymes with different prosthetic groups (e.g. *Heme*- vs *Manganese*-catalases) may be related with nutrient availability. Fifth, even when multiple defenses co-localize they may mediate different processes besides antioxidant protection. Some proteins such as peroxiredoxins also transduce redox signaling (Section 1.2.2 and see 1.4.1.2 for more detail). This could indicate that catalases and peroxidases could have different physiological roles, where the peroxidases may function in H_2O_2-dependent redox relays, and catalases would be limiting H_2O_2 accumulation to toxic levels.

We will now briefly discuss the main features of H_2O_2 decomposition by catalases and peroxiredoxins. Catalases are widely considered the main scavengers of H_2O_2 in many cells. In turn, peroxiredoxins' involvement in H_2O_2 metabolism seems not only to be H_2O_2 scavenging but also as mediators of redox signaling. While other peroxidases such as glutathione peroxidase may be important in H_2O_2 metabolism, they are mostly involved in protection against low H_2O_2 levels and organic peroxides and are reviewed elsewhere [435-438].

1.4.1.1 Catalase

Catalases (E.C. 1.11.1.6) are H_2O_2 dismutases ubiquitously distributed through the three kingdoms of life [439, 440]. Three families of catalases have evolved [441-443][12]: typical (monofunctional) catalases, (bifunctional) catalase-peroxidases, and non-heme (manganese-)catalases. Both typical catalases and catalase/peroxidases have heme groups buried in their catalytic site, accessible by H_2O_2 but not by organic peroxides through a narrow channel [444-446]. Heme catalases exhibit H_2O_2 dismutase activity but display many differences with respect to non-heme catalases including the absence of any sequence similarity, different active site and structural differences. In turn, non-heme catalases utilize manganese as a cofactor [447, 448]. Currently (Feb. 2016), 964 heme-catalases are annotated at Peroxibase (http://peroxibase.toulouse.inra.fr/ [449]), of which 534 are catalase-peroxidases. Manganese catalases comprise 101 annotated

[12] Some catalases were previously known as "atypical" catalases, such as chlorin-type heme catalase [442]. This and other formerly known "atypical" catalases were later classified as one of the three families above based on evolutionary studies [443].

sequences. While non-heme catalases are found only in bacteria, typical and bifunctional catalases are found in prokaryotic and eukaryotic organisms [440].

Monofunctional catalases have apparent K_m ≈40 – 600 mM and turnover numbers ≈54000 - 83000 s^{-1} [439]. Bifunctional catalases have apparent K_m ≈4-8 mM and turnover number of 3500-6000 s^{-1} [450]. These result $k_{cat}/K_m \approx 10^6\ M^{-1}s^{-1}$ for both bifunctional and typical catalases, suggesting that they are equally efficient in H_2O_2 reduction. In turn, manganese catalases display slightly lower $k_{cat}/K_m \approx 10^5$ $M^{-1}s^{-1}$ [447, 448, 451]. Though these parameters are indicative of the catalytic efficiency of the three families of catalases, one should bear in mind that catalases do not follow Michaelis-Menten kinetics unless at low H_2O_2 concentrations, and are not saturated by H_2O_2 (though catalase inactivation may occur as we will see) [439].

The utilization of these catalases varies with cell and growth conditions. For instance, monofunctional catalases are mostly used during stationary phase [452-454], whereas bifunctional catalases predominate under exponential growth and are induced by exposure to H_2O_2 [454-456] as observed in prokaryotes. In turn, manganese catalases are not essential in H_2O_2-treated organisms that have heme-catalases and peroxidases [457]. Though manganese catalase activity is observed in organisms naturally rich in manganese, it is not observed when heme sources are available [447]. Also, manganese importers are induced under low iron levels [458], which may suggest that manganese catalases are preferentially expressed under low heme conditions. Altogether, these observations suggest that manganese catalases are mostly utilized to compensate for the lack of heme catalase activity [429]. Other hypotheses [459] that could explain why manganese catalases are necessary are their ability to function under higher temperatures and their lower susceptibility to cyanide inhibition (which may be important during host invasion) in comparison to heme catalases. Additionally, it was observed that heme catalases may produce ROS upon exposure to UV radiation [460], possibly through Fenton reactions. It is unclear whether this process is a relevant source of ROS *in vivo*.

1. General Introduction

Typical catalases

Typical (or monofunctional) catalases (EC 1.11.1.6) are distributed through the three kingdoms of life, with 5 Archaea, 79 Bacteria and 346 are currently (Feb 2016) annotated sequences at Peroxibase (http://peroxibase.toulouse.inra.fr/ [449]). Monofunctional catalases are usually located in peroxisomes [461, 462], but may also be found in the cytoplasm (in human erythrocytes [425] and neutrophils [463]).

Enzymes in this superfamily display structural differences in subunit size, heme properties (e.g. orientation), and posttranslational modifications of amino acids in the active site, splitting them into three distinct subgroups with highly conserved active site [464, 465]. It is thought that they originally had large (≈750 residue) subunits but lost around 150 C-terminal residues during evolution [465].

Interestingly, few cyanobacteria display typical catalases [465]. Cyanobacteria are considered the pacemakers of aerobic evolution [466-469] due to their oxygenic photosynthesis metabolisms, to which it is attributed the accumulation of atmospheric oxygen from a previously anoxic environment. Because of this, it is thought [465] that typical catalases are not the oldest H_2O_2 scavenging enzymes developed immediately after oxygenic photosynthesis, the oldest being non-heme (manganese) catalases. A discussion of the structural properties of these catalases was done by [470, 471].

In heme catalases (i.e. mono- and bifunctional catalases) two redox centers are distinguishable, where iron is bound to the center of a porphyrin ring [472]. The reactions of typical catalases with H_2O_2 involve both redox centers and occur through two steps. First, H_2O_2 oxidizes the ground state enzyme (Ferricatalase, Por-Fe^{3+}) to Compound I (Por^{+}-Fe^{4+}=O) as showed in Reaction 1.16. Second, H_2O_2 reduces Compound I to ground state [473] (Reaction 1.17).

$$Ferricatalase(Por\text{-}Fe^{3+}) + H_2O_2 \rightarrow Compound\ I(Por^{+}\text{-}Fe^{4+}=O) + H_2O \qquad \textit{Reaction 1.16}$$

$$Compound\ I(Por^{+}\text{-}Fe^{4+}=O) + H_2O_2 \rightarrow Ferricatalase(Por\text{-}Fe^{3+}) + H_2O + O_2 \qquad \textit{Reaction 1.17}$$

Other reactions occur during its catalytic cycle. Compound I is slowly reduced to Compound II [473-475] by an unknown electron donor [476, 477]. Compound II is an inactive state of the enzyme, but its accumulation occurs very slowly

compared to the reactions of the enzyme with H_2O_2 (Reaction 1.16 and Reaction 1.17) in human erythrocytes and other eukaryotic cells, *E. coli* and *Aspergillus sp* [471, 475]. NADPH or other electron donors also prevent the accumulation of Compound II [478, 479]. NADPH prevents Compound II accumulation by reacting with an intermediate radical between Compound I and II, possibly through tyrosine residues neighboring the hemic iron [480].

Nevertheless, the fraction of inactive enzyme is relatively low even in high H_2O_2 doses and without added NADPH. For instance, *in vitro* observations using bovine liver catalase indicate that even in the absence of NADPH the inactive enzyme amounts to at most 20% of the enzyme even under 0.1 μM H_2O_2/s for 10 mins. It should be noted that NADPH is tightly bound to the enzyme [476, 478] but that not all catalases bind NADPH. It is also possible that externally added NADPH may not be an efficient protection mechanism if the enzyme-bound NADPH dissociates slowly as in the case of the erythrocyte enzyme ($K_D < 10^{-8}$ M [481]).

One additional inactive state exists, the Compound III. However, the fraction of the enzyme in this state is negligible even under high H_2O_2 doses and absence of NADPH [479].

Catalase-peroxidases

Bifunctional catalases (EC 1.11.1.21) are found in prokaryotes, protists and fungi [465]. Presently (Feb 2016), 534 catalase-peroxidases are found in Peroxibase (http://peroxibase.toulouse.inra.fr/ [449]), of which 17 are Archaea, 339 Bacteria and 178 Eukarya.

Bifunctional catalases are constituted by two-domain subunits, the N-terminal heme domain, and the C-terminal domain with no prosthetic group [470]. These enzymes exhibit H_2O_2 dismutase activity [482] and H_2O_2 reductase activity [483, 484]. They are thought to be at the origin of heme peroxidases, and similarly to the evolution of typical catalases, that of catalase-peroxidases also started with more complex proteins [465] where each subunit had the two-domains. At later stages in evolution the H_2O_2 dismutation functionality and C-terminal domain were eventually lost [485]. The superfamily of bifunctional catalases is comprised of 3 main clades with a few linking subclades [486]. One of the clades (Class I

catalase-peroxidases) contains both prokaryotic and eukaryotic representatives, whereas the two others (Class II and III) contain only eukaryotic proteins, each with various subclasses of peroxidase activities.

Catalase-peroxidases dismutate H_2O_2 (Reaction 1.14) but it is unclear whether they follow the same reactions of monofunctional catalases (Reaction 1.16 and Reaction 1.17) [440]. In addition, they display peroxidase activity when exogenous electron donors reduce Compound I to ground-state enzyme through two consecutive steps.

$$Compound\ I(Por^{+}\text{-}Fe^{4+}=O)+AH \rightarrow Compound\ II(Por\text{-}Fe^{4+}-OH)+A^{\cdot} \quad \textit{Reaction 1.18}$$

$$Compound\ II(Por\text{-}Fe^{4+}-OH)+AH \rightarrow Ferricatalase(Por\text{-}Fe^{3+})+H_2O+A^{-} \quad \textit{Reaction 1.19}$$

This activity is much slower compared to their dismutase activity [429, 487] which suggests that it has a negligible contribution to H_2O_2 scavenging. Instead, it is hypothesized to be a mechanism to reduce Compound I [429, 471]. The unknown Compound I reductants access the heme site through a different channel than that of H_2O_2 entry [439].

Although usually cytoplasmic these enzymes are also secreted to the periplasm in several pathogenic bacteria [197, 488, 489].

Non-heme catalases

Manganese catalases (EC 1.11.1.6) do not have heme groups in their catalytic pockets. These catalases are found in bacteria [447, 448, 457] and archaea [451], and currently (Feb 2016) 4 archaeal sequences (out of 101 total, prokaryotic) are annotated at Peroxibase (http://peroxibase.toulouse.inra.fr/ [449]). These enzymes evolved before heme catalases [465], and have been found in organisms grown in the absence of heme sources [447, 490].

In contrast to heme catalases, manganese catalases are single domain proteins where each subunit has a di-manganese active site [491, 492]. Their catalytic mechanism (Reaction 1.20 and Reaction 1.21) is similar to that of typical catalases (Reaction 1.16 and Reaction 1.17).

$$Catalase_{Ground\text{-}state}(Mn_2^{2+})+H_2O_2+2H^{+} \rightarrow Catalase_{Oxidized}(Mn_2^{3+})+2H_2O \quad \textit{Reaction 1.20}$$

$$Catalase_{Oxidized}(Mn_2^{3+}) + H_2O_2 \rightarrow Catalase_{Ground\text{-}state}(Mn_2^{2+}) + 2H^+ + O_2$$ Reaction 1.21

This group of catalases is not as widespread and is less catalytically efficient than heme catalases. It is frequently seen as secondary defenses against H_2O_2 [429, 459].

1.4.1.2 Peroxiredoxin

Peroxiredoxins (Prx, EC 1.11.1.15) reduce H_2O_2, peroxynitrite and other organic peroxides [493, 494] through their cysteine thiols. These proteins are present in all kingdoms [493] and are among the gene-induced responses to H_2O_2, particularly in unicellular organisms [495]. Prxs are among the most abundant proteins in *E. coli* [496], rat tissues [497], human erythrocytes [428] and in most human cells [498]. For instance, 0.1 – 0.8% of total protein content [499] and up to 5% of mitochondrial matrix protein [500] in mammal cells are Prxs. Prx1/AhpC peroxiredoxins are often highly expressed, accounting to 0.1 – 1% of total protein [501].

Families of Prxs

Based on their mechanisms of catalysis (Figure 1.6) three families of Prxs were initially proposed: 1-Cys peroxiredoxins, typical 2-Cys peroxiredoxins and atypical 2-Cys peroxiredoxins [197, 502]. 2-Cys Prxs are homodimers and contain 2 Cys per monomer whereas 1-Cys Prxs rely only on a single Cys per monomer. Their catalytic cycle involves a peroxidatic Cys (C_P or Cys_P) and a resolving Cys (C_R or Cys_R) in 2-Cys Prxs. In all three classes of Prxs, the catalytic cycle begins with the oxidation of C_P by H_2O_2 to sulfenic acid (C_P-OH). The sulfenic acid then forms an intermolecular (typical 2-Cys Prxs) or intramolecular (atypical 2-Cys Prxs) disulfide bond with the C_R, or with other proteins/small thiols (1-Cys Prxs [503]). This disulfide bond is then reduced to dithiol usually by reaction with thioredoxins or thioredoxin-like domains [504].

Although this classification of Prx families immediately indicates their catalytic properties, it groups structurally very different proteins together. More recent classifications take into account their structural features [505] and active site signatures and phylogeny [506]. These define six Prx families: Prx1/AhpC (include mammalian PrxI - IV), Prx5, Prx6, Tpx, BCP/PrxQ and AhpE. Each of

these six subclasses include 1-Cys and atypical/typical 2-Cys Prxs with exception to Prx1/AhpC which includes only typical 2-Cys Prxs. The structural differences between the six Prx families include different quaternary organization (e.g. dimers vs decamers vs dodecamers) and different location of C_R. The C_R locates in one of five possible locations where those close to the N- or C-termini form intermolecular disulfide bonds (as opposed to intramolecular disulfides). These structural differences are reviewed elsewhere [507, 508].

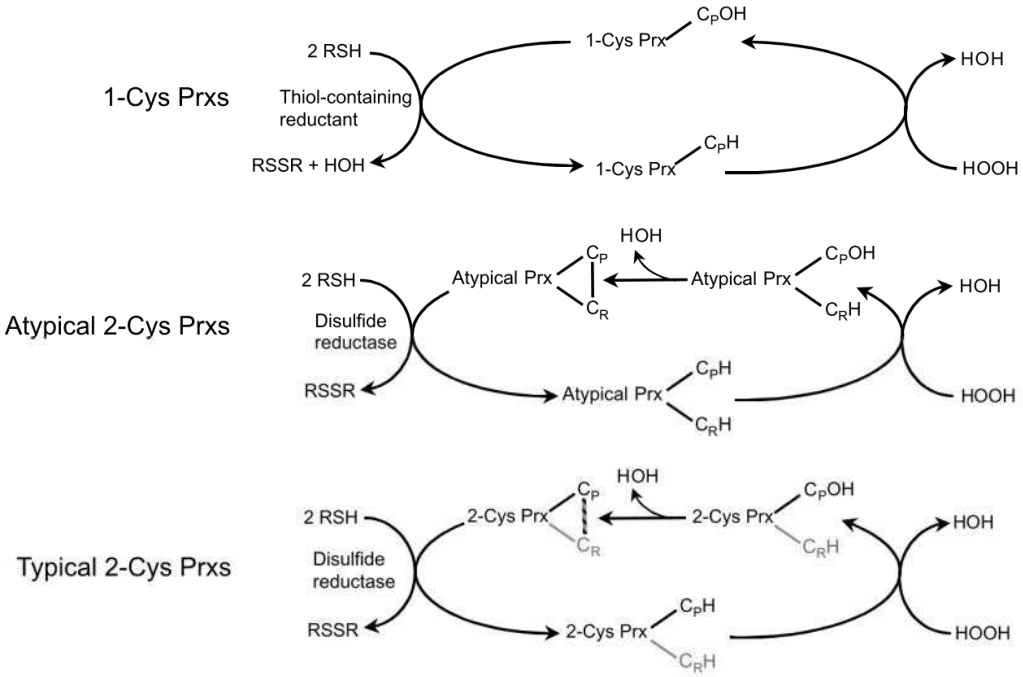

Figure 1.6 – Catalytic mechanisms of 1-Cys Prxs (top), atypical 2-Cys Prxs (middle) and typical 2-Cys Prxs (bottom). The attack of H_2O_2 on the peroxidatic Cys (C_P) leads to the formation of a sulfenic acid (C_POH) which condensates with other molecules (in the case of 1-Cys Prxs), or with C_R in the same monomer (in atypical Prxs) or in a different monomer (in typical 2-Cys Prxs). The coloring highlights that the C_R in typical 2-Cys Prxs comes from another monomer. Adapted from [197].

While catalases are primarily peroxisomal enzymes([425, 463]), Prxs are found in cytoplasm, mitochondria, chloroplasts, peroxisomes, endoplasmic reticulum and even extracellularly [493, 509-511]. For instance, mammalian proteins of the Prx1/AhpC family are found in the cytosol and nucleus (Prx1 and 2, respectively), mitochondria (Prx3), and endoplasmic reticulum (Prx4).

Phylogenetic analyses of these Prx families [506] indicates that Prx1/AhpC and Prx6 families are found in the three domains of life and are the most represented

Prxs. The BCP/PrxQ family is also present in the three domains, but absent in animals. The Prx5 family is not found in Archaea, and the Tpx and AhpE families are found almost exclusively in Bacteria (with exception for one species of Tpx in eukaryotes). Currently, (Feb. 2016) 1115 Peroxiredoxins are annotated at Peroxibase (http://peroxibase.toulouse.inra.fr/ [449]), but their annotation does not follow the 6 families above (Table 1.7).

Table 1.7 – Prxs deposited at Peroxibase (http://peroxibase.toulouse.inra.fr/ [449]) as of Feb. 2016. Total numbers of Prxs and distribution in Archaea, Bacteria and Eukarya.

	Total	**Archaea**	**Bacteria**	**Eukarya**
1-Cys	219	0	19	200
Typical 2-Cys	254	0	0	254
AhpC like	116	0	116	0
AhpE	23	0	23	0
BCP/PrxQ	195	9	85	101
Atypical 2-Cys	184	0	7	177
Tpx	26	0	23	3
Other*	53	0	53	0
Total	**1115**	**9**	**326**	**735**

* These are proteins where parts of the sequence show Prx and glutaredoxin homology.

Catalytic properties of Prxs

The reactivity of the peroxidatic Cys with H_2O_2 is much higher than those of other protein and low molecular weight thiols (Table 1.3). This high reactivity is due to two highly conserved features of the active site. Namely, the sequence Pro-$(Xaa)_3$-Thr/Ser-$(Xaa)_3$-Cys_P, and a nearby Arg [505, 506]. The presence of Pro, Thr/Ser and Arg residues near the peroxidatic Cys creates a hydrogen-bond network that aligns the H_2O_2 for attack by the thiolate [154] and lowers the activation energy for reaction of H_2O_2 with the Cys_P by stabilizing the Prx-H_2O_2 intermediate complex [193].

The catalytic cycle of 2-Cys Prxs involves the local unfolding and refolding of the active site [242, 512-514] (Figure 1.7A). The fully folded active site reacts with H_2O_2. Because the C_R is buried, rearrangement of the active site loop (10 residues containing the C_P) and disordering of the C-terminus beyond C_R is required for the formation of the C_P/C_R disulfide bond (Figure 1.7B).

Mutations that disrupt the fully folded active site decrease the reactivity with peroxides and rate of sulfinylation, whereas those that stabilize the fully fold state slow the formation of disulfide bonds but promote sulfinylation [515]. Therefore, the transition from fully folded to locally unfolded is important not only for governing the dynamics of catalysis, but also explains why some Prxs are not susceptible to sulfinylation [197][13]. For instance, Prx3 is less prone to sulfinylation than Prx2 owing to the 10-fold higher condensation rate constant of the former protein [517]. These kinetic differences may also contribute to promote selectivity of redox responses.

Additionally, other Cys residues facilitate Prx sulfinylation. Prx1 and 2 are >90% homologous [497] but whereas Prx1 is prone to sulfinylation, Prx2 is more resistant. Analysis of the two proteins indicates that this is due to a Cys that exists in Prx1 but not Prx2 [518]. The presence of this Cys facilitates the decameric organization and sulfinylation of Prx1 but not Prx2 [518].

The sulfinylation of Prxs is hypothesized to be important for three reasons. First, the inactivation of Prxs by sulfinylation is thought to allow less reactive molecules (e.g. protein tyrosine phosphatases) to react with H_2O_2. Second, to couple conserved redox circadian cycles with Prx function [519-521]. The levels of sulfiredoxin and H_2O_2, together with sulfinic Prx, display circadian rhythms in mitochondria in various tissues [522, 523]. And third, to permit chaperone function of 2-Cys Prxs in various species under severe oxidative stress [524, 525], though the *in vivo* relevance of Prxs' chaperone activity is still unclear.

Prxs as scavengers of low H_2O_2 concentrations

Due to their high reactivities with H_2O_2 (Table 1.3) and high abundance, Prxs are able to scavenge low H_2O_2 concentrations. However, under high H_2O_2 concentrations Prxs are inactivated due to sulfinylation [239, 242] or accumulate in disulfide form as result of limited thioredoxin recycling [205, 526-528].

In contrast, catalases can only function as efficient H_2O_2 dismutases at high H_2O_2 concentrations, becoming inefficient peroxidases at low H_2O_2 concentrations. For

[13] While some sulfenic acids of typical 2-Cys Prx from the Prx1/AhpC family are in fully fold form [515], human Prx IV (also a member of the Prx1/AhpC family) displays the locally unfolded sulfenic acid form [516].

this reason, Prx and catalases are believed to be functionally complementary in cells where they coexist in the same compartment.

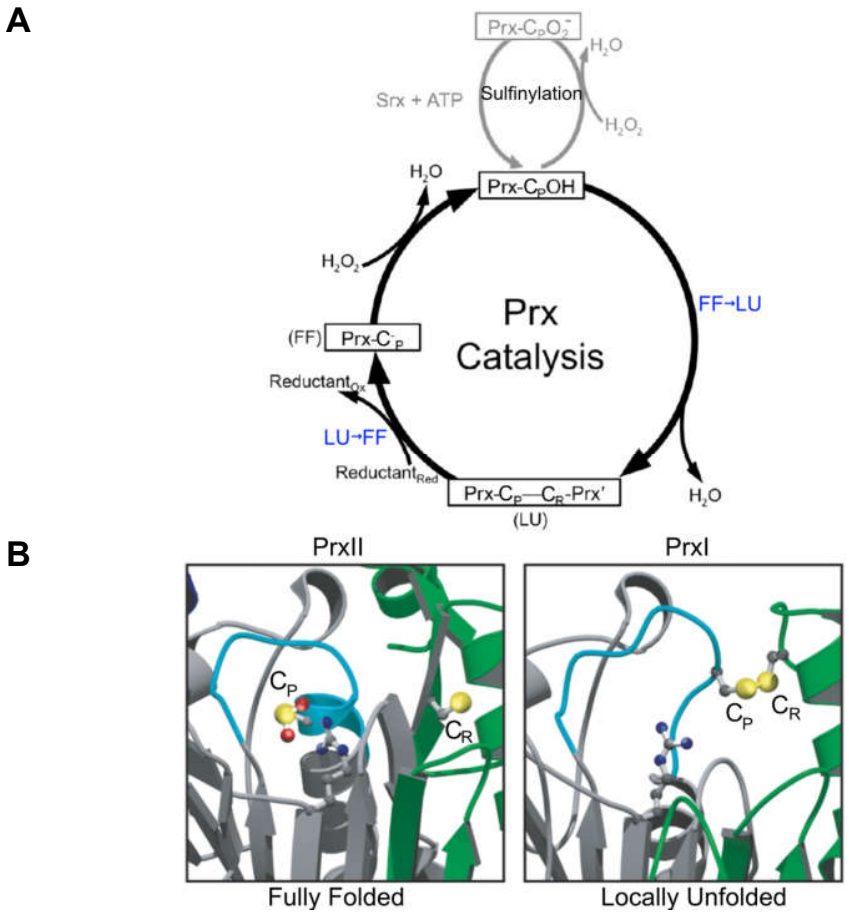

Figure 1.7 – The catalytic cycle of Prxs involves conformational changes in the protein. A) catalytic cycle showing the conformation change of Prxs, where FF is Fully Folded and LU is Locally Unfolded. The local unfolding (FF -> LU) is required for the formation of disulfide bond between C_P and C_R, and the local refolding (LU -> FF) is also required for the reaction between C_P and H_2O_2. The sulfinylation (gray) occurs in some but not all Prxs. Adapted from [515]. B) Detail of fully folded active site conformation of sulfinylated PrxII (left) and locally unfolded disulfide (PrxI). Represented are different Prx monomers (gray and green), the peroxidatic (C_P) and resolving (C_R) Cys, together with the Arg residue (blue ball and stick) and the loop that undergoes local unfolding (cyan). Adapted from [197].

This complementarity is illustrated by the following examples. AhpC in *E. coli* was one of the first Prxs to be described as scavenger of low H_2O_2 levels while its two catalases, KatG and KatE are the main defenses under higher H_2O_2 concentrations [433, 434]. In *S. cerevisae* there are five Prxs (cytosolic,

mitochondrial, and nuclear) [529, 530], of which Tsa1 is the main defense against H_2O_2 [531, 532] though the other Prxs are able to compensate the protection against endogenously generated H_2O_2 in null *tsa1* mutants [208, 533]. Mutants simultaneously lacking many of these thiol peroxidases are still viable [208] but sensitive to oxidative stress [534] indicating that Prxs are important but not essential. Likewise, acatalasemic mutants show no decrease in growth rate under basal oxidative conditions, but are sensitive to added H_2O_2 [535]. Similar observations were made for *S. pombe* [536]. Also, Prx2-mutant mice erythrocytes display similar catalase activities to wild type cells [537][14].

Altogether, these observations show that while Prxs are able to protect cells against low/endogenously-generated H_2O_2, they fail to do so at higher H_2O_2 concentrations.

Prxs in signaling

The high reactivity of Prxs with H_2O_2 (Table 1.3) and their high abundance makes them good H_2O_2 sensors and signaling transducers. Because Prxs use thioredoxins (Trx) as reductants, signaling properties of Prxs are intertwined with those of Trxs [198, 538].

As others have noted [198], Prxs may mediate H_2O_2 signaling through three non-mutually exclusive modes (Figure 1.8). First, H_2O_2 reacts directly with target molecules where Prxs control the local concentrations of H_2O_2. Second, H_2O_2 reacts with Prxs whose oxidized forms then transduce this redox signal to signaling targets. And third, Prx oxidation by H_2O_2 translates into oxidation of Trxs, which then react with the signaling targets. Below we present four examples of these processes, though many others are emerging [135, 510].

One of the most widely discussed features of H_2O_2-mediated signaling involves the oxidation of protein tyrosine phosphatases (PTP)[539]. How are PTPs oxidized in the presence of H_2O_2 [539] despite their lower concentrations and H_2O_2-reactivities compared to those of cellular defenses? One possible explanation is that PTPs co-localize with H_2O_2 sources and directly react with

[14] However, these mutant mice show several pathological effects, such as abnormally-sized erythrocytes, lower hematocrit, and higher levels of erythrocyte oxidized proteins.

H_2O_2 [27, 136]. However, a more likely explanation involves other more H_2O_2-reactive redox signaling partners that relay the oxidation to the phosphatases [139, 195, 228].

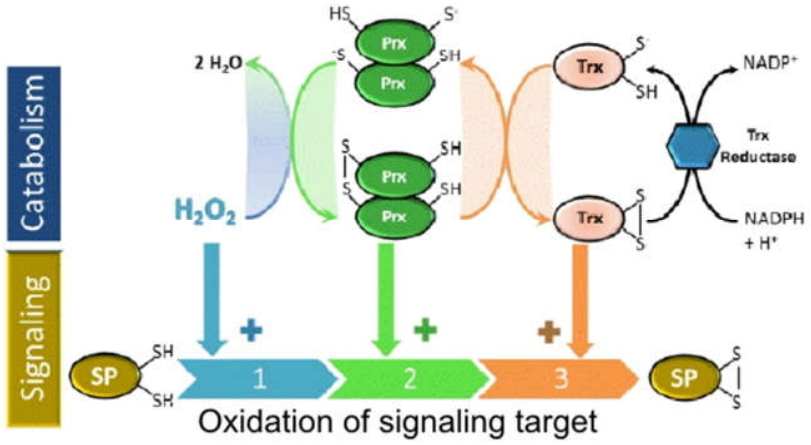

Figure 1.8 – Mechanisms of H_2O_2 signaling involving Prxs and Trxs. Three mechanisms are distinguished: direct oxidation of a signaling target by H_2O_2 (blue), oxidation of a Prx that then oxidizes the signaling target (green), and oxidation of signaling target by Trx (orange). Adapted from [198].

This is the case of the second and third modes of H_2O_2 signaling. For instance, Prx1 is involved in oxidation of the phosphatase PTEN by H_2O_2 in human cells [168, 170]. Prx1 binds PTEN and prevents its oxidation by H_2O_2 which in turn decreases Akt signaling therefore modulating cell survival and apoptosis [540]. Prx1 also binds MKP-1 and MKP-5, the phosphatases that regulate p38MAPK and JNK signaling. The mechanism of regulation is not fully understood, but it is clear that Prx1 has different effects depending on H_2O_2 levels [171]. Under low H_2O_2 concentrations Prx1 is bound to MKP-1 and MKP-5, maintaining these phosphatases active. Under higher H_2O_2 concentrations the Prx1/MKP-1 complexes dissociate, which oxidatively inactivates MKP-1 (similarly to the PTEN mechanism) and possibly allows for JNK activity and apoptosis [171, 541]. In turn, the Prx1/MKP-5 complex and MKP-5 activity are maintained even at high H_2O_2 concentrations, which inactivates p38MAPK and possibly leads to senescence [171]. It is therefore hypothesized that Prx1 modulates the senescence or apoptosis *via* MKP-1/5 depending on the cellular context and H_2O_2 concentrations [171].

Thioredoxins may also relay H_2O_2 signaling messages. Reduced Trx1 and 2 inhibit the kinase ASK1 in cytoplasm and mitochondria in mammalian cells [175, 542]. Upon oxidation of these Trxs, the Trx1/2-ASK1 complex dissociates, leading to ASK1 and caspase-3 activation and apoptosis. Additionally, some observations suggest that Trxs may work together with Prxs to regulate signaling targets. Trxs show much higher specificity of reaction with oxidized than reduced protein targets [543] (e.g. disulfide Prxs). And because Trxs ($k \approx 1\ M^{-1}s^{-1}$) are also much less H_2O_2-reactive than Prxs ($k > 10^5\ M^{-1}s^{-1}$, Table 1.3) the direct oxidation of Trxs by H_2O_2 is unlikely in a system where Prxs are also present. These observations suggest that where both Prxs and Trxs are present, the former may act as primary H_2O_2 sensors, transducing the oxidized moiety to Trxs which then regulate the activity of its targets. This is observed in the mechanism of Trx1/2 interaction with ASK1, where Prx2 sulfinylation maintains the integrity of the ASK1/Trx complex preventing ASK1 activation and apoptosis [176].

Prxs and inflammation

During inflammation, leukocytes release ROS and subject the nearby cells (e.g. erythrocytes) to higher levels of H_2O_2. In Chapter 2 we analyze the response of the Peroxiredoxin 2/Thioredoxin/Thioredoxin Reductase/Catalase system to various dynamics of erythrocyte exposure to H_2O_2. We consider high H_2O_2 concentrations (<1 μM) presumably attained during systemic inflammation or while crossing inflammation sites. It is therefore interesting to briefly examine the role of Prxs in inflammation in other cells[15].

Prx expression is significantly increased under acute inflammation in the lungs and other tissues [545-548]. The expression of these proteins in phagocytes and microglial cells is also upregulated by interferon γ and lipopolysaccharides in processes involving ROS [549-551]. These observations suggest that Prxs may be important in cells that produce high levels of ROS. Several comparisons of mice knockouts vs controls support this hypothesis: Prx2-knock outs are more sensitive to lipopolysaccharide-induced endotoxic shock, and expression of catalase or adenovirus-encoded Prx2 rescues the mice from endotoxic shock

[15] The roles of Prxs in inflammation are more extensively reviewed by [544].

[552]; Prx1-knock out mice are susceptible to induced pulmonary inflammation and fibrosis [553]. In turn, overexpressing human Prx4 leads to increased protection against inflammatory insults and apoptosis in model type 1 diabetes mellitus mice, and protects against type 2 diabetes mellitus [554, 555]. The activation of phagocytes is also mediated by Prxs. Microglial activation depends on Prx1 and is modulated by lipopolysaccharide but not by H_2O_2 [556]. Macrophages are also activated by Prx6-dependent NADPH oxidase activation [557]. Nevertheless, it is unclear whether these Prxs are mostly required for their role as peroxidase, redox-signaling transducers, or both.

Finally, Prxs have also been shown to initiate the inflammatory response. A 2-Cys Prx from *Plasmodium berghei* acts as a pathogen-associated molecular pattern (PAMP), binding a macrophage receptor and triggering pro-inflammatory responses [558]. Prxs also act as host-derived damage-associated molecular patterns (DAMP), molecules that initiate and perpetuate non-infectious inflammatory response, by triggering inflammatory cytokines by macrophages [559, 560]. Interestingly, it was observed [559] that this property of Prx1 is dependent on its ability to form decamers, but not on its peroxidase activity.

1.5 References

1. Sies, H. and D. Jones, *Oxidative stress*, in *Encyclopedia of Stress*, G. Fink, Editor. 2007, Elsevier: Amsterdam. p. 45-48.
2. Andreae, W.A., *A sensitive method for the estimation of hydrogen peroxide in biological materials.* Nature, 1955. **175**(4463): p. 859-60.
3. Sbarra, A.J. and M.L. Karnovsky, *The biochemical basis of phagocytosis. I. Metabolic changes during the ingestion of particles by polymorphonuclear leukocytes.* J Biol Chem, 1959. **234**(6): p. 1355-62.
4. Jensen, P.K., *No Title.* 1965. **122**: p. 157-166.
5. Boveris, a., et al., *The cellular production of hydrogen peroxide.* The Biochemical journal, 1972. **128**: p. 617-30.
6. Chance, B., H. Sies, and a. Boveris, *Hydroperoxide metabolism in mammalian organs.* Physiological reviews, 1979. **59**: p. 527-605.
7. Iyer, G., M. Islam, and J. Quastel, *Biochemical aspects of phagocytosis.* 1961.
8. Hampton, M.B., A.J. Kettle, and C.C. Winterbourn, *Inside the neutrophil phagosome: Oxidants, myeloperoxidase, and bacterial killing.* Blood, 1998. **92**(9): p. 3007-3017.
9. Learman, D., et al., *Formation of manganese oxides by bacterially generated superoxide.* Nature Geoscience, 2011. **4**(2): p. 95-98.
10. Smith, W.L. and R.C. Murphy, *Oxidized lipids formed non-enzymatically by reactive oxygen species.* Journal of Biological Chemistry, 2008. **283**: p. 15513-15514.
11. Cooke, M.S., et al., *Oxidative DNA damage: mechanisms, mutation, and disease.* The FASEB journal : official publication of the Federation of American Societies for Experimental Biology, 2003. **17**: p. 1195-1214.
12. Cabiscol, E., J. Tamarit, and J. Ros, *Oxidative stress in bacteria and protein damage by reactive oxygen species.* International Microbiology, 2000. **3**: p. 3-8.
13. Höhn, A., J. König, and T. Grune, *Protein oxidation in aging and the removal of oxidized proteins.* Journal of Proteomics, 2013. **92**: p. 132-159.
14. Garrison, W.M., *Reaction-mechanisms in the radiolysis of peptides, polypeptides, and proteins.* Chemical Reviews, 1987. **87**(2): p. 381-398.
15. Winterbourn, C.C., *Reconciling the chemistry and biology of reactive oxygen species.* Nature Chemical Biology, 2008. **4**(5): p. 278-286.
16. Peskin, A.V., et al., *The high reactivity of peroxiredoxin 2 with H2O2 is not reflected in its reaction with other oxidants and thiol reagents.* Journal Of Biological Chemistry, 2007. **282**(16): p. 11885-11892.
17. Trujillo, M., et al., *Pre-steady state kinetic characterization of human peroxiredoxin 5: taking advantage of Trp84 fluorescence increase upon oxidation.* Arch Biochem Biophys, 2007. **467**(1): p. 95-9106.

18. Manta, B., et al., *The peroxidase and peroxynitrite reductase activity of human erythrocyte peroxiredoxin 2.* Archives Of Biochemistry And Biophysics, 2009. **484**(2): p. 146-154.
19. Imlay, J.A., *Cellular Defenses against Superoxide and Hydrogen Peroxide.* Annual Review of Biochemistry, 2008. **77**(1): p. 755-776.
20. Fourquet, S., et al., *The Dual Functions of Thiol-Based Peroxidases in H2O2 Scavenging and Signaling.* Antioxidants & Redox Signaling, 2008. **10**(9): p. 1565-1576.
21. Toledano, M.B., et al., *Redox-dependent shift of OxyR-DNA contacts along an extended DNA-binding site: a mechanism for differential promoter selection.* Cell, 1994. **78**(5): p. 897-909.
22. Wood, M.J., G. Storz, and N. Tjandra, *Structural basis for redox regulation of Yap1 transcription factor localization.* Nature, 2004. **430**(7002): p. 917-21.
23. Dansen, T.B., et al., *Redox-sensitive cysteines bridge p300/CBP-mediated acetylation and FoxO4 activity.* Nat Chem Biol, 2009. **5**(9): p. 664-72.
24. Jarvis, R.M., S.M. Hughes, and E.C. Ledgerwood, *Peroxiredoxin 1 functions as a signal peroxidase to receive, transduce, and transmit peroxide signals in mammalian cells.* Free Radical Biology and Medicine, 2012. **53**(7): p. 1522-1530.
25. Woo, H.A., et al., *Inactivation of peroxiredoxin I by phosphorylation allows localized H 2 O 2 accumulation for cell signaling.* Cell, 2010. **140**(4): p. 517-528.
26. Gutscher, M., et al., *Proximity-based protein thiol oxidation by H2O2-scavenging peroxidases.* Journal of Biological Chemistry, 2009. **284**: p. 31532-31540.
27. Winterbourn, C.C., *The biological chemistry of hydrogen peroxide.* Methods Enzymol, 2013. **528**: p. 3-25.
28. Randall, L.M., G. Ferrer-Sueta, and A. Denicola, *Peroxiredoxins as preferential targets in H2O2-induced signaling.* Methods Enzymol, 2013. **527**: p. 41-63.
29. Conte, M.L. and K.S. Carroll, *The redox biochemistry of protein sulfenylation and sulfinylation.* Journal of Biological Chemistry, 2013. **288**(37): p. 26480-26488.
30. Lambeth, J.D., *NOX enzymes and the biology of reactive oxygen.* Nat Rev Immunol, 2004. **4**(3): p. 181-9.
31. Bedard, K. and K.H. Krause, *The NOX family of ROS-generating NADPH oxidases: physiology and pathophysiology.* Physiol Rev, 2007. **87**(1): p. 245-313.
32. Holmström, K.M. and T. Finkel, *Cellular mechanisms and physiological consequences of redox-dependent signalling.* Nature reviews. Molecular cell biology, 2014. **15**: p. 411-21.

33. Gough, D.R. and T.G. Cotter, *Hydrogen peroxide: a Jekyll and Hyde signalling molecule.* Cell Death and Disease, 2011. **2**: p. e213.
34. Sundaresan, M., et al., *Requirement for generation of H2O2 for platelet-derived growth factor signal transduction.* Science, 1995. **270**(5234): p. 296-9.
35. Foreman, J., et al., *Reactive oxygen species produced by NADPH oxidase regulate plant cell growth.* Nature, 2003. **422**(6930): p. 442-6.
36. Ikeda, S., et al., *IQGAP1 regulates reactive oxygen species-dependent endothelial cell migration through interacting with Nox2.* Arterioscler Thromb Vasc Biol, 2005. **25**(11): p. 2295-300.
37. Schmidt, K.N., et al., *The roles of hydrogen peroxide and superoxide as messengers in the activation of transcription factor NF-kappa B.* Chem.Biol., 1995. **2**(1): p. 13-22.
38. Brawn, K. and I. Fridovich, *Superoxide radical and superoxide dismutases: threat and defense.* Acta Physiol Scand Suppl, 1980. **492**: p. 9-18.
39. von Sonntag, C., et al., *Radiation-induced strand breaks in DNA: Chemical and enzymatic analysis of end groups and mechanistic aspects.* Adv. Radiat. Biol, 1981. **9**: p. 109-142.
40. Tien, M., B.A. Svingen, and S.D. Aust, *An investigation into the role of hydroxyl radical in xanthine oxidase-dependent lipid peroxidation.* Arch Biochem Biophys, 1982. **216**(1): p. 142-51.
41. Sokol, H.A., W. Bennett-Corniea, and W.M. Garrison, *A marked effect of conformation in the radiolysis of poly-α-l-glutamic acid in aqueous solution.* Journal of the American Chemical Society, 1965. **87**(6): p. 1391-1392.
42. Davies, M.J., *Protein and peptide alkoxyl radicals can give rise to C-terminal decarboxylation and backbone cleavage.* Archives of biochemistry and biophysics, 1996. **336**(1): p. 163-172.
43. Hawkins, C. and M. Davies, *EPR studies on the selectivity of hydroxyl radical attack on amino acids and peptides.* Journal of the Chemical Society, Perkin Transactions 2, 1998(12): p. 2617-2622.
44. Halliwell, B. and J.M. Gutteridge, *Oxygen toxicity, oxygen radicals, transition metals and disease.* Biochem J, 1984. **219**(1): p. 1-14.
45. Desesso, J.M., A.R. Scialli, and G.C. Goeringer, *D-mannitol, a specific hydroxyl free radical scavenger, reduces the developmental toxicity of hydroxyurea in rabbits.* Teratology, 1994. **49**(4): p. 248-59.
46. Del Maestro, R., et al., *Free radicals as mediators of tissue injury.* Acta Physiol Scand Suppl, 1980. **492**: p. 43-57.
47. Dikalov, S.I., M.P. Vitek, and R.P. Mason, *Cupric-amyloid beta peptide complex stimulates oxidation of ascorbate and generation of hydroxyl radical.* Free Radic Biol Med, 2004. **36**(3): p. 340-7.
48. Dawson, T.M. and V.L. Dawson, *Molecular pathways of neurodegeneration in Parkinson's disease.* Science, 2003. **302**(5646): p. 819-22.

49. Beauchamp, C. and I. Fridovich, *A mechanism for the production of ethylene from methional. The generation of the hydroxyl radical by xanthine oxidase.* J Biol Chem, 1970. **245**(18): p. 4641-6.

50. Halliwell, B., M.V. Clement, and L.H. Long, *Hydrogen peroxide in the human body.* Febs Letters, 2000. **486**(1): p. 10-13.

51. Weidinger, A. and A.V. Kozlov, *Biological Activities of Reactive Oxygen and Nitrogen Species: Oxidative Stress versus Signal Transduction.* Biomolecules, 2015. **5**(2): p. 472-84.

52. Gray, M.J., W.-Y. Wholey, and U. Jakob, *Bacterial responses to reactive chlorine species.* Annual review of microbiology, 2013. **67**: p. 141.

53. Halliwell, B., *Reactive species and antioxidants. Redox biology is a fundamental theme of aerobic life.* Plant physiology, 2006. **141**(2): p. 312-322.

54. Suh, Y.A., et al., *Cell transformation by the superoxide-generating oxidase Mox1.* Nature, 1999. **401**(6748): p. 79-82.

55. Lambeth, J.D., et al., *Novel homologs of gp91phox.* Trends Biochem Sci, 2000. **25**(10): p. 459-61.

56. Murphy, M.P., *How mitochondria produce reactive oxygen species.* Biochem J, 2009. **417**(1): p. 1-13.

57. Brand, M.D., *The sites and topology of mitochondrial superoxide production.* Exp Gerontol, 2010. **45**(7-8): p. 466-72.

58. Massey, V., et al., *The production of superoxide anion radicals in the reaction of reduced flavins and flavoproteins with molecular oxygen.* Biochem Biophys Res Commun, 1969. **36**(6): p. 891-7.

59. Geary, L.E. and A. Meister, *On the mechanism of glutamine-dependent reductive amination of alpha-ketoglutarate catalyzed by glutamate synthase.* J Biol Chem, 1977. **252**(10): p. 3501-8.

60. Messner, K.R. and J.A. Imlay, *The identification of primary sites of superoxide and hydrogen peroxide formation in the aerobic respiratory chain and sulfite reductase complex of Escherichia coli.* Journal Of Biological Chemistry, 1999. **274**(15): p. 10119-10128.

61. Messner, K.R. and J.A. Imlay, *Mechanism of superoxide and hydrogen peroxide formation by fumarate reductase, succinate dehydrogenase, and aspartate oxidase.* Journal Of Biological Chemistry, 2002. **277**(45): p. 42563-42571.

62. Korshunov, S. and J.A. Imlay, *Two sources of endogenous hydrogen peroxide in Escherichia coli.* Mol Microbiol, 2010. **75**(6): p. 1389-401.

63. Segal, A.W. and K.P. Shatwell, *The NADPH oxidase of phagocytic leukocytes.* Ann N Y Acad Sci, 1997. **832**: p. 215-22.

64. Harris, C.M. and V. Massey, *The reaction of reduced xanthine dehydrogenase with molecular oxygen. Reaction kinetics and measurement of superoxide radical.* J Biol Chem, 1997. **272**(13): p. 8370-9.

65. Harrison, R., *Structure and function of xanthine oxidoreductase: where are we now?* Free Radic Biol Med, 2002. **33**(6): p. 774-97.

66. Babior, B.M., J.D. Lambeth, and W. Nauseef, *The neutrophil NADPH oxidase.* Arch Biochem Biophys, 2002. **397**(2): p. 342-4.

67. Brown, G.C. and V. Borutaite, *There is no evidence that mitochondria are the main source of reactive oxygen species in mammalian cells.* Mitochondrion, 2012. **12**(1): p. 1-4.

68. Gross, E., et al., *Generating disulfides enzymatically: reaction products and electron acceptors of the endoplasmic reticulum thiol oxidase Ero1p.* Proc Natl Acad Sci U S A, 2006. **103**(2): p. 299-304.

69. Ozgur, R., et al., *Endoplasmic reticulum stress triggers ROS signalling, changes the redox state, and regulates the antioxidant defence of Arabidopsis thaliana.* Journal of experimental botany, 2014. **65**(5): p. 1377-1390.

70. Kukreja, R.C., et al., *PGH synthase and lipoxygenase generate superoxide in the presence of NADH or NADPH.* Circ Res, 1986. **59**(6): p. 612-9.

71. Roy, P., et al., *Superoxide generation by lipoxygenase in the presence of NADH and NADPH.* Biochim Biophys Acta, 1994. **1214**(2): p. 171-9.

72. Maker, H.S., et al., *Coupling of dopamine oxidation (monoamine oxidase activity) to glutathione oxidation via the generation of hydrogen peroxide in rat brain homogenates.* J Neurochem, 1981. **36**(2): p. 589-93.

73. Gillette, J.R., B.B. Brodie, and B.N. La Du, *The oxidation of drugs by liver microsomes: on the role of TPNH and oxygen.* J Pharmacol Exp Ther, 1957. **119**(4): p. 532-40.

74. Nordblom, G.D. and M.J. Coon, *Hydrogen peroxide formation and stoichiometry of hydroxylation reactions catalyzed by highly purified liver microsomal cytochrome P-450.* Arch Biochem Biophys, 1977. **180**(2): p. 343-7.

75. Korshunov, S. and J.A. Imlay, *Detection and quantification of superoxide formed within the periplasm of Escherichia coli.* J. Bacteriol., 2006. **188**(17): p. 6326-6334.

76. Seaver, L.C. and J.A. Imlay, *Are respiratory enzymes the primary sources of intracellular hydrogen peroxide?* Journal Of Biological Chemistry, 2004. **279**(47): p. 48742-48750.

77. Cadenas, E. and K.J. Davies, *Mitochondrial free radical generation, oxidative stress, and aging.* Free Radical Biology And Medicine, 2000. **29**(3-4): p. 222-230.

78. Turrens, J.F. and A. Boveris, *Generation of superoxide anion by the NADH dehydrogenase of bovine heart mitochondria.* Biochemical Journal, 1980. **191**(2): p. 421-427.

79. Petit, C., et al., *Oxygen consumption by cultured human cells is impaired by a nucleoside analogue cocktail that inhibits mitochondrial DNA synthesis.* Mitochondrion, 2005. **5**(3): p. 154-161.

80. Johnson, M.E. and G. Hummer, *Nonspecific binding limits the number of proteins in a cell and shapes their interaction networks.* Proceedings of the National Academy of Sciences, 2011. **108**.

81. Chance, B., et al., *The nature of the catalase intermediate in its biological function*, in *Oxidases and related redox systems*. 1973, University Park Press: Baltimore. p. 350-353.

82. Turrens, J.F., *Mitochondrial formation of reactive oxygen species.* The Journal of Physiology Online, 2003. **552**(2): p. 335-344.

83. Packer, M.A., C.M. Porteous, and M.P. Murphy, *Superoxide production by mitochondria in the presence of nitric oxide forms peroxynitrite.* Biochem Mol Biol Int, 1996. **40**(3): p. 527-34.

84. Szabo, C., H. Ischiropoulos, and R. Radi, *Peroxynitrite: biochemistry, pathophysiology and development of therapeutics.* Nat Rev Drug Discov, 2007. **6**(8): p. 662-80.

85. Huie, R.E. and S. Padmaja, *The reaction of NO with superoxide.* Free radical research, 1993. **18**(4): p. 195-199.

86. Kwong, L.K. and R.S. Sohal, *Substrate and site specificity of hydrogen peroxide generation in mouse mitochondria.* Archives Of Biochemistry And Biophysics, 1998. **350**(1): p. 118-126.

87. Tahara, E.B., F.D. Navarete, and A.J. Kowaltowski, *Tissue-, substrate-, and site-specific characteristics of mitochondrial reactive oxygen species generation.* Free Radical Biology and Medicine, 2009. **46**(9): p. 1283-1297.

88. !!! INVALID CITATION !!! [56, 82, 88].

89. Mailloux, R.J. and M.E. Harper, *Mitochondrial proticity and ROS signaling: lessons from the uncoupling proteins.* Trends Endocrinol Metab, 2012. **23**(9): p. 451-8.

90. Chen, K., et al., *Regulation of ROS signal transduction by NADPH oxidase 4 localization.* J Cell Biol, 2008. **181**(7): p. 1129-39.

91. Liu, R.M., et al., *Oxidative modification of nuclear mitogen-activated protein kinase phosphatase 1 is involved in transforming growth factor beta1-induced expression of plasminogen activator inhibitor 1 in fibroblasts.* J Biol Chem, 2010. **285**(21): p. 16239-47.

92. Graham, K.A., et al., *NADPH oxidase 4 is an oncoprotein localized to mitochondria.* Cancer Biol Ther, 2010. **10**(3): p. 223-31.

93. Geiszt, M., et al., *Identification of renox, an NAD(P)H oxidase in kidney.* Proc Natl Acad Sci U S A, 2000. **97**(14): p. 8010-4.

94. Cheng, G., et al., *Homologs of gp91phox: cloning and tissue expression of Nox3, Nox4, and Nox5.* Gene, 2001. **269**(1-2): p. 131-40.

95. Banfi, B., et al., *A Ca(2+)-activated NADPH oxidase in testis, spleen, and lymph nodes.* J Biol Chem, 2001. **276**(40): p. 37594-601.

96. De Deken, X., et al., *Cloning of two human thyroid cDNAs encoding new members of the NADPH oxidase family.* J Biol Chem, 2000. **275**(30): p. 23227-33.

97. Geiszt, M. and T.L. Leto, *The Nox family of NAD(P)H oxidases: host defense and beyond.* J Biol Chem, 2004. **279**(50): p. 51715-8.

98. Nauseef, W.M., *Biological roles for the NOX family NADPH oxidases.* Journal of Biological Chemistry, 2008. **283**(25): p. 16961-16965.

99. Wosniak, J., Jr., et al., *Cross-talk between mitochondria and NADPH oxidase: effects of mild mitochondrial dysfunction on angiotensin II-mediated increase in Nox isoform expression and activity in vascular smooth muscle cells.* Antioxid Redox Signal, 2009. **11**(6): p. 1265-78.

100. Dikalov, S.I., et al., *Mitochondrial reactive oxygen species and calcium uptake regulate activation of phagocytic NADPH oxidase.* Am J Physiol Regul Integr Comp Physiol, 2012. **302**(10): p. R1134-42.

101. De Duve, C. and P. Baudhuin, *Peroxisomes (microbodies and related particles).* Physiological Reviews, 1966. **46**(2): p. 323-357.

102. Antonenkov, V.D., et al., *Peroxisomes are oxidative organelles.* Antioxid Redox Signal, 2010. **13**(4): p. 525-37.

103. Fransen, M., et al., *Role of peroxisomes in ROS/RNS-metabolism: implications for human disease.* Biochim Biophys Acta, 2012. **1822**(9): p. 1363-73.

104. Bonekamp, N.A., et al., *Reactive oxygen species and peroxisomes: struggling for balance.* Biofactors, 2009. **35**(4): p. 346-55.

105. Leadsham, J.E., et al., *Loss of cytochrome c oxidase promotes RAS-dependent ROS production from the ER resident NADPH oxidase, Yno1p, in yeast.* Cell Metab, 2013. **18**(2): p. 279-86.

106. Liu, L., et al., *Mitochondrial dysfunction leads to telomere attrition and genomic instability.* Aging cell, 2002. **1**(1): p. 40-46.

107. Storz, G. and L.A. Tartaglia, *OxyR: a regulator of antioxidant genes.* J Nutr, 1992. **122**(3 Suppl): p. 627-630.

108. Jamieson, D.J., *Oxidative stress responses of the yeast Saccharomyces cerevisiae.* Yeast, 1998. **14**(16): p. 1511-1527.

109. Lee, J.W. and J.D. Helmann, *The PerR transcription factor senses H2O2 by metal-catalysed histidine oxidation.* Nature, 2006. **440**(7082): p. 363-7.

110. An, J.H. and T.K. Blackwell, *SKN-1 links C. elegans mesendodermal specification to a conserved oxidative stress response.* Genes Dev, 2003. **17**(15): p. 1882-93.

111. Sablina, A.A., et al., *The antioxidant function of the p53 tumor suppressor.* Nat Med, 2005. **11**(12): p. 1306-13.

112. Chen, K., et al., *Mitochondrial function is required for hydrogen peroxide-induced growth factor receptor transactivation and downstream signaling.* J Biol Chem, 2004. **279**(33): p. 35079-86.

113. Sauer, H., et al., *Role of reactive oxygen species and phosphatidylinositol 3-kinase in cardiomyocyte differentiation of embryonic stem cells.* FEBS Lett, 2000. **476**(3): p. 218-23.

114. Li, J., et al., *The NADPH oxidase NOX4 drives cardiac differentiation: Role in regulating cardiac transcription factors and MAP kinase activation.* Mol Biol Cell, 2006. **17**(9): p. 3978-88.

115. Kim, J.S., T.Y. Huang, and G.M. Bokoch, *Reactive oxygen species regulate a slingshot-cofilin activation pathway.* Mol Biol Cell, 2009. **20**(11): p. 2650-60.

116. Niethammer, P., et al., *A tissue-scale gradient of hydrogen peroxide mediates rapid wound detection in zebrafish.* Nature, 2009. **459**(7249): p. 996-U123.

117. Gianni, D., et al., *c-Src-mediated phosphorylation of NoxA1 and Tks4 induces the reactive oxygen species (ROS)-dependent formation of functional invadopodia in human colon cancer cells.* Mol Biol Cell, 2010. **21**(23): p. 4287-98.

118. Wang, Y., et al., *Regulation of VEGF-induced endothelial cell migration by mitochondrial reactive oxygen species.* Am J Physiol Cell Physiol, 2011. **301**(3): p. C695-704.

119. Ago, T., et al., *A redox-dependent pathway for regulating class II HDACs and cardiac hypertrophy.* Cell, 2008. **133**(6): p. 978-93.

120. Le Belle, J.E., et al., *Proliferative neural stem cells have high endogenous ROS levels that regulate self-renewal and neurogenesis in a PI3K/Akt-dependant manner.* Cell Stem Cell, 2011. **8**(1): p. 59-71.

121. Dickinson, B.C., et al., *Nox2 redox signaling maintains essential cell populations in the brain.* Nat Chem Biol, 2011. **7**(2): p. 106-12.

122. Haber, F. and J. Weiss. *The catalytic decomposition of hydrogen peroxide by iron salts*. in *Proceedings of the Royal Society of London A: Mathematical, Physical and Engineering Sciences*. 1934. The Royal Society.

123. McCord, J.M. and E.D. Day, Jr., *Superoxide-dependent production of hydroxyl radical catalyzed by iron-EDTA complex.* FEBS Lett, 1978. **86**(1): p. 139-42.

124. Hawkins, C.L. and M.J. Davies, *Generation and propagation of radical reactions on proteins.* Biochimica Et Biophysica Acta-Bioenergetics, 2001. **1504**(2-3): p. 196-219.

125. Levine, R.L., et al., *Turnover of bacterial glutamine synthetase: oxidative inactivation precedes proteolysis.* Proceedings of the National Academy of Sciences, 1981. **78**(4): p. 2120-2124.

126. Stadtman, E.R. and M.E. Wittenberger, *Inactivation of Escherichia coli glutamine synthetase by xanthine oxidase, nicotinate hydroxylase, horseradish peroxidase, or glucose oxidase: effects of ferredoxin, putidaredoxin, and menadione.* Archives of biochemistry and biophysics, 1985. **239**(2): p. 379-387.

127. Jang, S. and J.A. Imlay, *Micromolar intracellular hydrogen peroxide disrupts metabolism by damaging iron-sulfur enzymes.* Journal of Biological Chemistry, 2007. **282**(2): p. 929-937.

128. Pomposiello, P.J., M.H.J. Bennik, and B. Demple, *Genome-wide transcriptional profiling of the Escherichia coli responses to superoxide stress and sodium salicylate.* Journal Of Bacteriology, 2001. **183**(13): p. 3890-3902.

129. Kamata, H., et al., *Reactive oxygen species promote TNFalpha-induced death and sustained JNK activation by inhibiting MAP kinase phosphatases.* Cell, 2005. **120**(5): p. 649-61.

130. Gechev, T.S. and J. Hille, *Hydrogen peroxide as a signal controlling plant programmed cell death.* J Cell Biol, 2005. **168**(1): p. 17-20.

131. Aslund, F., et al., *Regulation of the OxyR transcription factor by hydrogen peroxide and the cellular thiol-disulfide status.* Proceedings Of The National Academy Of Sciences Of The United States Of America, 1999. **96**(11): p. 6161-6165.

132. Vivancos, A.P., et al., *A cysteine-sulfinic acid in peroxiredoxin regulates H2O2-sensing by the antioxidant Pap1 pathway.* Proceedings of the National Academy of Sciences of the United States of America, 2005. **102**(25): p. 8875-8880.

133. Bozonet, S.M., et al., *Oxidation of a eukaryotic 2-Cys peroxiredoxin is a molecular switch controlling the transcriptional response to increasing levels of hydrogen peroxide.* Journal of Biological Chemistry, 2005. **280**(24): p. 23319-23327.

134. Delaunay, A., et al., *A thiol peroxidase is an H2O2 receptor and redox-transducer in gene activation.* Cell, 2002. **111**(4): p. 471-481.

135. Veal, E.A., A.M. Day, and B.A. Morgan, *Hydrogen Peroxide Sensing and Signaling.* Molecular Cell, 2007. **26**(1): p. 1-14.

136. Marinho, H.S., et al., *Hydrogen peroxide sensing, signaling and regulation of transcription factors.* Redox Biol, 2014. **2**: p. 535-62.

137. Boronat, S., et al., *Thiol-based H2O2 signalling in microbial systems.* Redox Biology, 2014. **2**: p. 395-399.

138. Huxtable, R., *Biochemistry of sulfur*. Biochemistry of the elements. 1986, New York: Springer Science & Business Media.

139. Ferrer-Sueta, G., et al., *Factors Affecting Protein Thiol Reactivity and Specificity in Peroxide Reduction.* Chemical Research In Toxicology, 2011. **24**(4): p. 434-450.

140. Koppenol, W.H., D.M. Stanbury, and P.L. Bounds, *Electrode potentials of partially reduced oxygen species, from dioxygen to water.* Free Radical Biology and Medicine, 2010. **49**(3): p. 317-322.

141. Wunderlich, M. and R. Glockshuber, *Redox properties of protein disulfide isomerase (DsbA) from Escherichia coli.* Protein science: a publication of the Protein Society, 1993. **2**(5): p. 717.

142. Rouhier, N., et al., *Poplar peroxiredoxin Q. A thioredoxin-linked chloroplast antioxidant functional in pathogen defense.* Plant Physiology, 2004. **134**(3): p. 1027-1036.

143. Biteau, B., J. Labarre, and M.B. Toledano, *ATP-dependent reduction of cysteine-sulphinic acid by S. cerevisiae sulphiredoxin.* Nature, 2003. **425**(6961): p. 980-984.

144. Xu, G. and M.R. Chance, *Hydroxyl radical-mediated modification of proteins as probes for structural proteomics.* Chem Rev, 2007. **107**(8): p. 3514-43.

145. Griffiths, S.W., J. King, and C.L. Cooney, *The reactivity and oxidation pathway of cysteine 232 in recombinant human α1-antitrypsin.* Journal of Biological Chemistry, 2002. **277**(28): p. 25486-25492.

146. Gallogly, M.M. and J.J. Mieyal, *Mechanisms of reversible protein glutathionylation in redox signaling and oxidative stress.* Current opinion in pharmacology, 2007. **7**(4): p. 381-391.

147. Chang, T.-S.S., et al., *Characterization of mammalian sulfiredoxin and its reactivation of hyperoxidized peroxiredoxin through reduction of cysteine sulfinic acid in the active site to cysteine.* The Journal of biological chemistry, 2004. **279**: p. 50994-1001.

148. Polgar, L., *Ion-Pair Formation as a Source of Enhanced Reactivity of the Essential Thiol Group of d-Glyceraldehyde-3-Phosphate Dehydrogenase.* European Journal of Biochemistry, 1975. **51**(1): p. 63-71.

149. Roberts, D.D., et al., *Reactivity of small thiolate anions and cysteine-25 in papain toward methyl methanethiosulfonate.* Biochemistry, 1986. **25**(19): p. 5595-5601.

150. Pinitglang, S., et al., *A classical enzyme active center motif lacks catalytic competence until modulated electrostatically.* Biochemistry, 1997. **36**(33): p. 9968-9982.

151. Zhang, Z.Y. and J.E. Dixon, *Active site labeling of the Yersinia protein tyrosine phosphatase: the determination of the pKa of the active site cysteine and the function of the conserved histidine 402.* Biochemistry, 1993. **32**(36): p. 9340-9345.

152. Baburina, I., et al., *Three of four cysteines, including that responsible for substrate activation, are ionized at pH 6.0 in yeast pyruvate decarboxylase: evidence from Fourier transform infrared and isoelectric focusing studies.* Biochemistry, 1996. **35**(32): p. 10249-10255.

153. Declercq, J.-P., et al., *Crystal structure of human peroxiredoxin 5, a novel type of mammalian peroxiredoxin at 1.5 Å resolution.* Journal of molecular biology, 2001. **311**(4): p. 751-759.

154. Nelson, K.J., et al., *Cysteine pK(a) Values for the Bacterial Peroxiredoxin AhpC.* Biochemistry, 2008. **47**(48): p. 12860-12868.

155. Sun, C.H., M.J. Berardi, and J.H. Bushweller, *The NMR solution structure of human glutaredoxin in the fully reduced form.* Journal Of Molecular Biology, 1998. **280**(4): p. 687-701.

156. Kallis, G.-B. and A. Holmgren, *Differential reactivity of the functional sulfhydryl groups of cysteine-32 and cysteine-35 present in the reduced form of thioredoxin from Escherichia coli.* Journal of Biological Chemistry, 1980. **255**(21): p. 10261-10265.

157. Mavridou, D.A., et al., *Active-site properties of the oxidized and reduced C-terminal domain of DsbD obtained by NMR spectroscopy.* Journal of molecular biology, 2007. **370**(4): p. 643-658.

158. Li, L., et al., *The Electrostatic Driving Force for Nucleophilic Catalysis in l-Arginine Deiminase: A Combined Experimental and Theoretical Study†.* Biochemistry, 2008. **47**(16): p. 4721-4732.

159. Nordstrand, K., et al., *Direct NMR observation of the Cys-14 thiol proton of reduced Escherichia coli glutaredoxin-3 supports the presence of an active site thiol-thiolate hydrogen bond.* FEBS letters, 1999. **449**(2): p. 196-200.

160. Kortemme, T. and T.E. Creighton, *Ionisation of cysteine residues at the termini of model alpha-helical peptides. Relevance to unusual thiol pKa values in proteins of the thioredoxin family.* J Mol Biol, 1995. **253**(5): p. 799-812.

161. Darby, N. and T.E. Creighton, *Characterization of the active site cysteine residues of the thioredoxin-like domains of protein disulfide isomerase.* Biochemistry, 1995. **34**(51): p. 16770-16780.

162. Fomenko, D.E. and V.N. Gladyshev, *Identity and functions of CxxC-derived motifs.* Biochemistry, 2003. **42**(38): p. 11214-11225.

163. Guddat, L.W., J.C. Bardwell, and J.L. Martin, *Crystal structures of reduced and oxidized DsbA: investigation of domain motion and thiolate stabilization.* Structure, 1998. **6**(6): p. 757-767.

164. May, J.M. and C. de Haen, *Insulin-stimulated intracellular hydrogen peroxide production in rat epididymal fat cells.* J Biol Chem, 1979. **254**(7): p. 2214-20.

165. Zhang, Z.Y., et al., *The Cys(X)5Arg catalytic motif in phosphoester hydrolysis.* Biochemistry, 1994. **33**(51): p. 15266-70.

166. Irani, K., et al., *Mitogenic signaling mediated by oxidants in Ras-transformed fibroblasts.* Science, 1997. **275**(5306): p. 1649-52.

167. Yoshizumi, M., et al., *Src and Cas mediate JNK activation but not ERK1/2 and p38 kinases by reactive oxygen species.* J Biol Chem, 2000. **275**(16): p. 11706-12.

168. Kwon, J., et al., *Reversible oxidation and inactivation of the tumor suppressor PTEN in cells stimulated with peptide growth factors.* Proc Natl Acad Sci U S A, 2004. **101**(47): p. 16419-16424.

169. Salmeen, A., et al., *Redox regulation of protein tyrosine phosphatase 1B involves a sulphenyl-amide intermediate.* Nature, 2003. **423**(6941): p. 769-773.

170. Cao, J., et al., *Prdx1 inhibits tumorigenesis via regulating PTEN/AKT activity.* The EMBO journal, 2009. **28**(10): p. 1505-1517.

171. Turner-Ivey, B., et al., *Role for Prdx1 as a specific sensor in redox-regulated senescence in breast cancer.* Oncogene, 2013. **32**(45): p. 5302-5314.

172. Giannoni, E., et al., *Intracellular reactive oxygen species activate Src tyrosine kinase during cell adhesion and anchorage-dependent cell growth.* Mol Cell Biol, 2005. **25**(15): p. 6391-6403.

173. Cho, S.-H., et al., *Redox regulation of PTEN and protein tyrosine phosphatases in H 2 O 2-mediated cell signaling.* FEBS letters, 2004. **560**(1): p. 7-13.

174. Morinaka, A., et al., *Oligomeric peroxiredoxin-I is an essential intermediate for p53 to activate MST1 kinase and apoptosis.* Oncogene, 2011. **30**(40): p. 4208-4218.

175. Saitoh, M., et al., *Mammalian thioredoxin is a direct inhibitor of apoptosis signal-regulating kinase (ASK) 1.* The EMBO journal, 1998. **17**(9): p. 2596-2606.

176. Hu, X., et al., *Peroxiredoxin-2 protects against 6-hydroxydopamine-induced dopaminergic neurodegeneration via attenuation of the apoptosis signal-regulating kinase (ASK1) signaling cascade.* The Journal of Neuroscience, 2011. **31**(1): p. 247-261.

177. Hampton, M. and K. O'Connor, *Peroxiredoxins and the Regulation of Cell Death.* Molecules and cells, 2016.

178. Iwakami, S., et al., *Concentration-dependent dual effects of hydrogen peroxide on insulin signal transduction in H4IIEC hepatocytes.* PLoS One, 2011. **6**(11): p. e27401.

179. Matias, A.C., et al., *Biphasic modulation of fatty acid synthase by hydrogen peroxide in Saccharomyces cerevisiae.* Archives of biochemistry and biophysics, 2011. **515**(1): p. 107-111.

180. Vivancos, A.P., et al., *Activation of the redox sensor Pap1 by hydrogen peroxide requires modulation of the intracellular oxidant concentration.* Molecular microbiology, 2004. **52**(5): p. 1427-1435.

181. Toda, T., M. Shimanuki, and M. Yanagida, *Fission yeast genes that confer resistance to staurosporine encode an AP-1-like transcription factor and a protein kinase related to the mammalian ERK1/MAP2 and budding yeast FUS3 and KSS1 kinases.* Genes & development, 1991. **5**(1): p. 60-73.

182. Toone, W.M., et al., *Regulation of the fission yeast transcription factor Pap1 by oxidative stress: requirement for the nuclear export factor Crm1 (Exportin) and the stress-activated MAP kinase Sty1/Spc1.* Genes & Development, 1998. **12**(10): p. 1453-1463.

183. Delaunay, A., A.D. Isnard, and M.B. Toledano, *H2O2 sensing through oxidation of the Yap1 transcription factor.* The EMBO journal, 2000. **19**(19): p. 5157-5166.

184. Boveris, A. and E. Cadenas, *Mitochondrial production of hydrogen peroxide regulation by nitric oxide and the role of ubisemiquinone.* IUBMB.Life, 2000. **50**(4-5): p. 245-250.

185. Giorgio, M., et al., *Hydrogen peroxide: a metabolic by-product or a common mediator of ageing signals?* Nature reviews. Molecular cell biology, 2007. **8**: p. 722-728.

186. Dickinson, B.C. and C.J. Chang, *Chemistry and biology of reactive oxygen species in signaling or stress responses.* Nature chemical biology, 2011. **7**: p. 504-511.

187. Hamanaka, R.B. and N.S. Chandel, *Mitochondrial reactive oxygen species regulate cellular signaling and dictate biological outcomes.* Trends in Biochemical Sciences, 2010. **35**: p. 505-513.

188. Seaver, L.C. and J.A. Imlay, *Hydrogen peroxide fluxes and compartmentalization inside growing Escherichia coli.* Journal of Bacteriology, 2001. **183**(24): p. 7182-7189.

189. Polle, A., *Dissecting the superoxide dismutase-ascorbate-glutathione-pathway in chloroplasts by metabolic modeling. Computer simulations as a step towards flux analysis.* Plant Physiol, 2001. **126**(1): p. 445-62.

190. Antunes, F. and E. Cadenas, *Cellular titration of apoptosis with steady state concentrations of H(2)O(2): submicromolar levels of H(2)O(2) induce apoptosis through Fenton chemistry independent of the cellular thiol state.* Free Radical Biology And Medicine, 2001. **30**(9): p. 1008-1018.

191. Stone, J.R. and S.P. Yang, *Hydrogen peroxide: A signaling messenger.* Antioxidants & Redox Signaling, 2006. **8**(3-4): p. 243-270.

192. Nakamura, J., E.R. Purvis, and J.A. Swenberg, *Micromolar concentrations of hydrogen peroxide induce oxidative DNA lesions more efficiently than millimolar concentrations in mammalian cells.* Nucleic Acids Res, 2003. **31**(6): p. 1790-5.

193. Hall, A., et al., *Structural evidence that peroxiredoxin catalytic power is based on transition-state stabilization.* Journal of molecular biology, 2010. **402**(1): p. 194-209.

194. Nagy, P., et al., *Model for the Exceptional Reactivity of Peroxiredoxins 2 and 3 with Hydrogen Peroxide A KINETIC AND COMPUTATIONAL STUDY.* Journal of Biological Chemistry, 2011. **286**(20): p. 18048-18055.

195. Winterbourn, C.C. and M.B. Hampton, *Thiol chemistry and specificity in redox signaling.* Free Radical Biology And Medicine, 2008. **45**(5): p. 549-561.

196. Thorburn, D.R. and P.W. Kuchel, *Regulation of the human-erythrocyte hexose-monophosphate shunt under conditions of oxidative stress. A study using NMR spectroscopy, a kinetic isotope effect, a reconstituted system and computer simulation.* European Journal Of Biochemistry, 1985. **150**(2): p. 371-386.

197. Wood, Z.A., et al., *Structure, mechanism and regulation of peroxiredoxins.* Trends In Biochemical Sciences, 2003. **28**(1): p. 32-40.

198. Netto, L. and F. Antunes, *The Roles of Peroxiredoxin and Thioredoxin in Hydrogen Peroxide Sensing and in Signal Transduction.* Molecules and cells, 2016.

199. Saurin, A.T., et al., *Widespread sulfenic acid formation in tissues in response to hydrogen peroxide.* Proceedings Of The National Academy Of Sciences Of The United States Of America, 2004. **101**(52): p. 17982-17987.

200. Klomsiri, C., et al., *Use of dimedone-based chemical probes for sulfenic acid detection: evaluation of conditions affecting probe incorporation into redox-sensitive proteins.* Methods in enzymology, 2010. **473**: p. 77-94.

201. Barelier, S., et al., *Discovery of fragment molecules that bind the human peroxiredoxin 5 active site.* PloS one, 2010. **5**(3): p. e9744.

202. Paulsen, C.E., et al., *Peroxide-dependent sulfenylation of the EGFR catalytic site enhances kinase activity.* Nature chemical biology, 2012. **8**(1): p. 57-64.

203. Poole, L.B., P.A. Karplus, and A. Claiborne, *Protein sulfenic acids in redox signaling.* Annu. Rev. Pharmacol. Toxicol., 2004. **44**: p. 325-347.

204. Nagy, P. and C.C. Winterbourn, *Redox chemistry of biological thiols.* Advances in molecular toxicology, 2010. **4**: p. 183.

205. Low, F.M., et al., *Peroxiredoxin 2 functions as a noncatalytic scavenger of low-level hydrogen peroxide in the erythrocyte.* Blood, 2007. **109**(6): p. 2611-2617.

206. Cho, C.S., et al., *Irreversible Inactivation of Glutathione Peroxidase 1 and Reversible Inactivation of Peroxiredoxin II by H2O2 in Red Blood Cells.* Antioxidants & Redox Signaling, 2010. **12**(11): p. 1235-1246.

207. van Montfort, R.L., et al., *Oxidation state of the active-site cysteine in protein tyrosine phosphatase 1B.* Nature, 2003. **423**(6941): p. 773-7.

208. Fomenko, D.E., et al., *Thiol peroxidases mediate specific genome-wide regulation of gene expression in response to hydrogen peroxide.* Proceedings of the National Academy of Sciences, 2011. **108**.

209. Choi, H.J., et al., *Crystal structure of a novel human peroxidase enzyme at 2.0 A resolution.* Nature structural biology, 1998. **5**: p. 400-406.

210. Claiborne, A., et al., *Protein-sulfenic acids: diverse roles for an unlikely player in enzyme catalysis and redox regulation.* Biochemistry, 1999. **38**(47): p. 15407-15416.

211. Boschi-Muller, S., et al., *A Sulfenic Acid Enzyme Intermediate Is Involved in the Catalytic Mechanism of Peptide Methionine Sulfoxide Reductase fromEscherichia coli.* Journal of Biological Chemistry, 2000. **275**(46): p. 35908-35913.

212. Carballal, S., et al., *Sulfenic acid in human serum albumin.* Amino Acids, 2007. **32**(4): p. 543-551.

213. Ishii, A., K. Komiya, and J. Nakayama, *Synthesis of a stable sulfenic acid by oxidation of a sterically hindered thiol (thiophenetriptycene-8-thiol) 1 and its characterization.* Journal of the American Chemical Society, 1996. **118**(50): p. 12836-12837.

214. Goto, K., M. Holler, and R. Okazaki, *Synthesis, structure, and reactions of a sulfenic acid bearing a novel bowl-type substituent: the first synthesis of*

a stable sulfenic acid by direct oxidation of a thiol. Journal of the American Chemical Society, 1997. **119**(6): p. 1460-1461.

215. Riemer, J., N. Bulleid, and J.M. Herrmann, *Disulfide formation in the ER and mitochondria: two solutions to a common process.* Science, 2009. **324**(5932): p. 1284-1287.
216. Arner, E.S.J. and A. Holmgren, *Physiological functions of thioredoxin and thioredoxin reductase.* European Journal Of Biochemistry, 2000. **267**(20): p. 6102-6109.
217. Hogg, P.J., *Disulfide bonds as switches for protein function.* Trends in biochemical sciences, 2003. **28**(4): p. 210-214.
218. Lillig, C.H., C. Berndt, and A. Holmgren, *Glutaredoxin systems.* Biochimica et Biophysica Acta (BBA)-General Subjects, 2008. **1780**(11): p. 1304-1317.
219. Seo, M.S., et al., *Identification of a new type of mammalian peroxiredoxin that forms an intramolecular disulfide as a reaction intermediate.* J Biol Chem, 2000. **275**(27): p. 20346-20354.
220. Winterbourn, C.C. and D. Metodiewa, *Reactivity of biologically important thiol compounds with superoxide and hydrogen peroxide.* Free Radical Biology And Medicine, 1999. **27**(3-4): p. 322-328.
221. Barton, J.P., J.E. Packer, and R.J. Sims, *Kinetics of the reaction of hydrogen peroxide with cysteine and cysteamine.* Journal of the Chemical Society, Perkin Transactions 2, 1973(11): p. 1547-1549.
222. Goldman, R., et al., *Reduction of phenoxyl radicals by thioredoxin results in selective oxidation of its SH-groups to disulfides. An antioxidant function of thioredoxin.* Biochemistry, 1995. **34**(14): p. 4765-4772.
223. Denu, J.M. and K.G. Tanner, *Specific and reversible inactivation of protein tyrosine phosphatases by hydrogen peroxide: evidence for a sulfenic acid intermediate and implications for redox regulation.* Biochemistry, 1998. **37**(16): p. 5633-5642.
224. Barrett, W.C., et al., *Roles of superoxide radical anion in signal transduction mediated by reversible regulation of protein-tyrosine phosphatase 1B.* Journal Of Biological Chemistry, 1999. **274**(49): p. 34543-34546.
225. LaButti, J.N., et al., *Redox Regulation of Protein Tyrosine Phosphatase 1B by Peroxymonophosphate (O3POOH).* Journal of the American Chemical Society, 2007. **129**(17): p. 5320-5321.
226. Chen, C.-Y., D. Willard, and J. Rudolph, *Redox regulation of SH2-domain-containing protein tyrosine phosphatases by two backdoor cysteines.* Biochemistry, 2009. **48**(6): p. 1399-1409.
227. Zhou, H., et al., *The biological buffer bicarbonate/CO2 potentiates H2O2-mediated inactivation of protein tyrosine phosphatases.* Journal of the American Chemical Society, 2011. **133**(40): p. 15803-15805.

228. Brito, P.M. and F. Antunes, *Estimation of kinetic parameters related to biochemical interactions between hydrogen peroxide and signal transduction proteins.* Frontiers in chemistry, 2014. **2**.

229. Cross, A.R. and A.W. Segal, *The NADPH oxidase of professional phagocytes—prototype of the NOX electron transport chain systems.* Biochimica et Biophysica Acta (BBA)-Bioenergetics, 2004. **1657**(1): p. 1-22.

230. Lim, J.C., et al., *A low pKa cysteine at the active site of mouse methionine sulfoxide reductase A.* Journal of Biological Chemistry, 2012. **287**(30): p. 25596-25601.

231. Little, C. and P. O'brien, *Mechanism of Peroxide-Inactivation of the Sulphydryl Enzyme Glyceraldehyde-3-Phosphate Dehydrogenase.* European Journal of Biochemistry, 1969. **10**(3): p. 533-538.

232. Crane III, E.J., et al., *Analysis of the kinetic mechanism of enterococcal NADH peroxidase reveals catalytic roles for NADH complexes with both oxidized and two-electron-reduced enzyme forms.* Biochemistry, 1995. **34**(43): p. 14114-14124.

233. Andres-Mateos, E., et al., *DJ-1 gene deletion reveals that DJ-1 is an atypical peroxiredoxin-like peroxidase.* Proceedings of the National Academy of Sciences, 2007. **104**(37): p. 14807-14812.

234. Toledo, J.C., et al., *Horseradish peroxidase compound I as a tool to investigate reactive protein-cysteine residues: from quantification to kinetics.* Free Radical Biology and Medicine, 2011. **50**(9): p. 1032-1038.

235. Ogusucu, R., et al., *Reactions of yeast thioredoxin peroxidases I and II with hydrogen peroxide and peroxynitrite: rate constants by competitive kinetics.* Free Radical Biology and Medicine, 2007. **42**(3): p. 326-334.

236. Parsonage, D., P.A. Karplus, and L.B. Poole, *Substrate specificity and redox potential of AhpC, a bacterial peroxiredoxin.* Proc Natl Acad Sci U S A, 2008. **105**(24): p. 8209-14.

237. Fourquet, S., et al., *Activation of NRF2 by Nitrosative Agents and H2O2 Involves KEAP1 Disulfide Formation.* Journal of Biological Chemistry, 2010. **285**(11): p. 8463-8471.

238. Hamann, M., et al., *Quantitation of protein sulfinic and sulfonic acid, irreversibly oxidized protein cysteine sites in cellular proteins.* Protein Sensors and Reactive Oxygen Species, Pt B, Thiol Enzymes and Proteins, 2002. **348**: p. 146-156.

239. Yang, K.-S., et al., *Inactivation of human peroxiredoxin I during catalysis as the result of the oxidation of the catalytic site cysteine to cysteine-sulfinic acid.* J Biol Chem, 2002. **277**(41): p. 38029-38036.

240. Woo, H.A., et al., *Reversing the Inactivation of Peroxiredoxins Caused by Cysteine Sulfinic Acid Formation.* Science, 2003. **300**(5619): p. 653.

241. Rhee, S.G., *H2O2, a necessary evil for cell signaling.* Science, 2006. **312**(5782): p. 1882-3.

242. Wood, Z.A., L.B. Poole, and P.A. Karplus, *Peroxiredoxin Evolution and the Regulation of Hydrogen Peroxide Signaling.* Science, 2003. **300**(5619): p. 650.

243. Rabilloud, T., et al., *Proteomics Analysis of Cellular Response to Oxidative Stress EVIDENCE FOR IN VIVO OVEROXIDATION OF PEROXIREDOXINS AT THEIR ACTIVE SITE.* Journal of Biological Chemistry, 2002. **277**(22): p. 19396-19401.

244. Wagner, E., et al., *A method for detection of overoxidation of cysteines: peroxiredoxins are oxidized in vivo at the active-site cysteine during oxidative stress.* Biochem. J, 2002. **366**: p. 777-785.

245. Chang, T.-S., et al., *Regulation of peroxiredoxin I activity by Cdc2-mediated phosphorylation.* J Biol Chem, 2002. **277**(28): p. 25370-25376.

246. Lim, J.C., et al., *Irreversible oxidation of the active-site cysteine of peroxiredoxin to cysteine sulfonic acid for enhanced molecular chaperone activity.* Journal of Biological Chemistry, 2008. **283**(43): p. 28873-28880.

247. Hu, R.-G., et al., *The N-end rule pathway as a nitric oxide sensor controlling the levels of multiple regulators.* Nature, 2005. **437**(7061): p. 981-986.

248. Mishina, N.M., et al., *Does cellular hydrogen peroxide diffuse or act locally?* Antioxid. Redox Signal., 2011. **14**(1): p. 1-7.

249. Hilenski, L.L., et al., *Distinct subcellular localizations of Nox1 and Nox4 in vascular smooth muscle cells.* Arterioscler Thromb Vasc Biol, 2004. **24**(4): p. 677-83.

250. Ushio-Fukai, M., *Localizing NADPH oxidase-derived ROS.* Sci STKE, 2006. **2006**(349): p. re8.

251. Wu, R.F., et al., *Nox4-derived H2O2 mediates endoplasmic reticulum signaling through local Ras activation.* Mol Cell Biol, 2010. **30**(14): p. 3553-68.

252. Higdon, A., et al., *Cell signalling by reactive lipid species: new concepts and molecular mechanisms.* Biochemical Journal, 2012. **442**: p. 453-464.

253. van Stroe-Biezen, S., et al., *Diffusion coefficients of oxygen, hydrogen peroxide and glucose in a hydrogel.* Analytica chimica acta, 1993. **273**(1): p. 553-560.

254. Pelle, E., et al., *Keratinocytes act as a source of reactive oxygen species by transferring hydrogen peroxide to melanocytes.* Journal of investigative dermatology, 2005. **124**(4): p. 793-797.

255. Waghray, M., et al., *Hydrogen peroxide is a diffusible paracrine signal for the induction of epithelial cell death by activated myofibroblasts.* The FASEB journal, 2005. **19**(7): p. 854-856.

256. Antunes, F. and E. Cadenas, *Estimation of H2O2 gradients across biomembranes.* Febs Letters, 2000. **475**(2): p. 121-126.

257. Bienert, G.P., J.K. Schjoerring, and T.P. Jahn, *Membrane transport of hydrogen peroxide.* Biochimica et biophysica acta, 2006. **1758**: p. 994-1003.

258. Sousa-Lopes, A., et al., *Decreased cellular permeability to H2O2 protects Saccharomyces cerevisiae cells in stationary phase against oxidative stress.* Febs Letters, 2004. **578**(1-2): p. 152-156.

259. Mathai, J.C. and V. Sitaramam, *Stretch sensitivity of transmembrane mobility of hydrogen peroxide through voids in the bilayer. Role of cardiolipin.* Journal of Biological Chemistry, 1994. **269**(27): p. 17784-17793.

260. Mizoguchi, H. and S. Hara, *Effect of fatty acid saturation in membrane lipid bilayers on simple diffusion in the presence of ethanol at high concentrations.* Journal of fermentation and bioengineering, 1996. **81**(5): p. 406-411.

261. Sutherland, F., et al., *Characteristics of Fps1-dependent and-independent glycerol transport in Saccharomyces cerevisiae.* Journal of bacteriology, 1997. **179**(24): p. 7790-7795.

262. Rumyantseva, G., et al., *Permeation of liposome membrane by superoxide radical.* FEBS letters, 1979. **108**(2): p. 477-480.

263. Nicholls, P., *Activity of catalase in the red cell.* Biochimica Et Biophysica Acta, 1965. **99**: p. 286-297.

264. Lynch, R.E. and I. Fridovich, *Effects of superoxide on the erythrocyte membrane.* Journal Of Biological Chemistry, 1978. **253**(6): p. 1838-1845.

265. Takahashi, M.A. and K. Asada, *Superoxide anion permeability of phospholipid membranes and chloroplast thylakoids.* Archives Of Biochemistry And Biophysics, 1983. **226**(2): p. 558-566.

266. Branco, M.R., et al., *Decrease of H2O2 plasma membrane permeability during adaptation to H2O2 in Saccharomyces cerevisiae.* Journal Of Biological Chemistry, 2004. **279**(8): p. 6501-6506.

267. Lynch, R.E. and I. Fridovich, *Permeation of the erythrocyte stroma by superoxide radical.* Journal Of Biological Chemistry, 1978. **253**(13): p. 4697-4699.

268. Henzler, T. and E. Steudle, *Transport and metabolic degradation of hydrogen peroxide in Chara corallina: model calculations and measurements with the pressure probe suggest transport of H2O2 across water channels.* Journal of Experimental Botany, 2000. **51**(353): p. 2053-2066.

269. Bienert, G.P., et al., *Specific aquaporins facilitate the diffusion of hydrogen peroxide across membranes.* J Biol Chem, 2007. **282**(2): p. 1183-92.

270. Cadenas, E. and H. Sies, *Oxidative stress: excited oxygen species and enzyme activity.* Advances In Enzyme Regulation, 1985. **23**: p. 217-237.

271. Dynowski, M., et al., *Plant plasma membrane water channels conduct the signalling molecule H2O2.* Biochem J, 2008. **414**(1): p. 53-61.

272. Miller, E.W., B.C. Dickinson, and C.J. Chang, *Aquaporin-3 mediates hydrogen peroxide uptake to regulate downstream intracellular signaling.* Proceedings of the National Academy of Sciences, 2010. **107**.

273. Hara-Chikuma, M., et al., *Chemokine-dependent T cell migration requires aquaporin-3–mediated hydrogen peroxide uptake.* The Journal of experimental medicine, 2012. **209**(10): p. 1743-1752.

274. Buxton, G.V., et al., *Critical-review of rate constants for reactions of hydrated electrons, hydrogen-atoms and hydroxyl radicals (.OH/.O-) in aqueous-solution.* Journal of Physical and Chemical Reference Data, 1988. **17**(2): p. 513-886.

275. Roots, R. and S. Okada, *Estimation of life times and diffusion distances of radicals involved in x-ray-induced DNA strand breaks of killing of mammalian cells.* Radiat Res, 1975. **64**(2): p. 306-20.

276. Stein, G. and J. Weiss, *Chemical effects of ionizing radiations.* Nature, 1948. **161**(4095): p. 650.

277. Balashov, V.V., *Interaction of Particles and Radiation with Matter*. 1 ed. 1997, Moscow: Springer-Verlag Berlin Heidelberg.

278. McCormick, M.L., et al., *Eosinophil peroxidase-dependent hydroxyl radical generation by human eosinophils.* Journal of Biological Chemistry, 1994. **269**(45): p. 27914-27919.

279. Jomova, K. and M. Valko, *Advances in metal-induced oxidative stress and human disease.* Toxicology, 2011. **283**(2-3): p. 65-87.

280. Fenton, H., *LXXIII.—Oxidation of tartaric acid in presence of iron.* Journal of the Chemical Society, Transactions, 1894. **65**: p. 899-910.

281. Koppenol, W.H., *The Haber-Weiss cycle--70 years later.* Redox Rep, 2001. **6**(4): p. 229-34.

282. Koppenol, W., *Generation and thermodynamic properties of oxyradicals.* Focus on membrane lipid oxidation, 1989. **1**: p. 1-13.

283. Rigo, A., et al., *An attempt to evaluate the rate of the Haber-Weiss reaction by using OH radical scavengers.* FEBS Lett, 1977. **80**(1): p. 130-2.

284. Ferradini, C., et al., *The reaction between superoxide anion and hydrogen peroxide.* Photochemistry and Photobiology, 1978. **28**(4-5): p. 697-700.

285. Melhuish, W.H. and H.C. Sutton, *Study of the Haber–Weiss reaction using a sensitive method for detection of OH radicals.* Journal of the Chemical Society, Chemical Communications, 1978(22): p. 970-971.

286. Koppenol, W.H., *The centennial of the Fenton reaction.* Free Radic Biol Med, 1993. **15**(6): p. 645-51.

287. Borg, D.C., *Oxygen free radicals and tissue injury*, in *Oxygen free radicals in tissue damage*. 1993, Springer. p. 12-53.

288. Chen, S.X. and P. Schopfer, *Hydroxyl-radical production in physiological reactions. A novel function of peroxidase.* Eur J Biochem, 1999. **260**(3): p. 726-35.

289. Imlay, J.A., *Pathways of oxidative damage.* Annual Review Of Microbiology, 2003. **57**(1): p. 395-418.

290. Valko, M., H. Morris, and M.T. Cronin, *Metals, toxicity and oxidative stress.* Curr Med Chem, 2005. **12**(10): p. 1161-208.

291. Lemire, J.A., J.J. Harrison, and R.J. Turner, *Antimicrobial activity of metals: mechanisms, molecular targets and applications.* Nat Rev Microbiol, 2013. **11**(6): p. 371-84.

292. Pasternack, R.F. and W.R. Skowronek, Jr., *Catalysis of the disproportionation of superoxide by metalloporphyrins.* J Inorg Biochem, 1979. **11**(3): p. 261-7.

293. Bielski, B.H., et al., *Reactivity of HO2/O2 radicals in aqueous solution.* Journal of Physical and Chemical Reference Data, 1985. **14**(4): p. 1041-1100.

294. Imlay, J.A. and I. Fridovich, *Assay of metabolic superoxide production in Escherichia coli.* Journal Of Biological Chemistry, 1991. **266**(11): p. 6957-6965.

295. Winterbourn, C.C., *Comparison of superoxide with other reducing agents in the biological production of hydroxyl radicals.* Biochem J, 1979. **182**(2): p. 625-8.

296. Rowley, D.A. and B. Halliwell, *Superoxide-dependent formation of hydroxyl radicals in the presence of thiol compounds.* FEBS Lett, 1982. **138**(1): p. 33-6.

297. Rowley, D.A. and B. Halliwell, *Formation of hydroxyl radicals from hydrogen peroxide and iron salts by superoxide- and ascorbate-dependent mechanisms: relevance to the pathology of rheumatoid disease.* Clin Sci (Lond), 1983. **64**(6): p. 649-53.

298. Strlič, M., et al., *A comparative study of several transition metals in Fenton-like reaction systems at circum-neutral pH.* Acta Chim Slov, 2003. **50**(4): p. 619-632.

299. Stohs, S.J. and D. Bagchi, *Oxidative mechanisms in the toxicity of metal ions.* Free Radic Biol Med, 1995. **18**(2): p. 321-36.

300. Macomber, L., C. Rensing, and J.A. Imlay, *Intracellular copper does not catalyze the formation of oxidative DNA damage in Escherichia coli.* J Bacteriol, 2007. **189**(5): p. 1616-26.

301. Mello Filho, A.C. and R. Meneghini, *In vivo formation of single-strand breaks in DNA by hydrogen peroxide is mediated by the Haber-Weiss reaction.* Biochimica et Biophysica Acta (BBA)-Gene Structure and Expression, 1984. **781**(1): p. 56-63.

302. Rae, T.D., et al., *Undetectable intracellular free copper: the requirement of a copper chaperone for superoxide dismutase.* Science, 1999. **284**(5415): p. 805-808.

303. Woodmansee, A.N. and J.A. Imlay, *Reduced Flavins Promote Oxidative DNA Damage in Non-respiring Escherichia coli by Delivering Electrons to Intracellular Free Iron.* Journal Of Biological Chemistry, 2002. **277**(37): p. 34055-34066.

304. Park, S. and J.A. Imlay, *High levels of intracellular cysteine promote oxidative DNA damage by driving the Fenton reaction.* Journal Of Bacteriology, 2003. **185**(6): p. 1942-1950.

305. Rowley, D.A. and B. Halliwell, *Superoxide-dependent and ascorbate-dependent formation of hydroxyl radicals in the presence of copper salts: a physiologically significant reaction?* Arch Biochem Biophys, 1983. **225**(1): p. 279-84.

306. Walling, C., *Fenton's reagent revisited.* Accounts of chemical research, 1975. **8**(4): p. 125-131.

307. Keyer, K. and J.A. Imlay, *Superoxide accelerates DNA damage by elevating free-iron levels.* Proceedings Of The National Academy Of Sciences Of The United States Of America, 1996. **93**(24): p. 13635-13640.

308. Rush, J., Z. Maskos, and W. Koppenol, *Reactions of iron (II) nucleotide complexes with hydrogen peroxide.* FEBS letters, 1990. **261**(1): p. 121-123.

309. Gonzalez-Flecha, B. and B. Demple, *Homeostatic regulation of intracellular hydrogen peroxide concentration in aerobically growing Escherichia coli.* Journal of Bacteriology, 1997. **179**: p. 382-388.

310. Park, S., X.J. You, and J.A. Imlay, *Substantial DNA damage from submicromolar intracellular hydrogen peroxide detected in Hpx(-) mutants of Escherichia coli.* Proceedings Of The National Academy Of Sciences Of The United States Of America, 2005. **102**(26): p. 9317-9322.

311. Faulkner, M.J. and J.D. Helmann, *Peroxide stress elicits adaptive changes in bacterial metal ion homeostasis.* Antioxid Redox Signal, 2011. **15**(1): p. 175-89.

312. Simic, M.G., *Pulse radiolysis in study of oxygen radicals.* Methods Enzymol, 1990. **186**: p. 89-100.

313. Getoff, N. and G. Schenck, *Primary products of liquid water photolysis at 1236, 1470 and 1849 Å.* Photochemistry and Photobiology, 1968. **8**(3): p. 167-178.

314. Elliot, A., *Rate constants and g-values for the simulation of the radiolysis of light water over the range 0-300 deg C*. 1994, Atomic Energy of Canada Ltd., Chalk River, ON (Canada). Chalk River Nuclear Labs.

315. Bolton, J.R., S.J. Strickler, and J.S. Connolly, *Limiting and realizable ef ciencies of solar photolysis of water.* Nature, 1985. **316**: p. 495.

316. Ito, T. and K. Kobayashi, *Induction of lethal and genetic damage by vacuum-ultraviolet (163 nm) irradiation of aqueous suspensions of yeast cells.* Radiat Res, 1976. **68**(2): p. 275-83.

317. Davies, M.J. and R.T. Dean, *Radical-mediated protein oxidation: from chemistry to medicine*. Oxford science publications. 1997, Oxford ; New York: Oxford University Press. xii, 443 p.

318. Cox, R.A., R.G. Derwent, and M.R. Williams, *Atmospheric photooxidation reactions. Rates, reactivity, and mechanism for reaction of organic compounds with hydroxyl radicals.* Environmental Science & Technology, 1980. **14**(1): p. 57-61.

319. Pignatello, J.J., E. Oliveros, and A. MacKay, *Advanced oxidation processes for organic contaminant destruction based on the Fenton*

reaction and related chemistry. Critical reviews in environmental science and technology, 2006. **36**(1): p. 1-84.

320. Moise, T., et al., *Multiphase decomposition of novel oxygenated organics in aqueous and organic media.* Environ Sci Technol, 2005. **39**(14): p. 5203-8.

321. Gilbert, B., et al., *Electron spin resonance studies. Part L. Reactions of alkoxyl radicals generated from hydroperoxides and titanium-(III) ion in aqueous solution.* J. Chem. Soc., Perkin Trans, 1976. **2**: p. 1047-1052.

322. Gilbert, B.C., et al., *Electron spin resonance studies. Part 61. The generation and reactions of the t-butoxyl radical in aqueous solution.* Journal of the Chemical Society, Perkin Transactions 2, 1981(10): p. 1392-1400.

323. Bartlett, P.D. and G. Guaraldi, *Di-tert-butyl trioxide and di-tert-butyl tertoxide.* Journal of the American Chemical Society, 1967. **89**(18): p. 4799-4801.

324. Bennett, J.E., *Kinetic electron paramagnetic resonance study of the reactions of t-butylperoxyl radicals in aqueous solution.* J. Chem. Soc., Faraday Trans., 1990. **86**(19): p. 3247-3252.

325. Hawkins, C.L. and M.J. Davies, *Hypochlorite-induced damage to proteins: formation of nitrogen-centred radicals from lysine residues and their role in protein fragmentation.* Biochem J, 1998. **332 (Pt 3)**: p. 617-25.

326. Dizdaroglu, M. and M.G. Simic, *Hydroxycyclohexadienyl peroxy radicals*, in *Oxygen and oxy-radicals in chemistry and biology*, M.A.J. Rodgers and E.L. Powers, Editors. 1981, Academic Press: New York. p. 619-621.

327. Konermann, L., X. Tong, and Y. Pan, *Protein structure and dynamics studied by mass spectrometry: H/D exchange, hydroxyl radical labeling, and related approaches.* J Mass Spectrom, 2008. **43**(8): p. 1021-36.

328. Nukuna, B.N., G. Sun, and V.E. Anderson, *Hydroxyl radical oxidation of cytochrome c by aerobic radiolysis.* Free Radic Biol Med, 2004. **37**(8): p. 1203-13.

329. Sharp, J.S., J.M. Becker, and R.L. Hettich, *Analysis of protein solvent accessible surfaces by photochemical oxidation and mass spectrometry.* Anal Chem, 2004. **76**(3): p. 672-83.

330. Hambly, D.M. and M.L. Gross, *Laser flash photolysis of hydrogen peroxide to oxidize protein solvent-accessible residues on the microsecond timescale.* J Am Soc Mass Spectrom, 2005. **16**(12): p. 2057-63.

331. McClintock, C., V. Kertesz, and R.L. Hettich, *Development of an electrochemical oxidation method for probing higher order protein structure with mass spectrometry.* Anal Chem, 2008. **80**(9): p. 3304-17.

332. Sharma, V.K., *Oxidation of Amino Acids, Peptides, and Proteins: Kinetics and Mechanism*. Wiley series on reactive intermediates in chemistry and biology, ed. S.E. Rokita. 2013, NJ: John Wiley & Sons, Inc., Hoboken,. 126-180.

333. Wang, L. and M.R. Chance, *Structural mass spectrometry of proteins using hydroxyl radical based protein footprinting.* Anal Chem, 2011. **83**(19): p. 7234-41.

334. Heijman, M., et al., *A pulse radiolysis study of the reactions of OH/O with linoleic acid in oxygen-free aqueous solution.* Radiation Physics and Chemistry (1977), 1985. **26**(1): p. 83-88.

335. Boss, A., *NDRL/NIST solution kinetics database*. 1994: US Department of Commerce. Technology Administration. National Institute of Standards and Technology. Standard Reference Data Program.

336. Steenken, S., *Structure, acid/base properties and transformation reactions of purine radicals.* Free Radic Res Commun, 1989. **6**(2-3): p. 117-20.

337. Cadet, J. and J.R. Wagner, *Oxidatively generated base damage to cellular DNA by hydroxyl radical and one-electron oxidants: similarities and differences.* Arch Biochem Biophys, 2014. **557**: p. 47-54.

338. Linley, E., et al., *Use of hydrogen peroxide as a biocide: new consideration of its mechanisms of biocidal action.* J Antimicrob Chemother, 2012. **67**(7): p. 1589-96.

339. Touati, D., et al., *Lethal oxidative damage and mutagenesis are generated by iron in delta fur mutants of Escherichia coli: protective role of superoxide dismutase.* J Bacteriol, 1995. **177**(9): p. 2305-14.

340. Hoffmann, M.E., A.C. Mello-Filho, and R. Meneghini, *Correlation between cytotoxic effect of hydrogen peroxide and the yield of DNA strand breaks in cells of different species.* Biochim Biophys Acta, 1984. **781**(3): p. 234-8.

341. Halliwell, B. and J.M. Gutteridge, *Iron and free radical reactions: two aspects of antioxidant protection.* Trends in biochemical Sciences, 1986. **11**(9): p. 372-375.

342. Buettner, G.R., *The pecking order of free radicals and antioxidants: lipid peroxidation, alpha-tocopherol, and ascorbate.* Archives Of Biochemistry And Biophysics, 1993. **300**(2): p. 535-543.

343. Esterbauer, H., *Lipid peroxidation products: formation, chemical properties and biological activities*, in *Free radicals in liver injury*, G. Poli, et al., Editors. 1985, IRL Press: Oxford, England. p. 29-47.

344. Nigam, S. and T. Schewe, *Phospholipase A(2)s and lipid peroxidation.* Biochim Biophys Acta, 2000. **1488**(1-2): p. 167-81.

345. Green, D.R. and J.C. Reed, *Mitochondria and apoptosis.* Science, 1998. **281**(5381): p. 1309-12.

346. Simic, M., P. Neta, and E. Hayon, *Selectivity in the reactions of eaq-and OH radicals with simple peptides in aqueous solution. Optical absorption spectra of intermediates.* J Am Chem Soc, 1970. **92**(16): p. 4763-8.

347. Scholes, G., P. Shaw, and R. Willson, *Pulse radiolysis studies of aqueous solutions of nucleic acid*, in *Pulse Radiolysis*, M. Ebert, et al., Editors. 1965, Academic Press: New York. p. 151.

348. Scholes, G. and R. Willson, *γ-Radiolysis of aqueous thymine solutions. Determination of relative reaction rates of OH radicals.* Transactions of the Faraday Society, 1967. **63**: p. 2983-2993.

349. Adams, G.E., et al., *The pulse radiolysis of aqueous solutions of thiocyanate ion*, in *Pulse Radiolysis*, M. Ebert, et al., Editors. 1965, Academic Press: New York. p. 151.

350. Kraljic, I., *Kinetics of OH radical reactions in radiolysis, photolysis, and the Fenton system*, in *The Chemistry of Ionization and Excitation*, G.R.A. Johnson and G. Scholes, Editors. 1967, Taylor and Francis, Ltd: London. p. 303.

351. Morgan, P.E., D.I. Pattison, and M.J. Davies, *Quantification of hydroxyl radical-derived oxidation products in peptides containing glycine, alanine, valine, and proline.* Free Radic Biol Med, 2012. **52**(2): p. 328-39.

352. Swallow, A.J., *Effect of ionizing radiation on proteins, RCO groups, peptide bond cleavage, inactivation, -SH oxidation*, in *Radiation chemistry of organic compounds*, A.J. Swallow, Editor. 1960, Pergamon Press: New York. p. 211-224.

353. Prutz, W.A., et al., *The role of sulphur peptide functions in free radical transfer: a pulse radiolysis study.* Int J Radiat Biol, 1989. **55**(4): p. 539-56.

354. Lal, M., *Radiation induced oxidation of sulphydryl molecules in aqueous solutions. A comprehensive review.* Radiation Physics and Chemistry, 1994. **43**(6): p. 595-611.

355. Maleknia, S.D., M. Brenowitz, and M.R. Chance, *Millisecond radiolytic modification of peptides by synchrotron X-rays identified by mass spectrometry.* Analytical Chemistry, 1999. **71**(18): p. 3965-3973.

356. Shetty, V. and T.A. Neubert, *Characterization of novel oxidation products of cysteine in an active site motif peptide of PTP1B.* J Am Soc Mass Spectrom, 2009. **20**(8): p. 1540-8.

357. Boguta, G. and A.M. Dancewicz, *Radiation-induced dimerization of tyrosine and glycyltyrosine in aqueous solutions.* International Journal of Radiation Biology, 1981. **39**(2): p. 163-174.

358. Wheeler, O.H. and R. Montalvo, *Radiolysis of phenylalanine and tyrosine and aqueous solution.* Radiat Res, 1969. **40**(1): p. 1-10.

359. Winchester, R. and K. Lynn, *X-and γ-radiolysis of some tryptophan dipeptides.* International Journal of Radiation Biology, 1970. **17**(6): p. 541-548.

360. Josimović, L., I. Janković, and S. Jovanović, *Radiation induced decomposition of tryptophan in the presence of oxygen.* Radiation Physics and Chemistry, 1993. **41**(6): p. 835-841.

361. Tajima, M., M. Morita, and M. Fujimaki, *Radiation Chemistry of Foods: Part III. Radiolysis of Sulfur-Containing Amino Acids in Aqueous Glucose Solution.* Agricultural and Biological Chemistry, 1969. **33**(9): p. 1277-1281.

362. Hiller, K., et al., *Mechanism of the hydroxyl radical induced oxidation of methionine in aqueous solution.* Journal of the American Chemical Society, 1981. **103**(10): p. 2734-2743.

363. Dean, R.T., S.P. Wolff, and M.A. McElligott, *Histidine and proline are important sites of free radical damage to proteins.* Free Radical Research, 1989. **7**(2): p. 97-103.

364. Tomita, M., M. Irie, and T. Ukita, *Sensitized photooxidation of histidine and its derivatives. Products and mechanism of the reaction.* Biochemistry, 1969. **8**(12): p. 5149-60.

365. Uchida, K. and S. Kawakishi, *Selective oxidation of imidazole ring in histidine residues by the ascorbic acid—copper ion system.* Biochemical and biophysical research communications, 1986. **138**(2): p. 659-665.

366. Uchida, K., Y. Kato, and S. Kawakishi, *A novel mechanism for oxidative cleavage of prolyl peptides induced by the hydroxyl radical.* Biochemical and biophysical research communications, 1990. **169**(1): p. 265-271.

367. Kato, Y., K. Uchida, and S. Kawakishi, *Oxidative fragmentation of collagen and prolyl peptide by Cu(II)/H2O2. Conversion of proline residue to 2-pyrrolidone.* J Biol Chem, 1992. **267**(33): p. 23646-51.

368. Tong, X., J.C. Wren, and L. Konermann, *gamma-Ray-mediated oxidative labeling for detecting protein conformational changes by electrospray mass spectrometry.* Anal Chem, 2008. **80**(6): p. 2222-31.

369. Easton, C.J., *Advances in Detailed Reaction Mechanisms*. Vol. 1. 1991, Greenwich, CT: Jai Press, Inc.

370. Elad, D. and J. Sperling, *Photochemical modification of glycine-containing polypeptides.* Journal of the American Chemical Society, 1971. **93**(4): p. 967-971.

371. Garrison, W.M., W. Bennett, and M.E. Jayko, *Radiation-induced oxidation of protein in aqueous solution.* Radiation Research, 1962. **16**(4): p. 483-502.

372. Welle, F.M., H.-D. Beckhaus, and C. Rüchardt, *Thermochemical stability of α-amino-α-carbonylmethyl radicals and their resonance as measured by ESR.* The Journal of organic chemistry, 1997. **62**(3): p. 552-558.

373. Livingston, R., D.G. Doherty, and H. Zeldes, *Electron spin resonance study of liquids during photolysis. XIX. Aliphatic dipeptides.* J Am Chem Soc, 1975. **97**(11): p. 3198-3204.

374. Goshe, M.B., Y.H. Chen, and V.E. Anderson, *Identification of the sites of hydroxyl radical reaction with peptides by hydrogen/deuterium exchange: prevalence of reactions with the side chains.* Biochemistry, 2000. **39**(7): p. 1761-70.

375. Schuessler, H. and K. Schilling, *Oxygen effect in the radiolysis of proteins. Part 2. Bovine serum albumin.* Int J Radiat Biol Relat Stud Phys Chem Med, 1984. **45**(3): p. 267-81.

376. Neta, P., R.E. Huie, and A.B. Ross, *Rate constants for reactions of peroxyl radicals in fluid solutions.* Journal of Physical and Chemical Reference Data, 1990. **19**(2): p. 413-513.

377. Berlett, B.S. and E.R. Stadtman, *Protein oxidation in aging, disease, and oxidative stress.* Journal Of Biological Chemistry, 1997. **272**(33): p. 20313-20316.

378. Stadtman, E.R. and R.L. Levine, *Free radical-mediated oxidation of free amino acids and amino acid residues in proteins.* Amino Acids, 2003. **25**(3-4): p. 207-18.

379. Headlam, H.A. and M.J. Davies, *Beta-scission of side-chain alkoxyl radicals on peptides and proteins results in the loss of side-chains as aldehydes and ketones.* Free Radic Biol Med, 2002. **32**(11): p. 1171-84.

380. Karam, L.R., M. Dizdaroglu, and M.G. Simic, *OH radical-induced products of tyrosine peptides.* Int J Radiat Biol Relat Stud Phys Chem Med, 1984. **46**(6): p. 715-24.

381. Simic, M.G., E. Gajewski, and M. Dizdaroglu, *Kinetics and mechanisms of hydroxyl radical-induced crosslinks between phenylalanine peptides.* Radiation Physics and Chemistry (1977), 1984. **24**(5): p. 465-473.

382. Behrens, G. and G. Koltzenburg, *Elimination of Ammonium Ion from the a-Hydroxyalkyl Radicals of Serine and Threonine in Aqueous Solution and the Difference in the Reaction Mechanism.* Zeitschrift für Naturforschung C, 1985. **40**(11-12): p. 785-797.

383. Russell, G.A., *Deuterium-isotope Effects in the Autoxidation of Aralkyl Hydrocarbons. Mechanism of the Interaction of PEroxy Radicals1.* Journal of the American Chemical Society, 1957. **79**(14): p. 3871-3877.

384. Guan, J.-Q., S.C. Almo, and M.R. Chance, *Synchrotron radiolysis and mass spectrometry: a new approach to research on the actin cytoskeleton.* Accounts of chemical research, 2004. **37**(4): p. 221-229.

385. Kiselar, J.G., et al., *Hydroxyl radical probe of protein surfaces using synchrotron X-ray radiolysis and mass spectrometry.* International Journal Of Radiation Biology, 2002. **78**(2): p. 101-114.

386. Xu, G.Z. and M.R. Chance, *Radiolytic modification and reactivity of amino acid residues serving as structural probes for protein footprinting.* Analytical Chemistry, 2005. **77**(14): p. 4549-4555.

387. Barton, J. and J. Packer, *The radiolysis of oxygenated cysteine solutions at neutral pH. The role of RSSR and O 2 .* International Journal for Radiation Physics and Chemistry, 1970. **2**(3): p. 159-166.

388. Wardman, P. and C. von Sonntag, *Kinetic factors that control the fate of thiyl radicals in cells.* Methods Enzymol, 1995. **251**: p. 31-45.

389. Purdie, J., *Investigation of chain reactions and oxygen effects during radiolysis of peptide disulfide bonds using cysteine-glutathione disulfide as a model.* Radiation research, 1971. **48**(3): p. 474-483.

390. Owen, T.C. and A.C. Wilbraham, *Radiation chemistry of biochemical disulfides. II. Lipoic acid.* Journal of the American Chemical Society, 1969. **91**(12): p. 3365-3371.

391. Fahey, R.C., *Biologically important thiol-disulfide reactions and the role of cyst (e) ine in proteins: an evolutionary perspective*, in *Protein Crosslinking*. 1977, Springer. p. 1-30.

392. Ziegler, D., *Role of reversible oxidation-reduction of enzyme thiols-disulfides in metabolic regulation.* Annual review of biochemistry, 1985. **54**(1): p. 305-329.

393. Hwang, C., A.J. Sinskey, and H.F. Lodish, *Oxidized redox state of glutathione in the endoplasmic reticulum.* Science, 1992. **257**(5076): p. 1496-1502.

394. Jones, D.P., et al., *Cysteine/cystine couple is a newly recognized node in the circuitry for biologic redox signaling and control.* The FASEB journal, 2004. **18**(11): p. 1246-1248.

395. Valko, M., et al., *Free radicals, metals and antioxidants in oxidative stress-induced cancer.* Chem Biol Interact, 2006. **160**(1): p. 1-40.

396. Valko, M., et al., *Free radicals and antioxidants in normal physiological functions and human disease.* Int J Biochem Cell Biol, 2007. **39**(1): p. 44-84.

397. Francisco-Marquez, M. and A. Galano, *Role of the sulfur atom on the reactivity of methionine toward OH radicals: comparison with norleucine.* J Phys Chem B, 2009. **113**(14): p. 4947-52.

398. Lu, C., S. Yao, and N. Lin, *Studies on reactions of oxidizing sulfur–sulfur three-electron-bond complexes and reducing α-amino radicals derived from OH reaction with methionine in aqueous solution.* Biochimica et Biophysica Acta (BBA)-General Subjects, 2001. **1525**(1): p. 89-96.

399. Ray Jr, W., et al., *Evidence for involvement of a methionine residue in the enzymatic action of phosphoglucomutase and chymotrypsin.* Journal of the American Chemical Society, 1960. **82**(17): p. 4743-4744.

400. Wolff, J., et al., *Calmodulin activates prokaryotic adenylate cyclase.* Proceedings of the National Academy of Sciences, 1980. **77**(7): p. 3841-3844.

401. Levine, R.L., et al., *Methionine residues as endogenous antioxidants in proteins.* Proceedings Of The National Academy Of Sciences Of The United States Of America, 1996. **93**(26): p. 15036-15040.

402. Shao, B., et al., *Methionine Sulfoxide and Proteolytic Cleavage Contribute to the Inactivation of Cathepsin G by Hypochlorous Acid AN OXIDATIVE MECHANISM FOR REGULATION OF SERINE PROTEINASES BY MYELOPEROXIDASE.* Journal of Biological Chemistry, 2005. **280**(32): p. 29311-29321.

403. Moskovitz, J., H. Weissbach, and N. Brot, *Cloning the expression of a mammalian gene involved in the reduction of methionine sulfoxide residues in proteins.* Proceedings of the National Academy of Sciences, 1996. **93**(5): p. 2095-2099.

404. Moskovitz, J., et al., *Purification and characterization of methionine sulfoxide reductases from mouse and Staphylococcus aureus and their substrate stereospecificity.* Biochemical and biophysical research communications, 2002. **290**(1): p. 62-65.

405. Xu, G. and M.R. Chance, *Radiolytic modification of sulfur-containing amino acid residues in model peptides: fundamental studies for protein footprinting.* Anal Chem, 2005. **77**(8): p. 2437-49.

406. Davies, M.J., et al., *Stable markers of oxidant damage to proteins and their application in the study of human disease.* Free Radic Biol Med, 1999. **27**(11-12): p. 1151-63.

407. Morin, B., M.J. Davies, and R.T. Dean, *The protein oxidation product 3,4-dihydroxyphenylalanine (DOPA) mediates oxidative DNA damage.* Biochem J, 1998. **330 (Pt 3)**: p. 1059-67.

408. Hunter, E.P., M.F. Desrosiers, and M.G. Simic, *The effect of oxygen, antioxidants, and superoxide radical on tyrosine phenoxyl radical dimerization.* Free Radical Biology and Medicine, 1989. **6**(6): p. 581-585.

409. Heinecke, J.W., et al., *Tyrosyl radical generated by myeloperoxidase catalyzes the oxidative cross-linking of proteins.* Journal of Clinical Investigation, 1993. **91**(6): p. 2866.

410. Irwin, J.A., H. Østdal, and M.J. Davies, *Myoglobin-induced oxidative damage: evidence for radical transfer from oxidized myoglobin to other proteins and antioxidants.* Archives of biochemistry and biophysics, 1999. **362**(1): p. 94-104.

411. Savenkova, M., D.M. Mueller, and J.W. Heinecke, *Tyrosyl radical generated by myeloperoxidase is a physiological catalyst for the initiation of lipid peroxidation in low density lipoprotein.* Journal of Biological Chemistry, 1994. **269**(32): p. 20394-20400.

412. Armstrong, R. and A. Swallow, *Pulse-and gamma-radiolysis of aqueous solutions of tryptophan.* Radiation research, 1969. **40**(3): p. 563-579.

413. Østdal, H., H.J. Andersen, and M.J. Davies, *Formation of long-lived radicals on proteins by radical transfer from heme enzymes—a common process?* Archives of biochemistry and biophysics, 1999. **362**(1): p. 105-112.

414. Kiselar, J.G., et al., *Visualizing Arp2/3 complex activation mediated by binding of ATP and WASp using structural mass spectrometry.* Proceedings of the National Academy of Sciences, 2007. **104**(5): p. 1552-1557.

415. Samunl, A. and P. Neta, *Electron spin resonance study of the reaction of hydroxyl radicals with pyrrole, imidazole, and related compounds.* The Journal of Physical Chemistry, 1973. **77**(13): p. 1629-1635.

416. Bansal, K. and R. Sellers, *Polarographic and optical pulse radiolysis study of the radicals formed by hydroxyl radical attack on imidazole and related compounds in aqueous solutions.* The Journal of Physical Chemistry, 1975. **79**(17): p. 1775-1780.

417. Stadtman, E.R., *Metal ion-catalyzed oxidation of proteins: biochemical mechanism and biological consequences.* Free Radic Biol Med, 1990. **9**(4): p. 315-25.

418. Burgess, A.W., P. Ponnuswamy, and H. Scheraga, *Analysis of conformations of amino acid residues and prediction of backbone topography in proteins.* Israel Journal of Chemistry, 1974. **12**(1-2): p. 239-286.

419. Zimmerman, S.S. and H.A. Scheraga, *Influence of local interactions on protein structure. I. Conformational energy studies of N-acetyl-N'-methylamides of Pro-X and X-Pro dipeptides.* Biopolymers, 1977. **16**(4): p. 811-43.

420. Headlam, H.A., et al., *beta-Scission of C-3 (beta-carbon) alkoxyl radicals on peptides and proteins: a novel pathway which results in the formation of alpha-carbon radicals and the loss of amino acid side chains.* Chem Res Toxicol, 2000. **13**(11): p. 1087-95.

421. Halliwell, B., *Protection against tissue damage in vivo by desferrioxamine: what is its mechanism of action?* Free Radic Biol Med, 1989. **7**(6): p. 645-51.

422. Shang, F. and A. Taylor, *Ubiquitin–proteasome pathway and cellular responses to oxidative stress.* Free Radical Biology and Medicine, 2011. **51**(1): p. 5-16.

423. Jamieson, D.J. and G. Storz, *Transcriptional regulators of oxidative stress responses.* Cold Spring Harbor Monograph Archive, 1997. **34**: p. 91-115.

424. Gaballa, A. and J.D. Helmann, *A peroxide-induced zinc uptake system plays an important role in protection against oxidative stress in Bacillus subtilis.* Molecular microbiology, 2002. **45**(4): p. 997-1005.

425. Cohen, G. and P. Hochstein, *Glutathione Peroxidase: The Primary Agent for the Elimination of Hydrogen Peroxide in Erythrocytes.* Biochemistry, 1963. **2**(6): p. 1420-1428.

426. Mills, G.C., *Hemoglobin catabolism I. Glutathione peroxidase, an erythrocyte enzyme which protects hemoglobin from oxidative breakdown.* Journal Of Biological Chemistry, 1957. **229**(1): p. 189-197.

427. Moore, R.B., G.A. Plishker, and S.K. Shriver, *Purification and measurement of calpromotin, the cytoplasmic protein which activates calcium-dependent potassium transport.* Biochemical and Biophysical Research Communications, 1990. **166**(1): p. 146-153.

428. Moore, R.B., et al., *Reconstitution of Ca^{2+}-dependent K^{+} transport in erythrocyte-membrane vesicles requires a cytoplasmic protein.* Journal Of Biological Chemistry, 1991. **266**(28): p. 18964-18968.

429. Mishra, S. and J. Imlay, *Why do bacteria use so many enzymes to scavenge hydrogen peroxide?* Archives of biochemistry and biophysics, 2012. **525**(2): p. 145-160.

430. Dietz, K., *Thiol-Based Peroxidases and Ascorbate Peroxidases: Why Plants Rely on Multiple Peroxidase Systems in the Photosynthesizing Chloroplast?* Molecules and cells, 2016.

431. Gaetani, G.F., et al., *Predominant role of catalase in the disposal of hydrogen peroxide within human erythrocytes.* Blood, 1996. **87**(4): p. 1595-1599.

432. Johnson, R.M., et al., *Oxidation of glutathione peroxidase-deficient red cells by organic peroxides.* Blood, 2002. **100**: p. 1515-1516.

433. Seaver, L.C. and J.A. Imlay, *Alkyl hydroperoxide reductase is the primary scavenger of endogenous hydrogen peroxide in Escherichia coli.* Journal of Bacteriology, 2001. **183**(24): p. 7173-7181.

434. Imlay, J.A., *The molecular mechanisms and physiological consequences of oxidative stress: lessons from a model bacterium.* Nat Rev Micro, 2013. **11**(7): p. 443-454.

435. Ursini, F., et al., *Diversity of glutathione peroxidases.* Methods In Enzymology, 1995. **252**: p. 38-53.

436. Flohé, L. and F. Ursini, *Peroxidase: a term of many meanings.* Antioxidants & redox signaling, 2008. **10**(9): p. 1485-1490.

437. Flohe, L., et al., *A Comparison of Thiol Peroxidase Mechanisms.* Antioxidants & Redox Signaling, 2011. **15**(3): p. 763-780.

438. Hondal, R.J., S.M. Marino, and V.N. Gladyshev, *Selenocysteine in thiol/disulfide-like exchange reactions.* Antioxid. Redox Signal., 2013. **18**(13): p. 1675-1689.

439. Chelikani, P., I. Fita, and P.C. Loewen, *Diversity of structures and properties among catalases.* Cellular and Molecular Life Sciences, 2004. **61**(2): p. 192-208.

440. Zamocky, M., P.G. Furtmuller, and C. Obinger, *Evolution of catalases from bacteria to humans.* Antioxidants & Redox Signaling, 2008. **10**(9): p. 1527-1547.

441. Goldberg, I. and A. Hochman, *Three different types of catalases in Klebsiella pneumoniae.* Archives of biochemistry and biophysics, 1989. **268**(1): p. 124-128.

442. Goldberg, I. and A. Hochman, *Purification and characterization of a novel type of catalase from the bacterium Klebsiella pneumoniae.* Biochimica et Biophysica Acta (BBA)-General Subjects, 1989. **991**(2): p. 330-336.

443. Zamocky, M. and F. Koller, *Understanding the structure and function of catalases: clues from molecular evolution and in vitro mutagenesis.* Progress In Biophysics & Molecular Biology, 1999. **72**(1): p. 19-66.

444. Kalko, S.G., et al., *Theoretical study of the mechanisms of substrate recognition by catalase.* Journal of the American Chemical Society, 2001. **123**(39): p. 9665-9672.

445. Amara, P., et al., *Ligand diffusion in the catalase from Proteus mirabilis: A molecular dynamics study.* Protein Science, 2001. **10**(10): p. 1927-1935.

446. Carpena, X., et al., *Structure of the clade 1 catalase, CatF of Pseudomonas syringae, at 1.8 Å resolution.* Proteins: structure, function, and bioinformatics, 2003. **50**(3): p. 423-436.

447. Kono, Y. and I. Fridovich, *Isolation and characterization of the pseudocatalase of Lactobacillus plantarum.* Journal of Biological Chemistry, 1983. **258**(10): p. 6015-6019.

448. Allgood, G. and J. Perry, *Characterization of a manganese-containing catalase from the obligate thermophile Thermoleophilum album.* Journal of bacteriology, 1986. **168**(2): p. 563-567.

449. Passardi, F., et al., *PeroxiBase: the peroxidase database.* Phytochemistry, 2007. **68**(12): p. 1605-1611.

450. Hillar, A., et al., *Modulation of the activities of catalase-peroxidase HPI of Escherichia coli by site-directed mutagenesis.* Biochemistry, 2000. **39**: p. 5868-5875.

451. Amo, T., H. Atomi, and T. Imanaka, *Unique presence of a manganese catalase in a hyperthermophilic archaeon, Pyrobaculum calidifontis VA1.* Journal of bacteriology, 2002. **184**(12): p. 3305-3312.

452. Loewen, P.C. and J. Switala, *Purification and characterization of spore-specific catalase-2 from Bacillus subtilis.* Biochemistry and Cell Biology, 1988. **66**(7): p. 707-714.

453. Engelmann, S., C. Lindner, and M. Hecker, *Cloning, nucleotide sequence, and regulation of katE encoding a sigma B-dependent catalase in Bacillus subtilis.* Journal of bacteriology, 1995. **177**(19): p. 5598-5605.

454. Hahn, J.-S., et al., *H2O2-sensitive fur-like repressor CatR regulating the major catalase gene in Streptomyces coelicolor.* Journal of Biological Chemistry, 2000. **275**(49): p. 38254-38260.

455. Bol, D.K. and R.E. Yasbin, *Analysis of the dual regulatory mechanisms controlling expression of the vegetative catalase gene of Bacillus subtilis.* Journal of bacteriology, 1994. **176**(21): p. 6744-6748.

456. Bsat, N., et al., *Bacillus subtilis contains multiple Fur homologues: identification of the iron uptake (Fur) and peroxide regulon (PerR) repressors.* Molecular microbiology, 1998. **29**(1): p. 189-198.

457. Robbe-Saule, V., et al., *Identification of a non-haem catalase in Salmonella and its regulation by RpoS (σS).* Molecular microbiology, 2001. **39**(6): p. 1533-1545.

458. Martin, J.E. and J.A. Imlay, *The alternative aerobic ribonucleotide reductase of Escherichia coli, NrdEF, is a manganese-dependent enzyme that enables cell replication during periods of iron starvation.* Molecular microbiology, 2011. **80**(2): p. 319-334.

459. Whittaker, J.W., *Non-heme manganese catalase–the 'other'catalase.* Archives of biochemistry and biophysics, 2012. **525**(2): p. 111-120.

460. Heck, D.E., et al., *UVB Light Stimulates Production of Reactive Oxygen Species UNEXPECTED ROLE FOR CATALASE.* Journal of Biological Chemistry, 2003. **278**(25): p. 22432-22436.

461. De Duve, C., H. Beaufay, and P. Baudhuin, *Intracellular localization of catalase in rat liver.* Acta Chem. Scand, 1963. **17**: p. S210-S215.

462. Schrader, M. and H.D. Fahimi, *Peroxisomes and oxidative stress.* Biochimica et Biophysica Acta (BBA)-Molecular Cell Research, 2006. **1763**(12): p. 1755-1766.

463. Ballinger, C.A., et al., *Changes in the localization of catalase during differentiation of neutrophilic granulocytes.* Blood, 1994. **83**(9): p. 2654-2668.

464. Klotz, M.G., G.R. Klassen, and P.C. Loewen, *Phylogenetic relationships among prokaryotic and eukaryotic catalases.* Molecular biology and evolution, 1997. **14**(9): p. 951-958.

465. Zámocký, M., et al., *Molecular evolution of hydrogen peroxide degrading enzymes.* Archives of biochemistry and biophysics, 2012. **525**(2): p. 131-144.

466. Rasmussen, B., et al., *Reassessing the first appearance of eukaryotes and cyanobacteria.* Nature, 2008. **455**(7216): p. 1101-1104.

467. Bernroitner, M., et al., *Occurrence, phylogeny, structure, and function of catalases and peroxidases in cyanobacteria.* Journal of experimental botany, 2009: p. ern309.

468. Drews, G., et al., *Bioenergetic Processes of Cyanobacteria.* GA Peschek, C. Obinger, & G. Renger, Bioenergetic Processes of Cyanobacteria, 2011: p. 265-284.

469. Peschek, G.A., C. Obinger, and G. Renger, *Bioenergetic processes of Cyanobacteria*. 2011: Springer.

470. Díaz, A., et al., *Thirty years of heme catalases structural biology.* Archives of Biochemistry and Biophysics, 2012. **525**: p. 102-110.

471. Nicholls, P., *Classical catalase: ancient and modern.* Archives of biochemistry and biophysics, 2012. **525**(2): p. 95-101.

472. Dolphin, D., et al., *Compounds I of catalase and horse radish peroxidase: π-cation radicals.* Proceedings of the National Academy of Sciences, 1971. **68**(3): p. 614-618.

473. Chance, B., *The primary and secondary compounds of catalase and methyl or ethyl hydrogen peroxide; reactions with hydrogen peroxide. 2. Kinetics and activity.* Journal of Biological Chemistry, 1949. **179**(3): p. 1341-1369.

474. Nicholls, P., *The formation and catalytic role of catalase peroxide compound II.* Biochimica et Biophysica Acta (BBA) - Specialized Section on Enzymological Subjects, 1964. **81**(3): p. 479-495.

475. Johnson, R.M., et al., *Hemoglobin autoxidation and regulation of endogenous H2O2 levels in erythrocytes.* Free Radic Biol Med, 2005. **39**(11): p. 1407-1417.

476. Hillar, a. and P. Nicholls, *A mechanism for NADPH inhibition of catalase compound II formation.* FEBS Letters, 1992. **314**: p. 179-182.

477. Hillar, A., et al., *NADPH binding and control of catalase compound II formation: comparison of bovine, yeast, and Escherichia coli enzymes.* The Biochemical journal, 1994. **300 (Pt 2**: p. 531-539.

478. Kirkman, H.N., S. Galiano, and G.F. Gaetani, *The function of catalase-bound NADPH.* Journal Of Biological Chemistry, 1987. **262**(2): p. 660-666.

479. Kirkman, H.N., et al., *Mechanisms of protection of catalase by NADPH - Kinetics and stoichiometry.* Journal Of Biological Chemistry, 1999. **274**(20): p. 13908-13914.

480. Putnam, C.D., et al., *Active and inhibited human catalase structures: Ligand and NADPH binding and catalytic mechanism.* Journal Of Molecular Biology, 2000. **296**(1): p. 295-309.

481. Kirkman, H.N. and G.F. Gaetani, *Catalase: a tetrameric enzyme with four tightly bound molecules of NADPH.* Proceedings Of The National Academy Of Sciences Of The United States Of America, 1984. **81**(14): p. 4343-4347.

482. Vlasits, J., et al., *Mechanisms of catalase activity of heme peroxidases.* Archives of biochemistry and biophysics, 2010. **500**(1): p. 74-81.

483. Regelsberger, G., et al., *Spectral and kinetic studies of the oxidation of monosubstituted phenols and anilines by recombinant Synechocystis catalase-peroxidase compound I.* Biochemistry, 1999. **38**(32): p. 10480-10488.

484. Jakopitsch, C., et al., *Catalase-peroxidase from Synechocystis is capable of chlorination and bromination reactions.* Biochemical and biophysical research communications, 2001. **287**(3): p. 682-687.

485. Zámocký, M., P.G. Furtmüller, and C. Obinger, *Evolution of structure and function of Class I peroxidases.* Archives of Biochemistry and Biophysics, 2010. **500**(1): p. 45-57.

486. Zámocký, M., et al., *Turning points in the evolution of peroxidase–catalase superfamily: molecular phylogeny of hybrid heme peroxidases.* Cellular and Molecular Life Sciences, 2014. **71**(23): p. 4681-4696.

487. Smulevich, G., et al., *Probing the structure and bifunctionality of catalase-peroxidase (KatG).* Journal of inorganic biochemistry, 2006. **100**(4): p. 568-585.

488. Brunder, W., H. Schmidt, and H. Karch, *KatP, a novel catalase-peroxidase encoded by the large plasmid of enterohaemorrhagic Escherichia coli O157: H7.* Microbiology, 1996. **142**(11): p. 3305-3315.

489. Amemura-Maekawa, J., et al., *Identification of a novel periplasmic catalase-peroxidase KatA of Legionella pneumophila.* FEMS microbiology letters, 1999. **176**(2): p. 339-344.

490. Johnston, M. and E. Delwiche, *Distribution and characteristics of the catalases of Lactobacillaceae.* Journal of bacteriology, 1965. **90**(2): p. 347-351.

491. Beyer Jr, W.F. and I. Fridovich, *Pseudocatalase from Lactobacillus plantarum: evidence for a homopentameric structure containing two atoms of manganese per subunit.* Biochemistry, 1985. **24**(23): p. 6460-6467.

492. Barynin, V.V., et al., *Crystal structure of manganese catalase from Lactobacillus plantarum.* Structure, 2001. **9**(8): p. 725-738.

493. Hofmann, B., H.J. Hecht, and L. Flohe, *Peroxiredoxins.* Biological Chemistry, 2002. **383**(3-4): p. 347-364.

494. Flohé, L. and J.R. Harris, *Peroxiredoxin systems: structures and functions*. Vol. 44. 2007: Springer Science & Business Media.

495. Vandenbroucke, K., et al., *Hydrogen peroxide–induced gene expression across kingdoms: A comparative analysis.* Molecular Biology and Evolution, 2008. **25**(3): p. 507-516.

496. Link, A.J., K. Robison, and G.M. Church, *Comparing the predicted and observed properties of proteins encoded in the genome of Escherichia coli K-12.* Electrophoresis, 1997. **18**(8): p. 1259-1313.

497. Rhee, S.G., et al., *Peroxiredoxin, a novel family of peroxidases.* Iubmb Life, 2001. **52**(1-2): p. 35-41.

498. Dammeyer, P. and E.S.J. Arner, *Human Protein Atlas of redox systems - What can be learnt?* Biochimica et Biophysica Acta-General Subjects, 2011. **1810**(1): p. 111-138.

499. Chae, H.Z., et al., *Characterization of three isoforms of mammalian peroxiredoxin that reduce peroxides in the presence of thioredoxin.* Diabetes Research and Clinical Practice, 1999. **45**: p. 101 - 112.

500. Watabe, S., et al., *Purification and characterization of a substrate protein for mitochondrial ATP-dependent protease in bovine adrenal cortex.* Journal of biochemistry, 1994. **115**(4): p. 648-654.

501. Hall, A., P.A. Karplus, and L.B. Poole, *Typical 2-Cys peroxiredoxins - structures, mechanisms and functions.* Febs Journal, 2009. **276**(9): p. 2469-2477.

502. Chae, H.Z., et al., *Cloning and sequencing of thiol-specific antioxidant from mammalian brain: alkyl hydroperoxide reductase and thiol-specific antioxidant define a large family of antioxidant enzymes.* Proceedings of the National Academy of Sciences of the United States of America, 1994. **91**: p. 7017-7021.

503. Fisher, A.B., *Peroxiredoxin 6: a bifunctional enzyme with glutathione peroxidase and phospholipase A2 activities.* Antioxid Redox Signal, 2011. **15**(3): p. 831-844.

504. Chae, H.Z., S.J. Chung, and S.G. Rhee, *Thioredoxin-dependent peroxide reductase from yeast.* Journal Of Biological Chemistry, 1994. **269**(44): p. 27670-27678.

505. Hall, A., et al., *Structure-based insights into the catalytic power and conformational dexterity of peroxiredoxins.* Antioxid Redox Signal, 2011. **15**(3): p. 795-815.

506. Nelson, K.J., et al., *Analysis of the peroxiredoxin family: Using active-site structure and sequence information for global classification and residue analysis.* Proteins, 2011. **79**(3): p. 947-964.

507. Perkins, A., et al., *Peroxiredoxins: guardians against oxidative stress and modulators of peroxide signaling.* Trends in biochemical sciences, 2015. **40**(8): p. 435-445.

508. Poole, L. and K. Nelson, *Distribution and Features of the Six Classes of Peroxiredoxins.* Molecules and cells, 2016.

509. Okado-Matsumoto, A., et al., *Peroxiredoxin IV is a secretable protein with heparin-binding properties under reduced conditions.* Journal of Biochemistry, 2000. **127**(3): p. 493-501.

510. Rhee, S.G., et al., *Peroxiredoxin Functions as a Peroxidase and a Regulator and Sensor of Local Peroxides.* Journal of Biological Chemistry, 2012. **287**(7): p. 4403-4410.

511. Hanschmann, E.-M., et al., *Thioredoxins, glutaredoxins, and peroxiredoxins—molecular mechanisms and health significance: from cofactors to antioxidants to redox signaling.* Antioxidants & redox signaling, 2013. **19**(13): p. 1539-1605.

512. Schröder, E., et al., *Crystal structure of decameric 2-Cys peroxiredoxin from human erythrocytes at 1.7A resolution.* Structure, 2000. **8**(6): p. 605-615.

513. Wood, Z.A., et al., *Dimers to doughnuts: redox-sensitive oligomerization of 2-cysteine peroxiredoxins.* Biochemistry, 2002. **41**(17): p. 5493-5504.

514. Perkins, A., et al., *Mapping the active site helix-to-strand conversion of CxxxxC peroxiredoxin Q enzymes.* Biochemistry, 2012. **51**(38): p. 7638-7650.

515. Perkins, A., et al., *The sensitive balance between the fully folded and locally unfolded conformations of a model peroxiredoxin.* Biochemistry, 2013. **52**(48): p. 8708-8721.

516. Cao, Z., et al., *Crystal structure of reduced and of oxidized peroxiredoxin IV enzyme reveals a stable oxidized decamer and a non-disulfide-bonded intermediate in the catalytic cycle.* Journal of Biological Chemistry, 2011. **286**(49): p. 42257-42266.

517. Peskin, A.V., et al., *Hyperoxidation of peroxiredoxins 2 and 3: Rate constants for the reactions of the sulfenic acid of the peroxidatic cysteine.* J. Biol. Chem., 2013.

518. Lee, W.S., et al., *Human peroxiredoxin 1 and 2 are not duplicate proteins - The unique presence of Cys(83) in Prx1 underscores the structural and functional differences between Prx1 and Prx2.* Journal of Biological Chemistry, 2007. **282**(30): p. 22011-22022.

519. O'Neill, J.S. and A.B. Reddy, *Circadian clocks in human red blood cells.* Nature, 2011. **469**(7331): p. 498-U70.

520. Edgar, R.S., et al., *Peroxiredoxins are conserved markers of circadian rhythms.* Nature, 2012. **485**(7399): p. 459-464.

521. Olmedo, M., et al., *Circadian regulation of olfaction and an evolutionarily conserved, nontranscriptional marker in Caenorhabditis elegans.* Proceedings of the National Academy of Sciences, 2012. **109**(50): p. 20479-20484.

522. Kil, I.S., et al., *Feedback control of adrenal steroidogenesis via H2O2-dependent, reversible inactivation of peroxiredoxin III in mitochondria.* Molecular cell, 2012. **46**(5): p. 584-594.

523. Kil, I.S., et al., *Circadian Oscillation of Sulfiredoxin in the Mitochondria.* Molecular cell, 2015. **59**(4): p. 651-663.

524. Jang, H.H., et al., *Two enzymes in one; two yeast peroxiredoxins display oxidative stress-dependent switching from a peroxidase to a molecular chaperone function.* Cell, 2004. **117**(5): p. 625-635.

525. Moon, J.C., et al., *Oxidative stress-dependent structural and functional switching of a human 2-Cys peroxiredoxin isotype II that enhances HeLa cell resistance to H2O2-induced cell death.* Journal of Biological Chemistry, 2005. **280**(31): p. 28775-28784.

526. Baty, J.W., M.B. Hampton, and C.C. Winterbourn, *Proteomic detection of hydrogen peroxide-sensitive thiol proteins in Jurkat cells.* Biochemical Journal, 2005. **389**(3): p. 785-795.

527. Pillay, C.S., et al., *Enzymes or redox couples? The kinetics of thioredoxin and glutaredoxin reactions in a systems biology context.* Biochem J, 2009. **417**(1): p. 269-275.

528. Day, Alison M., et al., *Inactivation of a Peroxiredoxin by Hydrogen Peroxide Is Critical for Thioredoxin-Mediated Repair of Oxidized Proteins and Cell Survival.* Molecular Cell, 2012. **45**(3): p. 398-408.

529. Lee, J., et al., *A new antioxidant with alkyl hydroperoxide defense properties in yeast.* Journal Of Biological Chemistry, 1999. **274**(8): p. 4537-4544.

530. Park, S.G., et al., *Distinct physiological functions of thiol peroxidase isoenzymes in Saccharomyces cerevisiae.* Journal of Biological Chemistry, 2000. **275**(8): p. 5723-5732.

531. Jeong, J.S., et al., *Purification and characterization of a second type thioredoxin peroxidase (type II TPx) from Saccharomyces cerevisiae.* Biochemistry, 1999. **38**(2): p. 776-783.

532. Huang, M.E., et al., *A genomewide screen in Saccharomyces cerevisiae for genes that suppress the accumulation of mutations.* Proceedings Of The National Academy Of Sciences Of The United States Of America, 2003. **100**: p. 11529-11534.

533. Kaya, A., et al., *Thiol peroxidase deficiency leads to increased mutational load and decreased fitness in Saccharomyces cerevisiae.* Genetics, 2014. **198**(3): p. 905-917.

534. Wong, C.-M., K.-L. Siu, and D.-Y. Jin, *Peroxiredoxin-null yeast cells are hypersensitive to oxidative stress and are genomically unstable.* Journal of Biological Chemistry, 2004. **279**(22): p. 23207-23213.

535. Izawa, S., Y. Inoue, and A. Kimura, *Importance of catalase in the adaptive response to hydrogen peroxide: analysis of acatalasaemic Saccharomyces cerevisiae.* Biochemical Journal, 1996. **320 (Pt 1)**: p. 61-67.

536. Jara, M., et al., *The peroxiredoxin Tpx1 is essential as a H2O2 scavenger during aerobic growth in fission yeast.* Molecular biology of the cell, 2007. **18**(6): p. 2288-2295.

537. Lee, T.-H., et al., *Peroxiredoxin II is essential for sustaining life span of erythrocytes in mice.* Blood, 2003. **101**(12): p. 5033-5038.

538. Latimer, H. and E. Veal, *Peroxiredoxins in Regulation of MAPK Signalling Pathways; Sensors and Barriers to Signal Transduction.* Molecules and cells, 2016.

539. Mahadev, K., et al., *Insulin-stimulated hydrogen peroxide reversibly inhibits protein-tyrosine phosphatase 1b in vivo and enhances the early insulin action cascade.* Journal of Biological Chemistry, 2001. **276**(24): p. 21938-21942.

540. Song, G., G.L. Ouyang, and S.D. Bao, *The activation of Akt/PKB signaling pathway and cell survival.* Journal of Cellular and Molecular Medicine, 2005. **9**(1): p. 59-71.

541. Wang, Z., et al., *Mitogen-activated protein kinase phosphatase-1 represses c-Jun NH2-terminal kinase-mediated apoptosis via NF-κB regulation.* Journal of Biological Chemistry, 2008. **283**(30): p. 21011-21023.

542. Zhang, R., et al., *Thioredoxin-2 inhibits mitochondria-located ASK1-mediated apoptosis in a JNK-independent manner.* Circulation research, 2004. **94**(11): p. 1483-1491.

543. Palde, P.B. and K.S. Carroll, *A universal entropy-driven mechanism for thioredoxin–target recognition.* Proceedings of the National Academy of Sciences, 2015. **112**(26): p. 7960-7965.

544. Ishii, T., E. Warabi, and T. Yanagawa, *Novel roles of peroxiredoxins in inflammation, cancer and innate immunity.* J Clin Biochem Nutr, 2012. **50**(2): p. 91-105.

545. Knoops, B., et al., *Cloning and characterization of AOEB166, a novel mammalian antioxidant enzyme of the peroxiredoxin family.* Journal of Biological Chemistry, 1999. **274**(43): p. 30451-30458.

546. Kinnula, V., et al., *Cell specific expression of peroxiredoxins in human lung and pulmonary sarcoidosis.* Thorax, 2002. **57**(2): p. 157-164.

547. Wang, M.-X., et al., *Expression and regulation of peroxiredoxin 5 in human osteoarthritis.* FEBS letters, 2002. **531**(2): p. 359-362.

548. Yun, H.-M., et al., *PRDX6 controls multiple sclerosis by suppressing inflammation and blood brain barrier disruption.* Oncotarget, 2015. **6**(25): p. 20875.

549. Abbas, K., et al., *Signaling events leading to peroxiredoxin 5 up-regulation in immunostimulated macrophages.* Free Radical Biology and Medicine, 2009. **47**(6): p. 794-802.

550. Kim, S.-U., et al., *Peroxiredoxin I is an indicator of microglia activation and protects against hydrogen peroxide-mediated microglial death.* Biological and Pharmaceutical Bulletin, 2008. **31**(5): p. 820-825.

551. Sun, H.N., et al., *Microglial peroxiredoxin V acts as an inducible anti-inflammatory antioxidant through cooperation with redox signaling cascades.* Journal of neurochemistry, 2010. **114**(1): p. 39-50.

552. Yang, C.-S., et al., *Roles of peroxiredoxin II in the regulation of proinflammatory responses to LPS and protection against endotoxin-induced lethal shock.* The Journal of experimental medicine, 2007. **204**(3): p. 583-594.

553. Kikuchi, N., et al., *Aggravation of bleomycin-induced pulmonary inflammation and fibrosis in mice lacking peroxiredoxin I.* American journal of respiratory cell and molecular biology, 2011. **45**(3): p. 600-609.

554. Ding, Y., et al., *Overexpression of peroxiredoxin 4 protects against high-dose streptozotocin-induced diabetes by suppressing oxidative stress and cytokines in transgenic mice.* Antioxidants & redox signaling, 2010. **13**(10): p. 1477-1490.

555. Nabeshima, A., et al., *Peroxiredoxin 4 protects against nonalcoholic steatohepatitis and type 2 diabetes in a nongenetic mouse model.* Antioxidants & redox signaling, 2013. **19**(17): p. 1983-1998.

556. Kim, S.-U., et al., *Peroxiredoxin I is a ROS/p38 MAPK-dependent inducible antioxidant that regulates NF-κB-mediated iNOS induction and microglial activation.* Journal of neuroimmunology, 2013. **259**(1): p. 26-36.

557. Chatterjee, S., et al., *Peroxiredoxin 6 phosphorylation and subsequent phospholipase A2 activity are required for agonist-mediated activation of NADPH oxidase in mouse pulmonary microvascular endothelium and alveolar macrophages.* Journal of Biological Chemistry, 2011. **286**(13): p. 11696-11706.

558. Furuta, T., et al., *Mast cell-mediated immune responses through IgE antibody and Toll-like receptor 4 by malarial peroxiredoxin.* European journal of immunology, 2008. **38**(5): p. 1341-1350.

559. Riddell, J.R., et al., *Peroxiredoxin 1 stimulates secretion of proinflammatory cytokines by binding to TLR4.* The journal of immunology, 2010. **184**(2): p. 1022-1030.

560. Salzano, S., et al., *Linkage of inflammation and oxidative stress via release of glutathionylated peroxiredoxin-2, which acts as a danger signal.* Proceedings of the National Academy of Sciences, 2014. **111**(33): p. 12157-12162.

CHAPTER 2 – HYDROGEN PEROXIDE METABOLISM IN HUMAN ERYTHROCYTES

2. Hydrogen peroxide metabolism in human erythrocytes

ORIGINAL ARTICLE

Free Radical Biology and Medicine 74, 35-49.

Hydrogen peroxide metabolism and sensing in human erythrocytes: a validated kinetic model and reappraisal of the role of peroxiredoxin II

Rui Benfeitas[1,2,3], Gianluca Selvaggio[1], Fernando Antunes[4], Pedro M. B. M. Coelho[1], Armindo Salvador[1,5]

[1] CNC – Center for Neuroscience and Cell Biology, University of Coimbra, Portugal

[2] PhD Programme in Experimental Biology and Biomedicine (PDBEB), CNC-Center for Neuroscience and Cell Biology, University of Coimbra, Portugal

[3] Institute for Interdisciplinary Research (IIIUC), University of Coimbra, Portugal

[4] Departamento de Química e Bioquímica and Centro de Química e Bioquímica, Faculdade de Ciências, Universidade de Lisboa, Lisboa, Portugal.

[5] Coimbra Chemistry Centre, University of Coimbra, Portugal

2. Hydrogen peroxide metabolism in human erythrocytes

2.1 Abstract

Hydrogen peroxide (H_2O_2) metabolism in human erythrocytes has been thoroughly investigated, but unclear points persist. By integrating the available data into a mathematical model that accurately represents the current understanding and comparing computational predictions to observations we sought to (a) identify inconsistencies in present knowledge, (b) propose resolutions, and (c) examine their functional implications. The systematic confrontation of computational predictions to experimental observations of the responses of intact erythrocytes highlighted the following important discrepancy. The high rate constant (10^7-10^8 $M^{-1}s^{-1}$) for H_2O_2 reduction determined for purified peroxiredoxin II (Prx2) and the high abundance of this protein indicate that under physiological conditions it consumes practically all the H_2O_2. However, this is inconsistent with extensive evidence that Prx2's contribution for H_2O_2 elimination is comparable to catalase's. Models modified such that Prx2's *effective* peroxidase activity is just 10^5 $M^{-1}s^{-1}$ agree near-quantitatively with extensive experimental observations. This low effective activity is likely due to a strong but readily reversible inhibition of Prx2's peroxidatic activity in intact cells, implying that the main role of Prx2 in human erythrocytes is not to eliminate peroxide substrates. Simulations of the responses to physiological H_2O_2 stimuli highlight that a design combining abundant Prx2 with a low effective peroxidase activity spares NADPH while improving potential signaling properties of the Prx2/thioredoxin/thioredoxin reductase system.

2.2 Abbreviations

Cat	catalase
C-I	catalase compound I
C-II	catalase compound II
CPTTRS	Cat/Prx2/Trx1/TrxR system
Ferri	ferricatalase
GPx1	glutathione peroxidase 1
GSH	glutathione
GSR	glutathione reductase
GSSG	glutathione disulfide
KM,E,S	Michaelis-Menten constant of enzyme E for substrate S
MW	molecular weight
Prx2	peroxiredoxin II
PSH	Prx2 monomer with peroxidatic Cys in thiol form
PSO_2H	Prx2 monomer with peroxidatic Cys in sulfinic form
PSOH	Prx2 monomer with peroxidatic Cys in sulfenic form
PSS	Prx2 monomer with peroxidatic Cys in disulfide form
RT	plasma recirculation time
Srx	sulfiredoxin
t_c	erythrocyte transit time through an inflammation focus
t_r	mean recurrence period between successive crossing of inflammation foci by erythrocytes
Trx1	thioredoxin 1
$Trx1_{xy}$	Trx1 with active site dithiol in state x and regulatory dithiol in state y (T, thiol; D, disulfide)
TrxR	thioredoxin reductase
TrxSH	Trx1 with active site dithiol in reduced form
v_{sup}	rate of H_2O_2 supply.

Kinetic parameters are as defined in Table 2.1.

2.3 Introduction

The metabolism of H_2O_2 in human erythrocytes has been subject of scrutiny over many decades, which re-intensified recently [1-6]. Consequently, erythrocytes have become the most thoroughly understood model for H_2O_2 metabolism in human cells. Nevertheless, important aspects of this system and how its design relates to function remain unclear.

Mathematical modeling has consistently proved useful in clarifying the mechanisms of antioxidant defense and redox signaling [7-20]. Kinetic models help identifying gaps and inconsistencies in the state of the art, assessing alternative mechanistic hypotheses, understanding the interplay among multiple factors, and understanding the relationship between molecular-level design and phenotype. The availability of convenient kinetic modeling software [21] facilitated this approach. Attempts at quantitative modeling of H_2O_2 metabolism were crucial in highlighting the importance of Prx2 (EC 1.11.1.15) and addressing the relative

importance of glutathione peroxidase (GPx1, EC 1.11.1.9), catalase (Cat, EC 1.11.1.6) and Prx2 in mice erythrocytes [1, 3].

However, recent experimental data [4-6, 22] questions previous notions. The main open issues pertain to the role of the third most abundant protein in human erythrocytes, Prx2. Prx2 reduces H_2O_2 through a three-step cycle (Figure 2.1A) involving two conserved cysteine residues in each monomer. H_2O_2 oxidizes the peroxidatic cysteine C51-SH to a sulfenic acid, C51-SOH. C51-SOH then condenses with the resolving cysteine C172-SH from an adjacent monomer to form a disulfide C51-S-S-C172, which in turn is reduced by thioredoxin (Trx1), thereby closing the cycle. C51-SOH can also be further oxidized by H_2O_2 to sulfinic acid C51-SO_2H, which inactivates Prx2's peroxidase activity. Johnson *et al.* [1] found that a quantitative modeling of H_2O_2 metabolism in GPx-deficient mice erythrocytes required a substantial but not overwhelming contribution of Prx2. Experiments by Low *et al.* [2] confirmed the relevance of Prx2 for H_2O_2 consumption in human erythrocytes. Subsequent determinations [23, 24] of the rate constant for H_2O_2 reduction by Prx2 from human erythrocytes yielded values in the range 10^7-10^8 $M^{-1}s^{-1}$. As we will show below, these values imply an overwhelming contribution for H_2O_2 elimination should all Prx2 be peroxidatically active. Prx2 also protects hemoglobin against aggregation [5] and binds many proteins, some of which in a redox-dependent manner [25-28]. These observations raise the question of whether Prx2's main function in erythrocytes is to act as a peroxidase, a H_2O_2 sensor or a chaperone.

We began by critically reviewing the quantitative literature data about the physiological setting and mechanisms of H_2O_2 metabolism in human erythrocytes. Namely, we examined the pathophysiological concentrations range and time frames of exposure of these circulating cells to H_2O_2, as well as consumption mechanisms including the Cat, GPx1, and Prx2 pathways. We then introduce a kinetic model that seeks to accurately represent the current understanding of these processes, based on curated data from kinetic parameters determined *in vitro*. Comparing the predictions based on this model to experimental observations of intact erythrocytes we highlighted a fundamental discrepancy with the following implication. The *effective* peroxidase specific activity of Prx2 in erythrocytes is much lower than that determined for the purified

protein. This is most likely because Prx2 is subject to a strong but readily reversible inhibition by a hitherto unidentified factor. A modified kinetic model that accounts for the lowered peroxidase activity of Prx2 matches the experimental data near quantitatively. Our analysis of the functional implications of Prx2 inhibition indicates that such a design provides desirable signaling properties while avoiding NADPH waste in H_2O_2 elimination. Altogether, this work sums up the present understanding of the main aspects of the H_2O_2 metabolism and sensing in human erythrocytes and sets the stage for systematic analyses of the relationship between design and function of this system.

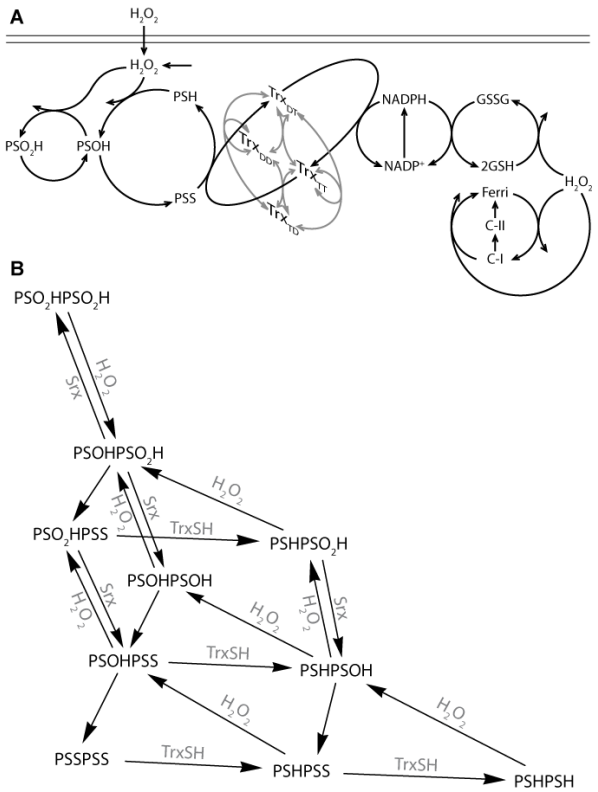

Figure 2.1 - Model of H_2O_2 metabolism in human erythrocytes. (A) Overall diagram of the model. The model accounts for the following processes: (i) Generation of intracellular H_2O_2 from both endogenous and exogenous sources; (ii) H_2O_2 consumption via Cat, Prx2 and GPx1; (iii) Prx2 sulfinylation and reduction of the sulfinic to the sulfenic form; (iv) Trx1 oxidation by Prx2, reduction via thioredoxin reductase and reactions between the active site dithiol and the regulatory dithiol (gray); (v) glutathione disulfide (GSSG) reduction via glutathione reductase (GSR); (vi) NADP+ reduction to NADPH by the hexose monophosphates shunt. (B) Modeling of the Prx2 redox cycle, taking the oxidation state of each monomer in each dimer into account. C-I, C-II, Ferri, catalase in Compound I, Compound II and Ferri form, respectively; PSH, PSOH, PSO2H, PSS, Prx2 monomer with the peroxidatic Cys residue in thiol, sulfenic, sulfinic and disulfide form, respectively; Srx, sulfiredoxin; Trxxy, thioredoxin with the active site dithiol in state x, and the regulatory dithiol in state y (T, thiol; D, disulfide); TrxSH, thioredoxin with the active site dithiol in reduced form.

2.4 Model formulation

Our mathematical model accounts for the processes displayed in Figure 2.1. Table 2.1 lists the reactions, rate expressions and kinetic parameters. Below we discuss the assumptions and estimations involved. All intracellular concentrations refer to dm^3 of erythrocyte water (conversion factors in Supplementary Materials section 2.10.1).

2. Hydrogen peroxide metabolism in human erythrocytes

*Table 2.1. Reactions, conservation relationships, rate expressions and parameter values considered in the kinetic model. Reactions whose rate expressions are omitted were considered to follow mass action kinetics with the indicated rate constant. The following four model variants are considered. Model A, K_{Prx2}= 0; Model B, all parameter values as displayed; Model C, K_{Prx2}= 0, $[Prx2\ dimers]_{tot}$= 0.5255 μM; Model D, K_{Prx2}= 0, k_{Ox}= 3.015×10^5 M^{-1}s^{-1}. All other parameter values are identical among the model variants. Except otherwise stated the extracellular concentration of H_2O_2 was treated as an independent (i. e., imposed) variable. Values in this table are presented as computationally implemented, and the number of significant figures does not necessarily reflect the accuracy of the estimates. SMn, Supplementary Materials section n. $Trx1_{xy}$, thioredoxin with the active site dithiol in state x, and the regulatory dithiol in state y (T, thiol; D, disulfide). iPS*PSH, Prx2 dimer where one monomer is in PS* state and the other is inactive PSH.*

Reaction	Rate (v) and pars	Ref.
→ H_2O_2	v_{prod} = 3.5×10^{-8} M s^{-1}	SM2.10.2
eH_2O_2 → H_2O_2	k_P = 10.9 s^{-1} [a]	SM2.10.3
H_2O_2 → eH_2O_2	k_P = 10.9 s^{-1} [a]	SM2.10.3
H_2O_2 + 2 GSH → GSSG + 2 H_2O	$v = \frac{1}{\frac{\phi_1}{[H_2O_2]} + \frac{\phi_2}{[GSH]}}$	[29]
	ϕ_1 = 3.99×10^{-2} s	SM2.10.5
	ϕ_2 = 9.72 s	SM2.10.5
GSSG + NADPH + H$^+$ → 2 GSH + NADP$^+$	$v = \frac{V_{Max,GSR}}{1 + \frac{K_{M,GSR,NADPH}}{[NADPH]} + \frac{K_{M,GSR,GSSG}}{[GSSG]}}$	[30]
	$V_{Max,GSR}$ = 4.9×10^{-5} M s^{-1}	[31]
	$K_{M,GSR,NADPH}$ = 8.5×10^{-6} M	[32]
	$K_{M,GSR,GSSG}$ = 6.5×10^{-5} M	[32]
Ferricatalase + H_2O_2 → Compound I + H_2O	k_{Ferri} = 6×10^6 M^{-1}s^{-1}	[33]
Compound I + H_2O_2 → Ferricatalase + O_2 + H_2O	k_{CI} = 1.8×10^7 M^{-1}s^{-1}	[33]
Compound I → Compound II	k_{Clinac} = 1.1×10^{-2} s^{-1}	[34]
Compound II → Ferricatalase	k_{CII} = 7.39×10^4 s^{-1}	[35]
PSHPSH + H_2O_2 → PSOHPSH + H_2O	$2k_{Ox}$ = 2×10^8 M^{-1}s^{-1} [b]	[24]
PSOHPSH → PSSPSH + H_2O	k_{Cond} = 1.7 s^{-1}	[22]
PSOHPSH + H_2O_2 → PSOHPSOH + H_2O	k_{Ox} = 10^8 M^{-1}s^{-1}	[24]
PSOHPSH + H_2O_2 →PSO_2HPSH + H_2O	k_{Sulf} = 1.2×10^4 M^{-1}s^{-1}	[22]
PSSPSH +H_2O_2 → PSSPSOH + H_2O	k_{Ox} = 10^8 M^{-1}s^{-1}	[24]
PSSPSH + $Trx1_{TT}$ → PSHPSH + $Trx1_{DT}$	k_{Red} = 2.1×10^5 M^{-1}s^{-1}	[24]
PSSPSH + $Trx1_{TD}$ → PSHPSH + $Trx1_{DD}$	k_{Red} = 2.1×10^5 M^{-1}s^{-1}	[24]
PSOHPSOH → PSSPSOH + H_2O	$2k_{Cond}$ = 3.4 s^{-1} [b]	[22]
PSOHPSOH + H_2O_2 →PSO_2HPSOH+ H_2O	$2k_{Sulf}$ = 2.4×10^4 M^{-1}s^{-1}	[22]

2. Hydrogen peroxide metabolism in human erythrocytes

Reaction	Rate (v) and pars	Ref.
$PSSPSOH \rightarrow PSSPSS + H_2O$	k_{Cond} = 1.7 s^{-1}	[22]
$PSSPSOH + H_2O_2 \rightarrow PSO_2HPSS + H_2O$	k_{Sulf} = 1.2×10^4 $M^{-1}s^{-1}$	[22]
$PSSPSOH + Trx1_{TT} \rightarrow PSOHPSH + Trx1_{DT}$	k_{Red} = 2.1×10^5 $M^{-1}s^{-1}$	[24]
$PSSPSOH + Trx1_{TD} \rightarrow PSOHPSH + Trx1_{DD}$	k_{Red} = 2.1×10^5 $M^{-1}s^{-1}$	[24]
$PSSPSS + Trx1_{TT} \rightarrow PSSPSH + Trx1_{DT}$	$2k_{Red}$ = 4.2×10^5 $M^{-1}s^{-1}$ [b]	[24]
$PSSPSS + Trx1_{TD} \rightarrow PSSPSH + Trx1_{DD}$	$2k_{Red}$ = 4.2×10^5 $M^{-1}s^{-1}$ [b]	[24]
$PSO_2HPSH + H_2O_2 \rightarrow PSO_2HPSOH + H_2O$	k_{Ox} = 10^8 $M^{-1}s^{-1}$	[24]
$PSO_2HPSH \rightarrow PSOHPSH$	k_{Srx} = 10^{-4} s^{-1}	[c]
$PSO_2HPSOH \rightarrow PSO_2HPSS + H_2O$	k_{Cond} = 1.7 s^{-1}	[22]
$PSO_2HPSOH + H_2O_2 \rightarrow PSO_2HPSO_2H + H_2O$	k_{Sulf} = 1.2×10^4 $M^{-1}s^{-1}$	[22]
$PSO_2HPSOH \rightarrow PSOHPSOH$	k_{Srx} = 10^{-4} s^{-1}	[c]
$PSO_2HPSS + Trx1_{TT} \rightarrow PSO_2HPSH + Trx1_{DT}$	k_{Red} = 2.1×10^5 $M^{-1}s^{-1}$	[24]
$PSO_2HPSS + Trx1_{TD} \rightarrow PSO_2HPSH + Trx1_{DD}$	k_{Red} = 2.1×10^5 $M^{-1}s^{-1}$	[24]
$PSO_2HPSS \rightarrow PSSPSOH$	k_{Srx} = 10^{-4} s^{-1}	[c]
$PSO_2HPSO_2H \rightarrow PSO_2HPSOH$	$2k_{Srx}$ = 2×10^{-4} s^{-1} [b]	[c]
$iPSHPSH + H_2O_2 \rightarrow iPSOHPSH$	k_{Ox} = 10^8 $M^{-1}s^{-1}$	[24]
$iPSOHPSH \rightarrow iPSSPSH$	k_{Cond} = 1.7 s^{-1}	[22]
$iPSOHPSH + H_2O_2 \rightarrow iPSO_2HPSH$	k_{Sulf} = 1.2×10^4 $M^{-1}s^{-1}$	[22]
$iPSO_2HPSH \rightarrow iPSOHPSH$	k_{Srx} = 10^{-4} s^{-1}	[c]
$iPSSPSH + Trx1_{TT} \rightarrow iPSHPSH + Trx1_{DT}$	k_{Red} = 2.1×10^5 $M^{-1}s^{-1}$	[24]
$iPSSPSH + Trx1_{TD} \rightarrow iPSHPSH + Trx1_{DD}$	k_{Red} = 2.1×10^5 $M^{-1}s^{-1}$	[24]
$PSHPSH \rightleftharpoons iPSHPSH$	K_{Prx2} = 166.9	
$PSOHPSH \rightleftharpoons iPSOHPSH$	K_{Prx2} = 166.9	
$PSSPSH \rightleftharpoons iPSSPSH$	K_{Prx2} = 166.9	[d]
$PSO_2HPSH \rightleftharpoons iPSO_2HPSH$	K_{Prx2} = 166.9	
$iPSHPSH \rightleftharpoons iPSHiPSH$	K_{Prx2} = 166.9	
$Trx1_{DT} + NADPH + H^+ \rightarrow Trx1_{TT} + NADP^+$	$v = \frac{V_{Max,TrxR}}{1 + \frac{K_{M,TrxR,NADPH}}{[NADPH]} + \frac{K_{M,TrxR,Trx1DT}}{[Trx1_{DT}]}}$	SM2.10.9
	$V_{Max,TrxR}$ = 1.0×10^{-5} M s^{-1}	SM2.10.9
	$K_{M,TrxR,NADPH}$ = 6×10^{-6} M	[36]
	$K_{M,TrxR,Trx1DT}$ = 1.83×10^{-6} M	[37]
$Trx1_{DD} + Trx1_{TT} \rightarrow 2\ Trx1_{TD}$	k_{Trxb} = 4.2×10^3 $M^{-1}s^{-1}$	SM2.10.8
$2\ Trx1_{TD} \rightarrow Trx1_{DD} + Trx1_{TT}$	$2k_{Trxa}$ = 4.2×10^5 $M^{-1}s^{-1}$ [b]	SM2.10.8
$Trx1_{DT} + Trx1_{TD} \rightarrow Trx1_{DD} + Trx1_{TT}$	k_{Trxa} = 2.1×10^5 $M^{-1}s^{-1}$	SM2.10.8
$Trx1_{DD} + Trx1_{TT} \rightarrow 2\ Trx1_{DT}$	k_{Trxa} = 2.1×10^5 $M^{-1}s^{-1}$	SM2.10.8
$2\ Trx1_{DT} \rightarrow Trx1_{DD} + Trx1_{TT}$	$2k_{Trxb}$ = 8.4×10^3 $M^{-1}s^{-1}$ [b]	SM2.10.8
$Trx1_{DD} + Trx1_{DT} \rightarrow Trx1_{DD} + Trx1_{TD}$	k_{Trxb} = 4.2×10^3 $M^{-1}s^{-1}$	SM2.10.8
$Trx1_{DD} + Trx1_{TD} \rightarrow Trx1_{DD} + Trx1_{DT}$	k_{Trxa} = 2.1×10^5 $M^{-1}s^{-1}$	SM2.10.8
$Trx1_{TT} + Trx1_{TD} \rightarrow Trx1_{TT} + Trx1_{DT}$	k_{Trxa} = 2.1×10^5 $M^{-1}s^{-1}$	SM2.10.8
$Trx1_{TT} + Trx1_{DT} \rightarrow Trx1_{TT} + Trx1_{TD}$	k_{Trxb} = 4.2×10^3 $M^{-1}s^{-1}$	SM2.10.8

Reaction	Rate (v) and pars	Ref.
$Trx1_{DD}$ + NADPH + H^+→ $Trx1_{TD}$ + $NADP^+$	$v = \frac{V_{Max,TrxR}}{1 + \frac{K_{M,TrxR,NADPH}}{[NADPH]} + \frac{K_{M,TrxR,Trx1DD}}{[Trx1_{DD}]}}$	SM2.10.9
	$V_{Max,TrxR}$ = 1.0×10^{-5} M s^{-1}	SM2.10.9
	$K_{M,TrxR,NADPH}$ = 6×10^{-6} M	[36]
	$K_{M,TrxR,Trx1DD}$ = 1.83×10^{-3} M	SM2.10.9
$NADP^+$ → NADPH + H^+	$v = \frac{V_{Max,HMS}[NADP^+]}{K_{M,HMS,NADP^+} + [NADP^+]}$	
	$V_{Max,HMS}$ = 2.4×10^{-6} M s^{-1}	SM2.10.11
	$K_{M,HMS,NADP^+}$ = 4.5×10^{-7} M	SM2.10.11
NADPH ⇌ $NADPH_{bound}$	K_{NADPH}= 9.6	SM2.10.10
$NADP^+$ ⇌ $NADP^+_{bound}$	K_{NADP+}=1.8	SM2.10.10
Conservation relationships		
[GSH] + 2×[GSSG] = $[GS]_{tot}$	$[GS]_{tot}$ = 3.2×10^{-3} M	[31]
[Ferricatalase] + [Compound I] + [Compound II] = = $[Cat]_{tot}$	$[Cat]_{tot}$ = 2.44×10^{-5} M	SM2.10.6
[PSHPSH] + [PSOHPSH] + [PSSPSH] + $[PSO_2HPSH]$ + [PSOHPSOH] + [PSSPSOH] + + [PSSPSS] + $[PSO_2HPSOH]$ + $[PSO_2HPSS]$ + + $[PSO_2HPSO_2H]$ + [iPSHPSH] + [iPSOHPSH] + + [iPSSPSH] + $[iPSO_2HPSH]$ + [iPSHiPSH] = = $[Prx2\ dimers]_{tot}$	$[Prx2\ dimers]_{tot}$ = 2.85×10^{-4} M	SM2.10.7
$[Trx1_{TT}]$ + $[Trx1_{TD}]$ + $[Trx1_{DT}]$ + $[Trx1_{DD}]$ = $[Trx]_{tot}$	$[Trx]_{tot}$= 5.6×10^{-7} M	[38]
[NADPH] + $[NADPH_{bound}]$ + $[NADP^+]$ + + $[NADP^+_{bound}]$ =$[NADP]_{tot}$	$[NADP]_{tot}$= 2.8×10^{-5} M	[39]

[a] Referred to erythrocyte water volume.

[b] Reaction can occur in two different ways.

[c] See Model Formulation – Sulfiredoxin.

[d] See Results - Observations with intact erythrocytes are inconsistent with a high effective peroxidase activity of Prx2.

2.4.1 Physiological setting

In order to appreciate the role of the various defenses in physiological context one must consider the dynamic regimes under which circulating erythrocytes are exposed to H_2O_2. Glutathione (GSH) and hemoglobin autoxidation are likely the main endogenous H_2O_2 sources. We estimate their joint H_2O_2 production as 35 nM s^{-1} (details in Supplementary Materials section 2.10.2). Recently it has been shown that erythrocytes carry several NADPH oxidases, which contribute to

oxidative stress in sickle cell disease [40]. However, the extent to which these enzymes contribute for H_2O_2 production in normal erythrocytes is unknown.

Erythrocytes are also very permeable to H_2O_2 (Supplementary Materials section 2.10.3), and as result, they are subject to substantial variations in H_2O_2 influx. We estimated the basal influx based on the following considerations. It is reasonable to assume, and indeed experimentally supported [2, 6, 41], that in absence of oxidative stress the thiol pools of both Prx2 and glutathione remain mostly in the reduced state. Because in human erythrocytes the reduction of these thiols is entirely dependent on NADPH, that predominantly reduced state can only be sustained if the thiol oxidation rate is substantially lower than the maximal rate of NADPH regeneration: 2.4 μM s^{-1} [42]. As we will analyze in further detail below, when most of the Prx2 is in reduced form it consumes a substantial fraction of the H_2O_2 entering the erythrocyte. Thus, it is reasonable to assume that under basal oxidative loads the H_2O_2 influx is no higher than 0.5 μM s^{-1}, which would correspond to a plasma concentration in the order of 50 nM. This upper bound is consistent with estimates of H_2O_2 production [43, 44] in plasma obtained from experiments *in vitro*. Although such experiments involved the determination of μM-scale H_2O_2 concentrations in the assay media, these media have a much lower H_2O_2 clearance capacity than human blood. Once this difference in clearance capacity is accounted for, the estimated H_2O_2 production rates translate into steady state plasma H_2O_2 concentrations no higher than 10 nM (computations in Supplementary Materials section 2.10.4). Accordingly, as reference for basal conditions we adopt 5 nM plasma H_2O_2, corresponding to a 55 nM s^{-1} influx.

Under systemic inflammation H_2O_2 influx may reach the μM s^{-1} range, but not much higher. Thus, steady state 7 μM extracellular H_2O_2 can already cause apoptosis of Jurkat T cells [45], and should thus not be sustainable for long in the systemic circulation. Also, erythrocytes of mice subject to endotoxemia and human erythrocytes exposed to *Staphylococcus aureus*-activated neutrophils at physiological neutrophil:erythrocyte ratios show an accumulation of 16% and 32% S-S crosslinked Prx2 dimers, respectively [6]. According to our mathematical model, sustaining this extent of Prx2 oxidation requires a steady ≈3 μM s^{-1} H_2O_2 influx, corresponding to ≈0.3 μM plasma H_2O_2. However, the above-mentioned

percentage of crosslinked Prx2 dimers may be a mean over an erythrocyte population with very heterogeneous Prx2 oxidation resulting from sporadic adhesion to phagocytes.

Erythrocytes are briefly exposed to high plasma H_2O_2 concentrations while circulating through inflammation sites. In inflamed tissues surrounding wounds in zebra fish tail intracellular H_2O_2 concentrations are 0.5-50 µM [46]. However, the upper limit of this range overestimates the plasma H_2O_2 concentrations erythrocytes face, because the fish tail is not blood-irrigated and has low H_2O_2 clearance capacity.

The duration of exposure in these events is determined by the capillary transit time (t_c) at the inflammation focus, because it is in capillaries that erythrocytes circulate most slowly. For the alveolar capillaries in resected lobes of human lung specimens mean transit times are ≈3.0 s, with a range 0.03 - 14.5 s [47]. Alveolar capillaries present a worst case scenario, as they are frequently crossed and are near the predominant site of leukocyte margination [48].

The recurrence period (t_r) between successive crossings of these regions by one given erythrocyte can be estimated from the following data. A plasma volume element has a recirculation time (RT) of 21.4 ± 3.4 s at the systemic vascular system and has a 0.17 probability of returning to the heart within RT seconds [47]. However, the average pulmonary recirculation time for erythrocytes can be just 7 - 9 s due to the Fahraeus–Lindqvist effect [49]. These values set a lower limit for t_r, corresponding to the case of an extensive pulmonary inflammation. The recurrence periods for crossing localized inflammations in the peripheral circulation are of many minutes to hours.

2.4.2 Intracellular processes

2.4.2.1 Glutathione peroxidase

GPx1 catalyzes the reduction of H_2O_2 and organic peroxides by GSH. The rate law characterized by Flohé *et al.* [29] for bovine GPx1 fits the time series obtained by Mueller *et al.* [50] for H_2O_2 consumption by GPx1 in human hemolyzates (estimations in Supplementary Materials section 2.10.5). Further, the values for ϕ_1 and ϕ_2 (Table 2.1) that were estimated from this time series are consistent with

other determinations [51] of GPx1 activity in human erythrocytes, and the ϕ_1/ϕ_2 ratio is in good agreement with the kinetic parameters determined in [52] for these cells. Because the data from [50] provide the most direct determination available of GPx1 kinetics in human erythrocytes, in our model we adopted the values for ϕ_1 and ϕ_2 estimated from this reference. As consequence of these values, at low to moderate oxidative stress the GPx1-catalized H_2O_2 reduction has zero-order kinetics with respect to GSH, and first-order kinetics with respect to H_2O_2. The estimated pseudo-first-order rate constant is 25 s^{-1}. The good agreement between independent determinations of the activity and kinetic parameters of GPx1 in human erythrocytes (further discussion in Supplementary Materials section 2.10.5) gives confidence about the accurate modeling of this enzyme's action.

2.4.2.2 Catalase

Cat behaves as a dismutase at H_2O_2 concentrations above nM, and as a peroxidase at lower concentrations [53]. We approximated its kinetics as described in Supplementary Materials section 2.10.6, and adjusted the effective concentration of Cat so that at high H_2O_2 concentrations the pseudo-first-order rate constant matched the value (218 s^{-1}) determined in [50]. The data from Mueller *et al.* [50] for hemolyzates shows that Cat eliminates H_2O_2 with much higher activity than GPx1 at H_2O_2 concentrations above 100 nM. However, it has been argued that this might not be the case at the sub-nM H_2O_2 concentrations prevailing in erythrocytes under physiological conditions because the activity of Cat as a peroxidase is lower than its activity as a dismutase. Our estimates based on the available data (Supplementary Materials section 2.10.6) strongly suggest that the activity of Cat remains much higher than that of GPx1 even under these conditions. Cat consumes NADPH for protection against inactivation [53, 54], but the rate of this process is negligible under physiological conditions (Supplementary Materials section 2.10.6)

2.4.2.3 Peroxiredoxin II

We explicitly consider the oxidation state of each peroxidatic Cys in each dimer (Figure 2.1B). This allowed us to compute the fractions of singly- and doubly-disulfide-crosslinked dimers. For the oxidation of C51-SH by H_2O_2 (k_{Ox}) and for

the reduction of the disulfide (k_{Red}) we adopted the rate constants determined by Manta *et al.* [24] for Prx2 purified from human erythrocytes: k_{Ox}= 1.0×10^{8} $M^{-1}s^{-1}$, k_{Red}=2.1×10^{5} $M^{-1}s^{-1}$ at 25 ºC, pH 7.4. This value for k_{Ox} is in the order of magnitude of the value 1.3×10^{7} $M^{-1}s^{-1}$ at 20 ºC, pH 7.4 determined by Peskin *et al.* [23]. For the condensation (k_{Cond}) and sulfinylation (k_{Sulf}) reactions we adopted the rate constants determined by Peskin *et al*. [22] for recombinant human Prx2: k_{Cond}=1.7 s^{-1}, k_{Sulf}=1.2×10^{4} $M^{-1}s^{-1}$ at 20 ºC (computations and further discussion in Supplementary Materials section 2.10.7).

2.4.2.4 Sulfiredoxin

Sulfiredoxin (EC 1.8.98.2) catalyzes the reduction Prx2's C51-SO_2H to C51-SOH using ATP and reducing equivalents from Trx or GSH [55]. This process is slow, as mammalian sulfiredoxins have k_{cat} ≈3.0×10^{-3} s^{-1} [55]. It remains poorly characterized in human erythrocytes, where it is also slow [2, 4]. Thus, we assumed a pseudo-first-order rate constant k_{Srx}=10^{-4} s^{-1}.

2.4.2.5 Thioredoxin

The reduction of Prx2 by Trx1 is coupled to the oxidation of the active site dithiol [C32,C35, E_o= –230 mV [56]] of the latter, which is in turn reduced *via* thioredoxin reductase (TrxR, EC 1.8.1.9). However, human Trx1 carries another conserved oxidizable dithiol (C62,C69), which has a higher midpoint potential (E_o > –210 mV) [56]. The corresponding disulfide is not directly reduced by TrxR and its oxidation prevents the direct reduction of the C32-C35 disulfide by TrxR. However, that disulfide can be reduced by the Trx C32-C35 dithiol [56]. We modeled these interactions (Figure 2.1A, gray, Supplementary Materials section 2.10.8) according to the following assumptions: the secondary dithiol of one Trx1 molecule can only be modified by the active site of another Trx1 molecule; and the redox state of one dithiol does not affect the properties of the other in the same molecule.

2.4.2.6 Thioredoxin reductase

TrxR catalyses the reduction of the Trx1 active site by NADPH in a ping-pong mechanism [57]. The maximal rate for this process (≈1.0 μM s^{-1}, Supplementary Materials section 2.10.9) is lower than the TrxR activity for two reasons. First, the

total concentration of Trx in human erythrocytes is lower than $K_{M,TrxR,Trx1DT}$. Second, at high oxidative loads part of the Trx is converted to the double-disulfide form [56].

2.4.2.7 NADP

Most NADP in human erythrocytes is bound to proteins. Out of the total 40 μM NADP pool, 12 μM is tightly bound to proteins [39, 54], and the remaining is loosely bound. We assumed that this remaining pool of NADPH and $NADP^+$ instantaneously equilibrates between bound and unbound forms (Supplementary Materials section 2.10.10).

2.4.2.8 NADPH regeneration

$NADP^+$ reduction proceeds *via* the hexose monophosphates shunt. We modeled its kinetics through a phenomenological Michaelis-Menten equation that approximates the behavior at both low and high oxidative loads accurately, and interpolates the behavior at intermediate oxidative loads (Supplementary Materials section 2.10.11).

2.5 Computational Methods

We formalized the models as systems of algebraic-differential equations. The concentrations of H_2O_2 in plasma, the cytoplasmic concentration of GPx1 and the total cytoplasmic concentrations of Prx2, NADP, glutathionyl moiety and Trx1 are independent variables whose values are prescribed at the outset. All other concentrations were treated as dependent variables.

We computed steady state solutions numerically, applying Newton-Raphson's method as implemented in *Mathematica*™ 9.0.1 [58] *FindRoot* function with default settings. All steady state solutions examined are stable. We have also evaluated the logarithmic sensitivities of all the concentrations and reaction rates to all the parameters as described in [59, 60]. This analysis indicates that the model is robust with respect to uncertainties of parameters and independent variables (Supplementary Materials section 2.10.12).

In order to analyze the time-dependent behavior we integrated the systems of equations numerically in *Mathematica*™ using the function *NDSolve with default*

values except for the setting MaximumStepSize→0.1. Critical results were double checked through simulations in COPASI [61]. The Systems Biology Markup Language (SBML) [62] file for the COPASI implementation is available from the authors upon request.

2.6 Results

2.6.1 Observations with intact erythrocytes are inconsistent with a high effective peroxidase activity of Prx2

The kinetic parameters in Table 2.1 were determined from experiments using purified proteins or hemolyzates. Is a kinetic model strictly based on these data able to accurately simulate the H_2O_2 metabolism in intact human erythrocytes? We addressed this question by comparing the predictions of such a kinetic model (Model A) to experimental observations with intact cells.

Under basal conditions, Model A predicts an intracellular H_2O_2 concentration of 1.6 pM (0.068 H_2O_2 molecules/erythrocyte) (Table 2.2). All the redox pools remain extensively reduced, due in part to the 90 nM s^{-1} H_2O_2 supply being 27-fold lower than the erythrocyte's NADPH supply capacity: 2.4 µM s^{-1} [42]. All H_2O_2-consuming processes operate far from maximal capacity, and as consequence they display pseudo-first-order kinetics. The relative contributions of the various processes to H_2O_2 scavenging thus do not depend on model details and can be understood based on the simple model in Figure 2.2A. They are proportional to their pseudo-first-order rate constants obtained by multiplying the concentrations of each protein by the respective second-order rate constant for the reaction with H_2O_2. Namely, Prx2 (57 000 s^{-1}, 99.7%) >> Cat (146 s^{-1}, 0.26%) > GPx1 (25 s^{-1}, 0.044%). The overwhelming contribution from Prx2 ensues from both the higher second-order rate constant and the much higher concentration of this protein relative to those of Cat and GPx1 (Figure 2.2B). But estimates based on lower experimentally determined rate constant [23] for H_2O_2 reduction by Prx2 (k_{Ox}) and Prx2 concentration [63] are qualitatively similar (Table 2.2, second column).

2. Hydrogen peroxide metabolism in human erythrocytes

*Table 2.2. Computed steady state variables under resting conditions. $d_{1/2}$: mean diffusion distance computed as per refs. [64, 65] using the lowest effective diffusion constant determined in [66] for a hydrogel (3.7×10^{-10} m^2s^{-1}); f_X: fraction in form X; PSH, PSOH, PSO2H, PSS: Prx2 monomers with the peroxidatic Cys in thiol, sulfenic, sulfinic and disulfide forms, respectively; PSSPS*H, PSSPSS: Prx2 dimers with one or two disulfide crosslinks; $Trx1_{TT}$, $Trx1_{TD}$, $Trx1_{DT}$, $Trx1_{DD}$: Trx1 with the active (first character) and regulatory (second character) site in disulfide (D) or thiol (T) form.*

	Model A	**Model A'** $[Prx2]_{tot}$ = 357 µM k_{Ox} = 1.3×10^{7} $M^{-1}s^{-1}$	**Model B**
v_{Prx2}/v_{Cat}	390	31	1.0
Fraction of inhibited Prx2	0	0	0.997
$[H_2O_2]$, M	0.016×10^{-10}	0.19×10^{-10}	2.4×10^{-10}
$t_{1/2}(H_2O_2)$, µs	12	149	2170
$d_{1/2}(H_2O_2)$, µm	0.16	0.58	2.2
Fraction of H_2O_2 consumed by Prx2	0.997	0.96	0.47
Fraction of H_2O_2 consumed by Cat	2.6×10^{-3}	3.1×10^{-2}	0.47
Fraction of H_2O_2 consumed by GPx	4.4×10^{-4}	5.2×10^{-3}	6.8×10^{-2}
NADPH consumption, Ms^{-1}	8.9×10^{-8}	8.7×10^{-8}	4.6×10^{-8}
NADPH consumed per H_2O_2 eliminated	1	0.97	0.53
Fraction of NADPH consumed by TrxR	1	0.99	0.87
E(GSSG|GSH), V	-0.43	-0.40	-0.36
$E(NADP^+|NADPH)$, V	-0.39	-0.39	-0.40
$E(Trx_{Ox}|Trx_{Red})$, V	-0.28	-0.28	-0.29
f_{PSH}	1.0	0.99	1.0
f_{PSOH}	9.2×10^{-5}	1.4×10^{-4}	4.3×10^{-5}
f_{PSO2H}	1.7×10^{-8}	3.2×10^{-7}	1.3×10^{-6}
f_{PSS}	1.4×10^{-3}	2.1×10^{-3}	6.3×10^{-4}
$f_{PSSPS*H}$	2.7×10^{-3}	4.2×10^{-3}	1.2×10^{-3}
f_{PSSPSS}	1.9×10^{-6}	4.5×10^{-6}	7.9×10^{-7}
f_{Trx1TT}	0.97	0.97	0.99
f_{Trx1TD}	2.5×10^{-4}	2.5×10^{-4}	1.7×10^{-4}
f_{Trx1DT}	3.0×10^{-2}	2.9×10^{-2}	1.4×10^{-2}
f_{Trx1DD}	4.0×10^{-4}	3.7×10^{-4}	1.1×10^{-4}

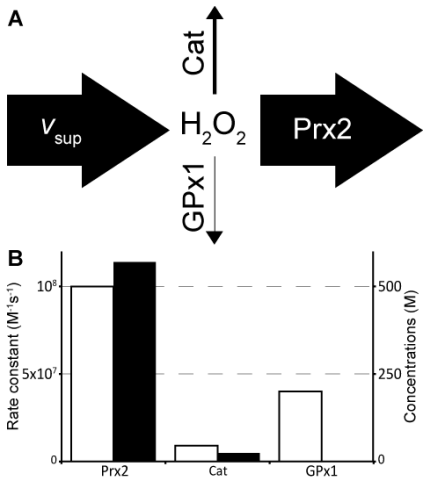

Figure 2.2. Simple model for H_2O_2 elimination at low H_2O_2 supply assuming that Prx2's peroxidase activity is as determined for the purified protein. (A) Main processes consuming H_2O_2 under these conditions follow pseudo-first-order kinetics. The fluxes are thus $v_{\mathrm{Prx2}} = k_{\mathrm{Ox}}[\mathrm{Prx2}][\mathrm{H_2O_2}] = k'_{\mathrm{Prx2}}[\mathrm{H_2O_2}]$, $v_{\mathrm{Cat}} = k_{\mathrm{Ferri}}[\mathrm{Cat}][\mathrm{H_2O_2}] = k'_{\mathrm{Cat}}[\mathrm{H_2O_2}]$, $v_{\mathrm{GPx1}} = \frac{[\mathrm{H_2O_2}]}{\phi_1} = k'_{\mathrm{GPx1}}[\mathrm{H_2O_2}]$ *, and the steady state concentration* $[\mathrm{H_2O_2}] = \frac{v_{\mathrm{sup}}}{k'_{\mathrm{Prx2}} + k'_{\mathrm{Cat}} + k'_{\mathrm{GPx1}}}$, *with vsup the H_2O_2 supply rate. If* k'_{Prx2} *is much higher than* k'_{Cat} *and* k'_{GPx1}*, then* $[\mathrm{H_2O_2}] \approx v_{\mathrm{sup}} / k'_{\mathrm{Prx2}}$*, and Cat inhibition or deletion cannot significantly affect [H2O2] and* v_{Prx2}*. (B) Protein rate constants (white bars) for reaction with H_2O_2 and monomer concentrations (black bars). The apparent second-order rate constant for Cat was computed by applying equation (4) from Supplementary Materials section 2.10.6 and the values for kFerri and kCl from Table 2.1; the second-order rate constant and the concentration of active monomers for GPx1 were inferred by comparing the value of $\phi 1$ determined in Supplementary Materials section 2.10.5 to the value of $\Phi 1$ determined in [52].*

Remarkably, the prediction that Prx2 consumes virtually all the H_2O_2 conflicts with substantial experimental evidence [1, 3, 67, 68] (discussed in Supplementary Materials section 2.10.13.1) that in intact erythrocytes at low H_2O_2 concentrations its contribution is comparable to Cat's. Further, simulations based on Model A show strong inconsistencies with experimental observations in [2] for human erythrocytes exposed to various H_2O_2 boluses (Figure 2.3A,E).

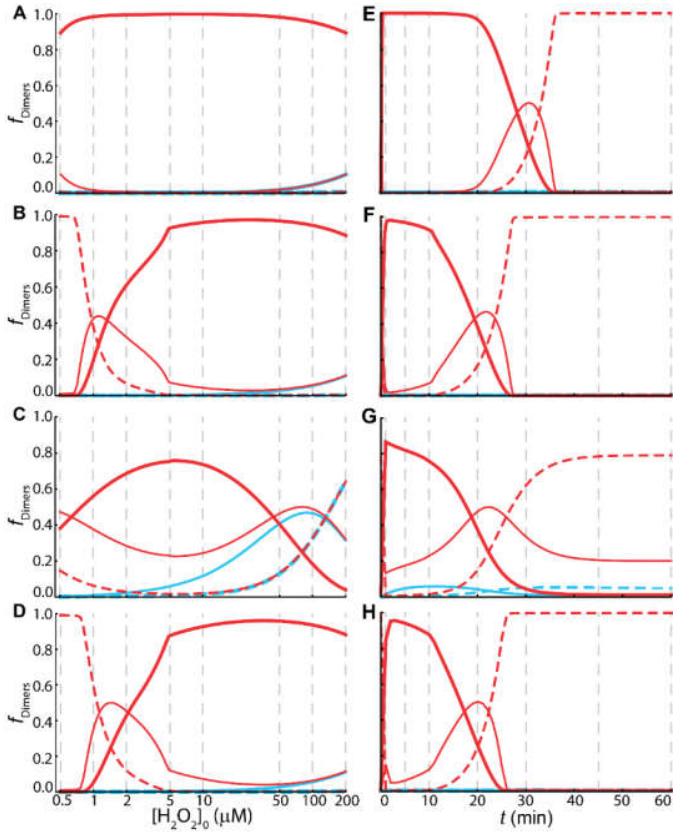

Figure 2.3. Simulation of responses of Prx2 in intact erythrocytes to H2O2 boluses as per experiments in [2]. Low et al. [2] exposed human erythrocytes (5×10⁹ cells dm⁻³, pH 7.4, 37° C, 5 mM glucose) to H2O2 boluses and determined the fractions of Prx2 monomers or disulfide-crosslinked dimers in non-reducing SDS–polyacrylamide gel electrophoresis gels for the boluses and times. Disulfide Prx2 ran in most cases as a double band, the upper and lower components of which corresponding to dimers with one and two disulfides, respectively [22]. Comparisons to simulation results must take into account that the experiments overestimate the fraction of oxidized Prx2, owing to adventitious oxidation during sample handling [2]. In order to simulate these experiments models were modified by (i) treating the extracellular concentration of H_2O_2 as a dependent variable, with compartment volumes accounting for the hematocrit of the assay medium, and (ii) assuming a 57 nM s^{-1} endogenous H_2O_2 production reflecting the higher rate of GSH autoxidation under atmospheric pressure (discussed in Supplementary Materials section 2.10.2). Plots represent the fractions of non-crosslinked (dashed), singly-crosslinked (thin solid lines) and doubly-crosslinked (thick solid line) Prx2 dimers, sulfinylated (cyan) or not (red), obtained by exposing 5×10⁹ cells dm^{-3} to H_2O_2 boluses according to the experiments in Figures 2 and 4 of [2]. (A – D) Simulations based on models A – D, respectively, at t= 10 min after exposure of erythrocytes to various boluses. Compare to Figure 2A,B of [2]. Vertical dashed lines indicate the experimental boluses. H2O2 concentrations are represented in logarithmic scale. In panels A, and B, the thin cyan lines overlap the thin red lines for high boluses, indicating that virtually all the singly-crosslinked dimers are sulfinylated under these conditions. Likewise, the dashed cyan line overlaps the dashed red line in panel C. (E – H) Simulations based on models A – D, respectively, for the 60 min following exposure of 5×10⁹ cells dm^{-3} to a 5 μM H_2O_2 bolus. Vertical dashed lines indicate the times at which dimer fractions were experimentally determined. Further information in Supplementary Materials section 2.10.13.2.

The conflict between the experimental observations with intact erythrocytes and the high peroxidase activity implied by the high Prx2 abundance [63, 68] and high value of k_{Ox} [23, 24] could have three alternative explanations. Below we use several modifications of Model A to assess the consistency of these explanations with the experimental data.

The first explanation is that the experimentally determined concentrations and rate constants are reliable but Prx2's peroxidase activity in erythrocytes is strongly inhibited. However, most of the Prx2 is oxidized to the disulfide form within 1 min when erythrocytes are exposed to a strong H_2O_2 bolus, and the timing of reduction of the disulfide is consistent with the determined activity of TrxR [2]. Therefore, the hypothetical inhibitor must essentially titrate active Prx2 out, readily release it from inhibition as the active pool is depleted, and not severely limit Prx2 reduction. In order to model this inhibition parsimoniously, we modified Model A by considering that reduced Prx2 monomers quickly equilibrate with a form that cannot reduce H_2O_2. The equilibrium constant (K_{Prx2}= 1.7×10^2) was chosen so that Prx2's contribution for H_2O_2 consumption matched Cat's at the basal steady state. This implies a >99% inhibition. The modified model (Model B) simulates near-quantitatively the detailed experimental observations in [2] and explains some puzzling phenomenology therein (Figure 2.3B, F and additional results in Supplementary Materials section 2.10.13.2). Additionally, the predicted redox potentials of Trx1 and NADPH agree with literature values (Table 2.2 and Supplementary Materials section 2.10.13.2). There is a strong disagreement with the high rates of Prx2 sulfinylation observed in experiments in [4]. However, this is likely because in these experiments H_2O_2 production *via* glucose oxidase in absence of erythrocytes strongly underestimated production in presence of erythrocytes (Supplementary Materials section 2.10.13.3). It should be noted that owing to lack of available data our models do not account for Prx1, which occurs in erythrocytes at 1.2% of Prx2's abundance [68]. Should Prx1 be as reactive with H_2O_2 as purified Prx2, it could account for virtually all the NADPH-dependent H_2O_2 consumption observed in erythrocytes that lack Cat activity (Supplementary Materials section 2.10.7). One would then have to hypothesize a complete inhibition of Prx2's peroxidase activity to explain these observations. However, an effective rate constant for H_2O_2 reduction by Prx2 in cells much lower than 10^5

$M^{-1}s^{-1}$ would be inconsistent with the observation [2] that Prx2 is rapidly oxidized upon exposure of 5×10^9 erythrocytes/dm^3 to a 5 μM H_2O_2 bolus (further details in Supplementary Materials section 2.10.7). This suggests that Prx2 does not contribute much less than Cat for H_2O_2 consumption under low H_2O_2 supplies, and that the *effective* rate constant for H_2O_2 reduction by Prx1 is also lower than 10^8 $M^{-1}s^{-1}$.

As a second explanation, Prx2's concentration [63, 68] might have been severely overestimated. We modeled this possibility by decreasing the total concentration of Prx2 in Model A to ≈1 μM, so that Prx2's contribution for H_2O_2 consumption matched Cat's at the basal steady state. However, this model (Model C) yielded results that are inconsistent with the experimental observations (Figure 2.3C,G). Further, the ≈1 μM Prx2 concentration is much lower than implied by the fraction of lysate protein obtained through the methods [69, 70] used to purify Prx2 for the determinations of k_{Ox} [23, 24]. And because the obtained values of k_{Ox} are referred to the mass of these Prx2 preparations, the estimated total Prx2's peroxidase activity in cells is practically independent of the latter's purity. Therefore, this explanation is unviable.

As a third explanation the value of k_{Ox} might have been severely overestimated. We modeled this possibility by decreasing that value in Model A to 3.015×10^5 $M^{-1}s^{-1}$, which makes Prx2's contribution for H_2O_2 consumption identical to Cat's at the basal steady state. The modified model (Model D) simulates the experimental observations in [2] as accurately as Model B (Figure 2.3D,H) and predicts similar redox potentials. Further, the observation that Prx2 forms complexes with many proteins [25-28], including Cat [26, 28], suggests that interactions with Cat or horseradish peroxidase (EC 1.11.1.7) in the competition assays might have interfered with the determinations [23, 24] of k_{Ox}. Such interactions might inhibit the competing enzyme or activate Prx2. However, the four different experiments in refs. [23, 24] all yield k_{Ox} values in the range 6×10^6–1.0×10^8 $M^{-1}s^{-1}$, with the most accurate experiments yielding the highest values. And despite having been carried out at a range of Prx2:Cat and Prx2:peroxidase ratios, none shows evidence of the anomalous behavior that interactions with Prx2 should cause (Supplementary Materials section 2.10.7). Further, an extensive inhibition of Cat by Prx2 is inconsistent with the observations [1-3, 67, 68] showing substantial

effects of Cat modulation in intact erythrocytes. In turn, activation of isolated Prx2 by Cat is inconsistent with observations [23] of Prx2 oxidation decreasing with increasing Cat activity.

Altogether, the whole body of experimental evidence favors the first explanation.

2.6.2 A low effective peroxidase activity of Prx2 spares NADPH and improves potential signaling properties

Prx2 is the third most abundant protein in human erythrocytes. Further, its very high reactivity requires a precise arrangement of aminoacyl residues in the active site [71], and would thus be lost to mutational drift in absence of a selective pressure requiring its maintenance. How can these considerations be reconciled with a strong inhibition of the peroxidase activity in human erythrocytes?

Below we examine the hypothesis that a large amount of reversibly inhibited Prx2 — the design represented by Model B — conveys advantages that cannot be achieved by a lower amount of Prx2 (Model/Design C) or a less H_2O_2-reactive Prx2 (Model/Design D). These advantages might be related to the management of the NADPH pool, and/or to the action of Prx2 as H_2O_2 sensor for the Cat/Prx2/Trx1/TrxR system (CPTTRS) functioning as a transducer of H_2O_2 supply (v_{sup}) into protein thiol redox states. We consider as potential signaling outputs the concentrations or redox potentials of any forms of Prx2 or Trx1 that can in principle specifically react with or bind to other proteins not part of the CPTTRS, regulating their activities. Additionally, the intracellular concentration of H_2O_2 is also an *output* because it is largely determined by the CPTTRS and it can be read by other cellular sensors. For the CPTTRS to be a good *analogic* transducer it must satisfy at least the following two criteria. First, the output must be sensitive to the input. This sensitivity is normally measured by the gain (g) of the output (y) with respect to the input (x): $g = \frac{\partial \log y}{\partial \log x} \approx \frac{x}{y}\frac{\Delta y}{\Delta x}$, for small Δx. A good gain normally means $g \geq 1$. Second, there should be a wide region of constant gain. That is, a region where a c-fold change in the input consistently translates into a c^g-fold change in the output so that the signal is transmitted undistorted. Constant gain regions are characterized by straight lines in plots of log y *vs*. log x. The ratio between the highest value of x in the constant gain region

and the lowest value of *x* in the region (or the basal value of *x* if the region extends to lower values) is denoted by “dynamic range”. For the CPTTRS to be a good *digital* transducer it has to satisfy at least the following criteria. First, the ratio between the output value at the “high” state and that at the “low” state must be high enough to clearly separate the two states despite sporadic fluctuations. Second, transition between the “low” and “high” state must occur within a narrow range of the input, a property denoted as “decisiveness”.

Armed with these concepts and terminology, we will now examine the extent to which Designs B-D of the CPTTRS fulfill the criteria above. Models B-D permit a meaningful comparison among these three otherwise equivalent designs, as the only differing parameters were adjusted so that the same steady state H_2O_2 concentrations, consumption rate and fractional contributions of Cat *vs.* Prx2 obtain under the reference (basal) conditions. We also compare to Model/Design A to examine the consequences of its high peroxidase activity.

At steady state, Designs A, B and D respond to increasing H_2O_2 supply (v_{sup}) as follows (Figure 2.4). At low v_{sup}, the fractions of Prx2 monomers in sulfenic and disulfide forms, as well as the fraction of Trx with the active site oxidized, increase near-linearly. In turn, the fraction of Prx2 monomers in sulfinic form increases quadratically with v_{sup}. The latter follows from this species forming upon two successive oxidations by H_2O_2. At higher v_{sup} the Prx2 oxidation rate approaches TrxR’s capacity to reduce Trx. As a consequence Trx accumulates in singly- and then doubly-oxidized forms. Because the latter is not a TrxR substrate, Prx2 reduction and the Trx redox potential (in absolute value) sharply decrease and cause a sharp accumulation of Prx2 disulfide and a steep decline in H_2O_2 reduction.

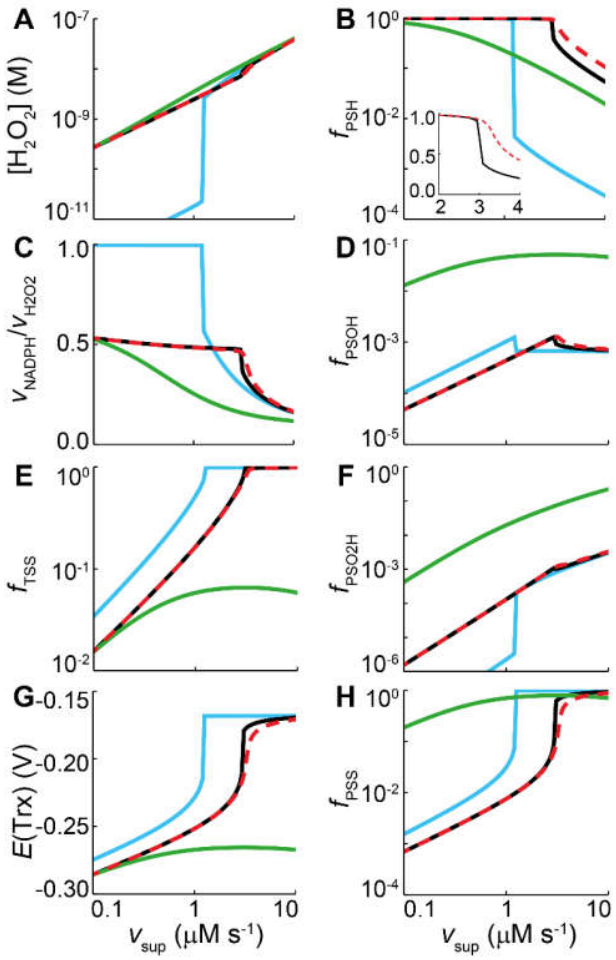

Figure 2.4. Steady state responses of alternative designs of the Prx2 redox cycle in H_2O_2 metabolism to changes in H_2O_2 supply. Cyan, Design A; Black, Design B; Green, Design C; Dashed red, Design D. Each design corresponds to the respective model variant described in Table 2.1. Note the logarithmic scales, except for E(Trx) in (G). (A) H_2O_2 concentration. Note (i) the extremely low H_2O_2 concentrations at low v_{sup} and very abrupt increase for Design A, and (ii) the higher H_2O_2 concentrations at intermediate v_{sup} for Design C. (B) Fraction of Prx2 monomers in reduced form. Note (i) the abrupt decrease for Design A occurring at v_{sup} values about half of those causing a milder decrease for Design B,D, and (ii) the gradual decrease for Design C, starting at very low v_{sup} and resulting in most Prx2 being oxidized at intermediate v_{sup}. (C) Ratio between rates of NADPH and H_2O_2 consumption. Note (i) the much higher NADPH consumed per H_2O_2 at low vsup for Design A, and (ii) lower NADPH consumption per H_2O_2 for Design C, reflecting respectively the high and low contributions of Prx2 for H_2O_2 elimination under these designs. (D) Fraction of Prx2 monomers in sulfenic form. (E) Fraction of Trx with the active site oxidized. Note the much lower accumulation of this form under Design C. (F) Fraction of Prx2 monomers in sulfinic form. Note (i) the much higher values under Design C, and (ii) the high gain (2) over most of the v_{sup} range under all designs. (G) Redox potential of the Trx active site. (H) Fraction of Prx2 monomers in disulfide form. In panels D-H, note (i) the higher dynamic ranges provided by Designs B, D as compared to Designs A, C; (ii) except in (F), the low gains and very low dynamic range provided by Design C. In panels B (inset), G, H note the better decisiveness provided by Design B vs. Design D. Accumulation of Prx2 in sulfenic (D) and sulfinic (F) forms is negligible under Designs A, B, D, but not under Design C.

These three designs provide sensitive constant-gain responses of various potential signaling outputs (Figure 2.4A,D,E,F,H) to changes in v_{sup}, over large dynamic ranges. The dynamic ranges extend to ≈2-fold higher values in Designs B and D relative to Design A, owing to less than half of the supplied H_2O_2 being consumed *via* Prx2. Further, the former two designs spend much less NADPH per H_2O_2 consumed than the latter (Figure 2.4C). Overall, the responses of Designs B and D are very similar, but Design B provides better digital transduction (Figure 2.4B,G,H) than Design D, separating the proportional response from the saturated regime through a stronger and more decisive threshold. This feature may be advantageous in activating a stress response at a sharp stress threshold.

In contrast, Design C fails to yield a constant-gain response or to achieve substantial oxidation of the Trx pool, owing to the low Prx2 concentration. Furthermore, it leads to extensive Prx2 sulfinylation at high values of v_{sup}. The latter due to Trx1 remaining mainly in reduced form even at high v_{sup}, therefore readily regenerating the Prx2 dithiol and ensuring a steady supply of sulfenic Prx2.

Erythrocytes are often exposed to brief H_2O_2 concentration pulses as they cross inflammation sites (see “Physiological setting” section), which makes the dynamic response relevant (Figure 2.5-7). Relative to Design A, Designs B and D are characterized by lower total NADPH expenditure (Figure 2.7A) and extended dynamic ranges (Figure 2.7B-G). Further, the latter two designs show faster recovery of the redox pools after H_2O_2 pulses (Figure 2.5,). This feature is advantageous to avoid a gradual build up of oxidized forms of Prx2, Trx1 and GSH as erythrocytes recurrently cross inflammation sites, as may happen in pulmonary infections (see “Physiological setting” section). Overall, Designs B and D show similar dynamic behavior. In contrast, in Design C even modest H_2O_2 pulses fully oxidize Prx2 (Figure 2.5E). As consequence, almost all the potential signaling outputs saturate at low pulse amplitudes: with the exception of the fraction of sulfinylated Prx2, the response to 3 s, 0.5 μM plasma H_2O_2 pulses is similar to the response to 50 μM pulses (Figure 2.5C-E).

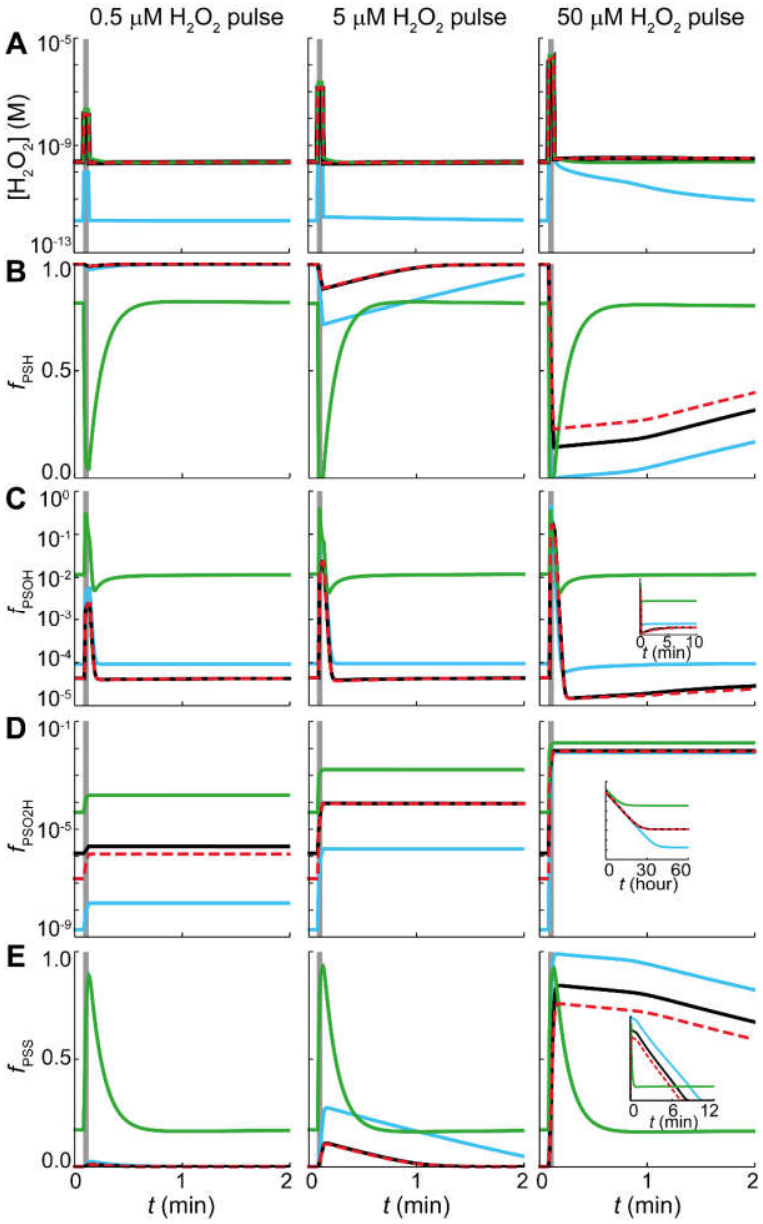

Figure 2.5. Responses of intracellular H_2O_2 concentration and Prx2 oxidation states to extracellular H_2O_2 pulses. Time courses of the intracellular H_2O_2 concentration (A), and of the fractions of Prx2 monomers with the peroxidatic Cys in thiol (B), sulfenic (C), sulfinic (D) and disulfide (E) form upon 3 s pulses of 0.5 μM, 5 μM, and 50 μM local plasma H_2O_2 concentrations. Vertical gray bars indicate the timing and duration of the H_2O_2 pulses. The correspondence of lines to designs is as for Figure 2.4. Recovery of the PSH pool after the strongest H_2O_2 pulses is delayed due to strong competition of GSR for NADPH following GSSG accumulation during the pulse (see Figure 2.6B,C). Note the strong oxidation of Prx2 caused by even relatively weak H_2O_2 (Figure 2.5 ctd.) pulses in Design C, due to the total concentration of Prx2 in this design being less than half the dose of H_2O_2 entering the erythrocyte during the pulse. Note also the very slow reduction of the sulfinic Prx2 accumulated during the pulse.

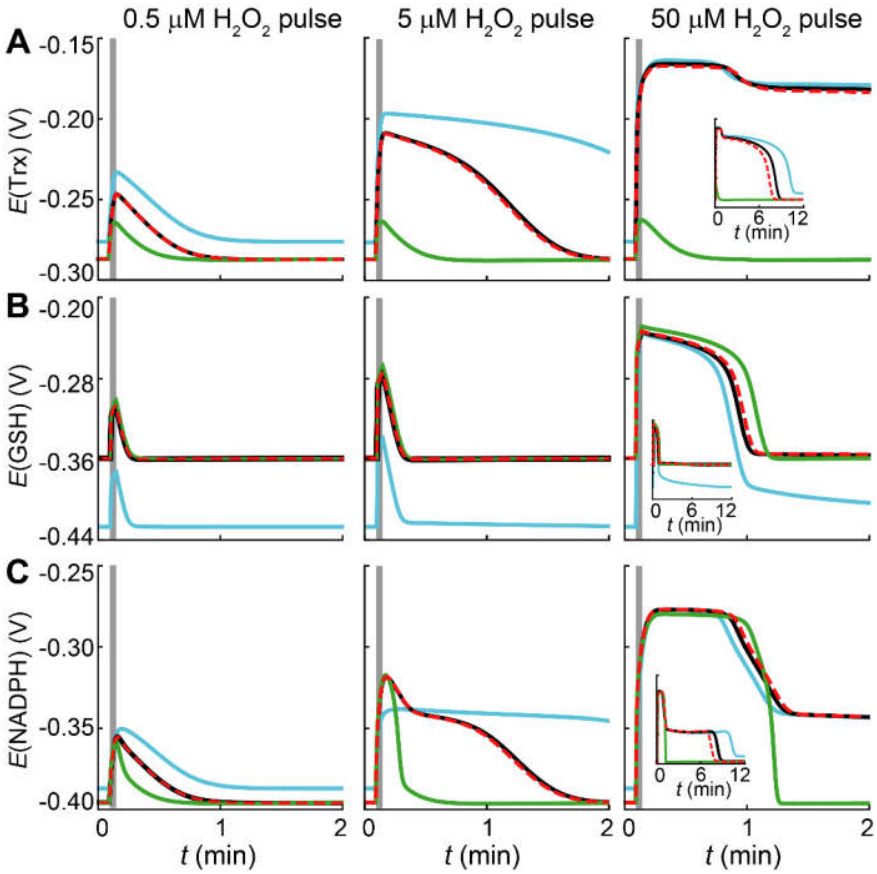

Figure 2.6. Responses of the potentials of redox pools to extracellular H_2O_2 pulses. The correspondence of lines to models is as for Figure 2.4. Time course of the redox potentials of Trx1 (A), GSH (B) and NADPH (C) upon 3 s pulses of 0.5 μM, 5 μM, and 50 μM local plasma H_2O_2 concentrations. Vertical gray bars indicate the timing and duration of the H_2O_2 pulses. Note the delay in the recovery of all the redox potentials after the strongest pulses. This ensues mainly from NADPH depletion by the GSR-catalyzed reduction of GSSG accumulated during the pulse and from the limited rate at which erythrocytes can reduce $NADP^+$ to NAPDH.

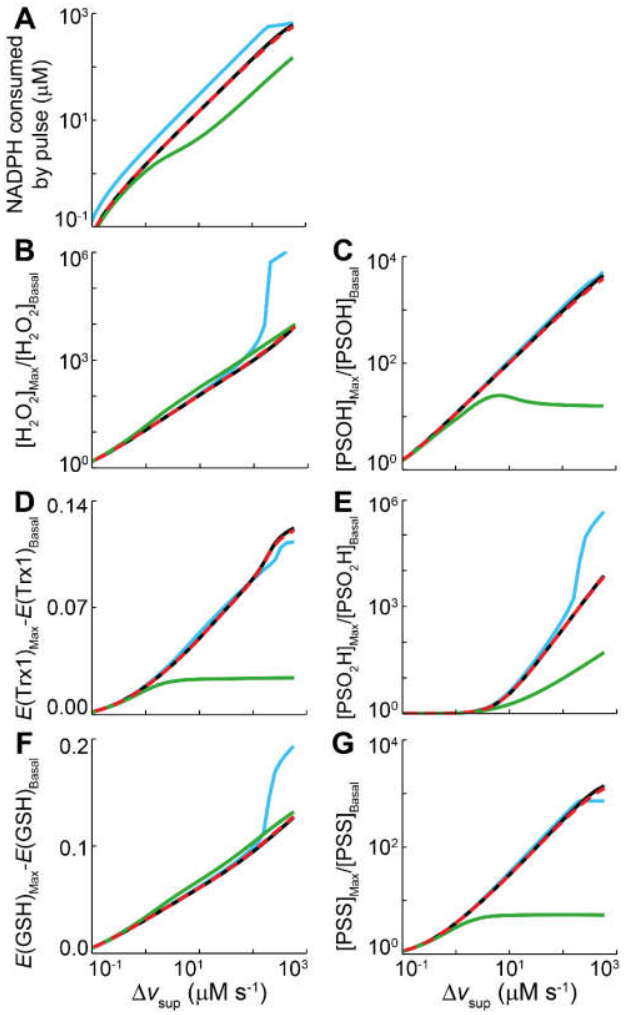

Figure 2.7. Responses of intracellular variables as function of the amplitude of 3 s H_2O_2 supply pulses. The correspondence of lines to models is as for Figure 2.4. Exception for the yy axes in D and F, all plots are in logarithmic scale. (A) NADPH consumed due to pulse, computed by integrating NADPH consumption from onset of 3 s pulse to full relaxation of all variables to within 1% of their pre-pulse steady state values and subtracting the NADPH consumed over the same time period in absence of a pulse. Note the higher consumption by Design A. The lower consumption by Design C is due to a lower contribution of Prx2 for H_2O_2 elimination, resulting in higher intracellular H_2O_2 concentrations (B). (B, C, E, G) Maximum fold changes of the concentrations of intracellular H_2O_2, sulfenic Prx2, sulfinic Prx2 and disulfide Prx2, respectively. (D, F) Maximum redox potential change of Trx and GSH, respectively. Note the larger dynamic ranges provided by Designs B, D in panels B, C, E-G, and the low dynamic range provided by Design C in panels C, D, G. The threshold effect in (E) ensues from the following. For a significant accumulation of Prx2 in sulfinic form to occur (E) the intracellular H_2O_2 concentration must be high enough for its reaction with the sulfenic acid to compete with the condensation reaction. The amplitude of the extracellular H_2O_2 concentration pulse ($\Delta[eH_2O_2]$) causing a Δv_{sup} pulse is given approximately by $\Delta[eH_2O_2] = \Delta v_{sup}/k_p = \Delta v_{sup}/(10.9\ s^{-1})$.

2.7 Discussion

This work presents an up-to-date quantitative assessment of the H_2O_2 metabolism in human erythrocytes, which allowed us to evaluate the consistency of the present knowledge about this process. Computational predictions based on available kinetic data were compared to experimental observations of intact human erythrocytes, and flagged a fundamental discrepancy. On one hand, the rate constants [23, 24] for H_2O_2 reduction by Prx2 and its concentration [63, 68] in reduced, non-sulfinylated form [2, 4, 72] would make it almost solely responsible for clearing H_2O_2 in human erythrocytes at physiological supply rates. On the other hand, extensive evidence (Supplementary Materials section 2.10.13.1) indicates that Prx2's contribution for H_2O_2 elimination is comparable to Cat's. Also, most Prx2 is oxidized to the disulfide form within 1 min when 5×10^9 erythrocytes/dm^3 are exposed to a 5 μM H_2O_2 bolus [2].

Altogether, these observations indicate that the *effective* rate constant for H_2O_2 reduction by Prx2 in erythrocytes is much lower than that determined for the purified protein. This may be because the experimental determinations over-estimated the rate constant by two orders of magnitude, or because Prx2's peroxidase activity is strongly (>99%) but reversibly inhibited in cells. Accounting for either one of these hypotheses permitted simulating the detailed experimental results in [2] accurately. However, the raw experimental data [67, 73] does not support the possibility of an over-estimation of the rate constant caused by the association of Prx2 to Cat or horseradish peroxidase, which adds weight to the alternative hypothesis.

The hypothetic inhibition is unlikely to be mediated by covalent post-translational modifications for the following two reasons. First, the Prx2 in the kinetic studies in [23, 24] should carry the same covalent modifications as in the human erythrocytes from which it was purified; yet it has very high peroxidase activity. Second, the fast turnover implied by the fast Prx2 oxidation observed in [2] makes regulation by covalent modification energetically forbidding (see Supplementary Materials section 2.10.14.1).

A binding-dissociation (near-)equilibrium is a more likely inhibitory mechanism. However, one must acknowledge the lack of obvious inhibitors. These must be in

sufficient excess over Prx2 to titrate it and form an inhibitory complex that is weak enough to permit ready dissociation. Few known erythrocyte metabolites and only two proteins — carbonic anhydrase and hemoglobin — are sufficiently abundant. No low molecular weight (MW) physiological effectors of Prx2 with the necessary characteristics are known at present. In turn, Prx2 binds hemoglobin and this binding is necessary for protecting the latter against H_2O_2-induced aggregation [5]. It is unknown if this interaction inhibits Prx2's peroxidase activity.

Prx2 also forms complexes with many less abundant proteins [25-28]. At least some of these complexes show peroxidase activity and can localize Prx2 to the membrane in a regulated way [26, 27]. An estimated 5% of the erythrocyte Prx2 is membrane-associated in absence of oxidative stress [63], and this fraction increases under oxidative stress [27]. Altogether, the strong inhibition suggested by our results and these observations suggest the following possibility. The peroxidase activity of Prx2 in human erythrocytes is deployed only where and when needed, through a process of regulated molecular transfer (a.k.a. "regulated recruitment") from inhibitory to non-inhibitory complexes (Figure 2.8).

The experimental observations above raise the question of whether H_2O_2 concentration gradients or the localization of a fraction of the Prx2 to the cell membrane might explain the discrepancy between the molecular data and the observations with intact erythrocytes. However, this would ensue only if Cat and not Prx2 was strongly localized to the sites of H_2O_2 supply, for which there is no evidence in the literature. The localization of Prx2 to the sites of H_2O_2 supply should instead further increase its contribution for consumption at low H_2O_2 concentrations.

Nevertheless, the peroxidase activity of Prx2 has strong implications for the spatial distribution of H_2O_2. The high peroxidase activity implied by the experimentally determined rate constants leads to H_2O_2 mean diffusion lengths (Table 2.2) substantially lower than the erythrocyte thickness (≈1 μm) and thus to substantial intracellular concentration gradients. In contrast, the much lower *effective* peroxidase activity implied by the observations with intact erythrocytes leads to a negligible gradient.

2. Hydrogen peroxide metabolism in human erythrocytes

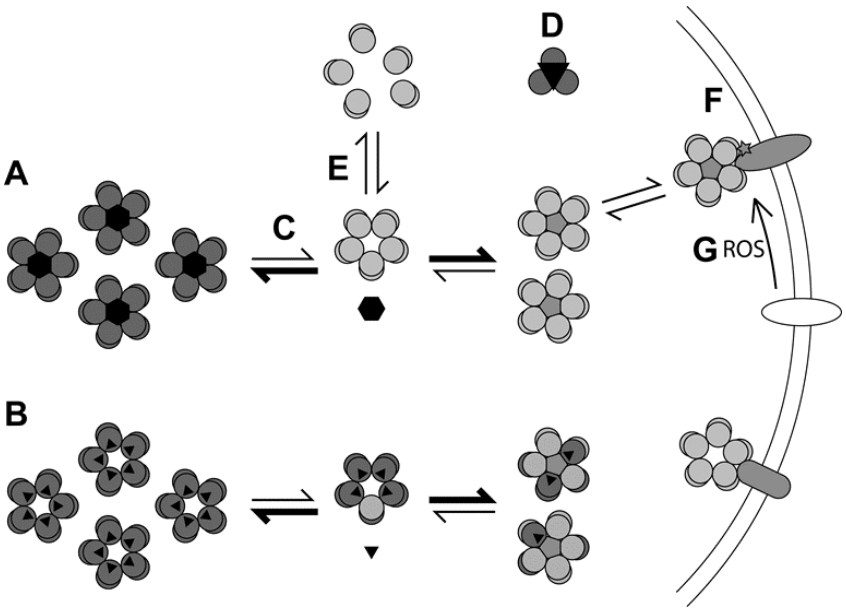

Figure 2.8. Prx2 binding states and peroxidase activity. We hypothesize that most Prx2 in human erythrocytes is bound to an agent that inhibits its peroxidase activity. This agent could be hemoglobin (black hexagons), eventually inhibiting at the Prx2 decamer level (A), or a metabolite (small black triangles), likely inhibiting at the Prx2 monomer level (B). For consistency with the experimental data for erythrocytes the inhibitor-Prx2 complex must be thermodynamically favored, but dissociate with a $k_{-} > \approx 0.1\ s^{-1}$ (C). Prx2 binds several cytoplasmic proteins in various oligomeric arrangements (D). Examples include Cat tetramers [28] (pentagons), and alcohol dehydrogenase 1 ($NADP^+$) homodimers (large triangle) [28]. The former complex does not inhibit Prx2's peroxidase activity [26], whereas the latter is presumed to inhibit this activity as it disrupts Prx2's dimers. Given the small fraction of peroxidatically active Prx2 and its propensity to bind other proteins, free Prx2 may occur at sub-μM concentrations, in which case it will be predominantly in dimeric form [24, 74] (E). A small fraction of Prx2 associates to membrane proteins such as stomatin [25] and Band 3 [27] (F). This fraction increases during oxidative stress, and this increase is at least in part mediated by changes in Band 3 [27] (G). Cat-Prx2 complexes bind the erythrocyte membrane under oxidizing conditions [26], but binding to Band 3 as depicted is uncertain. Circles, Prx2 monomers (peroxidatically active, light gray, or inactive, dark gray); black polygons, inhibitory binding agents (proteins, large, or metabolites, small); gray polygons, non-inhibitory binding agents; white, non-binding.

The hypothesis that Prx2's peroxidase activity is strongly inhibited has the following functional implication: the main role of Prx2 in human erythrocytes cannot be to minimize the intracellular concentration of H_2O_2 or of any other peroxide substrates. Indeed, H_2O_2 not being very reactive, the benefits of keeping its concentration at <0.1 molecules/cell (Table 2.2) can hardly balance their high

costs. Namely, the investment of 2.7% of this cell's cytoplasmic protein mass in Prx2 [68], and the waste of 1 NADPH/H_2O_2. More efficient protection against H_2O_2 could be achieved at much lower protein mass and ≈0 NADPH/H_2O_2 by doubling the amount of Cat. Further, the low H_2O_2 concentrations above would be too low to significantly oxidize less abundant [68] sensors such as Prx1 and Prx6 before Prx2 becomes fully oxidized. Instead, the large amount of Prx2 in erythrocytes may be required for it to protect proteins against unfolding and aggregation as a holdase [75] and/or for effective signaling. A strong but quickly reversible inhibition would then alleviate the NADPH cost of the "excessive" peroxidase activity while leaving the reducing equivalents in Prx2 available to help eliminating H_2O_2 under stress.

Although high-MW Prx2 (>240 kDa) multimers triggered by sulfinylation show the strongest holdase activity [75], lower-MW forms that predominate at low oxidative loads [24, 74] also show substantial activity [5, 72, 75]. In turn, Prx2 has also been involved in various signaling processes [76, 77].

Remarkably, our computational results indicate that a design with abundant Prx2 subject to strong reversible inhibition (Design B) has better signal transduction properties than a design with low Prx2 abundance (Design C). Namely (Figure 2.4, Figure 2.5), it provides (a) a large dynamic range where changes in H_2O_2 supply translate into proportional changes in potential signaling outputs, and (b) a sharp transition between a proportional response regime and a saturated regime where potential signaling outputs are at their maximum values. Property (a) is desirable for analogic signal transduction, whereas property (b) is desirable for digital signal transduction (e.g. for triggering an emergency response). Design B achieves these advantages at a lower NADPH cost, faster recovery of the Prx2 and Trx1 redox states after perturbation and extended range of proportional response relative to a design with normal Prx2 abundance and no inhibition (Design A). It is also the design that provides the best digital signal transduction.

Peroxiredoxins are very abundant in most cell types [78] where this poses similar problems of NADPH waste in H_2O_2 elimination and inhibition of competing H_2O_2 signaling pathways. An effective peroxidase activity that is well balanced with Cat's H_2O_2 dismutase activity and with the reactivities of other H_2O_2 sensors should have the same advantages in these cells as highlighted in this work for

human erythrocytes. These possibilities highlight the complexity of thiol redox systems and call for integrated theoretical-experimental approaches towards improving our understanding.

2.8 Highlights

- An accurate mathematical model of H_2O_2 metabolism in human erythrocytes is set up
- The physiological setting and dynamics of erythrocyte exposure to H_2O_2 are examined
- Observed responses of erythrocytes contradict a high peroxidase activity of Prx2
- A strong reversible inhibition of Prx2's peroxidase activity in cells is proposed
- Low effective Prx2's peroxidase activity spares NADPH, improves signaling

2.9 Acknowledgements

We acknowledge fellowship SFRH/BD/51199/2010 to RB and grants PEst-C/SAU/LA0001/2013-2014, PEst-OE/QUI/UI0612/2013, PEst-OE/QUI/UI0313/2014, and FCOMP-01-0124-FEDER-020978 financed by FEDER through the "Programa Operacional Factores de Competitividade, COMPETE" and by national funds through "FCT, Fundação para a Ciência e a Tecnologia" (project PTDC/QUI-BIQ/119657/2010).

2.10 Supplementary Materials

Additional information on parameter estimates and model validation.

2.10.1 Unit conversions

We refer all metabolite and protein concentrations and rates to erythrocyte water volume, rather than total cell volume as is more usual in the literature. We made this choice because the former concentrations are more relevant for determining the rates of intracellular biochemical processes. Conversions assume water volume to cell volume ratio of 0.717 [79] and an erythrocyte volume of 10^{-13} dm^3

[80]. Accordingly, in conversions from quantities expressed in terms of hemoglobin mass we consider an erythrocyte contents of 485 g hemoglobin / dm^3 erythrocyte water [79]. Except where otherwise stated, in converting from quantities expressed in terms of protein mass we assume that hemoglobin accounts for 90% of erythrocyte protein mass.

2.10.2 Endogenous H_2O_2 production

The autoxidation of oxyhemoglobin to methemoglobin is often cited as the main endogenous source of H_2O_2, *via* $O_2^{\bullet-}$, in the erythrocyte [1, 2, 81]. The mean rate of $O_2^{\bullet-}$ production *in vivo* from this process can be estimated as follows. The main enzyme responsible for methemoglobin reduction is Cyt b5 reductase, and in methemoglobinuria patients carrying a mutation that eliminates this activity 0.5 to 3% of the hemoglobin is oxidized to methemoglobin each day [82]. Considering [Hb]= 7 mM [83] and 3% oxidation/day, this gives $0.03\times4\times7\times10^{-3}/[(24\text{ h})\times(3600\text{ s/h})]$= 9.6 nM subunits/s, and an equal $O_2^{\bullet-}$ production. This rate is of the same order of magnitude as the 20 nM s^{-1} rate determined in ref.[84] for hemolyzates of packed cells at the pO_2= 90 Torr prevailing in arterial blood. Virtually all this $O_2^{\bullet-}$ is dismutated, yielding 1/2 H_2O_2 per $O_2^{\bullet-}$.

GSH autoxidation may also contribute relevantly to H_2O_2 production. This process occurs both enzymatically [85] and non-enzymatically [86]. The non-enzymatic oxidation is a multi-step process that follows overall second-order kinetics — and pseudo-first-order kinetics for O_2 and for GSH — with an apparent rate constant k_{spont}= 0.10 $M^{-1}s^{-1}$ (expressed in terms of GSSG production) determined at pH 9.2, 23 ºC [86]. In order to estimate the implied H_2O_2 production under physiological conditions one must take into account that it is the thiolate anion (GS^-), not the protonated thiol, that reacts with O_2. As follows from applying the Henderson-Hasselbach equation, the concentration of GS^- at the physiological pH (7.2) is just 5.0% of that at pH 9.2, considering that the thiol has pK_a= 8.7 [87]. The apparent rate constant will thus be proportionally lower at pH 7.2. Therefore, at pO_2= 90 Torr and a fully reduced GSH pool of 3.2 mM ref.[31], considering an O_2 solubility of 1.7×10^{-6} M $Torr^{-1}$ [88], this rate constant translates into a rate of H_2O_2 production of $0.05\times(90\text{ Torr})\times(1.7\times10^{-6}\text{ M Torr}^{-1})\times\times(0.10\text{ M}^{-1}\text{s}^{-1})\times(3.2\times10^{-3}\text{ M})$= 2.5 nM s^{-1} at 23 ºC.

2. Hydrogen peroxide metabolism in human erythrocytes

The enzymatic GSH autoxidation is catalyzed by Cu-Zn superoxide dismutase (SOD, EC 1.15.1.1) [85]. This thiol oxidase activity of SOD is still poorly characterized. However, Winterbourn *et al.* [85] have shown that 1.2 μM of bovine SOD incubated in air at pH 7.4 and 37 ºC, catalyzes the oxidation of 1 mM GSH at a rate of 8.3 nM s^{-1}. Given the higher concentrations of GSH and SOD (2 μM [89]) and slightly lower pH in human erythrocytes, the contribution of this process towards endogenous H_2O_2 production might be relevant.

The following experiment [31] further highlights the potential relevance of GSH autoxidation *in vivo.* In erythrocytes incubated at 37 ºC under a humidified stream of O_2:CO_2 19:1 (pO_2= 722 Torr) in absence of glucose the concentration of GSH decayed over 6 h with first-order kinetics. The rate constant was k_{ox}= 7.4×10^{-5} s^{-1} [16] (expressed in terms of GSSG production) [16]. One can estimate the pseudo-first-order rate constant and the rate of H_2O_2 production by this process under physiological conditions with a fully reduced 3.2 mM GSH pool by assuming that the kinetics of the reaction was first-order with respect to O_2 [86] and correcting for pO_2= 90 Torr: k= (90 Torr)×(7.4×10^{-5} s^{-1})/(722 Torr)= 9.2×10^{-6} s^{-1}, v= k×(3.2×10^{-3} M) = 30 nM s^{-1}.

Altogether, the reduction of the H_2O_2 generated from hemoglobin autoxidation plus the reduction of both the H_2O_2 and the oxidized glutathione generated by GSH autoxidation would require a NADPH expenditure of $0.5\times9.6\times10^{-9}$ M s^{-1} + $2\times30\times10^{-9}$ M s^{-1} = 65 nM s^{-1}. This value is in the range of the NADPH production — 56±13 nM s^{-1} — inferred from determinations of the activity of the pentose phosphates pathway [90], although these experiments were performed at pO_2= 160 Torr.

Determinations based on catalase inhibition by 3-aminotriazole yield lower H_2O_2 production for bovine erythrocytes [81]: 0.53 nM s^{-1} under atmospheric pressure. However, these experiments may have strongly underestimated H_2O_2 production because they overlooked the contribution of Prx2 for H_2O_2 reduction, and

---

[16] Should the observed GSH decay be due to GPx-catalyzed GSH oxidation it would have exhibited zero-order kinetics. This because at plausible intracellular H_2O_2 concentrations GPx1 shows a very low $K^{App}_{M,GPx1,GSH}$ and should thus remain effectively saturated with GSH down to very low GSH concentrations.

because most of the 3-aminotriazole might have been bound to proteins and therefore unavailable to inhibit catalase [1].

In all subsequent analyses in this work we will use 35 nM s^{-1} as reference value for endogenous H_2O_2 production, this value being the sum of the H_2O_2 production from GSH autoxidation estimated from the data in [31] plus the H_2O_2 production from hemoglobin autoxidation estimated in the first paragraph of this section.

2.10.3 H_2O_2 permeation

The permeability constant of horse erythrocyte membranes for H_2O_2 has been determined as 6×10^{-5} dm s^{-1} [91]. Experiments following the decay of extracellular H_2O_2 in presence of human erythrocytes (e.g. refs. [2, 50]) are consistent with this value after taking the hematocrit and the erythrocyte's geometry into account. This implies that H_2O_2 consumption by human erythrocytes is strongly limited by the membrane permeation step. Thus, we estimated the permeability constant of human erythrocyte membranes by fitting an exponential decay to the data in the first 10 minutes in Figure 4B from [2]. This yielded a first order rate constant of 3.9×10^{-3} s^{-1} (95% CI: [0.0033 s^{-1}, 0.0044 s^{-1}], R^2= 0.997) for a preparation containing 5×10^{9} cells dm^{-3} (Supplementary Figure 2.1). Considering an erythrocyte surface area of 1.35×10^{-8} dm^2 ref.[80], we obtain a permeability constant of $(3.9\times10^{-3}\ s^{-1})/[(5\times10^{9}\ \text{cells}\ dm^{-3})\times(1.35\times10^{-8}\ dm^2)]= 5.8\times10^{-5}$ dm s^{-1}. Indeed this is identical to the permeability constant for horse erythrocytes within experimental error.

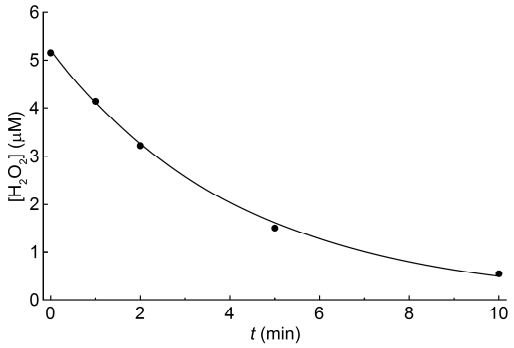

Supplementary Figure 2.1. Time evolution of extracellular H2O2 concentration in a suspension of 5×10^{9} human erythrocytes/dm^3 treated with 5 μM H_2O_2 [2] (dots), and best fit curve to the experimental points (line). See text for details.

This permeability constant translates into the following two effective first-order rate constants for H_2O_2 permeation, one referred to the erythrocyte water volume, the other to plasma volume. The former — $(5.8\times10^{-5}$ dm $s^{-1})\times(1.35\times10^{-8}$ $dm^2)/(0.72\times10^{-13}$ $dm^3)$ = 10.9 s^{-1} — considers a water contents of 72% of erythrocyte volume [79]. The latter — $(5.8\times10^{-5}$ dm $s^{-1})\times(1.35\times10^{-8}$ $dm^2)\times0.45/((1–0.45)\times10^{-13}$ $dm^3)$ = 6.4 s^{-1} — considers an hematocrit of 0.45.

2.10.4 H_2O_2 production and concentrations in blood plasma

The effective rate constant for H_2O_2 influx into erythrocytes from plasma estimated in the previous section is substantially lower than those for any of the H_2O_2-consuming enzymes in these cells (see following sections). Thus, permeation is the rate-limiting step in the consumption of plasma H_2O_2 by erythrocytes. This implies that the half-life of H_2O_2 in the general circulation is no higher than ln(2)/(6.4 s^{-1})= 0.11 s. Importantly, the rate constant above is directly proportional, and the half-life inversely proportional, to the total area of interface between plasma and erythrocytes, which in circulation amounts to $(1.35\times10^{-8}$ dm^2/erythrocyte)/[(1-0.45) (dm^3 plasma/dm^3 erythrocyte) × $(10^{-13}$ dm^3/erythrocyte)] = 2.5×10^3 m^2 interface area / dm^3 plasma. Any attempts to experimentally determine physiologically meaningful H_2O_2 concentrations in plasma thus have to contend with (a) this short half-life, (b) its strong dependence on the aggregation state of the erythrocytes (dispersed *vs.* sedimented) in the experimental setup, and (c) with the fact that in circulation plasma also makes extensive contact with the endothelial cells that form the vasculature walls, with an interface area comparable to that between plasma and erythrocytes [92]. As we discuss below for specific attempts that are often cited in support of micromolar-scale H_2O_2 concentrations in plasma, these challenges have yet to be addressed.

Using a radio-isotopic technique based on determination of $^{14}CO_2$ release from peroxide-dependent decarboxylation of 1-^{14}C-α-ketoacids, Varma & Devamanoharan [93] reported H_2O_2 concentrations of 288±185 μM for deproteinized whole blood samples and 34±18 μM for deproteinized plasma samples from human volunteers. However, H_2O_2 removal is blocked during the incubations, and the release of transition metals by the deproteinization treatment

may promote H_2O_2 production. These experiments are thus likely to severely overestimate H_2O_2 concentrations in blood and plasma.

Using a H_2O_2 electrode, Lacy *et al.* [94] determined a 2.14±0.13 µM H_2O_2 concentration in the plasma supernatant after centrifugation of blood samples taken from healthy patients without a family history of hypertension. However, this experimental setup is also conductive to potentially severe overestimation of the physiological H_2O_2 concentration. This because plasma lies directly on top of the buffy coat and has an extremely small interface area with the erythrocyte sediment, thus strongly hampering H_2O_2 removal. The fact that the H_2O_2 concentrations determined in plasma aliquots separated from the same samples are very similar to those determined in the former experiment further supports the notion that the erythrocyte sediment did not effectively consume the H_2O_2 generated in plasma. Nevertheless, the observation [94] that addition of SOD plus allopurinol (a xanthine oxidase inhibitor) to plasma leads to lower H_2O_2 concentrations than determined in absence of these additions indicate that xanthine oxidase may be responsible for a substantial fraction, though not all, of the H_2O_2 production in plasma.

Subsequent experiments [43] using the same electrochemical technique sought to determine the activity of xanthine oxidase in plasma from time courses of H_2O_2 concentration in presence of sufficient sodium azide to completely inhibit H_2O_2 consumption. These experiments detected the formation of a total of 36.1±7.6 µM H_2O_2 from the plasma of five healthy volunteers after azide addition. From the observation that it took on average 9.7±0.5 min for H_2O_2 to accumulate to its maximum level the authors estimate a xanthine oxidase activity of 6.5±0.3 mU/ml (= 6.2×10^{-8} M s^{-1}). However, a closer examination of these results raises the following questions. First, while the formation of 36.1 µM H_2O_2 under xanthine oxidase catalysis would consume at least as much xanthine, reported xanthine concentrations in blood plasma are much lower: 0.4-3.3 µM [95, 96]. Further, a substantial fraction of the available xanthine would have been consumed before azide addition, as this occurred after a 10 min centrifugation. Second, considering a K_M(xanthine) in the range of 1.7-3 µM [97, 98], an initial xanthine concentration of 22 µM would be saturating, and thus lead to a constant rate of H_2O_2 accumulation over most of the experiment. However, Figure 5 of ref [43] exhibits

a near-exponential approach to the final value, which is more consentaneous with a first-order process. Unfortunately the authors of [43] did not attempt to repeat these experiments in presence of allopurinol, which might have clarified whether the observed H_2O_2 production is really attributable to the xanthine oxidase reaction. Nevertheless, taking the computed 62 nM s^{-1} average H_2O_2 production rate at face value, this would imply a steady state plasma H_2O_2 concentration no higher than (62 nM s^{-1})/(6.4 s^{-1})= 9.7 nM in the systemic circulation.

The experiments in ref [94] suggest that lymphocytes, which are concentrated in the buffy coat, did not contribute overwhelmingly for H_2O_2 generation. Otherwise the H_2O_2 concentration determined in the supernatant immediately above the buffy coat, where lymphocytes are concentrated, would have been quite higher than that determined for isolated plasma. Further, should residual suspended lymphocytes have had a major contribution towards H_2O_2 production in isolated plasma, allopurinol would have inhibited a lower fraction of that production. However, the following experiments suggest that polymorphonuclear leukocytes (PMNs) may contribute majorly for H_2O_2 generation under pathological circumstances that cause their extensive activation. Using a H_2O_2 electrode, Liu & Zweier [44] determined the H_2O_2 production rates by human polymorphonuclear leukocytes activated by phorbol 12-myristate acetate. At the peak H_2O_2 concentration attained, the production rate was 0.16 fmol/s/PMN. Considering a normal granulocyte count of 10^{10} PMN/dm^3 plasma, we estimate a maximum total H_2O_2 production from granulocytes of 1.6 µM s^{-1}, if they were all simultaneously activated. However, even this extreme situation would translate into a steady state plasma H_2O_2 concentration no higher than (1.6 µM s^{-1})/(6.4 s^{-1})= 250 nM in the systemic circulation.

Two factors may contribute to make steady state plasma H_2O_2 concentrations in absence of inflammation even lower than the estimates above suggest. First, endothelial cells that form the vasculature walls may contribute substantially for H_2O_2 consumption as their overall interface area with plasma is comparable to that of the erythrocyte population [92]. Second, plasma also carries its own defenses against H_2O_2, such as GPx3 [99].

Altogether, the evidence reviewed above supports the notion that plasma H_2O_2 concentrations in the systemic circulation in absence of extensive inflammation

or infection are at most in the nM range. The source and exact concentrations of this H_2O_2 under basal conditions remain open problems, however.

2.10.5 GPx1 kinetics and concentration

We obtained the kinetic parameters for GPx1 by fitting the rate expression characterized by Flohé *et al.* [29] to the time course of GPx1-catalyzed H_2O_2 consumption in Figure 5 of [50]. In this rate expression [29]

$$v = \frac{[\mathrm{GPx1}]}{\frac{\Phi_1}{[\mathrm{H_2O_2}]} + \frac{\Phi_2}{[\mathrm{GSH}]}}, \tag{1}$$

the rate is invariant upon simultaneous changes of the enzyme concentration and of the kinetic parameters Φ_1 and Φ_2 by the same factor, which shows that one cannot independently estimate these three quantities from a progress curve. However, the rate expression can be rewritten as

$$v = \frac{1}{\frac{\phi_1}{[\mathrm{H_2O_2}]} + \frac{\phi_2}{[\mathrm{GSH}]}}, \tag{2}$$

and both parameters $\phi_1 = \Phi_1/[\mathrm{GPx1}]$, $\phi_2 = \Phi_1/[\mathrm{GPx1}]$ can be independently estimated. Thus, we sought to determine the values of ϕ_1, ϕ_2 that yield the best fit between the observed values of $\log_{10}([H_2O_2])$ (as per the logarithmic scale in Figure 5 of [50]) at the sampling times highlighted in Supplementary Figure 2.2 and the values computed by numerical integration of the following system of differential equations with the assay concentrations $[H_2O_2]_0$= 100 µM, $[GSH]_0$= 2 mM as initial conditions:

$$\begin{aligned} \frac{d[\mathrm{H_2O_2}]}{dt} &= -\frac{1}{\frac{\phi_1}{[\mathrm{H_2O_2}]} + \frac{\phi_2}{[\mathrm{GSH}]}} \\ \frac{d[\mathrm{GSH}]}{dt} &= -2\frac{1}{\frac{\phi_1}{[\mathrm{H_2O_2}]} + \frac{\phi_2}{[\mathrm{GSH}]}} \end{aligned} \tag{3}$$

2. Hydrogen peroxide metabolism in human erythrocytes

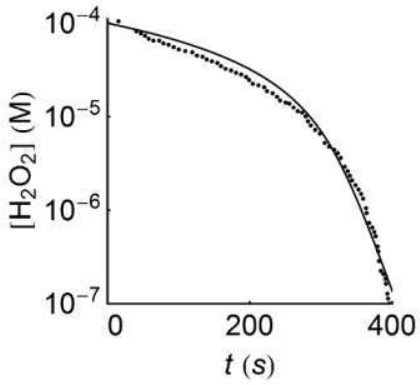

Supplementary Figure 2.2. GPx-catalyzed consumption of 100 µM H_2O_2 upon addition of 2 mM GSH as per the experimental setting of [50] (dots), and best fit curve to the experimental points (line). See text for details.

To estimate the best-fit parameters we applied the NonlinearModelFit function from *Mathematica*™ 9.0.1 [58] with default settings, after rescaling the data so that the variables had near-unit values. We obtained best-fit values ϕ_1 = 4.0×10^{-2} s (95% CI: [3.7×10^{-2} s, 4.3×10^{-2} s]) ϕ_2= 9.72 s (95% CI: [9.4 s, 10 s]), with an adjusted R^2=0.9996. These ϕ_1 and ϕ_2 values already reflect the conversion from assay hemoglobin concentration to erythrocyte water contents, considering a hemoglobin content of 485 g dm^{-3} erythrocyte water. The ratio $\frac{\phi_1}{\phi_2} = \frac{\Phi_1}{\Phi_2} = 4.1\times10^{-3}$ is in good agreement with that reported in [52] (5.6×10^{-3}).

This value of ϕ_2 is in excellent agreement with the pseudo-first-order rate constant of 3.6×10^{-2} s^{-1} determined Nicholls [100] for GSH decay in whole blood in presence of high H_2O_2 concentrations. Indeed, considering an hematocrit of 0.45 and a water contents of 0.717 dm^3 / dm^3 erythrocyte, this rate constant converts to an intracellular value of 0.11 s^{-1}, which is remarkably close to 1/ϕ_2= 0.10 s^{-1}. The values for ϕ_1 and ϕ_2 above are also in acceptable agreement with the GPx1 activity in human erythrocytes determined in [51], as the following computations show. These authors determined a mean GPx1 activity of 5.6±0.3 µmol GSH oxidized/min/10^{10} cells at 20 ºC, pH 7 in presence of 5 mM GSH and 73.3 µM H_2O_2 for a population of healthy individuals. Considering an activity increase by ≈25% between pH 7 and pH 7.2 [51] and a Q_{10} temperature coefficient of 1.18

[83], we estimate that the rate above should be 1.7-fold higher at 37 ºC, pH 7.2. Based on a water contents of 7.2×10^{-14} dm^3 $cell^{-1}$ [79, 80], the estimated activity expressed in terms of H_2O_2 consumption is then 1.1×10^{-4} M s^{-1}. In turn, replacing the estimated ϕ_1 and ϕ_2 values and the assay [51] GSH and H_2O_2 concentrations into equation (2) one obtains a rate of 4.0×10^{-4} M s^{-1}.

At micromolar H_2O_2 concentrations (*i. e.*, $[H_2O_2] \ll \frac{\phi_1}{\phi_2}[GSH]$ = 13 μM, considering [GSH]= 3.2 mM [31]) equation (2) reduces to a pseudo-first-order rate expression $v=k_{GPx1}[H_2O_2]$ with $k_{GPx1} = 1/\phi_1 = 25$ s^{-1}. This rate expression should be accurate under most physiological conditions, as intracellular H_2O_2 concentrations are expected to be much lower than 13 μM under most physiological circumstances and only drastic oxidative stresses cause strong GSH depletion.

Although there is relatively good agreement between GPx1 activity determinations in the literature [50-52, 101], these activities imply concentrations of active GPx1 monomers that are much lower than the total concentration of monomers determined through immunochemical methods [68]. Thus, from the data in refs. [50, 52] one estimates concentrations of 0.61 μM and 0.45 μM by dividing the values of Φ_1 and Φ_2 determined by [52] by the values of ϕ_1 and ϕ_2, respectively. From the above-mentioned data in [51] we estimate a 0.51 μM by applying the rate expression (1) with the kinetic parameters determined by [52]. From the reported activity in the outdated-blood hemolyzates used by Awasthi *et al.* [101] to purify GPx1 and again applying the values of Φ_1 and Φ_2 determined by [52] one can estimate a 0.11 μM GPx1 monomer concentration. Should one assume that all the final purified protein was 100% pure GPx1 and that this enzyme did not lose activity during purification, the estimated cellular GPx1 concentration would be 1.7 μM. However, using an immunochemical approach Cho *et al.* [68] determined an erythrocyte GPx1 contents of 6.0±2.0 μg/mg lysate protein, from which, considering an hemoglobin contents of 485 g dm^{-3} erythrocyte water and a monomer molecular weight of 23 kDa [101] we estimate a concentration of 1.3×10^{-4} M GPx1 monomers. The recent discovery [4] that peroxides gradually inactivate GPx1 by converting the selenocysteine residue at the active site to dehydroalanine can only partially explain this ≈270-fold

discrepancy between activity-based and immunochemistry-based determinations. This because the GPx1 activity decreases by just ≈50% over the erythrocyte life span [4].

This inactivation process did not affect the kinetic determinations in [50] because these used an initial 100 μM H_2O_2 which was rapidly consumed over a period of just 6 min, whereas in the experiments in [4] a 60 min exposure of GPx1 to a constant 200 μM H_2O_2 caused a 15% activity decrease.

2.10.6 Cat concentration and catalytic cycle

Experimental observations [50] indicate that at H_2O_2 concentrations > 0.1 μM the kinetics of catalase are well described by a pseudo-first-order rate expression over the whole biological range of H_2O_2 concentrations. We estimated the rate constant for this rate expression as k_{Cat}= 218 s^{-1} from the data obtained for the lowest H_2O_2 concentration assayed in [50] assuming an erythrocyte water contents of 2.06 dm^3/g hemoglobin [79].

This rate constant is consistent with a more indirect estimate that can be obtained from the catalase concentration in erythrocytes [68] as follows. Hemolyzate immunoblots from a population of 17 healthy individuals [68] contain 4.4±0.4 μg catalase/mg lyzate protein. Considering the same erythrocyte protein contents as assumed in [68], a monomer molar mass of 64 kDa [102], and referring the concentration to erythrocyte water (as per Supplementary Materials section 2.10.1) yields 32±3 μM Cat monomers. This is broadly consistent with other determinations [89, 103] in the range of 10-20 μM. In turn, considering that all Cat is present as ferricatalase and compound I, at steady state the pseudo-first-order rate constant can be expressed as

$$k_{Cat} = \frac{2}{\frac{1}{k_{\mathrm{Ferri}}} + \frac{1}{k_{\mathrm{CI}}}}[\mathrm{Cat}]. \qquad (4)$$

Replacing values one obtains k_{Cat}= 288 s^{-1}. The discrepancy between the two estimates can be fully accounted for by the partial heme occupancy of Cat [104] and for eventual interspecies differences in the values of k_{CI} and k_{Clinac}, as the available values for these parameters (Table 2.1 in main text) are for Cat purified from horse erythrocytes [33]. For consistency with the value of k_{Cat} determined in

[50], which is the most direct and reliable determination for human erythrocytes, we consider a 24.4 μM effective catalase concentration.

Very low H_2O_2 concentrations are insufficient for Compound I reduction to Ferricatalase by H_2O_2 to compete effectively with alternative non-productive reactions (Supplementary Figure 2.3). Namely, the conversion of Compound I to a postulated unstable Intermediate, which is then reduced to the inactive Compound II by an endogenous electron donor [105]. NADPH prevents the accumulation of Compound II under a steady H_2O_2 flux [53]. In this process, Cat-bound NADPH reduces the Intermediate to Ferricatalase [35], and free NADPH then reduces bound $NADP^+$ without concomitant association/dissociation of NADP [106].

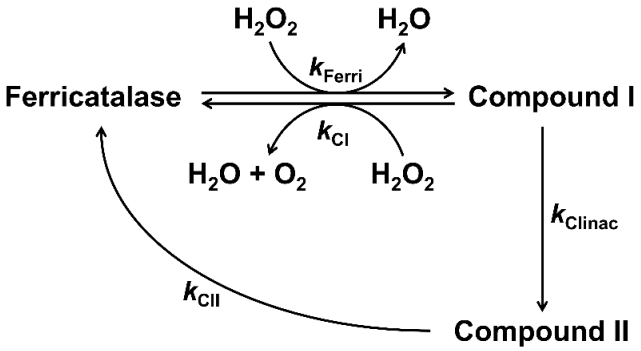

Supplementary Figure 2.3. Catalytic cycle considered in modeling the action of Cat. See text for details.

The Intermediate is unstable and is not detected even in absence of NADPH [35], indicating that the limiting step in the formation of Compound II is formation of Intermediate. We thus modeled the overall process as a direct conversion of Compound I into Compound II with k_{Clinac} = 0.011 s^{-1}, the rate constant for the formation of Compound II in horse Cat [34]. Compound II is reduced to Ferricatalase with a k_{CII} = 7.39×10^4 s^{-1} [35].

It is unclear whether significant Cat inactivation to Compound II occurs *in vivo*. The decay of Compound I to Intermediate competes with the reduction of Compound I by H_2O_2 when $[H_2O_2] < k_{CI}/k_{Clinac} = 6.9\times10^{-10}$ M. However, at such low oxidative loads a large NADPH pool is normally available for reduction of the Intermediate. NADPH consumption by the latter process is never very high, as the following analysis shows. The highest rates of NADPH consumption would

occur if all Intermediate formed were instantaneously converted to Ferricatalase. Under these conditions the steady state rate of Intermediate formation and NADPH consumption would be

$$v = \frac{\frac{k_{\mathrm{Ferri}} k_{\mathrm{CIinac}}}{k_{\mathrm{Ferri}} + k_{\mathrm{CI}}} [\mathrm{Cat}]_{tot} \ [\mathrm{H_2O_2}]}{\frac{k_{\mathrm{CIinac}}}{k_{\mathrm{Ferri}} + k_{\mathrm{CI}}} + [\mathrm{H_2O_2}]}$$

which at high H_2O_2 concentrations reduces to

$$v = \frac{k_{\mathrm{Ferri}} k_{\mathrm{CIinac}}}{k_{\mathrm{Ferri}} + k_{\mathrm{CI}}} [\mathrm{Cat}]_{tot}$$

Replacing values, we obtain the value of this upper limit for NADPH consumption as 67 nM s^{-1}, which is just 2.8% of the erythrocyte's capacity for NADPH regeneration — 2.4 μM s^{-1} [42]. Therefore it is justified to neglect NADPH consumption by Cat.

The reaction of Ferricatalase with $O_2^{\bullet-}$ ($k \approx 2\times10^5$ $M^{-1}s^{-1}$ [107]) or of Compound II with H_2O_2 yields another inactive form of Cat, Compound III. Compound III is unstable [107, 108] and reverts spontaneously to an active form of Cat in the absence of H_2O_2 [35]. The following evidence indicates that its occurrence *in vivo* can be neglected. Kirkman *et al.* [35] observed that <2.8% Compound III had accumulated after 1 hour of Cat incubation *in vitro* at a 2.47×10^{-7} M s^{-1} H_2O_2 generation rate in the absence of NADPH. They also observed <5% Cat as Compound III after 8 min under 1.3×10^{-7} M s^{-1} H_2O_2 and 0.68×10^{-7} M s^{-1} $O_2^{\bullet-}$ production. The fractions of Cat as Compound III *in vivo* should be lower than these because proteins such as Prx2 and SOD compete strongly with Cat for H_2O_2 and $O_2^{\bullet-}$, respectively.

Assuming that most Cat is in Ferricatalase form at low H_2O_2 concentration, H_2O_2 consumption by Cat under these conditions occurs with a pseudo-first-order rate constant of (24.4 μM Cat)×k_{Ferri}≈ 150 s^{-1}, *i. e.*, ≈67% of the value at high H_2O_2 concentrations.

2.10.7 Prx2 concentration and rate constant for H_2O_2 reduction

Moore *et al.* [63] determined a Prx2 contents of 5.6±1.7 mg / ml erythrocyte. This corresponds to a Prx2 monomer concentration of ≈3.6±1.1 ×10^{-4} M, considering a monomer molecular weight of 21892 Da and 0.717 dm^3 water/dm^3 erythrocyte. This is in reasonable agreement with the following more recent determination that we will take as reference in subsequent computations. Cho *et al.* [68] determined a Prx2 monomer contents of 26.8±7.7 µg Prx2/mg lyzate protein (2.68% of lyzate protein) in immunoblots from hemolyzates obtained from a population of 17 healthy individuals. From this we estimated a 570±164 µM Prx2 monomer concentration by dividing the reported 410 µmol/dm^3 erythrocyte [68] by the 0.717 dm^3 water/dm^3 erythrocyte water contents. Although there were no statistical differences between the erythrocyte Prx2 contents of 32 homozygous sickle cell patients and that in the control population, the data in [68] highlight a high variability in erythrocyte Prx2 contents, the analyzed population of 49 individuals covering a 2-fold range.

Prx1 and Prx6 were present in the erythrocytes of healthy individuals in amounts that represent 1.2% and 0.52% of that of Prx2, respectively [68].

The value of the rate constant (k_{Ox}) for H_2O_2 reduction by Prx2 was obtained in four different experiments [23, 24]. In the first two experiments [23] reduced Prx2 was treated for 5 min with H_2O_2 in presence of various amounts of either bovine liver Cat or human erythrocyte Cat. Analysis by nonreducing SDS-PAGE revealed that the fraction of Prx2 monomers increased and that of disulfide-linked dimers decreased with increasing Cat concentration. Therefore, interaction with Cat could not have substantially increased Prx2's reactivity with H_2O_2. Further, the amounts of each Cat necessary to achieve 50% protection against Prx2 oxidation reflect the relationship between the rate constants of these Cat, and both point to a $k_{Ox} \approx 6\times10^6$ $M^{-1}s^{-1}$.

The other two experiments [23, 24], were competition assays with horseradish peroxidase (HRP), based on the procedure of Ogusucu *et al.* [109]. Peskin *et al.* [23] used 10 µM HRP and 7 – 28 µM Prx2 monomers and plotted the values of $\frac{F}{1-F}k_{HRP}[\mathrm{HRP}]$ *vs*. [Prx2]. (Here, *F* and k_{HRP} stand for the fractional inhibition of HRP conversion to Compound I, and for the rate constant for this reaction of HRP

with H_2O_2.) The results are well fit by a straight line, and thus do not show evidence of potential artifacts caused by an eventual binding of Prx2 to HRP. This fit yields the value k_{Ox}= 1.3×10^7 M^{-1}s^{-1} for pH 7.4, 20 ºC.

In turn, Manta *et al.* [24] used 5 μM HRP and 0.4 – 1.7 μM Prx2 monomers and determined an estimate of k_{Ox} for each Prx2 concentration used. These estimates were all in the range 0.5×10^8 – 1.2×10^8 M^{-1}s^{-1} (mean 1.0×10^8 M^{-1}s^{-1} for pH 7.4, 25ºC), without a directional trend that could indicate eventual artifacts.

The 5 ºC temperature difference can only partially account for the discrepancy between the rate constants determined in refs. [23, 24], as the implied Q_{10}= 52 temperature coefficient is unrealistically high. Considering a more plausible Q_{10}= 2. to extrapolate to 37 ºC the value of k_{Ox} obtained in [24] at 25 ºC one would obtain a k_{Ox}= 2.×10^8 M^{-1}s^{-1}. Given the uncertainty in the experimental determinations, this value is not significantly different from that at 25 ºC. Adopting the value obtained in [24] at 25 ºC is a more conservative assumption considering the main point being made in the present work.

Given the high value of the rate constant, one may wonder whether the reaction might become diffusion limited in the cellular environment. The following estimate strongly argues against that possibility. The diffusion limit (k_d) for a bimolecular reaction is given by the expression $k_d = 4\pi R^* D N_A$, where R^* is the distance at which the molecules must come from each other in order to react, D is the sum of the diffusion coefficients of the molecules, and N_A is Avogadro's number [110]. By approximating R^* by the lower limit for the hydrodynamic radius of H_2O_2 (0.21 nm) and D by the diffusion constant for H_2O_2 in a hydrogel, 3.7×10^{-8} dm^2 s^{-1} [66], we estimate a lower limit 5.9×10^8 M^{-1}s^{-1} for k_d in the cellular environment.

The rate constant for H_2O_2 reduction by Prx6 is ≈3.3×10^6 M^{-1}s^{-1} [111], and the pseudo-first-order rate constant is thus (5.2×10^{-3})×(5.7×10^{-4} M)×(3.3×10^6 M^{-1}s^{-1})= 9.8 s^{-1}. This is much lower than the pseudo-first-order rate constant for catalase, and lower than that for GPx1. Therefore, we neglected the contribution of this protein for H_2O_2 elimination.

We are unaware of any determinations of the rate constant for H_2O_2 reduction by Prx1, and for this reason the model neglects this process. Shall this rate constant be similar to that for Prx2 [24], the pseudo-first-order rate constant will be

$(1.2\times10^{-2})\times(5.7\times10^{-4}\ M)\times(10^{8}\ M^{-1}s^{-1})= 6.8\times10^{2}\ s^{-1}$, which is ≈3-fold higher than that for catalase at low H_2O_2 concentrations and would make Prx1 the major contributor for H_2O_2 consumption where Prx2 is fully inhibited. However, the following estimates show that the *effective* rate constant for H_2O_2 reduction by Prx2 cannot be much lower than $10^5\ M^{-1}s^{-1}$. Low *et al.* [2] observed that exposure of 5×10^9 erythrocytes/dm^3 to a 5 μM H_2O_2 causes substantial Prx2 oxidation within 1 min. Figure 4B from [2] shows that the cells consumed ≈1 μM H_2O_2 during the first minute of the experiment. Because each cell carries $7.2\times10^{-13}\ dm^3$ water the H_2O_2 intake by each cell was $(1\ \mu M)/((5\times10^9\ cell\ dm^{-3})\times(7.2\times10^{-14}\ dm^3\ cell^{-1}))= 2.8$ mM. Based on Figure 4A from [2] we conservatively consider that 50% of the Prx2 peroxidatic thiols, amounting 285 μM, were oxidized to disulfides during the same time, corresponding to ≈10% of the intake. Conservatively assuming pseudo-first-order rate constants of 150 s^{-1} for Cat (Supplementary Materials section 2.10.6) and 25 s^{-1} for GPx1 (Supplementary Materials section 2.10.5) under these conditions, we find that the *effective* k_{Ox} must be at least $0.1\times(150\ s^{-1} + 25\ s^{-1})/(5.7\times10^{-4}\ M)= 3\times10^4\ M^{-1}s^{-1}$. Simulations based on Model D (Supplementary Figure 2.4) yield a more precise lower limit: $k_{Ox}> 3\times10^4\ M^{-1}s^{-1}$. This suggests that Prx2 does not contribute much less than 50% for H_2O_2 consumption under low H_2O_2 supplies, and that the effective rate constant for H_2O_2 reduction by Prx1 is also lower than $10^8\ M^{-1}s^{-1}$. The latter is consistent with the rate constant determined for *Saccharomyces cerevisiae* TSA1 (a Prx1 ortholog) using method and conditions similar to those used in [24] for Prx2: $\approx10^7\ M^{-1}s^{-1}$ at pH 7.4, 25ºC [109].

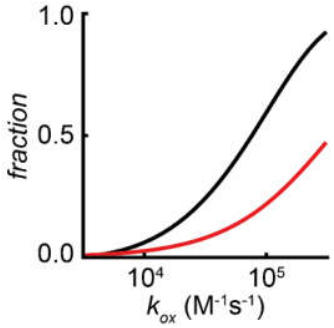

Supplementary Figure 2.4. Simulated Prx2 oxidation 1 min after a 5 μM H_2O_2 bolus under the conditions of the experiment in Fig. 4A of [2] as function of k_{Ox}. Black, fraction of crosslinked Prx2 monomers, based on Model D (Table 1 from main text) modified by (i) treating the extracellular concentration of H_2O_2 as a dependent variable, with compartment volumes accounting for the hematocrit of the assay medium, and (ii) assuming a 57 nM s^{-1} endogenous H_2O_2 production reflecting the higher rate of GSH autoxidation under atmospheric pressure (discussed in Supplementary Materials section 2.10.2). Red, fraction of H_2O_2 consumed by Prx2 under basal conditions implied by the same value of k_{Ox}, based on unmodified Model D.

2.10.8 Trx cycle

Human Trx1 possesses a regulatory dithiol (C62,C69) whose oxidation to disulfide prevents the reduction of the active site dithiol (C32,C35) via TrxR [56]. Go *et al.* [112] recently found that all Trx1 was in doubly oxidized form in HT29 cells (a colon cancer cell line) exposed to a 2 mM H_2O_2 bolus, and this form was also detectable in cells exposed to 20 μM auranofin, a TrxR inhibitor. The redox state of the regulatory dithiol is modulated by oxidation/reduction by the active site dithiol of a second Trx1 molecule [56]. In modeling these reactions we made the following three assumptions. First, oxidation of the regulatory dithiol fully prevents TrxR-catalyzed reduction of the active site. Second, the regulatory dithiol of a Trx1 can only be oxidized and reduced by the active site of other Trx1 molecule. Third, the redox state of the active site does not affect the redox potential nor the oxidation/reduction rate constants of the regulatory site. Fourth, all reactions between the active site of one molecule and the regulatory site of another molecule follow mass action kinetics. Under these assumptions, the possible reactions between active and regulatory dithiols are:

$$\begin{aligned} &\mathrm{Trx1_{DD}} + \mathrm{Trx1_{TT}} \rightleftharpoons 2\ \mathrm{Trx1_{TD}} \\ &\mathrm{Trx1_{DD}} + \mathrm{Trx1_{TT}} \rightleftharpoons 2\ \mathrm{Trx1_{DT}} \\ &\mathrm{Trx1_{DD}} + \mathrm{Trx1_{DT}} \rightleftharpoons \mathrm{Trx1_{TD}} + \mathrm{Trx1_{DD}} \\ &\mathrm{Trx1_{DT}} + \mathrm{Trx1_{TT}} \rightleftharpoons \mathrm{Trx1_{TT}} + \mathrm{Trx1_{TD}} \end{aligned} \quad (5)$$

Here, $\mathrm{Trx1_{xy}}$ indicates thioredoxin with the active site dithiol in state *x*, and the regulatory dithiol in state *y* where T stands for thiol and D for disulfide. We assumed that the redox state of each dithiol does not influence the midpoint potential nor the rate constants for the reduction/oxidation of the other dithiol, except for the above-mentioned effect on reduction of the $\mathrm{Trx1_{DD}}$ form via TrxR.

We coarsely estimated the equilibrium constant (K_{Trx1}) for the formal reaction

$$\mathrm{Trx1_{DT}} \rightleftharpoons \mathrm{Trx1_{TD}}$$

as follows. Watson *et al.* [56] found that $E_o(\mathrm{Trx1_{TD}} \rightleftharpoons \mathrm{Trx1_{TT}}) - E_o(\mathrm{Trx1_{DT}} \rightleftharpoons \mathrm{Trx1_{TT}})$ > –210 mV – (–230 mV) > 20.0 mV, which translates into K_{Trx1} > 4.5 according to Nernst's equation for 37 ºC. Accordingly, we found that the time course of Prx2 reduction in intact erythrocytes following a H_2O_2 bolus presented in [2] cannot be qualitatively reproduced by Models A, B or D with a K_{Trx1} lower than 50 (Supplementary Figure 2.5). On the other hand, because some C62,C69 disulfide is already observed [56] when Trx1 is incubated with redox buffer (GSSG+GSH) at *E*= -270 mV, the value of K_{Trx1} should not be much larger than 50.

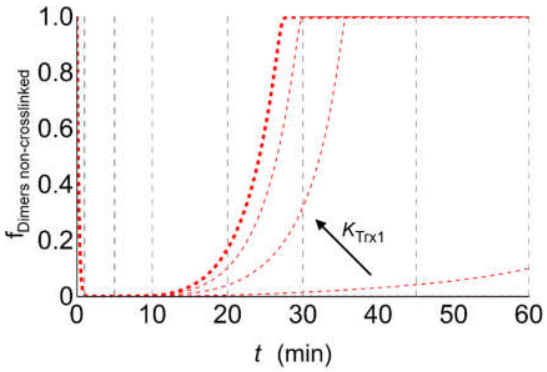

Supplementary Figure 2.5. Computed time courses of the fraction of non-crosslinked Prx2 dimers after exposing 5×10^9 erythrocytes dm^{-3} to a 5μM H_2O_2 bolus. Values K_{Trx1} = 10, 20, 30, 40, (thin dashed lines) or 50 (thick dashed line) were considered. K_{Trx1} increases in the direction of the arrow. Gray dashed lines indicate the times at which Prx2 forms were determined in ref.[2]. Results based on Model B.

Additionally, we assumed that the rate constant for oxidation of the regulatory dithiol by the active site disulfide of another Trx1 molecule is similar to the rate constant for the reduction of Prx2 disulfide by Trx, 2.1×10^5 $M^{-1}s^{-1}$ [24]. The observation that Trxs from phylogenetically distant organisms react with various substrates with rate constants in this order of magnitude [24, 113, 114] supports this assumption. The rate constant for the reverse reaction was obtained by dividing this value by the value of K_{Trx1}.

If one assumes that TrxR is completely unable to reduce the $Trx1_{DD}$ form of Trx1 the system lacks a steady state under conditions where all Trx1 is converted to this form. This situation complicates the numerical analysis of the model and is physiologically unrealistic, as in the cellular environment secondary reactions should reduce $Trx1_{DD}$ at a slow rate and this reaction will ultimately oxidize NADPH. In order to avoid these problems we considered that $Trx1_{DD}$ is a very poor substrate for TrxR, with a K_M 1000-fold higher than that for $Trx1_{DT}$. This assumption does not affect the relevant results in this work.

We implemented TrxR-catalyzed reduction of $Trx1_{DT}$ form as described in the next section.

2.10.9 TrxR activity

Low *et al.* [2] determined the Trx reductase activity in human erythrocytes for 5-(3-Carboxy-4-nitrophenyl)disulfanyl-2-nitrobenzoic acid (DTNB) as substrate

as 7.9 μM s^{-1} at 37 ºC, pH 7.4, and Urig *et al.* [36] determined a k_{cat}= 33.3 s^{-1} for the same substrate at 25 ºC, pH 7.4. Assuming that the ratio between the activity at 25 ºC and the activity at 37 ºC is 0.562 [83] as for the homologous enzyme GSR, this k_{cat} would translate into a k_{cat} = 59.2 s^{-1} at 37 ºC. The activity above would then correspond to 0.13 μM active protein, which is consistent with the lower estimate >44 nM obtained from the determinations by Meplan *et al.* [115]. In order to coarsely estimate the activity for the relevant physiological substrate, we drew on the determination by Turanov *et al.* [37] for recombinant human Trx: k_{cat} = 25.8 s^{-1} at 22ºC, pH 7.0. Assuming Q_{10}= 2.06 as determined for GSR from the activities ratio 25 ºC/37 ºC provided by [83], this implies a k_{cat} (Trx1) = 76.3 s^{-1} = 1.3 k_{cat}(DTNB), leading to a corresponding activity of $V_{Max,TrxR}$= 1.3×(7.9 μM s^{-1}) = 10 μM s^{-1}. However, the actual maximal rate of PSS reduction achievable is lower for the following two reasons. First, because the Trx concentration — 0.56 μM — is lower than $K_{M,TrxR,Trx1DT}$ = 1.83 μM [37]. One can estimate the maximal reduction rate knowing that TrxR follows a ping-pong catalytic mechanism [57, 116], assuming that $K_{M,TrxR,NADPH}$ = 6.0 μM [36] [17] and [NADPH]= 2.6 μM [12], considering $[Trx1_{DT}]$= $[Trx]_{Tot}$, and replacing values on the rate expression:

$$v = \frac{V_{\mathrm{Max,TrxR}}}{1 + \frac{K_{\mathrm{M,TrxR,NADPH}}}{[\mathrm{NADPH}]} + \frac{K_{\mathrm{M,TrxR,Trx1DT}}}{[\mathrm{Trx1_{DT}}]}} \qquad (6)$$

This computation yields v= 1.5 μM s^{-1} (1.2 μM s^{-1} if we consider the activity determined by [2]). The second reason is that under high oxidative loads Trx never fully accumulates in the $Trx1_{DT}$ form (Section 2.10.8) that is substrate for TrxR, but instead is further oxidized to the $Trx1_{DD}$ form, which is not reduced by TrxR. Using the model described in Section 2.10.8 we estimate that the maximal rate of Trx reduction is ≈1.0 μM s^{-1}, which is slightly lower than the estimated erythrocyte's capacity for NADPH regeneration. Thus, the capacity for NADPH

[17] Although this K_M was determined for DTNB as co-substrate it should hold as well for Trx as co-substrate. This because in a ping-pong mechanism the enzyme form binding one substrate is the same irrespective of the co-substrate.

supply, the TrxR activity and the concentration of Trx, all have some influence on the rate of PSS reduction at high oxidative loads.

At the maximal rate of Trx reduction estimated above it takes about (5.7×10^{-5} M)/(1.0×10^{-6} M s^{-1})= 570 s to fully regenerate Prx2 if it gets completely converted to the PSS form.

The pseudo-first-order rate constant for Trx reduction at low concentrations of $Trx1_{DT}$ is (1.0×10^{-5} M s^{-1})/(1.83 μM)= 5.5 s^{-1}.

To account for the slow reduction of $Trx1_{DD}$ we considered the same kinetic parameters as for the reduction of $Trx1_{DT}$ but assuming a higher $K_{M,TrxR,Trx1DD}$ (=1.83 mM).

2.10.10 NADPH concentration and binding equilibria

Human erythrocytes contain 39.9±7.0 μM NADPH [39] but most of it is bound to proteins [117]. Catalase tightly binds about 16 μM NADPH [117]. Because this NADPH exchanges with unbound NADPH very slowly [54] we discounted it from the total concentration of NADP. Thus, we consider $[NADP]_{tot}$ = 28 μM, as obtained in [39] with a method that determines only unbound and loosely bound NADP. The following evidence indicates that most of this NADP is loosely bound. First, 2.5-fold more NADP binds to proteins when submitting a chromatography column to 10 μM $NADP^+$ + 10 μM NADPH than when submitting a similar preparation to 2.5 μM $NADP^+$ + 2.5 μM NADPH [117]. As some of the major NADP binding peaks in the former chromatogram are barely detectable in the latter, NADP binding is probably not saturated at 10 μM $NADP^+$ + 10 μM NADPH. Thus, a substantial fraction of the NADP binding sites in erythrocytes have dissociation constants that are not much lower than $[NADP]_{tot}$. The data in [39] also indicates the existence of more than 154 μM NADP binding sites. Second, good fittings to published ultrafiltration data [117] are only achieveable by considering high concentrations of low-affinity binding sites for $NADP^+$ and NADPH. Third, [118] presents the concentrations of bound and unbound $NADP^+$ and NADPH in undiluted lyzates of both normal and G6PD-deficient erythrocytes. Although the total concentration of NADP in the latter erythrocytes is twice higher,

the ratios between bound and unbound forms of $NADP^+$ and NADPH are similar to those in normal erythrocytes.

Supplementary Table 1: Kinetic parameters of G6PD.

Parameter	Value	Reference
$V_{Max,G6PD}$	64 µM s^{-1}	[31]
$K_{D,G6PD,NADP^+}$	7.9 µM	[119]
$K_{I,G6PD,NADPH}$	7.1 µM	[31]
$K_{I,G6PD,DPG}$	2.3 mM	[83, 120]
$K_{M,G6PD,G6P}$	38 µM	[119]
$K_{M,G6PD,NADP^+}$	6.5 µM	[2-6, 8-20, 119]

Overall, these observations prompt us to model $NADP^+$ and NADPH binding to proteins as simple equilibria between loosely bound and unbound forms. With this assumption, we estimate from the data in [118]:

$$K_{NADP^+} = \frac{[\mathrm{NADP^+}]_{bound}}{[\mathrm{NADP^+}]} = 1.8, \quad K_{NADPH} = \frac{[\mathrm{NADPH}]_{bound}}{[\mathrm{NADPH}]} = 9.6.$$

Using these parameters, we estimate the physiological concentration of unbound NADPH at 2.6 µM.

We also assume that bound and unbound forms of $NADP^+$ and of NADPH equilibrate rapidly as compared to the redox turnover of the respective unbound forms, which is consistent with equilibrium constants near unity as noted above. Further details of the modeling of the NADP binding equilibria are available in [12].

2.10.11 NADPH regeneration by the hexose monophosphates shunt

At low oxidative loads NADPH supply by the hexose monophosphates shunt is controlled by demand for reducing equivalents [12, 15], whereas at high loads it is limited by hexokinase [31, 42]. The transition between these two regimes is complex to model. It depends on the possibility of recycling glucose 6-phosphate (G6P) from fructose 6-phosphate produced by the hexose monophosphates shunt (HMS) and on competition for this metabolite by phosphofructokinase, whose regulation is complex. Thus, we chose to represent NADPH regeneration

by a phenomenological rate expression that captures the behavior at both low and high oxidative loads realistically and interpolates the behavior at intermediate oxidative loads in the simplest way possible. Namely, we use a hyperbolic (*i. e.*, Michaelis-Menten-like) rate expression whose parameters are specified as follows. The $V_{Max,HMS}$= 2.4 μM s^{-1} is twice the maximum rate of the pentose phosphate pathway determined by [42], accounting for the fact that two molecules of NADPH are regenerated per G6P molecule consumed by the HMS. The $K_{M,HMS}$= 0.45 μM is such that the pseudo-first-order rate constant for $NADP^+$ reduction at low $NADP^+$ concentration is the same as that determined by G6PD kinetics: $V_{\mathrm{Max,HMS}} / K_{\mathrm{M,HMS,NADP^+}} = 2V^{\mathrm{App}}_{\mathrm{Max,G6PD}} / K^{\mathrm{App}}_{\mathrm{M,G6PD,NADP^+}}$. In order to estimate these apparent kinetic parameters of G6PD we considered the following rate expression [121]:

$$v = \frac{V_{\mathrm{Max,G6PD}}}{1+\frac{K_{\mathrm{M,G6PD,G6P}}}{[\mathrm{G6P}]}\left(1+\frac{K_{\mathrm{D,G6PD,NADP^+}}}{[\mathrm{NADP^+}]}\right)+\frac{K_{\mathrm{M,G6PD,NADP^+}}}{[\mathrm{NADP^+}]}\left(1+\frac{[\mathrm{NADPH}]}{K_{\mathrm{I,G6PD,NADPH}}}+\frac{[\mathrm{DPG}]}{K_{\mathrm{I,G6PD,DPG}}}\right)}, \quad (7)$$

with DPG standing for 2,3-diphosphoglycerate (DPG), the kinetic parameters as presented in Supplementary Table 1, [G6P]= 39 μM [83], [DPG] = 2.8 mM, which is the average concentration between arterial [122] and venous [123] blood, and unbound [NADPH] = 2.6 μM [12].

We obtain:

$$V^{\mathrm{App}}_{\mathrm{Max,G6PD}} = \frac{V_{\mathrm{Max,G6PD}}}{1+\frac{K_{\mathrm{M,G6PD,G6P}}}{[\mathrm{G6P}]}} = 32\ \mu\mathrm{M\,s^{-1}},$$

$$K^{\mathrm{App}}_{\mathrm{M,G6PD,NADP^+}} = \frac{K_{\mathrm{M,G6PD,NADP^+}}\left(1+\frac{[\mathrm{NADPH}]}{K_{\mathrm{I,G6PD,NADPH}}}+\frac{[\mathrm{DPG}]}{K_{\mathrm{I,G6PD,DPG}}}\right)+K_{\mathrm{D,G6PD,NADP^+}}\frac{K_{\mathrm{M,G6PD,G6P}}}{[G6P]}}{1+\frac{K_{\mathrm{M,G6PD,G6P}}}{[\mathrm{G6P}]}} = 12\ \mu\mathrm{M},$$

which yields $V_{Max,HMS}/K_{M,HMS}$ = 5.3 s^{-1}, translating into a $K_{M,HMS,NADP^+}$ = (2.4 μM s^{-1})/5.3 = 0.45 μM.

2.10.12 Sensitivity analysis

The logarithmic sensitivities of the concentrations to the parameters and independent variables are shown in Supplementary Figure 2.6. As expected, the most influential independent variable is the rate of H_2O_2 supply. Most sensitivities and gains are small, and sensitivities/gains higher than 1 (in absolute value) are circumscribed to a limited number of parameters and variables and do not exceed 3.9. Therefore, the concentrations are quite robust with respect to uncertainties

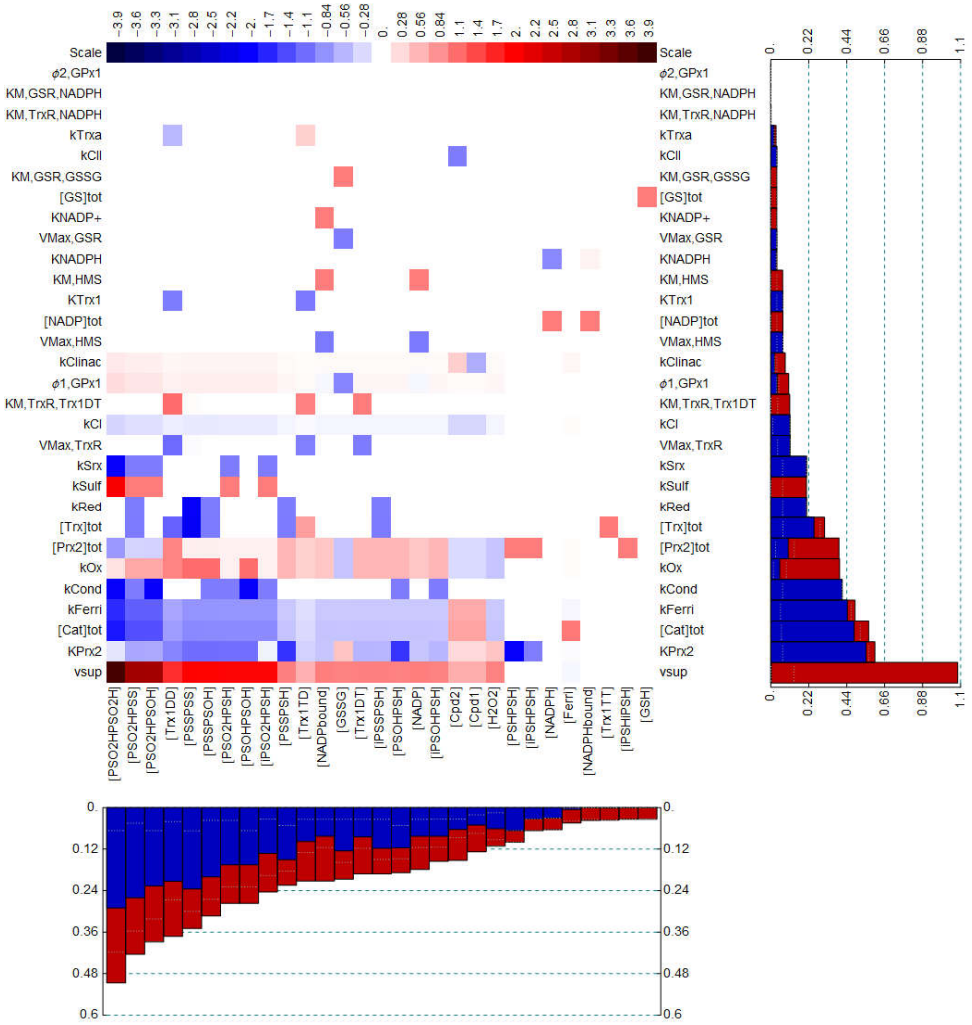

Supplementary Figure 2.6. Sensitivity analysis of Model B. Logarithmic sensitivities and gains of the steady state concentrations with respect to parameters and independent variables under the reference conditions. Vertical bars indicate the mean absolute value of the sensitivities or gains of each concentration, Horizontal bars indicate the mean absolute value of the sensitivities and gains with respect to each parameter or independent variable. Red, positive; blue, negative.

in the parameters and independent variables. The high gain (3.9) of the concentration of doubly sulfinylated Prx2 dimers with respect to the H_2O_2 supply reflects the fact that formation of this species requires four consecutive oxidations by H_2O_2. This species could thus be an extremely sensitive H_2O_2 sensor.

2.10.13 Model validation and refinement

2.10.13.1 Evidence that Prx2's contribution for H_2O_2 consumption in erythrocytes is comparable to Cat's

We are aware of the following five lines of evidence that Prx2's contribution for H_2O_2 consumption in intact erythrocytes at low oxidative loads is comparable to that of Cat.

First, Jakob *et al.* [67] found that erythrocytes from acatalasemic individuals exhibited 2.6-fold higher rates of NADPH production than those from normal individuals when incubated with glucose. This observation suggests that in the latter erythrocytes the Prx2- and GPx1-catalyzed processes together consume ≈40% of the H_2O_2 (Supplementary Materials section 2.10.13.4). Likewise, Gaetani *et al.* [90] found that the rate of the hexose monophosphate shunt in the erythrocytes from acatalasemic individuals was about twice that in the erythrocytes from healthy individuals.

Second, Johnson *et al.* [1] found that in erythrocytes from GPx1-deficient mice irreversible inactivation of Cat by 3-AT was substantially slower than expected if Cat were the sole enzyme eliminating H_2O_2. They were able to fit the observed data with a model that considered a contribution of peroxiredoxin consuming 55% of the H_2O_2, with a pseudo-first-order rate constant of 24 s^{-1}. Note that this value is just 0.04% of the one that we estimated in this work from the kinetic data obtained *in vitro* [24, 68]. Thus, Prx2 ought to be practically fully (99.96%) inhibited for that result to obtain if Prx2 in mice erythrocytes is as active and abundant as in human erythrocytes. Likewise, Matte *et al.* [124] observed that Cat inhibition caused a noticeable increase in Prx2 oxidation in mice erythrocytes.

Third, Johnson *et al*. [3] observed just 1.6-fold higher rates of Cat inactivation by 3-AT in the erythrocytes from $Prx2^{-/-}$ knockout mice than in the erythrocytes from wild type mice. From this result, and considering the diminished Cat activity in the

Prx2$^{-/-}$ mice [3], one estimates that in the erythrocytes from wild type mice Prx2 consumes 75% of the intracellular H_2O_2, according to a model [3] that already accounts for the lower specific activity of Cat at low H_2O_2 concentrations.

Fourth, Cho *et al.* [68] found that Cat inhibition caused a 5- to 10-fold increase in Prx2 sulfinylation in erythrocytes incubated for 3 h at a 50% hematocrit at a purportedly steady rate of H_2O_2 generation. Taken at face value, this observation suggests that Prx2 consumes no more than 45% of the H_2O_2, but questions can be raised about this experimental setup (Supplementary Materials section 2.10.13.3).

Fifth, Low *et al.* [2] observed that exposure of 5×10^9 erythrocytes/dm^3 to a 5 μM H_2O_2 causes incomplete Prx2 oxidation within 1 min. (Note that the second lane in Figure 4A from [2] exhibits a strong band corresponding to singly-crosslinked dimers, adjacent to the slightly more mobile band corresponding [22] to doubly-crosslinked dimers. Also, the incomplete crosslinking cannot be attributed to sulfinylation, of which Low *et al.* [2] did not detect any traces under the conditions of the experiment.) From Figure 4B in [2] we estimated (Supplementary Materials section 2.10.7) that during this time period 2.9 mM H_2O_2 entered the cell, which is 5-fold the concentration of Prx2 monomers. This $(2.9\times10^{-3}$ M)/(60 s)= 48 μM s^{-1} mean H_2O_2 influx rate far exceeds the estimated maximal rate of Prx2 reduction (1 μM s^{-1}, Supplementary Materials section 2.10.9). Therefore, should Prx2 be strongly competitive with Cat it should have been totally oxidized by the end of the first minute (see also Figure 2.3E in the main text).

2.10.13.2 Model validation

We validated the model by comparing the predicted responses to H_2O_2 under various conditions to the experimental observations reported by Low *et al*. [2]. In a first set of experiments these authors exposed human erythrocytes (5×10^9 or 5×10^{10} cells dm^{-3}, pH 7.4, 37º C, 5 mM glucose) to various H_2O_2 boluses for 10 min and determined the fractions of Prx2 monomers or disulfide-crosslinked dimers in non-reducing SDS-polyacrylamide gel electrophoresis (PAGE) gels. In another experiment these authors followed the cross-linking status of Prx2 over time upon exposing 5×10^9 erythrocytes dm^{-3} to a 5 μM H_2O_2 bolus for 60 minutes. We simulated these experiments as described in Figure 3 of the main text.

2. Hydrogen peroxide metabolism in human erythrocytes

Simulations based on Models B (inhibition of Prx2's peroxidase activity) and D (constitutively low peroxidase activity) reached near-quantitative agreement with the experimental results without requiring the adjustment of any further parameters (Figure 3B,D,F,H, Supplementary Figure 2.7A).

Comparisons must take into account that the experiments overestimate the fraction of oxidized Prx2, owing to adventitious oxidation during sample handling [2]. However, the simulations based on Models B and D for the incubation of 5×10^{10} cells dm^{-3} with 25 μM H_2O_2 and higher boluses (last five lanes in Figure 2 C from [2]) predict a slightly higher fraction of Prx2 oxidation than observed. This discrepancy may reflect reduction of Trx1 by GSH, catalyzed by glutaredoxin 1 [125], which was not taken into account owing to insufficient quantitative data.

Low *et al.* [2] have also observed that the incubation of 5×10^{9} erythrocytes dm^{-3} with 0 – 200 μM H_2O_2 boluses did not cause detectable sulfinylation. In turn, in erythrocytes pretreated with 3-aminotriazole to inhibit Cat incubation with 50 μM H_2O_2 also did not cause detectable sulfinylation, but incubation with 100 μM H_2O_2 caused a detectable accumulation of sulfinylated cross-linked dimers, and incubation with 200 μM H_2O_2 caused detectable accumulation of sulfinylated cross-linked dimers and a barely detectable accumulation of sulfinylated non-crosslinked dimers. Simulations using Models B and D are in quantitative agreement with these experimental observations if one assumes a detection limit of ≈30% sulfinylation (Figure 3B and Supplementary Figure 2.7A-C). The predicted absolute extent of sulfinylation depends on the pseudo-first order rate constant for the sulfiredoxin reaction, whose value in human erythrocytes remains very uncertain. Higher values of this rate constant will lead to the same qualitative result holding at lower detection limits.

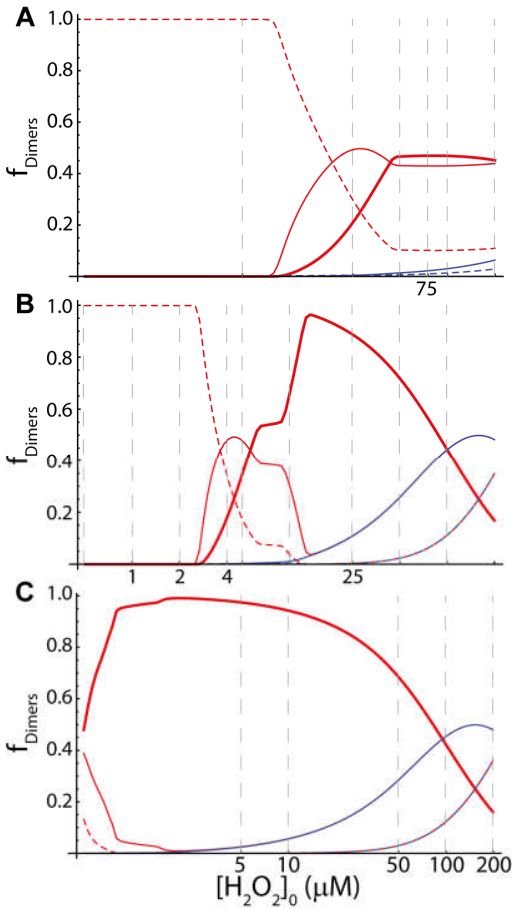

Supplementary Figure 2.7. Simulation of experiments in Figures 3 and 4 of [2]. Fractions of non-crosslinked (dashed), singly-crosslinked (thin solid lines) and doubly-crosslinked (thick solid line) dimers, sulfinylated (blue) or not (red), obtained after 10 min incubations of 5×10^{10} cells dm^{-3} (A, B) or 5×10^{9} cells dm^{-3} (C) with H_2O_2 boluses. (A) simulation based on Model B, compare to Figure 2C of [2]; (B, C) simulations based on Model B with $[Cat]_{tot}=0$, compare to Figures 2D and 3B of ref.[2], respectively. Simulations A-C based on Model D were very similar, whereas those based on Model C were inconsistent with experimental observations; those based on Model A were qualitatively distinct only at $[H_2O_2]_0$ not tested experimentally (not shown). Gray dashed lines indicate the boluses used in [2]. In panels B and C the thin blue lines overlap the thin red lines for high boluses, indicating that virtually all the singly-crosslinked dimers are sulfinylated under these conditions. Likewise, in these panels the dashed blue line overlaps the dashed red line. H_2O_2 concentrations are represented in logarithmic scale. Simulations based on Model D yield very similar results.

The simulation results in Supplementary Figure 2.7A reproduced the following puzzling experimental observation. Incubation of 5×10^{10} cells dm^{-3} with 50-200 μM H_2O_2 boluses caused incomplete Prx2 oxidation at 10 min, and the extent of oxidation did not change over this range of H_2O_2 concentrations. This behavior

has been attributed to more efficient H_2O_2 consumption by Cat at higher H_2O_2 concentrations [2]. However, we found that a model variant where the conversion of Compound I to Compound II was blocked, which abolishes any changes in Cat efficiency, yielded results that virtually overlap those in Supplementary Figure 2.7A. Instead, this phenomenon appears to be due to the following more complex interplay of factors. Strong H_2O_2 boluses lead to a transient state where the rate of Prx2 disulfide (PSS) production is limited by the rate of Prx2 thiol (PSH) regeneration by the Trx1/TrxR system (Supplementary Figure 2.8A). Due to the low activity of the latter system Prx2 accumulates almost completely in PSS form under these conditions, and the elimination of H_2O_2 is then mostly carried out by Cat with approximately pseudo-first-order kinetics. The intracellular H_2O_2 concentration thus decays exponentially (Supplementary Figure 2.8A, $t < 300$ s), tracking the permeation-limited exponential decay of extracellular H_2O_2. Therefore, at some point in time the oxidation of PSH by H_2O_2 becomes the rate-limiting step, and eventually becomes negligible compared to the rate (v_{red}) of PSS reduction (Supplementary Figure 2.8A, $t > 100$ s). Considering the exponential decay of intracellular H_2O_2, the time (t^*) at which net PSH accumulation begins scales approximately as the logarithm of bolus intensity ($[H_2O_2]_0$). Thus, each doubling of $[H_2O_2]_0$ will delay t^* by just $\Delta t^* \approx \ln(2)/(0.039\ s^{-1}) = 18$ s, where the denominator is the decay exponent of H_2O_2 concentration inferred from the curve in Figure 4B of [2] (Supplementary Materials section 2.10.3) corrected for 5×10^{10} cells dm^{-3}. From then on, the concentration of PSH increases at the approximately constant rate v_{red}, which is independent of the concentration of H_2O_2 (Supplementary Figure 2.8B). Each doubling in $[H_2O_2]_0$ thus decreases the extent of Prx2 reduction at 10 min by just $\approx v_{red}/\Delta t^*$.[18] The fraction of non-crosslinked dimers changes even less due to the following compensatory factor (Supplementary Figure 2.8B). Sulfinylated Prx2 (PSO_2H) accumulates for a short period while there is some accumulation of PSOH. This

[18] The value of v_{red} is much lower than $V_{Max,TrxR}$ because such strong H_2O_2 boluses cause substantial GSSG accumulation, leading GSR to outcompete TrxR for NADPH. The fact that the less GSSG accumulated in response to lower H_2O_2 boluses can be reduced in less than 10 min explains the higher extent of Prx2 reduction at 10 min after those boluses.

accumulation increases with $[H_2O_2]_0$ and hinders the formation of disulfide crosslinks.

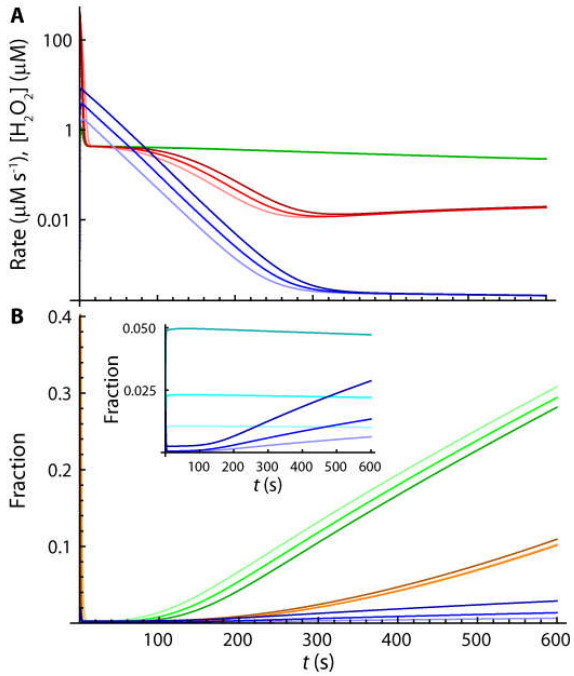

*Supplementary Figure 2.8. Analysis of time courses after H_2O_2 boluses. Simulations consider the experimental conditions for Figure 2C from ref.[2] and 50 μM (lightest curves), 100 μM and 200 μM (darkest) H_2O_2 boluses. (A) Rate of PSS formation (red) and reduction (green), and intracellular H_2O_2 concentration (blue). (B) Fraction of Prx2 monomers in PSH form (green), fraction of Prx2 dimers that lack disulfide crosslinks (PS*HPS*H, orange), fraction of dimers that lack disulfide crosslinks and carry at least one sulfinic Cys (PSO_2HPS^*H, blue), and fraction of sulfinylated Prx2 monomers (PSO_2H, cyan, inset). Note that sulfinylated monomers only accumulate very early on, and that the increase in the fraction of PSO_2HPS^*H at t>100 s is due to the reduction of sulfinylated singly-crosslinked dimers ($PSSPSO_2H$) to non-crosslinked sulfinylated dimers ($PSHPSO_2H$).*

When Cat is inhibited as per the experiment in Figure 3B of [2], all the redox pools are strongly depleted, and Prx2 is not significantly reduced over the 10 min duration of the incubation. Further, the concentration of H_2O_2 stays high during this period, leading to progressive Prx2 sulfinylation.

Model B predicts redox potentials of the Trx and NADPH pools at rest (Table 2 in main text) that are in line with those characterized experimentally in other cells: –280 mV for Trx1 in proliferating THP1 human monocytes [56] and –400 mV for NADPH [126]. However, it predicts a more negative redox potential for GSH than the –250 mV determined [127] for human erythrocytes or the –259 mV

determined [56] for proliferating THP1 human monocytes. This discrepancy is mainly due to the following two reasons. First, the model neglects various processes that oxidize the GSH pool, such as the reduction of organic peroxides and of protein sulfenic acids and dithiols. Second, experimental determinations tend to overestimate the extent of GSH oxidation *in vivo* because they are usually carried out at O_2 partial pressures much above physiological values. This discrepancy could be resolved by assuming an additional process oxidizing GSH and does not change the conclusions of this work.

Despite the good agreement with the experimental observations in [31], Models B and D are inconsistent with the high Prx2 sulfinylation observed by Cho *et al.* [4] at low H_2O_2 supplies. However, this discrepancy is likely due to a strong underestimation of H_2O_2 supply in this experiment. We examine this problem in the next section.

2.10.13.3 Analysis of experiments by Cho *et al.* [4]

Cho *et al.* [4] incubated erythrocytes at a 50% hematocrit with glucose oxidase (GO) at an activity that generates H_2O_2 at a purported rate of 4.5 μM min^{-1}= 75 nM s^{-1}. They found that ≈10% of Prx2 becomes sulfinylated after 3 h, corresponding to a mean sulfinylation rate of 0.1×(5.7×10^{-4} M)/(3×3600 s)= 5.3 nM s^{-1} in excess of the sulfiredoxin-catalyzed sulfinic acid reduction rate.

The extracellular H_2O_2 concentration at steady state in this experiment can be estimated from the purported H_2O_2 production rate as follows. The 50% hematocrit corresponds to a pseudo-first-order rate constant for H_2O_2 clearance by erythrocytes of (5.8×10^{-5} dm s^{-1})×(1.35×10^{-8} dm^2)×0.5/((1–0.5)×10^{-13} dm^3) = 7.8 s^{-1}, considering the permeability constant estimated in Supplementary Materials section 2.10.3, an erythrocyte surface area of 1.35×10^{-8} dm^2 [80] and an erythrocyte volume of 10^{-13} dm^3 [80]. Thus, the steady state extracellular H_2O_2 concentration is (75 nM s^{-1})/(7.8 s^{-1})= 9.6 nM.

In order to examine the consistency of Model A with the mean sulfinylation rate implied by the experiment above we first estimate the H_2O_2 influx referred to intracellular concentrations. Because the hematocrit is 50% and considering a water to cell volume ratio of 0.717 [79] this influx is simply (75 nM s^{-1})/0.717= 0.11 μM s^{-1}. The endogenous H_2O_2 production can be estimated as 0.057 μM s^{-1}, per

Supplementary Materials section 2.10.2 and accounting for the higher H_2O_2 production from GSH autoxidation under atmospheric pressure (pO_2= 160 Torr) (Supplementary Materials section 2.10.2). The total H_2O_2 supply is thus around 0.16 μM s^{-1}. This is still sufficiently low that the GSH, Trx1 and Prx2 pools remain overwhelmingly in the reduced forms. Therefore, the intracellular H_2O_2 concentration according to Model A will be approximately the ratio between the supply rate and the sum of the pseudo-first-order rate constants (k_{Prx2} + k_{Cat} + k_{GPx1} = 57000 s^{-1} + 218 s^{-1} + 25 s^{-1} = 57243 s^{-1}) for H_2O_2 elimination by the three main defenses: (0.16 μM s^{-1})/(57243 s^{-1}= 2.8 pM. This concentration will form (5.7×10^4 s^{-1})×(2.8×10^{-12} M)= 0.16 μM s^{-1} sulfenic Prx2. Neglecting the activity of sulfiredoxin and considering the rate constants for condensation and sulfinylation (k_{Cond}= 1.7 s^{-1}, k_{Sulf}= 1.2×10^4 $M^{-1}s^{-1}$) determined in [22] this flux leads to a (0.16 μM s^{-1})/[1.7 s^{-1} + (1.2×10^4 $M^{-1}s^{-1}$)×(2.8 pM)]= 94 nM steady state concentration of sulfenic Prx2, and a (1.2×10^4 $M^{-1}s^{-1}$)×(2.8 pM)×(94 nM)= 3.2 fM s^{-1} sulfinylation rate. This rate is six orders of magnitude lower than that implied by the results in [4]. Further, in order to achieve consistency the value of k_{Sulf} would have to be (1.7 s^{-1} × 5.3 nM s^{-1})/[2.8 pM ×(0.16 μM s^{-1} – 0.0053 μM s^{-1})] = 2.1×10^{10} $M^{-1}s^{-1}$, which is unrealistically high.

Cho *et al.* [4] further observed that under the same conditions as in the experiment described above Cat inhibition caused a 5- to 10-fold increase in the Prx2 sulfinylation rate. In order to examine the implications of this observation with respect to the fraction of H_2O_2 consumed by Prx2 we considered the simplified model outlined in Supplementary Figure 2.9A.

A steady state analysis of this model shows that the ratio (r) between the sulfinylation rate at the normal Cat activity and that with Cat fully inhibited can be written as function of two reduced parameters as follows:

$$r = \frac{\gamma - 1}{2}\left(\left(\frac{1}{\rho}+1\right)\left(\sqrt{\left(\gamma+(\gamma+1)\rho\right)^2 - 4\gamma\rho^2} - \gamma\right) - \left(\gamma + 1 + (\gamma-1)\rho\right)\right), \qquad (8)$$

where $\rho = \dfrac{\dfrac{1}{\dfrac{1}{k_{\mathrm{Cond}}}+\dfrac{1}{k_R}}[\mathrm{Prx2}]_{Tot}}{\Phi} > 1$ corresponds to the ratio between the maximal rate of regeneration of Prx2 in thiol form and the H_2O_2 supply rate, and

2. Hydrogen peroxide metabolism in human erythrocytes

$\rho = \frac{k_{Ox}[\mathrm{Prx2}]_{Tot}}{k_{Cat}}$ corresponds to the ratio between the pseudo-first-order rate constant for H_2O_2 reduction by the thiol form of Prx2 and that for H_2O_2 dismutation by Cat. Solving Equation (8) for the value of ρ that would yield r= 1/5 one finds

$$\rho_{1/5} = \frac{10\gamma^2 - 5\gamma - 4 + (5\gamma - 4)\sqrt{20\gamma(\gamma - 1) + 1}}{40(\gamma - 1)^2} \qquad (9)$$

Under the conditions of the experiment γ=296, which yields $\rho_{1/5}$= 0.81. [The value of $\rho_{1/5}$ is remarkably constant over a wide range of γ values (Supplementary Figure 2.9B)]. Thus, the above mentioned experimental observation implies that Prx2 consumes no more than 0.81/(1+0.81)= 45% of the H_2O_2. But for a value ρ= 0.81 to obtain, Prx2 would have to be 1-(0.81×218 s^{-1})/(5.7×10^4 s^{-1})= 99.7% inhibited.

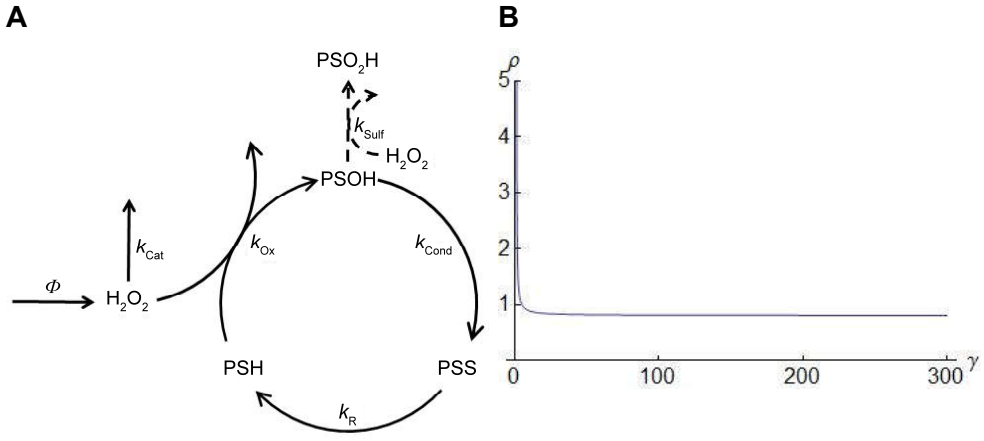

Supplementary Figure 2.9. Simplified model for the analysis of the effect of Cat inhibition on sulfinylation rate. A) Diagram of the model. The parameters are: Φ, H_2O_2 supply; k_{Cat}, pseudo-first-order rate constant for H_2O_2 consumption by Cat; k_{Ox}, rate constant for H_2O_2 reduction by the thiol form of Prx2; k_{Cond}, rate constant for sulfenic acid condensation with the resolving Cys; k_R= $k_{Red}[Trx]_{Tot}$, pseudo-first-order rate constant for the reduction of the Prx2 disulfide by thioredoxin, assuming all thioredoxin in reduced form; k_{Sulf}, rate constant for sulfinylation. Sulfinylation (dashed arrows) was considered negligible in the calculation of the steady state concentrations. We neglected the contribution of the GPx1 reaction for H_2O_2 consumption. B) Plot of the values of ρ that yield r= 1/5 as function of γ. See text for explanation.

Although a strong reversible inhibition of Prx2 can explain the experimentally observed effects of changes in Cat activity in intact cells the following analysis shows that it cannot explain the extent of Prx2 sulfinylation observed by Cho *et al.* [4].

Consider that Prx2 oxidation to the sulfenic form is inhibited to the extent that it accounts for the consumption of 50% of the H_2O_2. Under these circumstances the intracellular steady state concentrations of H_2O_2 and of Prx2 sulfenic form are $[\mathrm{H_2O_2}] = \frac{\Phi}{2k_O}$ and $[\mathrm{PSOH}] = \frac{1}{2}\frac{\Phi}{k_{\mathrm{Cond}} + k_{\mathrm{Sulf}}[\mathrm{H_2O_2}]} = \frac{\Phi}{2k_{\mathrm{Cond}} + k_{\mathrm{Sulf}}\frac{\Phi}{k_{\mathrm{O}}}}$, with k_O standing for the pseudo-first-order rate constant for all the other processes consuming H_2O_2. The sulfinylation rate will thus be

$$v_S = k_{\mathrm{Sulf}}[\mathrm{PSOH}][\mathrm{H_2O_2}] = \frac{1}{2}\frac{\Phi^2}{2\frac{k_O k_{\mathrm{Cond}}}{k_{\mathrm{Sulf}}} + \Phi} \approx \frac{1}{4}\frac{\Phi^2}{k_O}\frac{k_{\mathrm{Sulf}}}{k_{\mathrm{Cond}}} \qquad (10)$$

Considering k_O= 243 s^{-1}, as per the estimated contributions of Cat and GPx1, and replacing values one finds v_S= 190 fM s^{-1}, which is still four orders of magnitude lower than the mean sulfinylation rate implied by the experiments of Cho *et al.* [4]. In order to explain the reported sulfinylation flux under these conditions, k_{Sulf}/k_{Cond} would have to exceed the 7.1×10^3 M^{-1} determined in [22] by a 4×10^4 factor.

In order to determine if such values of k_{Sulf}/k_{Cond} would be consistent with the results from [2] described in Supplementary Materials section 2.10.13.2 in the framework of Model B we proceeded as follows. We varied the value of k_{Cond} from 10^{-5} s^{-1} up to 20 s^{-1} while keeping the ratio k_{Sulf}/k_{Cond} fixed at 2.8×10^8 M^{-1} and examined whether any values in this range would yield results qualitatively consistent with those in Figures 2, 3 and 4 of [2]. ($k_{Cond} \leq 10^{-5}$ s^{-1} yields <7% reduced Prx2 monomers without exogenous H_2O_2 addition, contrary to observations [2] that most Prx2 is reduced under such conditions; $k_{Cond} > 20$ s^{-1} yield k_{Sulf} values beyond the diffusion limit.) All k_{Cond} values in the considered range yielded results that are qualitatively inconsistent with the experimental observations in [2]. Therefore, the observations by Cho *et al.* [4] cannot be explained in the framework of Model B simply by assuming that the values of k_{Cond} and k_{Sulf} differ from the experimentally determined ones.

As follows from equation (10), v_S depends quadratically on the rate of H_2O_2 production and therefore any error in the latter rate will have a strong effect on the former. This prompted us to investigate if Cho *et al.* [4] could have

underestimated the H_2O_2 production rate. The reported 4.5 μM min^{-1} rate of H_2O_2 production *via* GO was determined in an experiment where H_2O_2 accumulated for 3 h to concentrations in excess of 6 mM. The concentration of O_2 in the medium cannot exceed 186 μM as per the water solubility, and can be much lower owing to consumption by the GO reaction under only mild agitation. Because H_2O_2 is a competitive inhibitor of GO with a K_I that is similar to the K_M for O_2 [128], GO is strongly inhibited under these conditions. However, in presence of erythrocytes at a 50% hematocrit the situation is dramatically different for the following two reasons. First, the steady state H_2O_2 concentration in the assay medium is much lower owing to consumption by the cells. Second, erythrocytes carry a total ≈10 mM O_2 bound to hemoglobin, which can be readily delivered owing to the very large total area of contact between cells and the medium. Therefore, the ratio between the concentrations of H_2O_2 and O_2 will be much lower, GO will be much less inhibited and the rate of H_2O_2 production will be much higher under these conditions. The extent of this effect is difficult to determine accurately because the O_2 concentrations attained in the control experiment are dependent on geometrical factors that were not reported. However, we can obtain a lower estimate under the optimistic assumption that the medium was saturated with O_2 in both experiments. Considering that at the solubility limit $[O_2] \approx K_M(O_2)$ [128], that $K_I \approx K_M(O_2)$ and that $[H_2O_2] >> [O_2]$, the ratio between the non-inhibited and the inhibited rate of H_2O_2 production is approximately

$$\frac{v_{GO}}{v_{GO,inh}} = \frac{\dfrac{V_{Max}^{App}[O_2]}{K_M + [O_2]}}{\dfrac{V_{Max}^{App}[O_2]}{K_M\left(1+\dfrac{[H_2O_2]}{K_I}\right)+[O_2]}} = \frac{K_M\left(1+\dfrac{[H_2O_2]}{K_I}\right)+[O_2]}{K_M+[O_2]} \approx \frac{[H_2O_2]}{2[O_2]} \approx \frac{3\,\mathrm{mM}}{0.372\,\mathrm{mM}} \approx 8.1$$

(Here, 3 mM is taken as the mean H_2O_2 concentration over the experiment for determining the rate of H_2O_2 production.) Thus, even under this optimistic assumption the sulfinylation rate would be $8.1^2 \approx 66$-fold higher than predicted based on the reported rate of H_2O_2 production. Furthermore, the long incubation with high initial glucose concentrations (25 mM) may have caused strong acidification of the medium owing to lactate accumulation from glucose

catabolism. Acidic conditions have recently been shown to promote Prx2 oxidation in human erythrocytes [128], presumably due to enhanced superoxide production via hemoglobin autoxidation [6, 129].

Recent carefully designed experiments did not detect Prx2 sulfinylation in HEK293 cells exposed to steady 3.7 μM H_2O_2 up to 24h, but showed evidence of Prx2 overoxidation following administration of >25 μM H_2O_2 boluses [130]. The computational results based on Models B and D, which consider the condensation and sulfinylation rate constants determined in [22], are consistent with these experimental observations and also with those in [2]. Therefore, there is no substantial reason to question the ability of these models to simulate the responses of Prx2 sulfinylation to H_2O_2.

2.10.13.4 Analysis of experiments of Jacob *et al.* [67]

Jacob *et al.* [67] incubated normal and acatalasemic erythrocytes at a hematocrit of 35% with 15 mM glucose plus tracer quantities of ^{14}C-glucose at 37 ºC and quantified the amount of $^{14}CO_2$ accumulated after 4 hours. Whereas normal erythrocytes produced 48 μmol CO_2/dm^3 cells/hour, corresponding to 38 nM NADPH/s, acatalasemic erythrocytes produced 123 μmol CO_2/dm^3 cells/hour, corresponding to 98 nM NADPH/s. This suggests that in normal erythrocytes Prx2 and GPx1 together consume ≈39% of the H_2O_2. This estimate follows from the following analysis based on the assumptions that most NADPH was being used towards H_2O_2 reduction, that H_2O_2 production is identical in both normal and acatalasemic cells, and that acatalasemic erythrocytes have normal GPx1 and Prx2 activities. The intracellular concentration of H_2O_2 in normal and acatalasemic erythrocytes at steady state are given by $[H_2O_2] = \frac{\Phi}{k_{GPx1} + k_{Prx2} + k_{Cat}}$ and $[H_2O_2] = \frac{\Phi}{k_{GPx1} + k_{Prx2}}$, respectively. Thus, the rates of NADPH consumption in each case are $v_{normal} = [H_2O_2](k_{Prx2} + k_{GPx1}) = \frac{\Phi}{1 + \frac{k_{Cat}}{k_{GPx1} + k_{Prx2}}}$ and

$v_{acatalasemic} = [H_2O_2](k_{Prx2} + k_{GPx1}) = \Phi$, respectively, from which it follows $\frac{v_{normal}}{v_{acatalasemic}} = \frac{k_{GPx1} + k_{Prx2}}{k_{Cat} + k_{GPx1} + k_{Prx2}} = \frac{38\,\mathrm{nMs^{-1}}}{98\,\mathrm{nMs^{-1}}} \approx 0.39$.

The estimated contribution of GPx1 and Prx2 will be even lower for the following two reasons. First, because part of the NADPH is consumed for processes other than H_2O_2 reduction the ratios of NADPH regeneration rates above underestimate the ratio between NADPH consumption by H_2O_2 reduction in normal erythrocytes and that in acatalasemic erythrocytes. Second, the rate of endogenous H_2O_2 generation may have been higher in normal than in acatalasemic erythrocytes. This because normal erythrocytes accumulated more lactate than acatalasemic ones, which should have caused higher acidification in the former than in the latter erythrocytes. Acidic environments exacerbate Prx2 oxidation, presumably due to increased hemoglobin autoxidation generating superoxide [6].

2.10.14 Additional notes

2.10.14.1 Energetic cost of inhibiting the peroxidase activity of Prx2 through covalent modification

The observation that most Prx2 is oxidized to disulfide form within 1 min after erythrocytes are exposed to a 5 μM H_2O_2 bolus [2] implies an inhibition-activation turnover in the order of 0.1 s^{-1}. This turnover amounts to a flux approaching (0.1 s^{-1})×(570 μM)= 57 μM s^{-1}, which is 18-fold the erythrocyte's maximal ATP production rate [42]. Because each covalent modification cycle costs at least one ATP or one reducing equivalent, this mode of regulation would make such a rate of cycling energetically forbidding.

2.11 References

1. Johnson, R. M., G. Goyette, Y. Ravindranath and Y•-S. Ho (2005). "Hemoglobin autoxidation and regulation of endogenous H2O2 levels in erythrocytes." Free Radic Biol Med **39**(11): 1407-1417.

2. Low, F. M., M. B. Hampton, A. V. Peskin and C. C. Winterbourn (2007). "Peroxiredoxin 2 functions as a noncatalytic scavenger of low-level hydrogen peroxide in the erythrocyte." Blood **109**(6): 2611-2617.

3. Johnson, R. M., Y•-S. Ho, D•-Y. Yu, F. A. Kuypers, Y. Ravindranath and G. W. Goyette (2010). "The effects of disruption of genes for peroxiredoxin-2, glutathione peroxidase-1, and catalase on erythrocyte oxidative metabolism." Free Radical Biology And Medicine **48**(4): 519-525.

4. Cho, C. S., S. Lee, G. T. Lee, H. A. Woo, E. J. Choi and S. G. Rhee (2010). "Irreversible Inactivation of Glutathione Peroxidase 1 and Reversible Inactivation of Peroxiredoxin II by H2O2 in Red Blood Cells." Antioxidants & Redox Signaling **12**(11): 1235-1246.

5. Han, Y•-H., S•-U. Kim, T•-H. Kwon, D•-S. Lee, H•-L. Ha, D•-S. Park, E•-J. Woo, S•-H. Lee, J•-M. Kim, H•-B. Chae, S. Y. Lee, B. Y. Kim, D. Y. Yoon, S. G. Rhee, E. Fibach and D•-Y. Yu (2012). "Peroxiredoxin II is essential for preventing hemolytic anemia from oxidative stress through maintaining hemoglobin stability." Biochem. Biophys. Res. Commun. **426**(3): 427-432.

6. Bayer, S. B., G. Maghzal, R. Stocker, M. B. Hampton and C. C. Winterbourn (2013). "Neutrophil-mediated oxidation of erythrocyte peroxiredoxin 2 as a potential marker of oxidative stress in inflammation." FASEB J.

7. Antunes, F., A. Salvador and R. E. Pinto (1995). "PHGPx and phospholipase A2/GPx: comparative importance on the reduction of hydroperoxides in rat liver mitochondria." Free Radical Biology and Medicine **19**(5): 669-677.

8. Salvador, A., F. Antunes and R. E. Pinto (1995). "Kinetic modelling of in vitro lipid peroxidation experiments--'low level' validation of a model of in vivo lipid peroxidation." Free Radical Research **23**(2): 151-172.

9. Antunes, F., A. Salvador, H. S. Marinho, R. Alves and R. E. Pinto (1996). "Lipid peroxidation in mitochondrial inner membranes. I. An integrative kinetic model." Free Radical Biology and Medicine **21**(7): 917-943.

10. Salvador, A., J. Sousa and R. E. Pinto (2001). "Hydroperoxyl, superoxide and pH gradients in the mitochondrial matrix: a theoretical assessment." Free Radical Biology and Medicine **31**(10): 1208-1215.

11. Gardner, R., A. Salvador and P. Moradas-Ferreira (2002). "Why does SOD overexpression sometimes enhance, sometimes decrease, hydrogen peroxide production? A minimalist explanation." Free Radical Biology and Medicine **32**(12): 1351-1357.

12. Salvador, A. and M. A. Savageau (2003). "Quantitative evolutionary design of glucose 6-phosphate dehydrogenase expression in human erythrocytes." Proceedings of the National Academy of Sciences of the U. S. A. **100**: 14463-14468.

13. Makino, N., K. Sasaki, K. Hashida and Y. Sakakura (2004). "A metabolic model describing the H2O2 elimination by mammalian cells including H2O2 permeation through cytoplasmic and peroxisomal membranes: comparison with experimental data." Biochimica et Biophysica Acta-General Subjects **1673**(3): 149-159.

14. Gardner, R., P. Moradas-Ferreira and A. Salvador (2006). "Why does superoxide dismutase overexpression often increase hydrogen peroxide

concentrations? An alternative explanation." Journal of Theoretical Biology **242**(3): 798-800.

15. Salvador, A. and M. A. Savageau (2006). "Evolution of enzymes in a series is driven by dissimilar functional demands." Proceedings of the National Academy of Sciences of the U. S. A. **103**: 2226-2231.

16. Coelho, P. M. B. M., A. Salvador and M. A. Savageau (2009). "Quantifying Global Tolerance of Biochemical Systems: Design Implications for Moiety-Transfer Cycles." PLoS Comput Biol **5**(3): e1000319.

17. Adimora, N. J., D. P. Jones and M. L. Kemp (2010). "A Model of Redox Kinetics Implicates the Thiol Proteome in Cellular Hydrogen Peroxide Responses." Antioxidants & Redox Signaling **13**(6): 731-743.

18. Coelho, P. M. B. M., A. Salvador and M. A. Savageau (2010). "Relating Mutant Genotype to Phenotype via Quantitative Behavior of the NADPH Redox Cycle in Human Erythrocytes." PLoS ONE **5**(9): e13031.

19. Pillay, C., J$^{\bullet-}$H. Hofmeyr and J. Rohwer (2011). "The logic of kinetic regulation in the thioredoxin system." BMC Systems Biology **5**(1): 15.

20. Aon, M. A., B. A. Stanley, V. Sivakumaran, J. M. Kembro, B. O'Rourke, N. Paolocci and S. Cortassa (2012). "Glutathione/thioredoxin systems modulate mitochondrial H2O2 emission: An experimental-computational study." Journal Of General Physiology **139**(6): 479-491.

21. Alves, R., F. Antunes and A. Salvador (2006). "Tools for kinetic modeling of biochemical networks." Nature Biotechnology **24**(6): 667-672.

22. Peskin, A. V., N. Dickerhof, R. A. Poynton, L. N. Paton, P. E. Pace, M. B. Hampton and C. C. Winterbourn (2013). "Hyperoxidation of peroxiredoxins 2 and 3: Rate constants for the reactions of the sulfenic acid of the peroxidatic cysteine." J. Biol. Chem.

23. Peskin, A. V., F. M. Low, L. N. Paton, G. J. Maghzal, M. B. Hampton and C. C. Winterbourn (2007). "The high reactivity of peroxiredoxin 2 with H2O2 is not reflected in its reaction with other oxidants and thiol reagents." Journal Of Biological Chemistry **282**(16): 11885-11892.

24. Manta, B., M. Hugo, C. Ortiz, G. Ferrer-Sueta, M. Trujillo and A. Denicola (2009). "The peroxidase and peroxynitrite reductase activity of human erythrocyte peroxiredoxin 2." Archives Of Biochemistry And Biophysics **484**(2): 146-154.

25. Moore, R. B. and S. K. Shriver (1997). "Protein 7.2 b of human erythrocyte membranes binds to calpromotin." Biochemical and biophysical research communications **232**(2): 294-297.

26. Rinalducci, S., G. M. D'Amici, B. Blasi and L. Zolla (2011). "Oxidative stress-dependent oligomeric status of erythrocyte peroxiredoxin II (PrxII) during storage under standard blood banking conditions." Biochimie **93**(5): 845-853.

27. Matte, A., M. Bertoldi, N. Mohandas, X. An, A. Bugatti, A. M. Brunati, M. Rusnati, E. Tibaldi, A. Siciliano, F. Turrini, S. Perrotta and L. De Franceschi (2013). "Membrane association of peroxiredoxin-2 in red cells is mediated by the N-terminal cytoplasmic domain of band 3." Free Radical Biology And Medicine **55**: 27-35.

28. Pallotta, V., A. D'Alessandro, S. Rinalducci and L. Zolla (2013). "Native protein complexes in the cytoplasm of red blood cells." Journal of proteome research **12**(7): 3529-3546.

29. Flohé, L., G. Loschen, W. A. Gunzler and E. Eichele (1972). "Glutathione peroxidase, V. The kinetic mechanism." Hoppe-Seylers Zeitschrift Fur Physiologische Chemie **353**(6): 987-999.

30. Mannervik, B. (1973). "A branching reaction mechanism of glutathione reductase." Biochemical and Biophysical Research Communications **53**(4): 1151-1158.

31. Thorburn, D. R. and P. W. Kuchel (1985). "Regulation of the human-erythrocyte hexose-monophosphate shunt under conditions of oxidative stress. A study using NMR spectroscopy, a kinetic isotope effect, a reconstituted system and computer simulation." European Journal Of Biochemistry **150**(2): 371-386.

32. Worthington, D. J. and M. A. Rosemeyer (1976). "Glutathione reductase from human erythrocytes. Catalytic properties and aggregation." European Journal Of Biochemistry **67**(1): 231-238.

33. Chance, B. (1952). "The state of catalase in the respiring bacterial cell." Science **116**(3008): 202-203.

34. Nicholls, P. (1964). "The formation and catalytic role of catalase peroxide compound II." Biochimica et Biophysica Acta (BBA) - Specialized Section on Enzymological Subjects **81**(3): 479-495.

35. Kirkman, H. N., M. Rolfo, A. M. Ferraris and G. F. Gaetani (1999). "Mechanisms of protection of catalase by NADPH - Kinetics and stoichiometry." Journal Of Biological Chemistry **274**(20): 13908-13914.

36. Urig, S., J. Lieske, K. Fritz-Wolf, A. Irmler and K. Becker (2006). "Truncated mutants of human thioredoxin reductase 1 do not exhibit glutathione reductase activity." Febs Letters **580**(15): 3595-3600.

37. Turanov, A. A., D. Su and V. N. Gladyshev (2006). "Characterization of alternative cytosolic forms and cellular targets of mouse mitochondrial thioredoxin reductase." Journal Of Biological Chemistry **281**(32): 22953-22963.

38. Grattagliano, I., S. Russmann, V. O. Palmieri, P. Portincasa, G. Palasciano and B. H. Lauterburg (2005). "Glutathione peroxidase, thioredoxin, and membrane protein changes in erythrocytes predict ribavirin-induced anemia[ast]." Clin Pharmacol Ther **78**(4): 422-432.

39. Wagner, T. C. and M. D. Scott (1994). "Single extraction method for the spectrophotometric quantification of oxidized and reduced pyridine-nucleotides in erythrocytes." Analytical Biochemistry **222**(2): 417-426.

40. George, A., S. Pushkaran, D. G. Konstantinidis, S. Koochaki, P. Malik, N. Mohandas, Y. Zheng, C. H. Joiner and T. A. Kalfa (2013). "Erythrocyte NADPH oxidase activity modulated by Rac GTPases, PKC, and plasma cytokines contributes to oxidative stress in sickle cell disease." Blood **121**(11): 2099-2107.

41. Giustarini, D., I. Dalle-Donne, R. Colombo, A. Milzani and R. Rossi (2004). "Interference of plasmatic reduced glutathione and hemolysis on glutathione disulfide levels in human blood." Free Radical Research **38**(10): 1101-1106.

42. Albrecht, V., H. Roigas, M. Schultze, G. Jacobasch and S. Rapoport (1971). "The influence of pH and methylene blue on the pathways of glucose utilization and lactate formation in erythrocytes of man." European Journal Of Biochemistry **20**(1): 44-50.

43. Lacy, F., D. A. Gough and S. Schmid (1998). "Role of xanthine oxidase in hydrogen peroxide production." Free Radical Biology And Medicine **25**(6): 720-727.

44. Liu, X. P. and J. L. Zweier (2001). "A real-time electrochemical technique for measurement of cellular hydrogen peroxide generation and consumption: Evaluation in human polymorphonuclear leukocytes." Free Radical Biology And Medicine **31**(7): 894-901.

45. Antunes, F. and E. Cadenas (2001). "Cellular titration of apoptosis with steady state concentrations of H(2)O(2): submicromolar levels of H(2)O(2) induce apoptosis through Fenton chemistry independent of the cellular thiol state." Free Radical Biology And Medicine **30**(9): 1008-1018.

46. Niethammer, P., C. Grabher, A. T. Look and T. J. Mitchison (2009). "A tissue-scale gradient of hydrogen peroxide mediates rapid wound detection in zebrafish." Nature **459**(7249): 996-U123.

47. Hogg, J. C., H. O. Coxson, M. L. Brumwell, N. Beyers, C. M. Doerschuk, W. MacNee and B. R. Wiggs (1994). "Erythrocyte and polymorphonuclear cell transit time and concentration in human pulmonary capillaries." J.Appl.Physiol **77**(4): 1795-1800.

48. Kuebler, W. M., K. Parthasarathi, J. Lindert and J. Bhattacharya (2007). "Real-time lung microscopy." Journal of applied physiology **102**(3): 1255-1264.

49. Sutton, G. C., J. Karnell and G. Nylin (1950). "Studies on the rapidity of complete blood circulation in man." American heart journal **39**(5): 741-748.

50. Mueller, S., H. D. Riedel and W. Stremmel (1997). "Direct evidence for catalase as the predominant H2O2-removing enzyme in human erythrocytes." Blood **90**(12): 4973-4978.

51. Paglia, D. E. and W. N. Valentine (1967). "Studies on quantitative and qualitative characterization of erythrocyte glutathione peroxidase." Journal of Laboratory and Clinical Medicine **70**(1): 158-169.

52. Takebe, G., J. Yarimizu, Y. Saito, T. Hayashi, H. Nakamura, J. Yodoi, S. Nagasawa and K. Takahashi (2002). "A comparative study on the hydroperoxide and thiol specificity of the glutathione peroxidase family and selenoprotein P." Journal Of Biological Chemistry **277**(43): 41254-41258.

53. Kirkman, H. N., S. Galiano and G. F. Gaetani (1987). "The function of catalase-bound NADPH." Journal Of Biological Chemistry **262**(2): 660-666.

54. Kirkman, H. N. and G. F. Gaetani (1984). "Catalase: a tetrameric enzyme with four tightly bound molecules of NADPH." Proceedings Of The National Academy Of Sciences Of The United States Of America **81**(14): 4343-4347.

55. Chang, T•-S. S., W. Jeong, A. W. Hyun, M. L. Sun, S. Park, G. R. Sue, H. A. Woo, S. M. Lee, S. Park and S. G. Rhee (2004). "Characterization of mammalian sulfiredoxin and its reactivation of hyperoxidized peroxiredoxin

through reduction of cysteine sulfinic acid in the active site to cysteine." The Journal of biological chemistry **279**: 50994-51001.

56. Watson, W. H., J. Pohl, W. R. Montfort, O. Stuchlik, M. S. Reed, G. Powis and D. P. Jones (2003). "Redox potential of human thioredoxin 1 and identification of a second dithiol/disulfide motif." J. Biol. Chem. **278**(35): 33408-33415.

57. Gromer, S., L. D. Arscott, C. H. Williams, R. H. Schirmeri and K. Becker (1998). "Human placenta thioredoxin reductase. Isolation of the selenoenzyme, steady state kinetics, and inhibition by therapeutic gold compounds." Journal of Biological Chemistry **273**: 20096-20101.

58. Wolfram Research, I. (2012). Mathematica. Champaign, Illinois, Wolfram Research, Inc.

59. Salvador, A. (2000). "Synergism analysis of metabolic processes: I. Conceptual framework." Mathematical Biosciences **163**(2): 105-129.

60. Salvador, A. (2000). "Synergism analysis of metabolic processes: II. Tensor formulation and treatment of stoichiometric constraints." Mathematical Biosciences **163**(2): 131-158.

61. Hoops, S., S. Sahle, R. Gauges, C. Lee, J. Pahle, N. Simus, M. Singhal, L. Xu, P. Mendes and U. Kummer (2006). "COPASI—a complex pathway simulator." Bioinformatics **22**(24): 3067-3074.

62. Hucka, M., A. Finney, H. M. Sauro, H. Bolouri, J. C. Doyle, H. Kitano, A. P. Arkin, B. J. Bornstein, D. Bray, A. Cornish-Bowden, A. A. Cuellar, S. Dronov, E. D. Gilles, M. Ginkel, V. Gor, I. I. Goryanin, W. J. Hedley, T. C. Hodgman, J. H. Hofmeyr, P. J. Hunter, N. S. Juty, J. L. Kasberger, A. Kremling, U. Kummer, N. Le Novere, L. M. Loew, D. Lucio, P. Mendes, E. Minch, E. D. Mjolsness, Y. Nakayama, M. R. Nelson, P. F. Nielsen, T. Sakurada, J. C. Schaff, B. E. Shapiro, T. S. Shimizu, H. D. Spence, J. Stelling, K. Takahashi, M. Tomita, J. Wagner and J. Wang (2003). "The systems biology markup language (SBML): a medium for representation and exchange of biochemical network models." Bioinformatics **19**(4): 524-531.

63. Moore, R. B., M. V. Mankad, S. K. Shriver, V. N. Mankad and G. A. Plishker (1991). "Reconstitution of Ca^{2+}-dependent K^{+} transport in erythrocyte-membrane vesicles requires a cytoplasmic protein." Journal Of Biological Chemistry **266**(28): 18964-18968.

64. Einstein, A. (1905). "Über die von der molekularkinetischen Theorie der Wärme geforderte Bewegung von in ruhenden Flüssigkeiten suspendierten Teilchen." Ann. Phys. **322**(8): 549-560.

65. Smoluchowski, M. V. (1906). "Zur kinetischen Theorie der Brownschen Molekularbewegung und der Suspensionen." Ann. Phys. **326**(14): 756-780.

66. van Stroe-Biezen, S., F. Everaerts, L. Janssen and R. Tacken (1993). "Diffusion coefficients of oxygen, hydrogen peroxide and glucose in a hydrogel." Analytica chimica acta **273**(1): 553-560.

67. Jacob, H. S., S. H. Ingbar and J. H. Jandl (1965). "Oxidative hemolysis and erythrocyte metabolism in hereditary acatalasia." J. Clin. Invest. **44**: 1187-1199.

68. Cho, C•-S., G. J. Kato, S. H. Yang, S. W. Bae, J. S. Lee, M. T. Gladwin and S. G. Rhee (2010). "Hydroxyurea-induced expression of glutathione peroxidase 1 in red blood cells of individuals with sickle cell anemia." Antioxid. Redox Signal. **13**(1): 1-11.

69. Moore, R. B., G. A. Plishker and S. K. Shriver (1990). "Purification and measurement of calpromotin, the cytoplasmic protein which activates calcium-dependent potassium transport." Biochemical and Biophysical Research Communications **166**(1): 146-153.

70. Shau, H., R. K. Gupta and S. H. Golub (1993). "Identification of a natural killer enhancing factor (NKEF) from human erythroid cells." Cellular immunology **147**(1): 1-11.

71. Ferrer-Sueta, G., B. Manta, H. Botti, R. Radi, M. Trujillo and A. Denicola (2011). "Factors Affecting Protein Thiol Reactivity and Specificity in Peroxide Reduction." Chemical Research In Toxicology **24**(4): 434-450.

72. Ogasawara, Y., T. Ohminato, Y. Nakamura and K. Ishii (2012). "Structural and functional analysis of native peroxiredoxin 2 in human red blood cells." International Journal of Biochemistry & Cell Biology **44**(7): 1072-1077.

73. Jaeschke, H., A. Bautista, Z. Spolarics and J. Spitzer (1992). "Superoxide generation by neutrophils and Kupffer cells during in vivo reperfusion after hepatic ischemia in rats." Journal of Leukocyte Biology **52**(4): 377-382.

74. Barranco-Medina, S., S. Kakorin, J. J. Lázaro and K•-J. Dietz (2008). "Thermodynamics of the Dimer Decamer Transition of Reduced Human and Plant 2-Cys Peroxiredoxin." Biochemistry **47**(27): 7196-7204.

75. Moon, J. C., Y•-S. Hah, W. Y. Kim, B. G. Jung, H. H. Jang, J. R. Lee, S. Y. Kim, Y. M. Lee, M. G. Jeon and C. W. Kim (2005). "Oxidative stress-dependent structural and functional switching of a human 2-Cys peroxiredoxin isotype II that enhances HeLa cell resistance to H2O2-induced cell death." Journal of Biological Chemistry **280**(31): 28775-28784.

76. Choi, M. H., I. K. Lee, G. W. Kim, B. U. Kim, Y•-H. Han, D•-Y. Yu, H. S. Park, K. Y. Kim, J. S. Lee, C. Choi, Y. S. Bae, B. I. Lee, S. G. Rhee and S. W. Kang (2005). "Regulation of PDGF signalling and vascular remodelling by peroxiredoxin II." Nature **435**(7040): 347-353.

77. Pace, P. E., A. V. Peskin, M•-H. Han, M. B. Hampton and C. C. Winterbourn (2013). "Hyperoxidized peroxiredoxin 2 interacts with the protein disulphide isomerase ERp46." Biochem. J.

78. Dammeyer, P. and E. S. J. Arner (2011). "Human Protein Atlas of redox systems - What can be learnt?" Biochimica et Biophysica Acta-General Subjects **1810**(1): 111-138.

79. Savitz, D., V. W. Sidel and A. K. Solomon (1964). "Osmotic properties of human red cells." Journal Of General Physiology **48**(1): 79-94.

80. Evans, E. and Y. C. Fung (1972). "Improved measurements of the erythrocyte geometry." Microvasc Res **4**(4): 335-347.

81. Giulivi, C., P. Hochstein and K. J. Davies (1994). "Hydrogen peroxide production by red blood cells." Free Radical Biology And Medicine **16**(1): 123-129.

82. Eder, H. A., C. Finch and R. W. McKee (1949). "CONGENITAL METHEMOGLOBINEMIA - A CLINICAL AND BIOCHEMICAL STUDY OF A CASE." Journal of Clinical Investigation **28**(2): 265-272.

83. Beutler, E. (1984). Red cell metabolism: a manual of biochemical methods. New York, Grune and Stratton.

84. Scarpa, M., P. Viglino, D. Contri and A. Rigo (1984). "Generation of superoxide ion in human red blood cell lysates." Journal Of Biological Chemistry **259**(17): 10657-10659.

85. Winterbourn, C. C., A. V. Peskin and H. N. Parsons-Mair (2002). "Thiol oxidase activity of copper,zinc superoxide dismutase." Journal Of Biological Chemistry **277**(3): 1906-1911.

86. Scarpa, M., F. Momo, P. Viglino, F. Vianello and A. Rigo (1996). "Activated oxygen species in the oxidation of glutathione - A kinetic study." Biophysical Chemistry **60**(1-2): 53-61.

87. Houk, J., R. Singh, G. M. Whitesides and O. W. G. William B. Jakoby (1987). Measurement of thiol-disulfide interchange reactions and thiol pKa values. Methods In Enzymology, Academic Press. **Volume 143:** 129-140.

88. Wilhelm, E., R. Battino and R. J. Wilcock (1977). "Low-pressure solubility of gases in liquid water." Chemical reviews **77**(2): 219-262.

89. Hartz, J. W., S. Funakoshi and H. F. Deutsch (1973). "The levels of superoxide dismutase and catalase in human tissues as determined immunochemically." Clinica Chimica Acta **46**(2): 125-132.

90. Gaetani, G. F., S. Galiano, L. Canepa, A. M. Ferraris and H. N. Kirkman (1989). "Catalase and glutathione peroxidase are equally active in detoxification of hydrogen peroxide in human erythrocytes." Blood **73**(1): 334-339.

91. Nicholls, P. (1965). "Activity of catalase in the red cell." Biochimica Et Biophysica Acta **99**: 286-297.

92. Aird, W. C. (2005). "Spatial and temporal dynamics of the endothelium." Journal of Thrombosis and Haemostasis **3**(7): 1392-1406.

93. Varma, S. D. and P. S. Devamanoharan (1991). "Hydrogen peroxide in human blood." Free Radic Res Commun **14**(2): 125-131.

94. Lacy, F., D. T. Connor and S. Schmid (1998). "Plasma hydrogen peroxide production in hypertensives and normotensive subjects at genetic risk of hypertension." J Hypertens **16**(3): 291-303.

95. Harkness, R. A., S. B. Coade and A. D. Webster (1984). "ATP, ADP and AMP in plasma from peripheral venous blood." Clinica Chimica Acta **143**(2): 91-98.

96. Kock, R., B. Delvoux and H. Greiling (1993). "A high-performance liquid chromatographic method for the determination of hypoxanthine, xanthine, uric acid and allantoin in serum." Eur J Clin Chem Clin Biochem **31**(5): 303-310.

97. Radi, R., H. Rubbo, K. Bush and B. A. Freeman (1997). "Xanthine oxidase binding to glycosaminoglycans: Kinetics and superoxide dismutase interactions of immobilized xanthine oxidase-heparin complexes." Archives Of Biochemistry And Biophysics **339**(1): 125-135.

98. Kudo, M., T. Moteki, T. Sasaki, Y. Konno, S. Ujiie, A. Onose, M. Mizugaki, M. Ishikawa and M. Hiratsuka (2008). "Functional characterization of human xanthine oxidase allelic variants." Pharmacogenetics and Genomics **18**(3): 243-251.

99. Maddipati, K. R., C. Gasparski and L. J. Marnett (1987). "Characterization of the hydroperoxide-reducing activity of human-plasma." Archives of Biochemistry and Biophysics **254**(1): 9-17.

100. Nicholls, P. (1972). "Contributions of catalase and glutathione peroxidase to red cell peroxide removal." Biochimica et Biophysica Acta (BBA) - General Subjects **279**(2): 306-309.

101. Awasthi, Y. C., E. Beutler and S. K. Srivastava (1975). "Purification and properties of human erythrocyte glutathione peroxidase." Journal Of Biological Chemistry **250**(13): 5144-5149.

102. Bonaventura, J., W. A. Schroeder and S. Fang (1972). "Human erythrocyte catalase: an improved method of isolation and a reevaluation of reported properties." Archives Of Biochemistry And Biophysics **150**(2): 606-617.

103. Ben, Y. and E. Shapira (1973). "Specific immunoassay for quantitative determination of human erythrocyte catalase." Journal of Laboratory and Clinical Medicine **81**(1): 133-139.

104. Sies, H., T. Bücher, N. Oshino and B. Chance (1973). "Heme occupancy of catalase in hemoglobin-free perfused rat liver and of isolated rat liver catalase." Archives Of Biochemistry And Biophysics **154**(1): 106-116.

105. Hillar, A., P. Nicholls, J. Switala and P. C. Loewen (1994). "NADPH BINDING AND CONTROL OF CATALASE COMPOUND-II FORMATION - COMPARISON OF BOVINE, YEAST, AND ESCHERICHIA-COLI ENZYMES." Biochemical Journal **300**: 531-539.

106. Gaetani, G. F., A. M. Ferraris, P. Sanna and H. N. Kirkman (2005). "A novel NADPH :(bound) NADP(+) reductase and NADH :(bound) NADP(+) transhydrogenase function in bovine liver catalase." Biochemical Journal **385**: 763-768.

107. Shimizu, N., K. Kobayashi and K. Hayashi (1984). "The reaction of superoxide radical with catalase. Mechanism of the inhibition of catalase by superoxide radical." Journal of Biological Chemistry **259**(7): 4414-4418.

108. Lardinois, O. M. (1995). "Reactions of bovine liver catalase with superoxide radicals and hydrogen peroxide." Free radical research **22**(3): 251-274.

109. Ogusucu, R., D. Rettori, D. C. Munhoz, L. E. S. Netto and O. Augusto (2007). "Reactions of yeast thioredoxin peroxidases I and II with hydrogen peroxide and peroxynitrite: rate constants by competitive kinetics." Free Radical Biology and Medicine **42**(3): 326-334.

110. Atkins, P. W. (1994). Physical chemistry. Oxford, Oxford University Press.

111. Fisher, A. B., C. Dodia, Y. Manevich, J. W. Chen and S. I. Feinstein (1999). "Phospholipid hydroperoxides are substrates for non-selenium glutathione peroxidase." Journal Of Biological Chemistry **274**(30): 21326-21334.

112. Go, Y•-M., J. R. Roede, D. Walkers, D. M. Duong, N. T. Seyfried, M. Orr, Y. Liang, K. D. Pennell and D. P. Jones (2013). "Selective targeting of the cysteine proteome by thioredoxin and glutathione redox systems." Mol. Cell Proteomics.

113. Holmgren, A. (1979). "Reduction of disulfides by thioredoxin. Exceptional reactivity of insulin and suggested functions of thioredoxin in mechanism of hormone action." J. Biol. Chem. **254**(18): 9113-9119.

114. Perez-Jimenez, R., J. Y. Li, P. Kosuri, I. Sanchez-Romero, A. P. Wiita, D. Rodriguez-Larrea, A. Chueca, A. Holmgren, A. Miranda-Vizuete, K. Becker, S. H. Cho, J. Beckwith, E. Gelhaye, J. P. Jacquot, E. Gaucher, J. M. Sanchez-Ruiz, B. J. Berne and J. M. Fernandez (2009). "Diversity of chemical mechanisms in thioredoxin catalysis revealed by single-molecule force spectroscopy." Nature Structural & Molecular Biology **16**(8): 890-U120.

115. Meplan, C., L. K. Crosley, F. Nicol, G. J. Beckett, A. F. Howie, K. E. Hill, G. Horgan, J. C. Mathers, J. R. Arthur and J. E. Hesketh (2007). "Genetic polymorphisms in the human selenoprotein P gene determine the response of selenoprotein markers to selenium supplementation in a gender-specific manner (the SELGEN study)." Faseb Journal **21**(12): 3063-3074.

116. Zhong, L. W., E. S. J. Arner and A. Holmgren (2000). "Structure and mechanism of mammalian thioredoxin reductase: The active site is a redox-active selenolthiol/selenenylsulfide formed from the conserved cysteine-selenocysteine sequence." Proceedings Of The National Academy Of Sciences Of The United States Of America **97**(11): 5854-5859.

117. Kirkman, H. N. and G. F. Gaetani (1986). "Regulation of glucose-6-phosphate dehydrogenase in human erythrocytes." Journal Of Biological Chemistry **261**(9): 4033-4038.

118. Canepa, L., A. M. Ferraris, M. Miglino and G. F. Gaetani (1991). "Bound and unbound pyridine dinucleotides in normal and glucose- 6-phosphate dehydrogenase-deficient erythrocytes." Biochimica Et Biophysica Acta **1074**(1): 101-104.

119. Kirkman, H. N., W. G. Wilson and E. H. Clemons (1980). "Regulation of glucose-6-phosphate-dehydrogenase .1. Intact red- cells." Journal of Laboratory and Clinical Medicine **95**(6): 877-887.

120. Buckwitz, D., G. Sch"nian, H. G. Holzh tter and G. Jacobasch (1986). "Kinetic model of glucose-6-phosphate dehydrogenase from red blood cells. Parameter estimation from progress curves and simulation of regulatory properties." Biomedica Biochimica Acta **45**(4): 429-439.

121. Wang, X. T., S. W. N. Au, V. M. S. Lam and P. C. Engel (2002). "Recombinant human glucose-6-phosphate dehydrogenase." European Journal Of Biochemistry **269**(14): 3417-3424.

122. Mulquiney, P. J. and P. W. Kuchel (1999). "Model of 2,3-bisphosphoglycerate metabolism in the human erythrocyte based on detailed enzyme kinetic equations: equations and parameter refinement." Biochemical Journal **342 Pt 3**: 581-596.

123. Hickey, T. M., D. E. Uddin and L. A. Kiesow (1979). "Measurement of Erythrocyte 2, 3-diphosphoglycerate with a centrifugal analyzer." Clinical chemistry **25**(7): 1314-1317.

124. Matte, A., P. S. Low, F. Turrini, M. Bertoldi, M. E. Campanella, D. Spano, A. Pantaleo, A. Siciliano and L. De Franceschi (2010). "Peroxiredoxin-2 expression is increased in beta-thalassemic mouse red cells but is displaced from the membrane as a marker of oxidative stress." Free Radical Biology and Medicine **49**(3): 457-466.

125. Du, Y., H. Zhang, J. Lu and A. Holmgren (2012). "Glutathione and glutaredoxin act as a backup of human thioredoxin reductase 1 to reduce thioredoxin 1 preventing cell death by aurothioglucose." Journal of Biological Chemistry **287**: 38210-38219.

126. Jones, D. P. (2002). Redox potential of GSH/GSSG couple: assay and biological significance. Methods in enzymology, protein sensors and reactive oxygen species - part B: Thiol enzymes and proteins. H. Sies and L. Packer. San Diego, California, Academic Press**:** 93-112.

127. Colombo, G., I. Dalle-Donne, D. Giustarini, N. Gagliano, N. Portinaro, R. Colombo, R. Rossi and A. Milzani (2010). "Cellular redox potential and hemoglobin S-glutathionylation in human and rat erythrocytes: A comparative study." Blood Cells Molecules and Diseases **44**(3): 133-139.

128. Bao, J., K. Furumoto, M. Yoshimoto, K. Fukunaga and K. Nakao (2003). "Competitive inhibition by hydrogen peroxide produced in glucose oxidation catalyzed by glucose oxidase." Biochemical engineering journal **13**(1): 69-72.

129. Brown, W. D. and L. B. Mebine (1969). "Autoxidation of Oxymyoglobins." Journal Of Biological Chemistry **244**(24): 6696-6701.

130. Sobotta, M. C., A. G. Barata, U. Schmidt, S. Mueller, G. Millonig and T. P. Dick (2013). "Exposing cells to H2O2: a quantitative comparison between continuous low-dose and one-time high-dose treatments." Free Radical Biology and Medicine **60**: 325-335.

CHAPTER 3 – PROTEOME COMPOSITION AND AEROTOLERANCE

3. Proteome composition and aerotolerance

ARTICLE IN PREPARATION

The imprint of aerotolerance on protein amino acid composition

Benfeitas, R.[1,2,3]; Moura, A.[1,4]; Alves, R.[3, 5]*, Salvador, A.[1,6]*

[1] - Center for Neuroscience and Cell Biology, University of Coimbra, 3004-517 Coimbra, Portugal

[2] - Institute for Interdisciplinary Research, University of Coimbra, 3030-789 Coimbra, Portugal

[3] Institut de Recerca Biomèdica de Lleida IRBLLeida, Edifici de Recerca Biomédica I, Av Rovira Roure 80, 25198 Lleida, Catalunya, Spain.

[4] Current address: Institut Pasteur International Network, Units of Biology of Infection & Microbial Evolutionary Genomics, Paris, France

[5] Departament de Ciencies Mèdiques Bàsiques, Universitat de Lleida

[6] Coimbra Chemistry Center, University of Coimbra, 3004-535 Coimbra, Portugal

3.1 Abstract

Virtually all organisms are exposed to reactive oxygen species (ROS) from both intra- and extracellular sources. There are various types of ROS that attack cellular components causing oxidative stress that can impair normal function and/or kill the cell. The hydroxyl radical (•OH) is one of the most deleterious ROS, reacting with certain amino acids at a rate that is diffusion-limited. •OH promotes protein carbonylation and misfolding. It cannot be efficiently scavenged by known antioxidant defenses. This suggests that proteomes may be a target for significant •OH-related oxidative damage, which should be more severe for organisms living in O_2-rich environments. Here we investigate if and how natural selection against utilization of highly •OH-reactive amino acids affected proteome amino acid composition.

To address this issue we studied 1099 fully-annotated unicellular organisms from the three domains of life using multilinear regression modelling and controlling for all major known sources of bias in amino acid composition, as well as for type of energy producing metabolism (fermentation vs. respiration). Genomic G+C content, thermophily, protein size and phylogeny are known main determinants of relative amino acid composition (AAC). After controlling for these variables, we observe that aerotolerance emerges as one of the most important factors to influence protein oxidability, translating into significantly lower protein oxidabilities in AT vs AI organisms. However, we find no significant differences in protein biosynthetic costs between aerotolerant and intolerant organisms, despite the higher energetic yield of respiratory-based (AT-associated) metabolisms vs fermentation-based (AI-associated) metabolisms.

We observe that aerotolerance is one of the most important variables to explain the relative frequencies of Cys (20 – 26% variability) and Met (~19%). Further, aerotolerant (AT) Bacteria, and to some extent Archaea, show significantly (p-value $<6.25\times10^{-4}$) lower utilization of highly oxidizable amino acids ($k_{\bullet OH} \approx 10^{10}$ $M^{-1}s^{-1}$) Cys, Tyr and Met than aerointolerant (AI). In contrast, the 3rd most oxidizable amino acid, Trp, is used with higher frequencies by AT-organisms. Nevertheless, amino acid frequencies translate into widespread lower protein oxidabilities in AT- than AI-organisms (p-value < 0.0045) in all domains and in most phyla tested, whether residue solvent-accessibility is considered or not. Cys and Tyr together explain ≈40% and 30%

of protein oxidability in AI and AT organisms, respectively. However, when we consider solvent accessibility, Tyr and Arg become the residues with most significant contribution for protein oxidability. This reflects an evolutionary pressure towards shielding some of the most oxidizable residues from oxidants in the solvent.

To our knowledge, this is the first study where amino acid/protein oxidability and biosynthetic costs were compared between organisms as function of their aerotolerance while controlling for all known sources of compositional bias.

3.2 Abbreviations

AT	Aerotolerant (Aerobes and Facultative Aerobes)
AI	Aerointolerant (Microaerophilic and Anaerobes)
cDNA	Coding DNA
Aerotol	Aerotolerance
Therm	Thermophily
PSize	Protein size
nProts	Number of proteins
nAA	Number of amino acids
q	Average protein •OH-oxidability per residue
r	Average protein •OH-oxidability per residue, weighted by amino acid exposure to solvent

3.3 Introduction

Aerobic environments pose opportunities and threats to unicellular organisms, potentially influencing the proteomic patterns of amino acid usage on an evolutionary timescale. The use of O_2 as final electron acceptor in respiratory chains permits a more efficient metabolic use of available carbon sources. These gains ensue in part from the increased ATP yield of aerobic respiration [1, 2]. In addition, whereas anaerobic organisms have to spend carbon units in eliminating the excess reducing equivalents generated by the biosynthesis of some amino acids, aerobic organisms can use those reducing equivalents for ATP synthesis. These ATP gains are particularly significant in the synthesis of Arg, Cys, His, and Lys (Table 3.2). Because there is substantial evidence that natural selection tends to minimize the biosynthetic costs of proteins [3-6], proteins from aerotolerant organisms may thus be enriched in the above-mentioned aminoacyl residues, relative to those from aerointolerant organisms.

On the other hand, aerobic environments promote oxidative damage to cellular components (for reviews see [7-11] and references therein). O_2 freely diffuses across

cell membranes and increases intracellular concentrations of reactive oxygen species (ROS). Among these, superoxide and hydrogen peroxide show a modest reactivity with protein aminoacyl chains [12]. Hydrogen peroxide can attack Met and Cys residues at relevant rates only when these residues are located in favorable protein environments, such as near Lys residues [13-15]. Further, these ROS are quickly scavenged by superoxide dismutases, catalases, peroxidases and peroxiredoxins [16-19]. In contrast, the hydroxyl radical (•OH) reacts with most cellular components at nearly diffusion-limited rate constants [12]. For this reason, it cannot be efficiently trapped by any antioxidant defenses and reacts near the sites of production. Further, its formation cannot be fully prevented *in vivo* because it is a primary product of water photolysis and radiolysis [20], and •OH reactions with Cys, Tyr, Trp, Met, Phe, His, Arg and Ile are diffusion-limited [12]. The oxidation of amino acid-side chains in proteins by •OH is generally irreversible [21], leads to misfolding and cross-linking [22], and in the presence of O_2 may fragment peptide chains [11, 23]. Additionally, Asp and Glu can promote protein damage by binding Fe^{2+} ions, thereby facilitating the *in situ* generation of •OH through the Fenton reaction of hydrogen peroxide with these ions [24]. Natural selection may thus disfavor the usage of the above-mentioned amino acids in the proteins from aerotolerant organisms, relative to those of aerointolerant organisms.

Indeed, an analysis of 306 genomes [25] found that cysteine and methionine tend to be underrepresented in the proteins of aerotolerant organisms. However, these authors also found that Trp was over-represented in the proteins of aerobes and did not detect other consistent amino acid usage trends with respect to aerotolerance. Nevertheless, this study did not control for many of the factors that are now known to influence protein amino acid usage, and that we briefly review below.

The main determinant of amino acid composition (AAC) of proteomes is nucleotide composition of DNA, expressed in terms of genomic G+C content [26-29] or intergenic nucleotide sequences [30]. This influence is due to the degenerate structure of the genetic code and explains 20 to 80% of the variation in AAC [28, 30].

The second main factor affecting proteome AAC is organisms' thermophily [27, 28, 31], explaining about 20% of the variability [28]. AAC signatures allow for a clear segregation of organisms between temperature ranges [27, 28, 30, 31], with species following a high GC/temperature vs low GC/temperature trend [31]. Amino acids that

improve thermo-stability (*e.g.* Arg, Ile, Asp, Glu) are favored in the proteins of organisms growing at higher temperatures [32-34].

The third most important factor influencing AAC is the biosynthetic cost of amino acids. More expensive residues (*e.g.* Trp, Phe, Cys) are significantly underrepresented relative to cheaper amino acids (*e.g.* Glu, Asp, Gly), especially in abundant [3] and extracellular proteins [35].

Protein size also influences AAC [36-39]. Smaller proteins exhibit a larger fraction of solvent-exposed residues than larger proteins. Because of this, and owing to the importance of hydrophobicity for structure stabilization [36, 37, 40], the relative abundance of charged and highly hydrophilic amino acids tends to be lower in larger proteins [38].

Here, we investigate the effects of adaptation to aerobic environments on the AAC of proteomes from unicellular organisms while controlling for various factors. This is done by studying 1099 unicellular organisms from all three domains of life with fully sequenced and annotated genomes. We started by examining whether and how the proteome •OH-oxidabilities, estimated from the primary protein sequence, differ between aerotolerant and aerointolerant organisms. Aerotolerant organisms consistently display lower proteome oxidabilities than aerointolerant organisms. These biases are due to distinctive and widespread patterns of amino acid utilization between the two aerotolerance groups, and result of the utilization of highly oxidizable amino acids (e.g. cysteine, tyrosine, and methionine) at lower frequencies in aerotolerant organisms. We then used regression models to test whether aerotolerance significantly explains these biases when other sources of compositional bias are considered (e.g. coding sequence GC content, thermophily, etc.). We observe that aerotolerance emerges as one of the most important factors to explain the observed protein oxidability in Archaea, and the second most important after genomic GC content in Bacteria. It is also one of the most important factors to explain the frequencies of some of the amino acids (e.g. Cys). Lastly, we tested whether aerotolerance of organisms imposes significant AAC-biases with respect to biosynthetic costs of amino acids. We find no significant differences in protein biosynthetic costs between aerotolerant and intolerant organisms, despite the higher energetic yield of respiration-based metabolisms (associated with AT lifestyle) in comparison with fermentative-based metabolisms (associated with AI lifestyle).

3.4 Methods

3.4.1 Organism selection and genome and proteome collection

We focused on unicellular organisms with fully sequenced and annotated genomes, covering all three phylogenetic domains. Whenever sequences for multiple subspecies of a given organism were available, only the subspecies and strain that is considered to be the organism's representative as indicated on the respective genome page on NCBI's RefSeq [41] was analyzed. Multicellular organisms were neglected because the differential O_2 exposure of distinct tissues would complicate aerotolerance classifications. In addition, only organisms with a complete taxonomic description were considered. This allowed to control for the effect of phylogeny on amino acid usage. Genome/proteome files whose coding sequences had not been annotated were also excluded. Overall, we selected 1099 genomes/proteomes from the 10105 that we downloaded either from Genbank [42] or from RefSeq [41] on October 22, 2014. The selected collection comprised 429 obligate aerobes, 281 facultative aerobes, 38 microaerophiles and 351 obligate anaerobes. Aerobes and facultative aerobes were classified as aerotolerant (AT), whereas microaerophiles and anaerobes were classified as aerointolerant (AI). In all statistical analyses AI and AT was coded as 1 and 2, respectively. The phylogenetic distribution of these organisms is as shown in Table 3.1.

Table 3.1 – Distribution of organisms considered in this work. An extended version of this table including thermophily and number of organisms with known growth rates is present in Supplementary Table 3.1, Section 3.8. Bacter./Chlorob. – Bacteroidetes/Chlorobi.

Domain	Phylum or group	Total	AI	AT
Archaea	All	81	53	28
	Euryarchaeota	54	39	15
	Others	27	14	13
Bacteria	All	965	325	640
	Actinobacteria	120	25	95
	Bacter./Chlorob.	59	25	34
	Firmicutes	237	140	97
	Proteobacteria	394	74	320
	Others	156	61	94
Eukarya	All	53	11	42
All		1099	710	389

3.4.2 Obtaining and curating physiological and genomic control parameters

We consider the following parameters potentially influencing AAC: genomic G+C content, growth rates, presence/absence of oxidative defense proteins in the genome, phylogenetic lineage, temperature range, aerotolerance, and cost of amino acid biosynthesis. For each organism, information about these features was extracted from the organism's main genome page in NCBI, with the exception of G+C content, growth rate, presence/absence of oxidative defense proteins in the genome, and cost of amino acid biosynthesis (Supporting Information 3.8.2).

We directly calculated the genomic G+C content from the coding sequences of each genome using an in-house script and parsing the cDNA sequences downloaded from NCBI. Some cDNA files were not correctly parsed and annotated (Supporting Information 3.8). In such cases we considered the G+C content specified in the organism's main genome page at NCBI. As a control to estimate the error that using this number might introduce, we compared NCBI's reported whole-genome G+C content with our calculated coding sequence G+C content (%GC) for the 956

organisms with well annotated cDNA files. The difference between the two values was <1% in 76% of the organisms, and <5% in all.

Growth rates were manually extracted and curated from the literature using Bionumbers [43] and [44]. Whenever multiple growth rates were available for the same species, we used the fastest rate determined for the representative subspecies.

Thermophily data was obtained from each organism's genome page at NCBI. Whenever a thermophily group was not indicated but the organism's optimum growth temperature was present, we corresponded the organism's optimum growth temperature to the following four thermophily groups: psychrophiles (optimal growth temperature <20ºC, coded as 1 for statistical analysis); mesophiles (20 to <45ºC, coded as 2); thermophiles (45ºC to <80ºC, coded as 3), and hyperthermophiles (>80ºC, coded as 4). Data on host association, biotic relationship and pathogenicity were obtained from the organism's genome page at NCBI, from the BacMap genome atlas (http://bacmap.wishartlab.com/genomes) [45] or from the primary literature.

We identified presence/absence of various antioxidant defenses and other proteins in each proteome by considering synonyms and EC numbers of each enzyme taken from BRENDA [46].

3.4.3 Calculating relative amino acid usage and protein size

We calculated protein size and relative amino acid usage as follows. Relative amino acid usage per protein was computed from the ratio between the total counts of each of the 20 essential amino acids and the total number of residues in each protein sequence. In all cases, we discarded the initial methionine, as consideration of this initial amino acid would introduce a bias in relative methionine composition with respect to protein size: because the translation initiation codon mostly codes for methionine, the fraction of methionine in smaller proteins would be amplified with respect to that of larger proteins. We also discarded amino acids that were unclear (e.g. represented as X in the sequence) or rare (e.g. seleno-cysteine).

3.4.4 Calculating amino acid and protein •OH-reactivity indices

To compare protein reactivity with •OH between organisms we proceeded as follows. We first estimated amino acyl side chain reactivity with •OH (k_j, Table 3.2) by computing the difference between whole amino acid •OH-reactivity in solution, as per

NDRL-NIST solution kinetics database [12], and the rate constant for Gly. Because this amino acid has an unreactive hydrogen atom as side chain, its reactivity with •OH is mostly due to the carboxyl and amine groups common to all amino acids.

We then estimated the mean •OH reactivity per amino acid (*q*) for each protein based on the primary sequence, given by

$$q_i = \frac{1}{s_i} \cdot \sum_{j=1}^{20} k_j \cdot n_{ij} \qquad \textit{Equation 1}$$

where n_{ij} is the number of residues of type *j* in protein *i* and s_i is the total number of residues in protein *i*.

The effective reactivity of hydrophobic residues is substantially lower than that of hydrophilic ones, as the former tend to be less accessible to the solvents, especially in larger proteins. We thus also computed an accessibility-corrected mean reactivity per amino acid (*r*):

$$r_i = \frac{1}{s_i} \cdot \sum_{j=1}^{20} k_j \cdot n_{ij} \cdot p_{ij} \qquad \textit{Equation 2}$$

where p_{ij} is the solvent accessibility of amino acid *j* in a protein of size s_i and ranges from 0 to 1, for a totally hidden vs totally exposed amino acid.

Available solvent-accessibility predictors [47-49] either yield very poor predictions for less abundant amino acids (Cys, Trp and Tyr) or are too slow to handle the >3.9 million proteins in our sample (results not shown). Therefore we used the following simpler approach to estimate p_{ij} while accounting for the effect of protein size. For each of the 20 amino acids, *j*, we considered a second order polynomial $a_j(s_i)$ of solvent accessibility (a_j) as function of number of amino acids s_i in a protein. We fitted these polynomials to a dataset of van der Waals solvent accessibilities determined using Abstract [50]. This was done for 9821 proteins with experimentally determined structures downloaded from the Protein DataBank (www.rcsb.org, [51]), for proteins from organisms covering the three phylogenetic domains. This approach yields r_i values in very good agreement to those obtained using solvent accessibilities computed from experimentally determined structures (Supporting Information 3.8.3).

Note that *r* must not be taken as a realistic reactivity estimate but just as an overall indicator of protein reactivity. This because a residue's local chemical environment in a protein can strongly influence its reactivity. Further, aminoacyl residues such as Glu and Asp that are not themselves very •OH-reactive but bind Fe^{2+} ions that can greatly increase proteins' vulnerability to damage by •OH [24].

Amino acid *j*'s relative contributions for protein *i*'s reactivity and accessibility-corrected reactivity were computed as

$$q_{ij} = \frac{k_j \cdot n_{ij}}{q_i \cdot s_i} \qquad \textit{Equation 3}$$

and

$$r_{ij} = \frac{k_j \cdot n_{ij} \cdot p_{ij}}{r_i \cdot s_i}, \qquad \textit{Equation 4}$$

respectively.

3.4.5 Biosynthetic costs of amino acids

The biosynthesis cost of each amino acid is expressed in terms of glucose equivalents and reflects the net moles of glucose, reducing equivalents (NADH/NADPH), ATP equivalents, ammonia, sulfur/sulfate, CO_2, single carbon units, acetyl-coA and other metabolites, generated or consumed per mole of amino acid produced under glucose-limited growth. Previous cost calculations for amino acid biosynthesis accounted only for a subset of these biosynthetic units [3, 52-56].

These costs were estimated under fermentative and respiratory growth conditions for *E. coli* and *S. cerevisiae*. This was done by manual inspection of the biosynthesis pathways under the alternative growth conditions as reported in Ecocyc [57], *Saccharomyces* Genome Database [58], and KEGG [59] for *E. coli* K-12 MG1655 (KEGG: *eco*) and *S. cerevisiae* (KEGG: *sce*). Whenever alternative pathways that produce/consume the same amino acid are reported, we consider the one that is reported in the literature as being responsible for the majority of the production/consumption flux for cells growing in the absence of O_2 (anaerobic cost) or in the presence of O_2 (aerobic cost). Where no such information was available we selected the pathway that yields the lowest biosynthetic cost. Details are given in

Supporting Information 3.8.2. Amino acid biosynthesis costs in *E. coli* (Table 3.2) were considered representative for those of other bacteria, given the strong conservation of amino acid biosynthesis pathways. Unlike the respiratory chains of other O_2-respiring eukaryotes, that of *S. cerevisae* yields only one ATP molecule per NADH consumed, because it lacks respiratory complex I [60]. This yeast uses a NADH:ubiquinone oxidoreductase to catalyze the transfer of electron pairs from the mitochondrial matrix NADH to ubiquinone [61, 62] but is unable to pump protons across the inner mitochondrial membrane [63]. For this reason the P/O ratio approaches 1 [64]. This means that biosynthesis of amino acids under respiratory-based metabolism is cheaper in other eukaryotes, making our estimation an upper limit of the eukaryotic cost. Because of this and of the fact that little information is available for most of the other eukaryotes we use the S. cerevisiae costs as a proxy for those of all eukaryotes. Any difference we find would be even bigger, and thus more significant, with the exact numbers for each organism.

The scalar biosynthesis cost was estimated from the ratio of fermentation/respiration costs indicated in Table 3.2. By using these cost ratios rather than the direct biosynthetic costs we are able to compare how amino acid biosynthesis varies between aerotolerant vs intolerant organisms whilst controlling for the energetic differences of respiratory- vs fermentative-based metabolisms. Higher ratios indicate a lower biosynthesis cost minimization, whereas smaller ratios indicate higher biosynthesis cost minimization.

Table 3.2 – Amino acid reactivity with •OH and biosynthetic costs in glucose equivalents. Rate constants for reaction between amino acyl side chain reaction with •OH were estimated from whole amino acids in solution (see Calculating amino acid and protein •OH-reactivity indices *for details). Biosynthetic costs in Bacteria and Eukarya, under fermentative and respiratory growth, based on the biosynthetic costs of amino acids in E. coli and S. cerevisae.*

		Biosynthetic costs			
	Reactivity with •OH	*Bacteria*		*Eukarya*	
	($M^{-1}s^{-1}$)	Respiration	Fermentation	Respiration	Fermentation
Ala (A)	4.8×10^{7}	0.484	0.887	0.526	1.62
Arg (R)	3.5×10^{9}	1.19	5.44	1.63	10.5
Asn (N)	3.2×10^{7}	0.612	2.00	0.838	4.12
Asp (D)	5.8×10^{7}	0.484	0.887	0.588	2.12
Cys (C)	4.1×10^{10}	0.896	3.72	1.96	8.50
Gln (Q)	5.2×10^{8}	0.795	2.72	0.992	5.60
Glu (E)	2.1×10^{8}	0.743	2.28	0.867	4.60
Gly (G)	1.7×10^{7}	0.267	0.665	0.325	1.31
His (H)	5.7×10^{9}	1.06	4.49	1.36	7.45
Ile (I)	1.8×10^{9}	1.29	2.66	1.44	4.62
Leu (L)	1.7×10^{9}	1.19	3.33	1.24	5.75
Lys (K)	3.3×10^{8}	1.22	2.66	1.51	10.5
Met (M)	8.5×10^{9}	1.46	8.22	1.69	7.68
Phe (F)	6.5×10^{9}	1.78	3.67	1.91	5.42
Pro (P)	4.6×10^{8}	0.954	2.83	1.11	5.35
Ser (S)	3.0×10^{8}	0.445	1.72	0.526	3.12
Thr (T)	4.9×10^{8}	0.733	1.78	0.890	3.37
Trp (W)	1.3×10^{10}	2.12	5.27	2.36	8.25
Tyr (Y)	1.3×10^{10}	1.70	4.17	1.82	5.29
Val (V)	7.4×10^{8}	0.954	1.66	0.989	2.75

3.4.6 Modeling amino acid frequency, biosynthetic cost and protein oxidability

In order to examine the potential effect of %GC, temperature, aerotolerance, median protein size, total number of amino acids in the proteome, total number of proteins in the proteome and doubling time on average amino acid frequency, average protein oxidability and biosynthesis cost for each proteome we proceeded as follows. We constructed multilinear regression models for the variation of each dependent variable *y* as function of the control variables ***x***:

$$m_y(\mathbf{x}) = \varepsilon + \sum_{i=1}^{n} \alpha_i \cdot x_i$$

Here α_i are the regression coefficients for the control variables (sources of bias), and ε is an error term [65]. We fitted these models to the pertinent data sets and estimated

the R^2 coefficients of determination adjusted for total number of fitted parameters and the regression coefficients. Because variance in protein size is (broadly) proportional to protein size, we applied a logarithmic transform to this variable in all multivariate models.

Multilinear regression models were implemented in Wolfram's Mathematica 10.0.1.0 [66] using the function *LinearModelFit* with default parameters, or in R [67] using the function *lm*. Further details about the implementation of multilinear regression models is indicated in Supplementary Information 3.8.5.

3.4.7 Statistical analyses

Distributions were compared using the Mann-Whitney test with the null hypothesis that the difference between true location parameters is 0. Minimum group size considered was 15 except where otherwise stated. This sample size is robust to potential errors that may arise from comparing very small and non-normally distributed samples, regardless of their shape [68]. We relaxed the sample size requirement in comparisons involving AI eukaryotes because we could retrieve only 11 suitable genome sequences for this important group.

Whenever necessary, corrections for multiple hypothesis testing were done using False Discovery Rates and Bonferroni corrections indicated at each figure legend.

The p-values of estimated model regression coefficients α_i were calculated by comparing the estimated two-tailed t-distribution with a t-distribution with median 0 and (sample size)-(number of fitted coefficients) degrees of freedom.

3.4.8 Software

All parsing and file editing was done using Perl and Bioperl modules. All mathematical and statistical calculations were done using Mathematica [66] and R [67].

3.5 Results

3.5.1 Proteomes from aerotolerant organisms are consistently less •OH-reactive than those from aerointolerant organisms

We first examined the influence of adaptation to O_2-rich environments as inferred from the organisms' aerotolerance on proteome reactivity with the •OH radical. The analysis was based on the proteome sequences from 1099 unicellular organisms selected and partitioned into aerotolerant (AT) and aerointolerant (AI) groups as described in Methods. For each proteome we computed the medians ($\tilde{q}$, $\tilde{r}$) of the accessibility-corrected (*r*) and uncorrected (*q*) •OH-reactivities per amino acid (equations 1 and 2) across its component proteins. The $\tilde{q}$ and $\tilde{r}$ values for AT organisms are significantly lower than those for AI organisms (Figure 3.1 and Supplementary Figure 1, Mann-Whitney U statistic 211840 and 187680, respectively, $p < 2.2\times10^{-16}$ for one-sided comparison).

Although intermediate median *q* values do not achieve discrimination between AI and AT organisms, 130 (94%) out of the 138 organisms with $\tilde{q}$ <2.0×10^9 $M^{-1}s^{-1}$ are AT, and 87 (77%) out of the 113 organisms with $\tilde{q}$ > 2.45×10^9 $M^{-1}s^{-1}$ are AI. Further, 19 out of the 24 AT organisms in the latter $\tilde{q}$ range with documented biotic relationship (compared to 72/611 in the whole sample) are intracellular parasites, commensals or symbionts, which are likely under relaxed selection due to their lower population sizes[69].

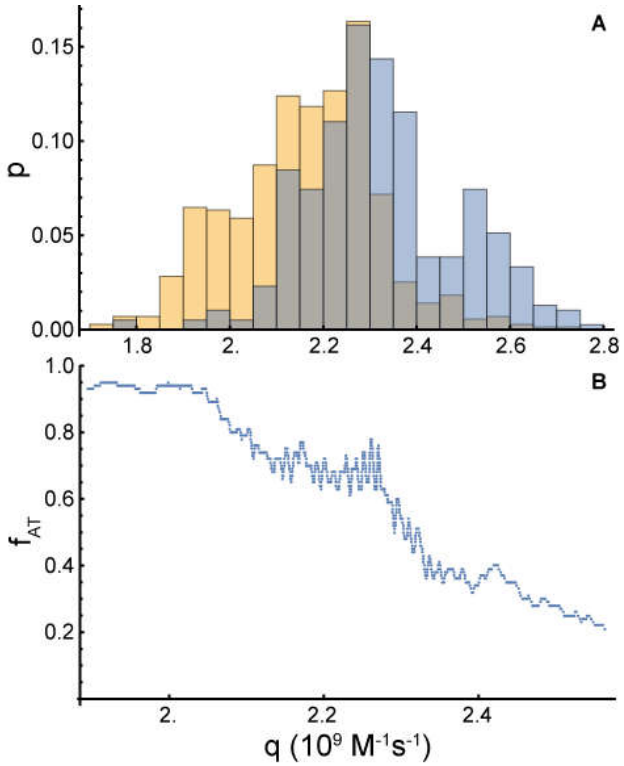

Figure 3.1 – AT organisms have lower median proteome oxidability q *than AI organisms. A) Probability distribution bins determined for AT (orange) and AI (blue) populations as function of median proteome* q. *B) Moving median of the fraction of AT organisms in the total population as function of median proteome* q.

Median *r* values are less discriminating (Supplementary Figure 3.1), perhaps because the solvent accessibility estimates reflect just means for each residue and not the real accessibility in each protein.

In order to assess whether these trends just reflect phylogenetic inertia or are a result of adaptation to O_2-rich environments, we then compared the median values of *q* and *r* between AT and AI organisms within the same clade (Figure 3.2).

3. Proteome composition and aerotolerance

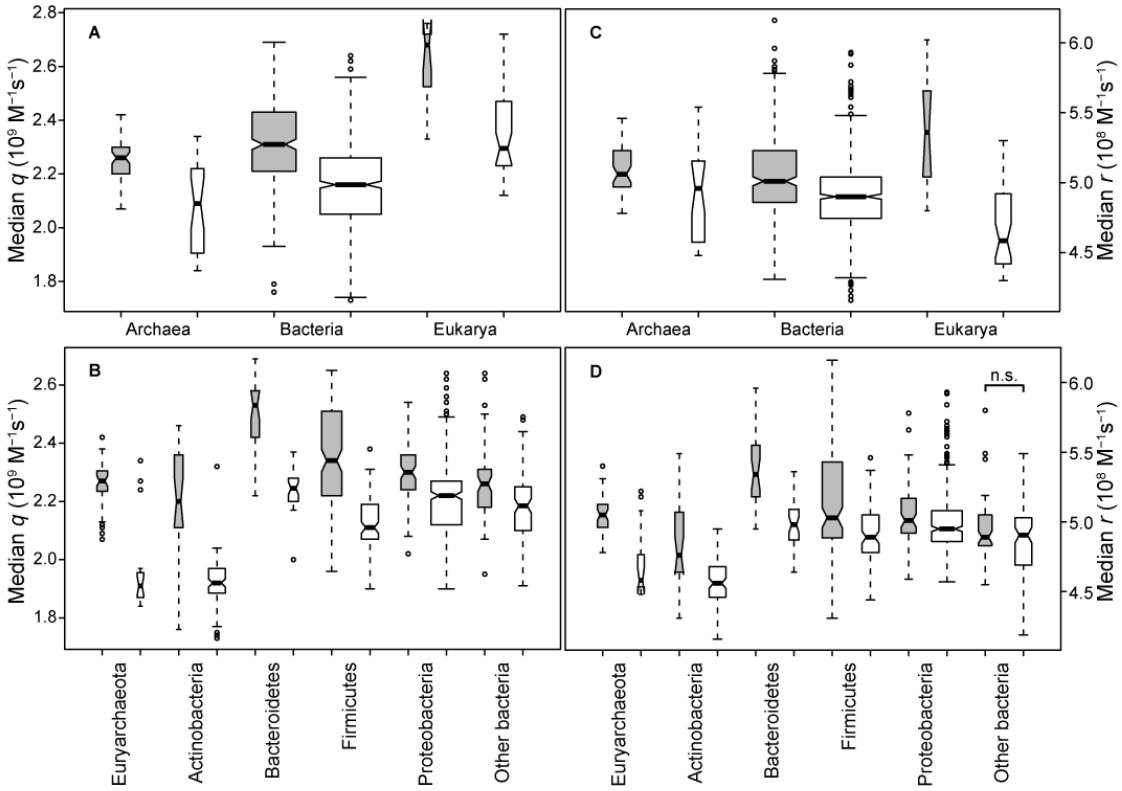

Figure 3.2 - Distribution of proteome median q (A, B) and r (C, D) values for AI (gray) and AT organisms (white) for the three phylogenetic domains (A, C) and for the sufficiently represented archaeal and bacterial phyla. Whiskers extend to 1.5 the interquartile differences, bar widths are proportional to the square root of sample sizes, notches mark approximate 95% confidence intervals for the medians. Mann-Whitney tests comparing the distributions of median q and r values in AI vs. AT organisms of the same clade indicate that true location shifts are significantly greater than zero for all but one (n.s.) cases at a 1% false discovery ratio.

The $\tilde{q}$ values for the proteomes of AT organisms are significantly lower than those for the proteomes of AI organisms in all the analyzed clades (Figure 3.2A,B). This is true for comparisons at both the phylogenetic domain and phyla levels. Likewise, the $\tilde{r}$ values for the proteomes of AT organisms are significantly lower than those for the proteomes of AI organisms (Figure 3.2C,D). Because the probability of 7 independently evolving lineages (*i.e.*, the six phyla in Figure 3.2B,D plus the Eukarya domain) showing the same trend by chance is just 2^{-7}= 0.0078, these results indicate with substantial confidence that evolutionary adaptation of microorganisms to O_2-rich environments is mediated at least in part by adaptation of the proteome so as to make proteins less $^{\bullet}$OH-reactive.

Median $\tilde{q}$ ($\tilde{r}$) values for AT organisms are 3% to 16% (1% to 14%) lower than those for AI organisms from the same clade. Further, in Bacteria median $\tilde{q}$ values follow the relationship aerobes $\cong$ facultative aerobes < microaerophiles < anaerobes (Supplementary Figure 3.2). We note that sample sizes are insufficient for a robust comparison in other prokaryotic phylogenetic clades.

Eukaryotes have higher median $\tilde{q}$ values than organisms from the other two domains. Although AT eukaryotes' $\tilde{q}$ values are comparable to those of AI bacteria, their $\tilde{r}$ values are lower than those of AT bacteria (Figure 3.2A,C). The latter is due to AT eukaryotes having very large proteins (Supplementary Figure 3.3) and therefore their aminoacyl side chains being on average less accessible to the solvent.

The following additional observations are consistent with natural selection against highly $^{\bullet}$OH-reactive proteins. First, intracellular parasites, commensals and symbionts show significantly higher $\tilde{q}$ than free-living organisms, but even in this set AT organisms show significantly lower $\tilde{q}$ than AI ones ($p= 0.0015$ for one-tailed Mann-Whitney test, Supplementary Figure 3.4). Many of these organisms have low %GC and small proteomes that result from gene loss, due to Muller's ratchet and to the use of host metabolism to perform many biological functions (Supplementary Figure 3.5). These two observations are consistent with relaxed selection owing to small effective population sizes [70].

Second, distributions of *q* values among the proteins of AT organisms are narrower and have lower skewness ($i.e.$, leaner left hand tails) than those from AI organisms (Supplementary Figure 3.6). This is suggestive of weaker selection against very $^{\bullet}$OH-reactive proteins in the latter organisms.

The correlations of *q* with protein size are negative for all but 21 of the 1099 proteomes analyzed, and the Spearman rank correlation coefficients tend to be stronger for AT than for AI organisms (Supplementary Figure 3.7). This suggests that the selective pressure for low reactivity with $^{\bullet}$OH is not weaker on the buried aminoacyl residues than on solvent-accessible ones, and/or that solvent-exposed residues in large proteins are under stronger selective pressure than those in small proteins. It is possible that amino acids are exposed to oxidants in the solvent during protein synthesis, particularly in nascent chains, which are enriched in highly oxidizable

residues (e.g. Met and Thr) and rarefied in lowly oxidizable residues (e.g. Gly and Asn) [71].

3.5.2 Proteomes from aerotolerant organisms show consistent bias in the usage of most aminoacyl residues

The observed $\tilde{q}$ and $\tilde{r}$ differentials between AT and AI organisms reflect differences in the proteomes' relative aminoacyl composition between these groups of organisms. We examined the nature of these differences by comparing the AT/AI group medians of the median relative frequencies of each of the twenty amino acids in the proteomes of the same organism groups as above (Figure 3.3). The trends of amino acid under-/over-representation in AT vs. AI organisms show remarkable consistency over independently evolving microbial lineages. Thus, Cys, Tyr and Met are under-represented, and Thr is over-represented in the proteomes of AT organisms form all lineages examined as compared to AI organisms from the same lineages. Ile and Lys are under-represented, and Trp, His, Pro and Ala are over-represented in AT organisms from all lineages except Bacteroidetes. Leu and Gln are over-represented in AT organisms form all lineages except Archaea and Actinobacteria, respectively. Phe is under-represented, and Arg is over-represented in AT organisms from all lineages except Bacteroidetes and Firmicutes. Asn is under-represented, and Val is over-represented in AT organisms form all lineages except Bacteroidetes and "Other bacterial phyla". Glu is under-represented in AT organisms form all lineages except Bacteroidetes and Euryarchaeota.

Altogether, the pattern of biases in relative AAC in AT *vs* AI organisms within the phylum Bacteroidetes differs substantially from that in all other lineages observed.

Although the mean proteome frequencies of the amino acids are more prone to be biased by groups of proteins with extreme aminoacyl composition, they follow essentially the same trends (Supplementary Figure 3.8).

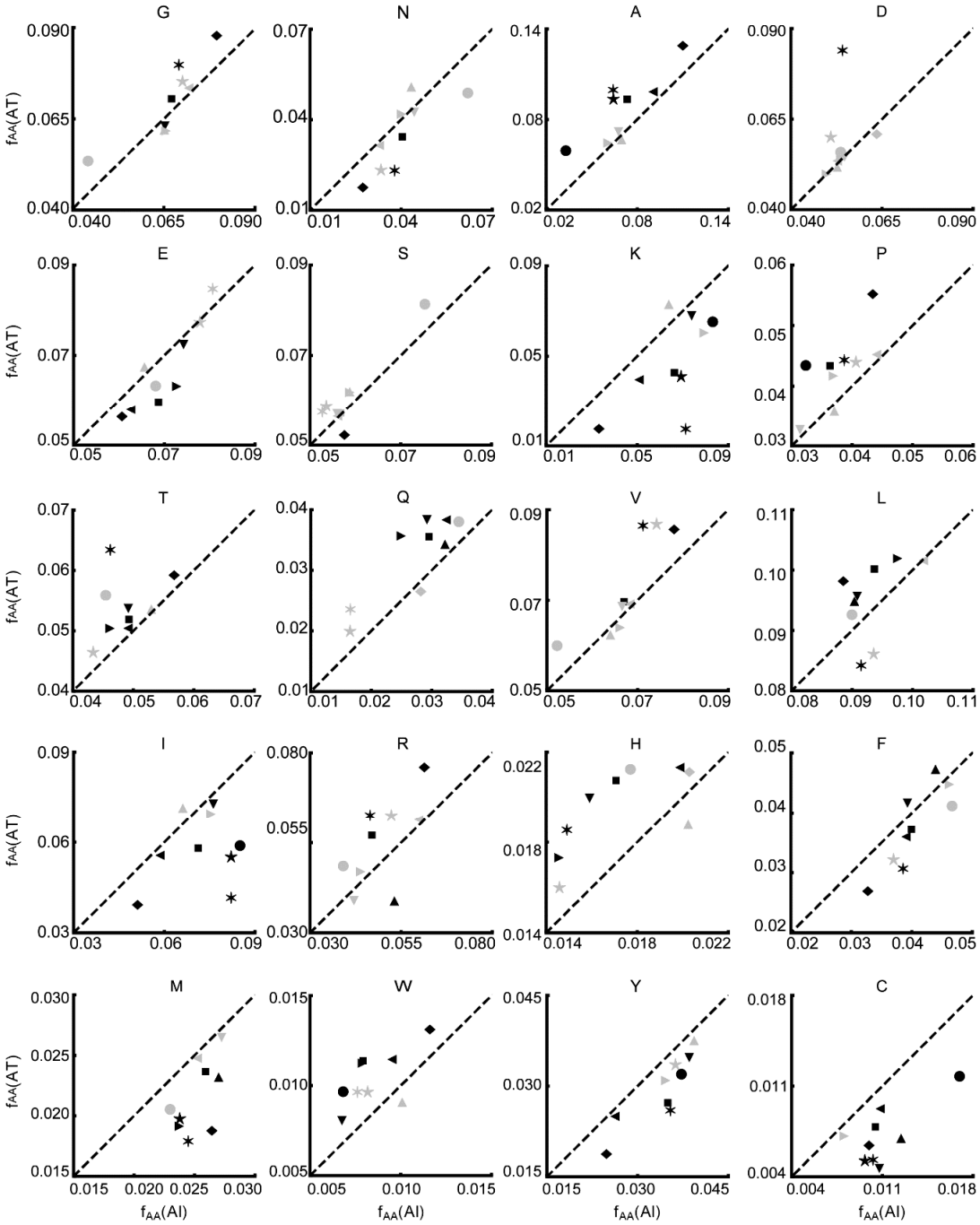

Figure 3.3 - Distribution of median amino acid frequencies in AT [$f_{AA}(AT)$] and AI [$f_{AA}(AI)$] in the three phylogenetic domains (★ - Archaea, ■ - Bacteria, ● - Eukarya) and in the sufficiently represented archeal (✸ - Euryarchaeota) and bacterial phyla (◆ - Actinobacteria, ▲ - Bacteroidetes/Chlorobi, ▼ - Firmicutes, ◀ - Proteobacteria, ▶ - Other). Mann-Whitney tests comparing the distributions of median frequency values in AI vs. AT organisms of the same clade indicate that true location shifts are significantly greater than zero at a 1% false discovery ratio for all cases indicated by black symbols. Amino acids ordered by increasing •OH-reactivity.

3.5.3 Biases in amino acid usage in aerotolerant vs. aerointolerant organisms reflect aminoacyl residues' reactivity with •OH

Tyr, Cys, Phe and Met are the main contributors for the overall •OH-reactivity of the proteomes, together contributing 60%-70% of the value of $\tilde{q}$ in most AI organisms (Supplementary Figure 3.9 and Supplementary Figure 3.10). It is thus remarkable that these aminoacyl residues are consistently depleted in the proteomes of AT organisms. The lower values of $\tilde{q}$ and $\tilde{r}$ in these organisms are due mainly to a substantial depletion of Cys, with depletions of Tyr and Met also playing an important role in most lineages (Supplementary Figure 3.9 and Supplementary Figure 3.10). However, the results in the previous section also show that the proteomes of AT organisms are enriched in some very •OH-reactive residues. This is the case of Trp, His and Arg, the latter of which is one of the two main contributors for $\tilde{r}$ in most lineages (Supplementary Figure 3.9 and Supplementary Figure 3.10). This apparent discrepancy may be explained by the fact that natural selection favors amino acid substitutions that preserve side chains' physical-chemical properties [72, 73]. Remarkably, Trp, His and Arg are among the most selectively favored substituents for Tyr and Lys, which are among the most strongly depleted residues in AT organisms.

In general, if there is an overall trend in AT organisms to replace •OH-reactive residues by less reactive ones with compatible physical-chemical properties the following should hold. First, the ratios (R_f) between the abundances of the most reactive amino acids and their preferred less reactive substituents should be consistently lower in AT than in AI organisms. Second, this trend should be strongest for the cases where the amino acid in the numerator contributes more substantially for the overall reactivity of the proteome. We examined these possibilities by considering separately the sets of preferred substitutions for buried and for solvent-accessible aminoacyl residues defined by [73] (Figure 3.4, Supplementary Table 3.3, Supplementary Figure 3.11). For the former set of substitutions both trends are indeed observed (A,B). First, most preferred-substitution sets show $R_f(AT)/R_f(AI) < 1$, the only exceptions being for very unreactive aminoacyl residues. Second, $R_f(AT)/R_f(AI)$ shows strong and very significant negative correlations with the difference [$\Delta k_{\bullet OH}$, Δ(accessibility×$k_{\bullet OH}$)] between the •OH reactivity of the most reactive amino acid and the mean of the

reactivities of the other amino acids in each set, irrespective of the reactivities being weighted by the solvent accessibility of the residues (Spearman rank correlation -0.67, $p < 0.03$) or not (Spearman rank correlation -0.61, $p < 0.05$).

Several groups of preferred substitutions for solvent-exposed residues show $R_f(AT)/R_f(AI) < 1$ but no statistically significant correlation between $R_f(AT)/R_f(AI)$ is observed (Figure 3.4B). This mainly ensues from Lys being substantially more depleted in the proteomes of AT organisms than expected from its reactivity with $^{\bullet}OH$, perhaps because Lys can enhance the reactivity of Cys with peroxides and is itself quite reactive with autoxidation products [13-15]. If Lys is considered to have an effective reactivity similar to His, $R_f(AT)/R_f(AI)$ becomes <1 for all groups involving very reactive aminoacyl groups and shows negative correlations with $\Delta k_{\bullet OH}$ and $\Delta(\text{accessibility} \times k_{\bullet OH})$ (Figure 3.4C, Spearman rank correlation -0.66, $p=0.014$).

The substantially decreased Cys and increased Trp abundances in the proteomes of AT are remarkable because these are the two least mutable amino acids, due to their unique properties [72].

3. Proteome composition and aerotolerance

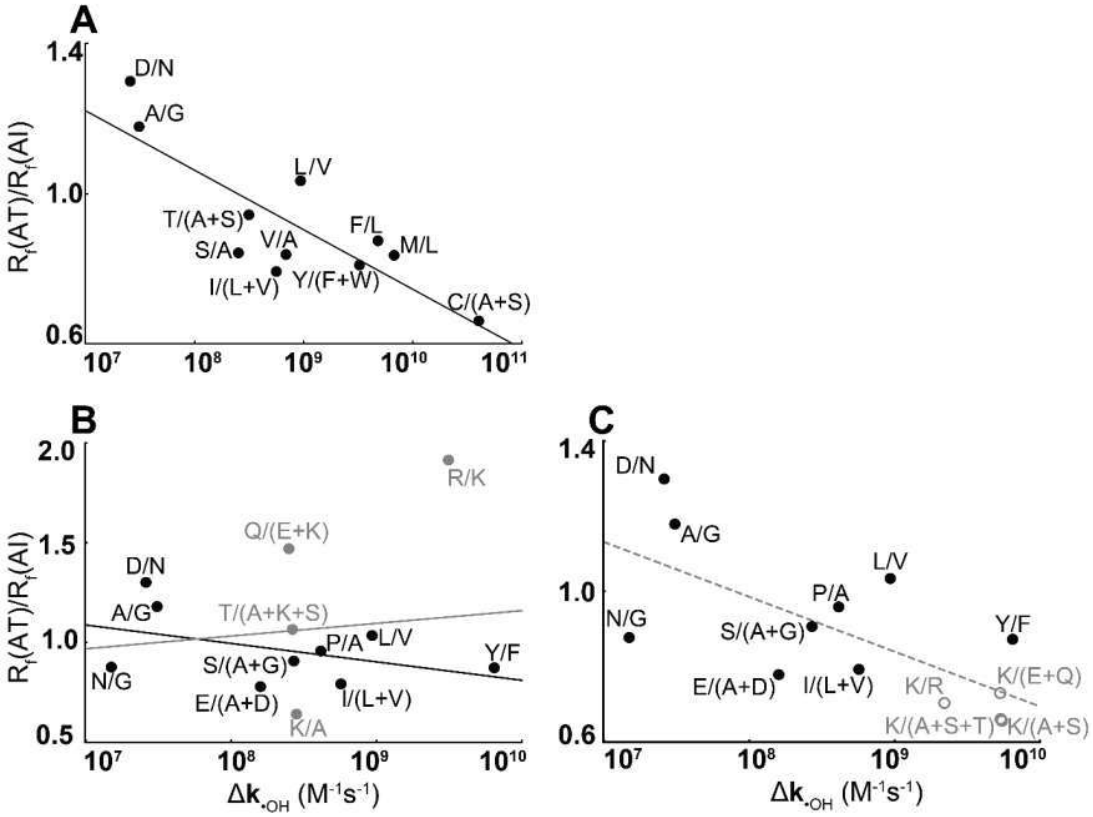

Figure 3.4 – Ratios of frequencies of groups of frequently substituted non-exposed (top) or solvent-exposed (bottom) amino acids as function of differences of amino acid •OH reactivity of the residues for Bacteria. For each group of frequently substituted amino acyl residues in proteins [73] we computed the ratios (R_f) between the median amino acid frequency of the most reactive aminoacyl residues and the means of the median frequencies of the other aminoacyl residues in the group for AI and AT bacteria. We then plotted the ratios $R_f(AT)/R_f(AI)$ as function of $\log_{10}$ of the differences between •OH reactivity of the amino acid in the numerator of R_f and the mean of those in the denominator. In panels B, C the gray symbols indicate the ratios for the replacement groups involving Lys, either considering its reactivity with •OH (closed circles) or an effective reactivity similar to His (circumferences). Lines are least squares regression lines of $R_f(AT)/R_f(AI)$ vs. $\log_{10}(\Delta k_{\bullet OH})$ (B, D) for the ratios represented by closed black circles (black), by all closed circles (solid gray), and by the closed black circles plus the gray circumferences (dashed gray). Ratios compared as function of $\Delta k_{\bullet OH}$ weighted by amino acid exposure to solvent are found in *Supplementary Figure 3.11*. Spearman rank correlation coefficients are: (A) -0.67 (p=0.023), (B) all circles, -0.10 (p=0.73), black circles -0.28 (p=0.46), (C) black circles plus gray circumferences -0.66 (p=0.014).

3.5.4 Aerotolerance is by itself an important determinant of proteome •OH-reactivity and relative AAC

The results above suggest that the evolution of aerotolerance is mediated in part by the proteome-scale adaptation of relative AAC in such way as to decrease proteins' susceptibility to oxidative damage. However, such adaptation might conceivably be explained by aerotolerant organisms being biased with respect to coding sequence G+C contents (%GC), thermophily and protein size, all of which have a substantial effect on AAC [26-29, 31, 36, 37, 40]. Indeed, in the three phylogenetic domains the genomic coding sequences of AT organisms tend to be GC-richer than those from AI organisms (Supplementary Figure 3.12) The distribution of AI and AT organisms over the four thermophily categories (Supplementary Table 3.6) suggests an increased preference for a AI life style with increasing optimal growth temperature in Bacteria and to a certain extent in Archaea, perhaps mirroring the decreasing O_2 solubility in water. Also, eukaryotic AT organisms tend to have larger proteins than AI organisms, though this trend is not observed in the other phylogenetic domains (Supplementary Figure 3.3). Supplementary Figure 3.13 highlights a substantial influence of all these factors and phylogeny on $\tilde{q}$. Below we show that aerotolerance is an important determinant of proteome •OH-reactivity and relative AAC independent of these biasing factors.

Our sample of organisms contains too few AI Eukaryotes for a statistically robust multifactorial analysis, and temperature extremophiles are very unevenly represented across phyla. Therefore, we first analyzed the interplay among phylogeny, aerotolerance, %GC and median protein size in determining $\tilde{q}$ for the 862 mesophilic Archaea and Bacteria (Set M). Then, using separate models, we analyzed the interplay among optimal growth temperature, aerotolerance, %GC and median protein size for the 80 mesophilic, thermophilic and hyperthermophilic Archaea (Set A), and for the 934 mesophilic and thermophilic Bacteria, with all phyla pooled together (Set B).

Supplementary Figure 3.13 and Supplementary Figure 3.14 show that $\tilde{q}$ has nonlinear relationships with %GC and median protein size, respectively. We thus started with a maximal model (henceforth denoted MMM) considering $\%GC^2$ and $(\text{protein size})^2$ terms plus all possible interaction terms among phyla, aerotolerance, %GC and

protein size. Then, we assessed the contribution of variable *x* to the variance in $\tilde{q}$ by comparing the residual variance of models that neglect variable *x* (MMM-*x*) to that of MMM (details in Supplementary Information 3.8.5). This analysis (Supplementary Table 3.7) flagged aerotolerance as the most important explanatory variable, followed by phylum, %GC and median protein size.

In order to assess the effect of aerotolerance on $\tilde{q}$ after discounting the effect of the other variables we simplified MMM to achieve a minimal adequate model (mAMM, details in Supporting Information 3.8.5). This simplified model was fitted to the data set, after which we determined the fitted $\tilde{q}$ values considering 50% G+C and the grand mean of the median protein sizes, or considering the phylum means of both these variables. These *adjusted* $\tilde{q}$ values are 3% to 20% lower for AT than for AI organisms from the same phylum considering 50% G+C and the mean of median protein sizes, or 3% to 14% lower for AT than for AI organisms from the same phylum if %GC and median protein sizes are considered per phylum (Table 3.3). Differences are very significant in all phyla.

The low cardinality of Set A only permits accounting for two-way interactions, but a good maximal and minimal adequate models (MMA, adjusted R^2= 0.75, mAMM, adjusted R^2= 0.73, details in Supporting Information 3.8.5) were achieved nevertheless. In turn, although the starting model for analysis of Set B accounted for all possible interactions among aerotolerance, %GC, temperature and median protein size, the maximal and minimal adequate models (MMB, mAMB, details in Supporting Information 3.8.5) have adjusted R^2 of just 0.56. This is in line with the adjusted R^2 for model MMM-*phylum* and likely reflects the substantial contribution of phylogeny to the variance of $\tilde{q}$.

Aerotolerance is the first and second most important explanatory variable for variance in $\tilde{q}$ in Sets A and B, respectively (Supplementary Table 3.7), with %GC being the most important variable in the latter model. Optimal growth temperature and median protein size are respectively the third and fourth most important variables in both models. Both models highlight significant interactions between aerotolerance and optimal growth temperature: $\tilde{q}$ decreases with increasing optimal growth temperature among AI organisms, whereas it increases among AT organisms (Supplementary Figure 3.16). Thus, $\tilde{q}$ differences between AT and AI in hyperthermophilic archaea and in thermophilic bacteria become non-significant after adjusting for differences in

%GC and median protein size as described above (Table 3.4). However, these differences remain highly significant in mesophilic archaea and bacteria and in thermophilic archaea.

Similar trends are observed when using simpler multilinear regression models (Supporting Information 3.8.6). Because these models consider only first order terms, the trends of *q* are easily interpretable and one does not need hold each variable constant, though the variability is only partially explained in some of these models. Similar analyses performed on amino acid frequencies also highlights that aerotolerance is the main explanatory variable in the frequencies of Cys, Gln, Met, and one of the most important variables in explaining the aerotolerance in Leu and Trp (Supporting Information 3.8.6).

Overall, these analyses indicate that aerotolerance is an important variable to explain the observed patterns of AAC and protein oxidability.

Table 3.3 - %GC- and median-protein-size-adjusted relative differences in $\tilde{q}$ between AT and AI organisms. Values represent the predicted relative differences $\frac{\tilde{q}_{AT}-\tilde{q}_{AI}}{\tilde{q}_{AI}}$ that obtain from MMM by setting %GC= 50 and median protein size = sample mean (left hand column) or %GC= phylum mean and median protein size = phylum mean (right hand column).

Phylum	**%GC = 50, median protein size = grand mean**			**%GC, median protein size = phylum mean**		
	Relative difference	**Standard error**	**p ****	**Relative difference**	**Standard error**	**p ****
Euryarchaea*	-0.20	0.057	6×10^{-3}	-0.14	0.032	6×10^{-5}
Actinobacteria	-0.16	0.026	1×10^{-8}	-0.084	0.013	4×10^{-9}
Chlorobi	-0.089	0.014	1×10^{-9}	-0.095	0.011	$<3\times10^{-15}$
Firmicutes	-0.14	0.012	$<3\times10^{-15}$	-0.12	0.0061	$<3\times10^{-15}$
Proteobacteria	-0.027	0.0064	4×10^{-4}	-0.031	0.0063	2×10^{-5}
Other bacteria	-0.043	0.012	5×10^{-3}	-0.047	0.0091	4×10^{-6}

* Includes one AT Crenarchaeota. ** Includes Bonferroni correction for 12 hypotheses.

Table 3.4 - %GC- and median-protein-size-adjusted relative differences in $\tilde{q}$ between AT and AI organisms. Values represent the predicted relative differences $\frac{\tilde{q}_{AT}-\tilde{q}_{AI}}{\tilde{q}_{AI}}$ that obtain from MMM by setting %GC= 50 and median protein size = sample mean (left hand column) or %GC= phylum mean and median protein size = phylum mean (right hand column).

Thermophily	**Fitted $\tilde{q}_{AI}$ (10^9 $M^{-1}s^{-1}$)**	**Std. error (10^9 $M^{-1}s^{-1}$)**	**Fitted $\tilde{q}_{AT}$ (10^9 $M^{-1}s^{-1}$)**	**Std. error (10^9 $M^{-1}s^{-1}$)**	**%diff**	**p ***
			Archaea			
Mesophiles	2.29	0.019	2.04	0.030	-11%	4×10^{-9}
Thermophiles	2.25	0.013	2.12	0.019	-5.7%	1×10^{-7}
Hyperthermophiles	2.21	0.016	2.20	0.022	-0.34%	n.s.
			Bacteria			
Mesophiles	2.39	0.0084	2.23	0.0070	-6.6%	$<10^{-15}$
Thermophiles	2.24	0.016	2.24	0.019	0.06%	n.s.

* Includes Bonferroni correction for 5 hypotheses. n.s., non-significant

3.5.5 Minimization of proteins' biosynthetic cost cannot explain the differential proteome amino acid usage in AT vs. AI organisms

The relative biosynthetic costs of the various amino acids depend on the organisms' ability to use O_2 as a final electron acceptor in respiratory chains (Table 1). Because natural selection tends to minimize the biosynthetic costs of proteins [3, 54], the proteins from aerobic and anaerobic organisms might be enriched in the amino acids that are cheapest under respiratory and fermentative conditions, respectively. This phenomenon might thus provide an alternative explanation for the observed AAC differentials between AT and AI organisms.

Given the wide diversity and still limited understanding of the metabolic capabilities among microorganisms it is difficult to determine representative estimates of the biosynthetic costs in each condition except for the most thoroughly studied model organisms. However, one can draw on the fact that amino acid biosynthesis pathways are strongly conserved and that the changes in biosynthetic cost ranks between aerobic and anaerobic conditions are strongly influenced by the fate of the generated NADH to obtain a rough approximation. Based on this principle, we estimated the biosynthetic costs of amino acids in Bacteria and Eukarya (Table 3.2) as described in Methods and computed the ratio (RC) between the sum of the biosynthetic cost of all the proteins under fermentation and the sum of the costs under respiratory metabolism. (Archaea were disregarded due to the lack of reliable data.) Evolutionary adaptation to minimize the biosynthetic cost of the proteins according to the ability to use oxygen in respiration should lead to lower RC in AI than in AT organisms. However, the data did not reveal significant differences in RC between AI and AT Eukaryotes, or a consistent trend across bacterial phyla (Supplementary Figure 3.15).

3.6 Discussion

Considering that cells cannot entirely prevent the production of the hydroxyl radical in O_2-rich environments nor effectively scavenge it, we hypothesized that natural selection leads to a decreased reactivity of proteins from aerotolerant microorganisms with this radical. We thus used the mean reactivity with •OH per aminoacyl residue (q) as a bioinformatic proxy of each protein's •OH-reactivity, and compared proteome-median q values ($\tilde{q}$) of AT organisms to those of AI organisms. Supporting the hypothesis, $\tilde{q}$ values for AT organisms were significantly lower than those for AI organisms in all independently evolving lineages analyzed (Figure 3.2, AT group medians 3%-16% lower). That is, proteins from AT organisms are made of less-reactive amino acids than those from AI. This trend remains significant when the amino acids' reactivities are weighted by their mean protein-size-controlled solvent accessibilities (Figure 3.2). Moreover, the proteome distributions of q values in AT organisms tend to be narrower and to have leaner right-hand tails than those of AI organisms, consistent with stronger selection against proteins with high q. Further, this happens despite the AT organisms in general having more proteins than AI organisms, which argues against the possibility that the low $\tilde{q}$ of the former being due to a "special" low-q set of proteins without orthologues in the latter.

Organisms' $\tilde{q}$ values tend to decrease with increasing %GC of the genomes for G+C > 55% in all phylogenetic domains, and with increasing optimal growth temperature and median protein size in bacteria. However, aerotolerance remains the main explanatory factor for the variance in $\tilde{q}$ even after controlling for these factors.

The lower $\tilde{q}$ values of AT organisms are mainly due to the rarefaction of the four strongest contributors for proteins' •OH-reactivity: Cys, Tyr, Met and Phe. These residues are less abundant in AT than in AI organisms from all (Cys, Tyr, Met) or most (Phe) lineages examined. However, other very •OH-reactive residues — Trp, His and Arg — are more abundant in the proteins from AT organisms than in those of AI organisms in most lineages examined; and a moderately •OH-reactive residue — Lys — is among the most depleted in the former organisms.

Two alternative hypotheses may explain these patterns of aminoacyl frequency bias between AT and AI organisms. The first one, henceforth denoted "conservative substitution hypothesis", is that the proteomes of AT organisms are enriched in the

above-mentioned •OH-reactive residues because these are the only substituents for the rarefied reactive residues that preserve their main structural and physical properties. Indeed, Trp, His and Arg are the most selectively favored substituents for Tyr and Lys, according to Dayoff's point accepted mutation matrices [72-75]. Although Trp's reactivity with •OH is similar to Tyr's, Trp is less solvent-accessible and does not form protein-protein cross-links upon attack by •OH, unlike Tyr [76]. Likewise, although Lys is less •OH-reactive than Arg or His, it is more reactive with electrophilic products that are generated by the autoxidation of lipids and sugars in O_2-rich environments [77], and the products formed can cause protein unfolding, aggregation and cross-linking [78, 79]. Further, if located in the neighborhood of a Cys, Lys favors the ionization of the thiol, making it more reactive with ROS [13-15]. Therefore, Tyr $\rightarrow$ Trp, Lys $\rightarrow$ Arg and Lys $\rightarrow$ His substitutions may be specially favored in AT organisms.

The conservative substitution hypothesis is supported by the following results (see Results Section 3.5.3). First, the ratios (R_f) between the relative frequency of the most •OH-reactive residue in each "equivalence" group (as per ref. [73]) and the sum of the relative frequencies of the other residues in the group are lower in AT than in AI organisms. The only exceptions are for the least reactive of all residues, which together contribute <0.1% of the proteins' *q* values, and for the groups including Lys. Second, the ratios Rf(AT)/Rf(AI) show a strong negative correlation with the •OH-reactivity of the most reactive residue in each group. This is true for the "equivalence" groups for buried residues, and for the groups for solvent-exposed residues when Lys is neglected or considered to have an effective reactivity similar to that of His. Third, in Bacteria, the regression coefficients with respect to aerotolerance are significantly lower than zero for all the R_f involving the most reactive residues in a regression model accounting also for G+C content of the coding sequence, optimal growth temperature and median protein size.

The second hypothesis, henceforth denoted by "GC bias hypothesis" is that the patterns of aminoacyl frequency bias are largely a result of %GC differences between AT and AI organisms. Indeed, AT organisms tend to have higher %GC than AI ones (Supplementary Figure 3.12), and for %GC > 55 the correlation coefficients of the frequencies of the most reactive residues with %GC have the same signs as the bias between AT and AI organisms. Namely, negative for Cys, Tyr, Met, Phe and Lys, and

positive for Trp, His and Arg. However, for %GC < 50 the relative frequencies of Cys and Met increase with increasing %GC.

The two hypotheses above are not mutually exclusive, and the following observations suggest that both contribute to explain the patterns of aminoacyl usage bias between AT and AI organisms.

Adaptation is likely mediated both by purifying selection on reactive amino acids with strong structural and/or functional importance in AT organisms and by selection on processes affecting GC

Comparing seven bacteria that are pathogenic to vertebrates to seven non-pathogenic bacteria Vidovic *et al.* (2012) [80] found that the former were more resistant to oxidative stress and HSP90 chaperone inhibition, and had proteomes less susceptible to carbonylation. Based on a comparison of the amino acid usage patterns in a subset of the proteins from 46 pathogenic to that in 40 non-pathogenic firmicutes and γ-proteobacteria they then defined a "Pathogen Proteome Signature" that maximally separated pathogens from non-pathogens. Intriguingly, our results stand in contrast to these findings. First, all indices of adaptation to aerotolerance and oxidative stress tested — $\tilde{q}$, fraction of proteins devoted to antioxidant defense, frequency of Cys in the proteome — are either not significantly different between vertebrate pathogens and non-pathogens or indicate weaker adaptation for aerotolerance in non-pathogens than in pathogens. This holds irrespective of whether organisms with small genomes are excluded from the sample.

Interestingly, intracellular parasites, commensals and symbionts (henceforth denoted "intracellular associates") display higher protein oxidabilities than free-living organisms, suggesting weaker adaptation indices. Organisms with an obligatory host-associated life-style usually have a vertical mode of transmission and are subject to frequent population bottlenecks [81]. Consequently, they tend to have low effective population sizes, which leaves them vulnerable to accumulation of deleterious mutations (Muller's ratchet) [69]. The reduced genomes and low %GC of many of the intracellular associates (Supplementary Figure 3.5) indicate that they are subject to Muller's ratchet, which would also explain their elevated $\tilde{q}$ values. However, this cannot explain the high $\tilde{q}$ values of many intracellular associates, many of them pathogenic, that have large genomes and high G+C content.

3. Proteome composition and aerotolerance

Altogether, these results suggest that most pathogens' success is not due to adaptation to survive oxidative stress but by avoiding activating the immune defenses of the host organisms. Many intracellular pathogens in particular may live in a redox-protected environment, eventually using the host's antioxidant defenses to their own benefit. The latter behavior is illustrated by the malaria pathogen *Plasmodium falciparum*, which imports peroxiredoxin 2 from the host's erythrocytes to survive oxidative stress [82] which is a very efficient and abundant antioxidant defense in the human erythrocyte [83].

Overall, our observations indicate that organisms' proteomes are highly adapted to deal with the added oxidative stress of exposure to oxygen-rich environments. This is expressed at the level of AAC and reflects in a lower protein oxidability. These observations follow multiple studies that indicate that environmental conditions such as temperature [27, 28, 31], but not habitat [84], affect amino acid signatures of organisms.

3.7 Acknowledgments

We acknowledge Fellowship SFRH/BD/51199/2010 to R.B.

3.8 Supporting Information

3.8.1 Organism Information

Supplementary Table 3.1 – Number of organisms in the various groups considered. AT – Aerotolerant; AI – Aerointolerant.

Domain	Phylum or group	Total	Aerotolerance		Thermophily				With known growth rate
			AI	AT	Psychrophiles	Mesophiles	Thermophiles	Hyperthermophiles	
Archaea	All	81	53	28	1	27	14	39	25
	Euryarchaeota	54	39	15	1	26	12	15	13
	Others	27	14	13	0	1	2	24	12
Bacteria	All	965	325	640	26	835	99	5	184
	Actinobacteria	120	25	95	1	112	7	0	15
	Bacter./Chlorob.	59	25	34	4	54	1	0	7
	Firmicutes	237	140	97	5	190	41	1	32
	Proteobacteria	394	74	320	16	373	5	0	95
	Others	155	61	94	0	106	45	4	35
Eukarya	All	53	11	42	1	51	1	0	9
Total		1099	389	710	28	913	114	44	218

Organisms whose cDNA was not correctly annotated and whose G+C content was obtained from each organism's genome page at NCBI were the following: *Brachybacterium paraconglomeratum, Burkholderia oklahomensis, Burkholderia ubonensis, Carnobacterium maltaromaticum, Chlamydia muridarum, Citromicrobium bathyomarinum, Clostridium cellulovorans, Corynebacterium aurimucosum, Cryptosporidium hominis, Desulfotomaculum nigrificans, Enterococcus casseliflavus, Gemmata obscuriglobus, Lactobacillus iners, Methylosinus trichosporium, Micrococcus luteus, Pseudoalteromonas flavipulchra, Succinivibrionaceae bacterium, Thermococcus zilligii, Verrucomicrobium spinosum, Vibrio campbellii*.

3.8.2 Estimates of amino acid biosynthetic costs in *E. coli* and *S. cerevisiae*

To estimate each amino acid's biosynthesis costs (Table 2 of the main text) we first estimated the net number of precursor molecules, one-carbon units, ATP (~P) and NADPH/NADH equivalents consumed or produced in the biosynthesis of each amino acid. Because ammonium, sulfate and CO_2/bicarbonate are also necessary for synthesizing some amino acids we then estimated the costs to uptake each of these molecules. All these costs were then converted to ~P and NADH equivalents, which finally are converted to number of glucose equivalents.

3.8.2.1 Estimating number of precursor molecules, one-carbon units, ATP, NADPH/NADH equivalents and Acetyl-CoA spent/generated

The biosynthesis pathway we considered for each amino acid in each organism was obtained by manually inspecting the *E. coli* metabolic pathways at EcoCyc [57] and the Yeast Metabolic Pathways at the *Saccharomyces* Genome Database [58]. These pathways were then compared to the equivalent pathways deposited in KEGG [59] for the two organisms (KEGG ids *eco* and *sce*). Where multiple pathways are available for the synthesis of a given amino acid, we considered the pathway that has been experimentally determined to carry most of the flux for biosynthesis of that amino acid in the relevant conditions. If this information was not available, we considered the pathway through each the biosynthesis of the amino acid is cheapest.

The following costs are implicit in the ~P and NADPH counts. Where pathways use acetyl-CoA and release acetate in a later step we consider a net cost of 2 ~P for recycling acetate as acetyl-CoA, reflecting the activity of AMP-forming acetate-CoA ligase (EC 6.2.1.1) and the absence of ADP-forming acetate-CoA ligase (EC 6.2.1.13) in both organisms.

We also computed the cost of precursors (pyruvate, oxaloacetate, etc), single carbon units, NADPH and transport processes in terms of glucose, ~P and NADH reducing equivalents. This is necessary because the ~P yields of both glucose and NADH equivalents depend on the extent to which cells rely on fermentative vs respiratory metabolism for ~P production and NADH oxidation (see below). The costs attributed

to precursors (3-phosphoglyceratte, phosphoenolpyruvate, pyruvate, oxaloacetate, 2-oxoglutarate) were derived from the stoichiometry of glycolysis and tricarboxylic acids cycles in *E. coli* and *S. cerevisae*. The costs assigned to erythrose 4-phosphate, ribose 5-phosphate, and NADPH reducing equivalents reflect different modes of operation of the pentose phosphates pathway, both in *E. coli* and *S. cerevisae*, and were computed from the overall reactions as catalyzed by enzymes in central carbon metabolism. The costs of acetyl-CoA reflect this molecule's formation from pyruvate through the activity of pyruvate dehydrogenase (EC 1.2.4.1). The cost of single carbon units was based on the methyl transfer reactions catalyzed by serine hydroxymethyltransferase (EC 2.1.2.1) and glycine cleavage complex, often considered the main source of single carbon units in the cell [85, 86](Supplementary Table 3.2), and then estimated by taking into account the cost of Ser biosynthesis (in glucose, NADH, ~P and CO_2 equivalents).

Supplementary Table 3.2 – Overall reactions for synthesis of precursors of amino acid synthesis.

Reaction	Enzymes catalyzing intermediate steps
Serine + 2 tetrahydrofolate $\rightarrow$ $\rightarrow$ 2 5,10-methylenetetrahydrofolate + NADH + NH_4^+ + CO_2	EC 2.1.2.1; Glycine cleavage complex
2 Glucose + 3 ATP $\rightarrow$ 3 erythrose 4-phosphate + 3 ADP	EC 2.7.1.1; EC 2.7.1.2; EC 5.3.1.9; EC 2.7.1.11; EC 4.1.2.13; EC 5.3.1.1; EC 5.1.3.1; EC 5.3.1.6; EC 2.2.1.2
5 Glucose + 6 ATP $\rightarrow$ 6 ribose 5-phosphate + 6 ADP	EC 2.7.1.1; EC 2.7.1.2; EC 5.3.1.9; EC 2.7.1.11; EC 4.1.2.13; EC 5.3.1.1; EC 2.2.1.1; EC 2.2.1.2; EC 5.1.3.1; EC 5.3.1.6
Glucose + ATP + 7 H_2O + 12 $NADP^+$ $\rightarrow$12 NADPH + + 12 H^+ + 6 CO_2 + ADP + P_i	EC 2.7.1.1; EC 2.7.1.2; EC 1.1.1.49; EC 3.1.1.31; EC 1.1.1.44; EC 5.1.3.1; EC 5.3.1.6; EC 2.2.1.2; EC 2.2.1.1; EC 5.3.1.1; EC 4.1.2.13; EC 3.1.3.11

3.8.2.2 Estimating transport costs for ammonium, sulfate and CO_2/bicarbonate

Ammonium intake dissipates the electrochemical potential across the plasma membrane, an effect that has to be compensated through active proton extrusion. In *E. coli* this is mostly accomplished through the F0/F1 ATPase [87], whereas yeast

mostly uses the Pma1p proton pump [88]. The bacterial pump has a stoichiometry of 2 to 3 H^+ per ATP hydrolyzed, with the most recent determinations supporting the larger value [87, 89, 90]. The yeast pump has a stoichiometry of 1 H^+/ATP under abundant glucose [91]. These stoichiometries were considered for the cost of utilizing ammonium.

Sulfate uptake in *E. coli* occurs through multiple sulfate transporters. Studies with the CysP and SBP (EC 3.6.3.25) transporters of the ABC family, indicate that these are the most important for sulfate intake given that their mutation renders the cell auxotrophic for cysteine due to blocking of sulfate and thiosulfate transport [92, 93]. CysP is also among the 5-25% most abundant proteins in *E. coli* [94-96], allowing us to consider the stoichiometry of their activity for our cost of sulfate uptake: 1 ~P consumed per sulfate uptaken. In *S. cerevisae* sulfate uptake is mediated by two high-affinity transporters SUL1 and SUL2 [97, 98], and is coupled with the net influx of 3 H^+ and efflux of 1 K^+ per SO_4^{2-} uptaken [99]. These studies also indicate that sulfate intake is generally coupled with anion/cation with concomitant charge balance and null net potential change. No ATP hydrolysis coupled to SUL1/SUL2 activity was reported, and no cost of sulfate uptake was considered in yeast.

We assumed that CO_2 – or bicarbonate derived from it through the action of carbonic anhydrase — can be imported from the environment or extruded at no cost for the cell. This assumption is consistent with the detection of a functional carbonic anhydrase (EC 4.2.1.1) in *E. coli* [100] and yeast [101, 102], of bicarbonate transporters in *E. coli* [103] and a presumably non-electrogenic plasma membrane anion transporter in *S. cerevisae* [104]. The cost of dissipating carbon as CO_2 is already implicit in the stoichiometry of synthesis of the metabolic precursors from glucose.

3.8.2.3 Converting net costs of all precursors into glucose equivalents

In this step we convert all the costs estimated above into number of glucose equivalents, under fermentative and respiratory conditions. The following two alternatives could be considered as intuitive scalar measures of metabolic cost. First [54, 105], the net number of “high energy” phosphate bond equivalents (~P) hydrolyzed to synthesize each amino acid from precursor molecules plus the number of ~P that would have been produced from each spent precursor should it have been

catabolized for energy production. Alternatively, we can express the cost of synthesizing any given amino acid in terms of glucose molecules spent in generating the precursors and ~P equivalents and, where necessary, oxidizing the excess NADH. We opted for the latter alternative because most available proteomic data for *E. coli* and yeast [95, 106-110] were obtained for aerobic glucose-limited growth, which is carbon- rather than energy-limited. However, the two cost measures are approximately proportional, the proportionality constant being the ATP yield of glucose catabolism under the condition of interest.

In order to compute the biosynthetic cost of each amino acid in terms of glucose equivalents we convert all ~P and NADH reducing equivalents into glucose equivalents for two extreme situations: fully respiratory energy metabolism and fully fermentative energy metabolism. The ~P equivalents are straightforwardly converted to glucose equivalents in yeast by dividing by the ~P yield of glucose in each condition: 2 ~P/glucose for fermentation and 16 ~P/glucose for respiration. The latter value is much lower than the respiratory yield of most known eukaryotic cells because *S. cerevisiae* lacks respiratory complex I [60]. Instead, it has a single-subunit NADH:ubiquinone oxidoreductase which catalyzes the transfer of electron pairs from mitochondrial matrix NADH to ubiquinone [61, 62] but is unable to pump protons across the mitochondrial inner membrane [61]. For this reason, the P/O ratio approaches 1 [64], meaning that only 1 ATP is generated per NADH oxidized. In *E. coli* there are 3 ~P/glucose formed during fermentation, and 26 ~P/glucose under respiration [111]. The latter value comes short of the theoretically predicted 33 ~P/glucose [112] owing to proton leakage [113] and to the utilization of NADH dehydrogenases and cytochrome oxidases with differential contributions to the proton motive force: the proton-pumping NADH:quinone oxidoreductase NADH dehydrogenase I catalyzes the translocation of 2 H^+/e^- to the periplasm [114], whereas NDH-II is not electrogenic [115]. The cytochrome *bd*-oxidase does not translocate protons but leads to transmembrane charge separation with net 1 H^+/e^- [116-120], whereas cytochrome *bo*-oxidase has a yield of 2 H^+/e^- [116], with the choice of oxidase depending on the growth conditions [121]. Another possible factor contributing to the lower energy yield is the maintenance energy requirement [122, 123].

The conversion of NADH reducing equivalents into glucose equivalents was treated as follows. Biosynthetic pathways generate excess NADH reducing equivalents, which

have to be eliminated so that the reactions proceed. If respiration is sufficiently active, all the excess this NADH can be reoxidized by the respiratory chain, yielding 1 ~P per NADH oxidized in yeast. Therefore, each excess NADH reducing equivalent generated by amino acid biosynthesis under these conditions reduces the amino acid cost by 1/16 glucose equivalents.

The corresponding estimate for *E. coli* has to account for the coupled proton translocation yield of NDH-I (2 H^+/e^-) and NDH-II (0 H^+/e^-). Both dehydrogenases can be used, but cytochrome *bo*-oxidase (2 H^+/e^-) predominates over *bd*-oxidase under high oxygen pressure [121]. Considering the activity of cytochrome *bo*-oxidase, we estimate that each NADH molecule yields an average 6 H^+ translocated, resulting in 2 ~P/NADH after considering F0/F1 ATPase activity. Therefore, each excess NADH reducing equivalent reduces amino acid synthesis in 1/13 glucose equivalents.

Under fermentative conditions NADH must be reoxidized through other pathways. In yeast, ethanolic fermentation is unsuitable for this task, because it is redox neutral (*i. e*. as many NADH reducing equivalents are produced as are consumed). Instead, yeast cells use glycerol [124]. This pathway entails a cost because it shifts one DHAP molecule away from both energy production and biosynthesis and spends 1 ~P per NADH oxidized. Therefore, each excess NADH reducing equivalent generated by amino acid biosynthesis under these conditions *increases* the amino acid cost by 1 glucose equivalent. *E. coli* uses mixed acid fermentation under anaerobiosis to recycle NADH back to NAD^+ whilst excreting various products. From the five possible branches of this pathway only ethanol formation is not redox neutral, oxidizing one more NADH than it produces [125] with an overall cost of 0.5 Glucose equivalents per NADH equivalents oxidized.

Overall, these considerations were taken into account to compute the amino acid biosynthesis costs indicated in Table 3.2 of the main text.

The following groups of amino acids and their ratio of costs fermentation/respiration were considered based on physico-chemical similarity of their side chains and on observed frequent amino acid substitutions [73].

Supplementary Table 3.3 – Amino acids grouped based on structure similarity and frequency of substitutions [73]. Cys, Pro and His do not group together with other amino acids. Asn and Gln are not acidic amino acids but are frequently substituted by Glu or Asp. Ratios of costs based on Table 3.2 of main text. Underlined amino acids are the biosynthetically cheapest in each group and were considered as reference amino acids for the frequency ratios estimated.

		Ratio of costs (fermentation/respiration)	
Group	**Amino acid**	***E. coli***	***S. cerevisae***
Acidic	<u>Asp</u>	1.84	3.61
	Glu	3.06	5.31
	Asn	3.27	4.92
	Gln	3.42	5.65
Aromatic	<u>Phe</u>	2.06	2.84
	Tyr	2.45	2.91
	Trp	2.49	3.49
Lipophilic	<u>Val</u>	1.74	2.78
	Ile	2.06	3.21
	Leu	2.81	4.64
	Met	5.63	4.54
Neutral	<u>Ala</u>	1.83	3.09
	Thr	2.42	3.79
	Gly	2.49	4.04
	Ser	3.87	5.94
Basic	Lys	2.19	6.96
	Arg	4.56	6.42
	Cys	4.15	4.34
	Pro	2.97	4.84
	His	4.25	5.49

3.8.3 Estimate of amino acid solvent accessibility

We tested how our algorithm's predictions for each protein's r_i ($r_{i,pred}$), which takes into account the predicted amino acid exposure as function of protein size, with the r_i obtained using the solvent accessibilities computed from experimentally determined structures ($r_{i,obs}$). To do this we used a set of 9821 proteins with experimentally determined structures from which amino acid exposure to solvent was computed (see Methods in main text). To compare $r_{i,pred}$ with $r_{i,obs}$ we selected 50 random subsets of 7000 out of the 9821 experimentally determined proteins. Each subset was used as template for determining the best fit polynomials $a_j(s_i)$ of amino acid exposure a_i as function of the number of amino acids s_i in a protein.

3. Proteome composition and aerotolerance

For each of the 50 randomly chosen sets we then computed the ratio r_{pred} / r_{obs} for the subset of excluded 2821 proteins, and determined medians, standard deviations and quartiles for those ratios for all organisms with more than 100 experimentally determined proteins (Supplementary Table 3.5). All other organisms with less than 100 experimentally determined protein structures were grouped together and a similar comparison was carried out. The median r_{pred} / r_{obs} ratios estimated per organism are all close to 1 (Supplementary Table 3.5). Although some of the standard deviations are comparatively large, both the first and third quartiles are very close to 1. These observations indicate that using $a_j(s_i)$ as predictor for amino acid exposure to solvent yields *r* values very close to those that would be determined with experimentally-determined solvent accessibility. Further, because coefficients were so similar in each of the 50 runs (all coefficients had coefficients of variation <0.1, Supplementary Table 3.4), these observations also indicate that any of the 50 yield similar results. The final polynomial functions $a_j(s_i)$ were the ones with the best fit (Supplementary Table 3.4) from the sets above. Despite the regression polynomials explaining a small fraction of the variance in amino acid solvent accessibility, this does not affect the estimates of protein *r* and a good agreement with the values computed from the experimentally determined structures is observed (properties of r_{pred} / r_{obs}: median = 1.024, first quartile = 0.884, third quartile = 1.198, standard deviation = 0.259).

Supplementary Table 3.4 – Summary of estimated regression coefficients for $a_j(s_i)$ used to estimate exposure to solvent (columns Reference) and respective Adj R^2, and coefficients attained based on 50 randomly chosen sets of 7000 proteins. A polynomial function of the form $a_j(s_i) = b + c \cdot s_i + d \cdot s_i^2$ was used to fit amino acid exposure to solvent as function of protein size (s_i). See text above for details. b, c, d – fitted coefficients; SE – standard error of the mean; CV – coefficient of variation.

	Adj R^2	b				c				d			
		Reference	Mean	SE ($\times 10^{-6}$)	CV	Reference	Mean ($\times 10^{-4}$)	SE ($\times 10^{-8}$)	CV	Reference	Mean ($\times 10^{-7}$)	SE ($\times 10^{-11}$)	CV
A	0.16	0.398	0.398	5.43	0.00808	-4.83	-4.807	2.11	-0.0259	2.97	2.96	1.69	0.0338
C	0.05	0.194	0.188	7.17	0.0225	-3.47	-3.206	2.60	-0.0479	2.40	2.18	2.01	0.0546
D	0.14	0.586	0.589	3.57	0.00358	-3.78	-3.866	1.38	-0.0211	2.25	2.31	1.16	0.0296
E	0.14	0.607	0.604	4.23	0.00413	-3.43	-3.335	1.57	-0.0278	2.11	2.03	1.30	0.0378
F	0.10	0.252	0.255	6.71	0.0156	-3.72	-3.818	2.38	-0.0370	2.44	2.51	1.84	0.0434
G	0.22	0.599	0.603	4.34	0.00427	-5.98	-6.102	1.81	-0.0176	3.62	3.73	1.59	0.0252
H	0.12	0.504	0.497	6.78	0.00808	-5.70	-5.548	2.70	-0.0289	3.49	3.42	2.21	0.0382
I	0.12	0.220	0.216	4.92	0.0135	-3.29	-3.182	1.79	-0.0334	2.17	2.09	1.38	0.0390
K	0.10	0.617	0.619	3.47	0.00331	-3.00	-3.056	1.40	-0.0271	1.78	1.83	1.20	0.0388
L	0.17	0.252	0.250	4.04	0.00956	-3.84	-3.798	1.45	-0.0226	2.58	2.55	1.12	0.0259
M	0.15	0.382	0.379	6.95	0.0108	-6.91	-6.838	2.57	-0.0223	4.68	4.63	2.10	0.0268
N	0.11	0.545	0.552	5.51	0.00590	-4.00	-4.297	2.10	-0.0289	2.20	2.43	1.71	0.0414
P	0.17	0.511	0.515	4.94	0.00567	-4.85	-4.964	1.98	-0.0236	2.95	3.02	1.64	0.0323
Q	0.19	0.598	0.599	4.80	0.00474	-5.37	-5.489	1.96	-0.0212	3.13	3.27	1.68	0.0303
R	0.20	0.552	0.548	5.70	0.00614	-5.06	-4.939	2.21	-0.0266	3.12	3.02	1.83	0.0359
S	0.20	0.512	0.512	5.05	0.00584	-5.43	-5.472	2.01	-0.0218	3.29	3.36	1.72	0.0303
T	0.17	0.458	0.460	5.19	0.00669	-4.62	-4.709	2.06	-0.0259	2.72	2.80	1.74	0.0367
V	0.13	0.251	0.253	4.36	0.0102	-3.56	-3.656	1.72	-0.0280	2.36	2.43	1.41	0.0342
W	0.03	0.272	0.274	6.90	0.0149	-2.69	-2.758	2.84	-0.0608	1.62	1.66	2.38	0.0847
Y	0.10	0.321	0.325	5.34	0.00974	-3.63	-3.803	1.91	-0.0297	2.22	2.36	1.54	0.0386

3. Proteome composition and aerotolerance

Supplementary Table 3.5 – Summary of comparisons between oxidability indices predicted using a randomly chosen set of experimentally determined proteins (r_{pred}) and an oxidability index based on experimentally determined amino acid exposures (r_{obs}). See text above for details. Organisms, their domains, number of proteins considered (# prots) are given. Properties of the estimated ratios are shown (Median, SD – Standard Deviation, Q1 – first quartile, Q3 – third quartile).

Organism	**Domain**	**# prots**	r_{pred} / r_{obs}		
			Median	**Q1**	**Q3**
Saccharomyces cerevisiae	Eukaryota	716	1.068	0.902	1.290
Salmonella typhimurium DT104	Bacteria	189	1.068	0.912	1.349
Bacillus subtilis 168	Bacteria	332	1.028	0.819	1.237
Methanocaldococcus jannaschii DSM 2661	Archaea	105	0.946	0.815	1.080
Thermotoga maritima MSB8	Bacteria	232	0.958	0.840	1.079
Pyrococcus horikoshii OT3	Archaea	236	0.927	0.856	1.010
Aquifex aeolicus VF5	Bacteria	116	0.892	0.769	1.055
Mycobacterium tuberculosis H37Rv	Bacteria	346	0.996	0.885	1.118
Escherichia coli K 12 substr MG1655	Bacteria	2055	1.042	0.892	1.206
Helicobacter pylori 26695	Bacteria	104	0.973	0.832	1.035
Staphylococcus aureus N315	Bacteria	311	0.977	0.916	1.181
Pseudomonas putida KT2440	Bacteria	120	0.941	0.845	1.013
Pseudomonas aeruginosa PAO1	Bacteria	247	1.086	0.935	1.332
Thermus thermophilus HB27	Bacteria	375	0.992	0.852	1.089
All others		4337	1.026	0.875	1.203

3.8.4 Additional figures and tables

Unless otherwise stated, all boxwhisker plots below have whiskers extending to 1.5 the interquartile differences, bar widths are proportional to the square root of sample sizes, notches mark approximate 95% confidence intervals for the medians.

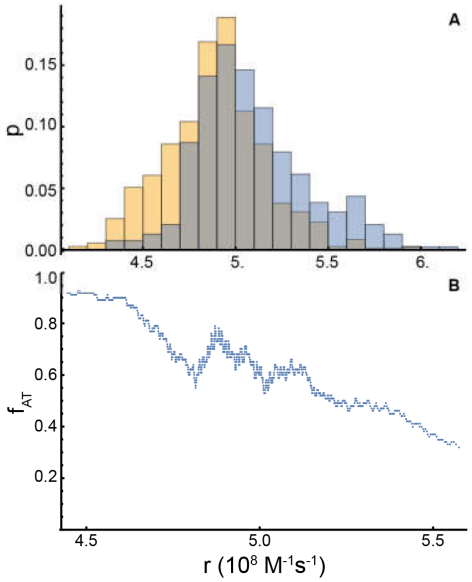

Supplementary Figure 3.1 - AT organisms have lower median proteome oxidability r *than AI organisms. A) Probability distribution bins determined for AT (orange) and AI (blue) populations as function of median proteome* r. *B) Moving median fraction of AT organisms in the total population as function of median proteome* r.

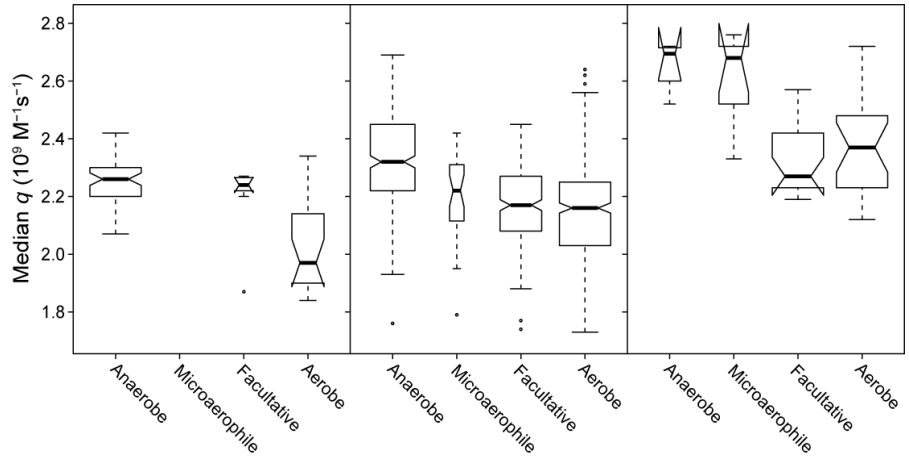

Supplementary Figure 3.2 – Median proteome q as function of oxygen tolerance in Archaea (left), Bacteria (middle) and Eukarya (right).

3. Proteome composition and aerotolerance

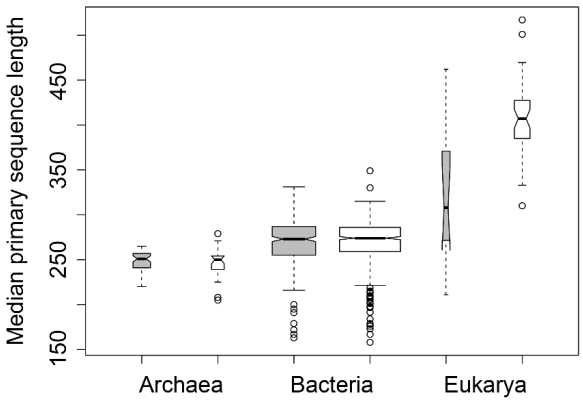

Supplementary Figure 3.3 – Median size of primary protein sequence in AI (gray) and AT (white) organisms.

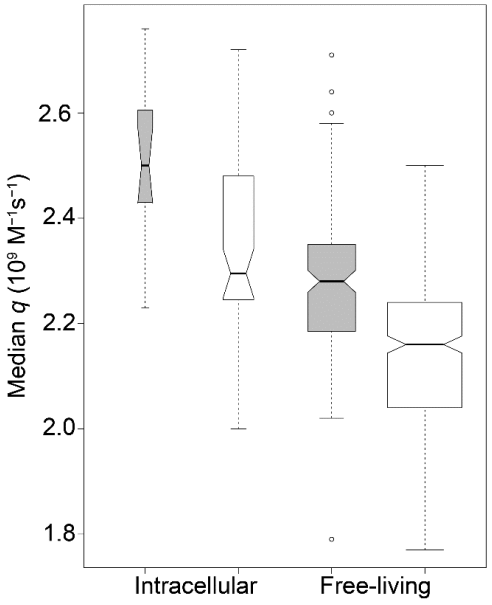

Supplementary Figure 3.4 – Median proteome oxidability in intracellular parasites versus free-living AI (gray) and AT (white) organisms.

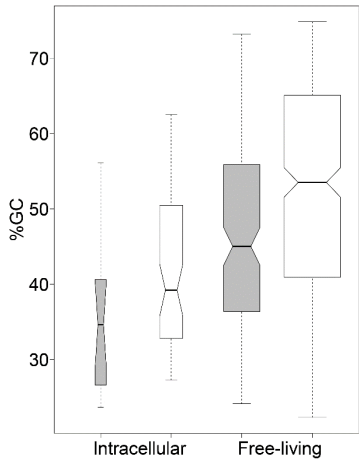

Supplementary Figure 3.5 – Median proteome genomic G+C content in intracellular parasites and free-living AI (gray) and AT (white) organisms.

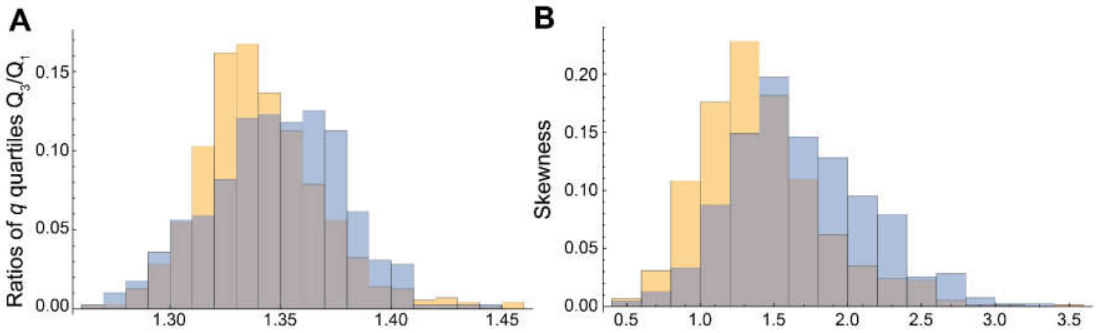

Supplementary Figure 3.6 – Distribution of q *values within AI (yellow) and AT (blue) organisms. A) Histograms of the ratios between the third and first quartiles of the distribution of protein q values in each organism ($p = 4.5\times10^{-6}$ for comparison of AT vs. AI, by one sided Mann-Whitney test). B) Histograms of the skewness of the distribution of protein q values in each organism ($p = 3.3\times10^{-22}$ for comparison of AT vs. AI, by one sided MW test).*

3. Proteome composition and aerotolerance

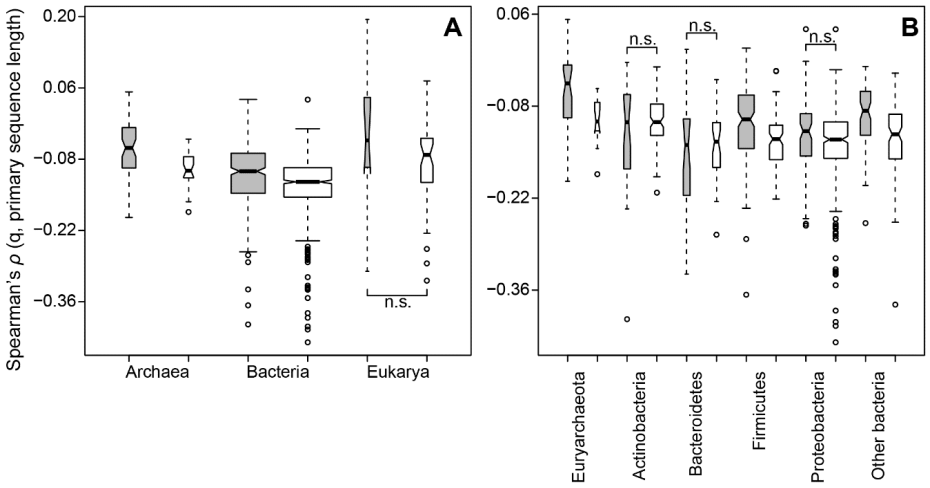

Supplementary Figure 3.7 – Correlation between protein q *and size of the primary protein sequence in AI (gray) and AT (white) domain (A) and phyla (B). Spearman's rank correlations were computed for each organism. Mann-Whitney tests comparing the distributions of the correlations in AI vs. AT organisms of the same clade indicate that true location shifts are significantly greater than zero except where indicated (n.s.) at a 1% false discovery ratio.*

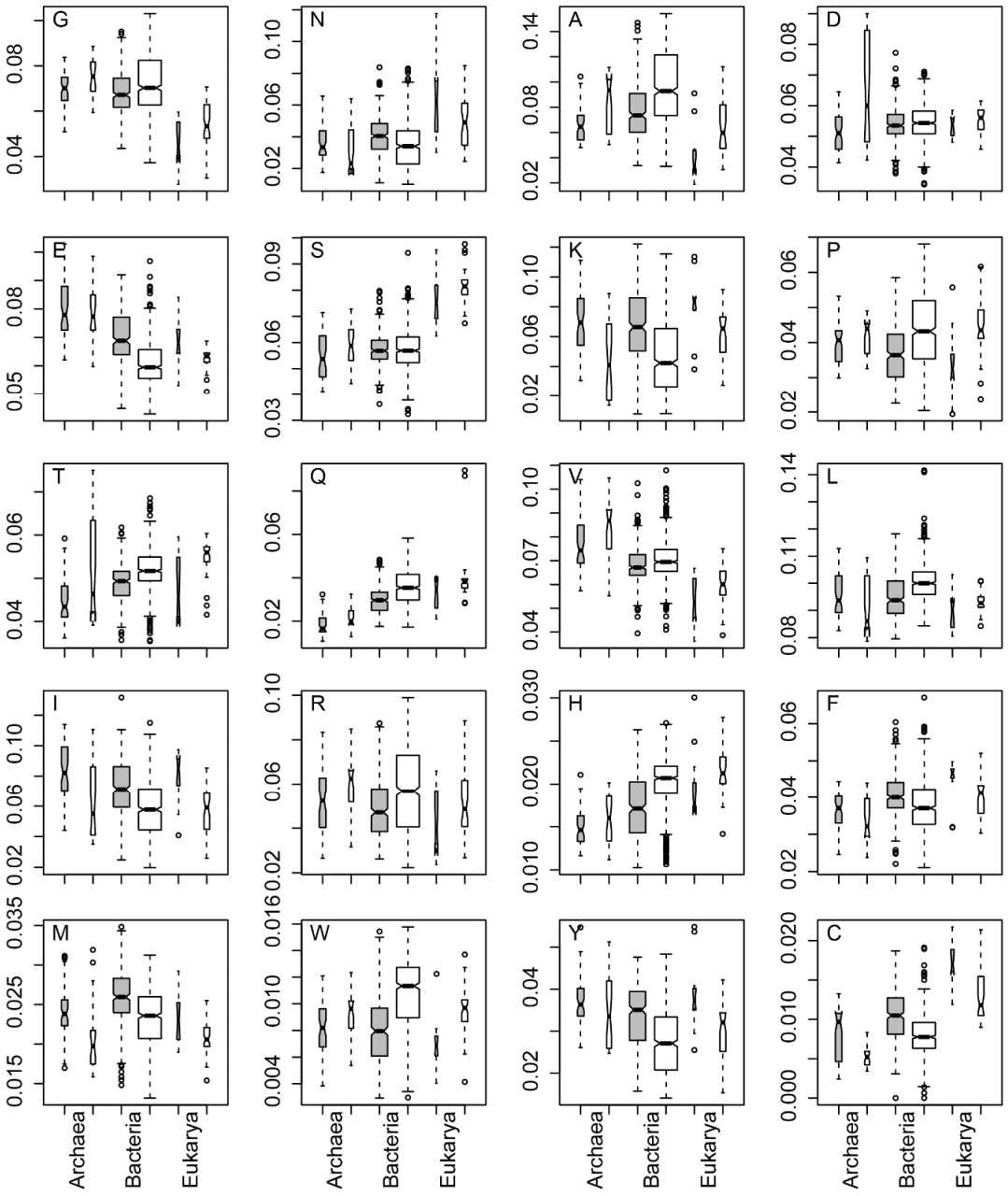

Supplementary Figure 3.8 – Distribution of median amino acid frequencies in AI (gray) and AT organisms (white) for the three phylogenetic domains and phyla.

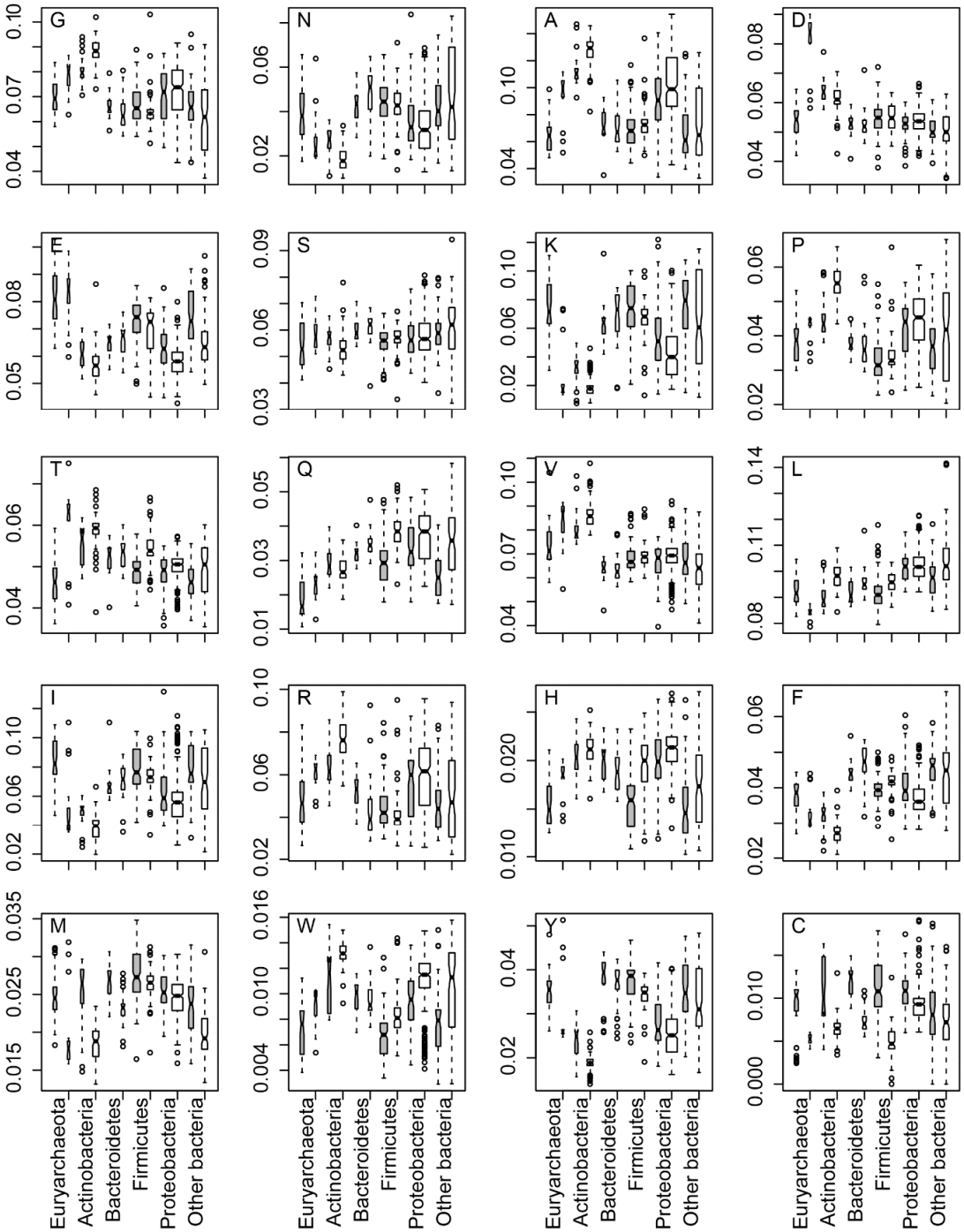

Supplementary Figure 3.8 (continued)

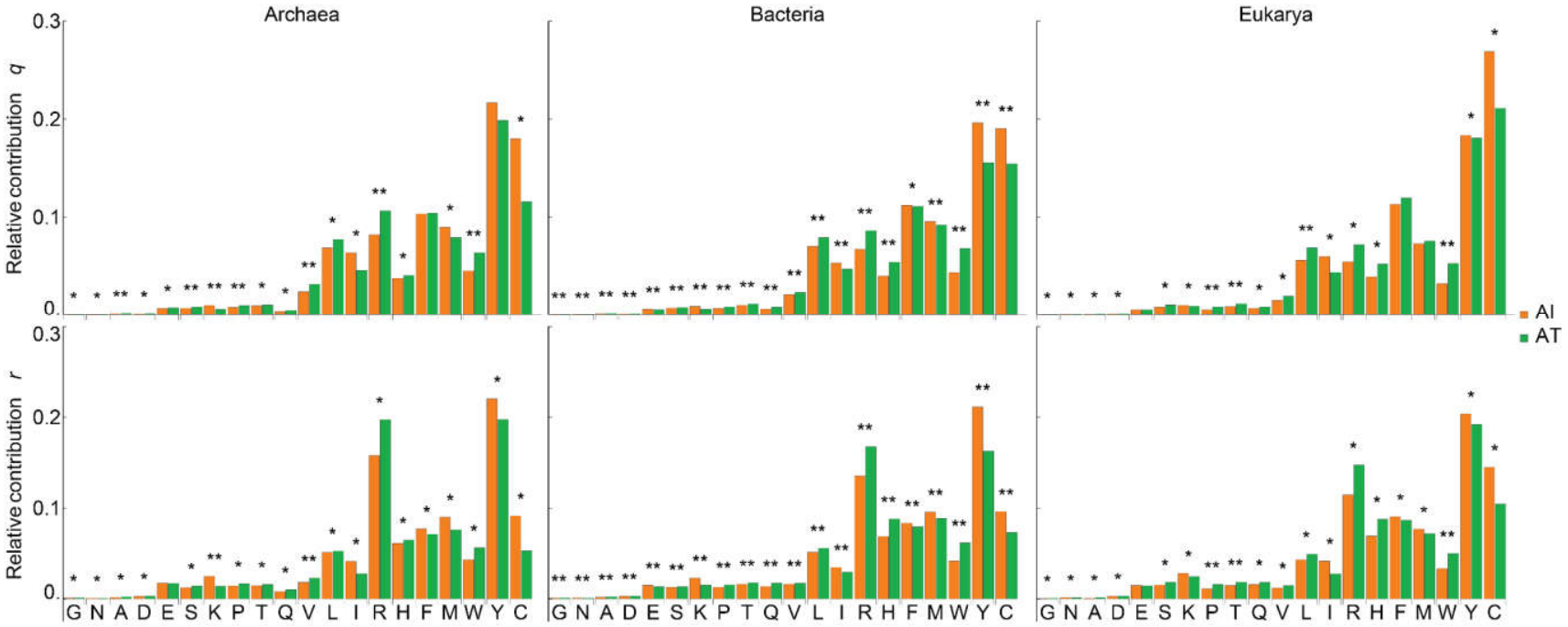

Supplementary Figure 3.9 – Median amino acid contribution to oxidability q *(top) or* r *(bottom) in AI (orange) and AT (green) Archaea (left), Bacteria (middle) and Eukarya (right). Mann-Whitney test performed for the comparison of median relative contributions of AI vs AT in each domain. * p-value < 0.05, p-value < 0.00028 (corrected for 180 tested hypotheses).*

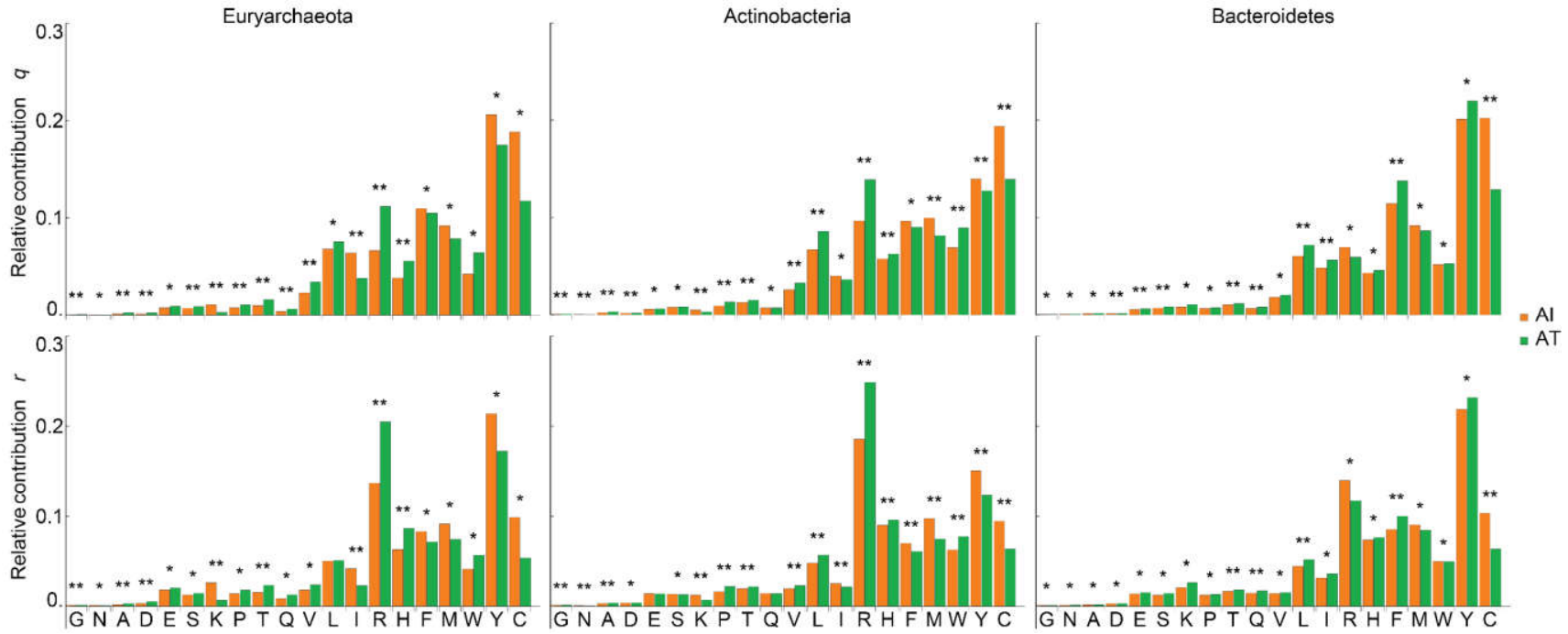

Supplementary Figure 3.10 – Median amino acid contribution to oxidability q *(top) or* r *(bottom) in AI (orange) and AT (green) for the sufficiently represented archaeal and bacterial phyla. Mann-Whitney test performed for the comparison of median relative contributions of AI vs AT in each domain. * p-value < 0.05, p-value < 0.00028 (corrected for 180 tested hypotheses).*

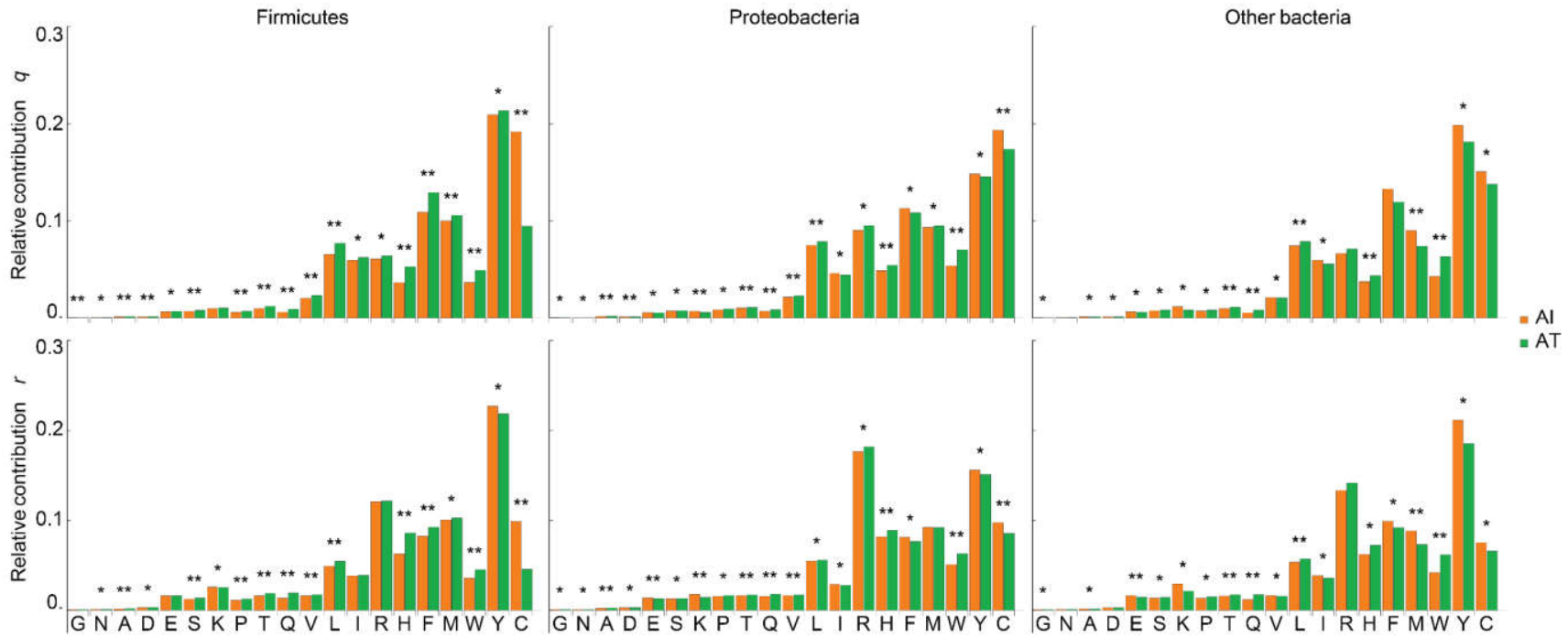

Supplementary Figure 3.10 (cont.)

3. Proteome composition and aerotolerance

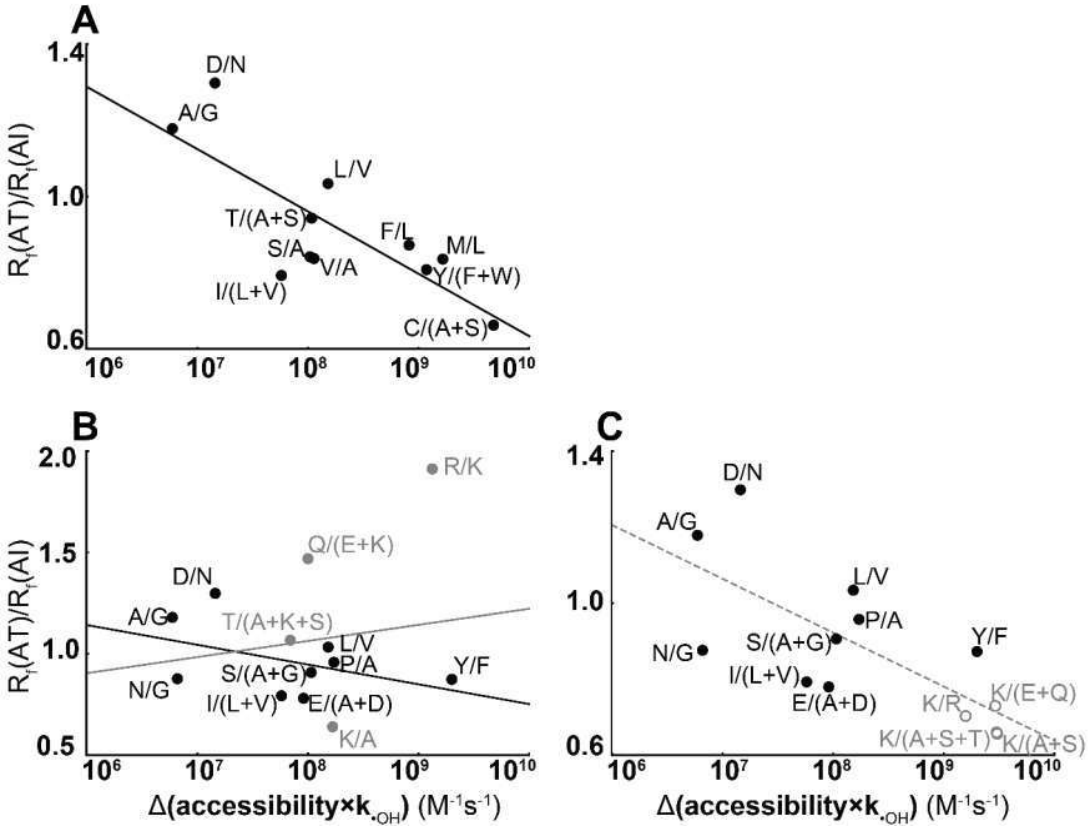

Supplementary Figure 3.11 - Ratios of frequencies of groups of frequently substituted non-exposed (top) or solvent-exposed (bottom) amino acids as function of differences of amino acid •OH reactivity weighted by solvent accessibility of the residues for Bacteria. For each group of frequently substituted amino acyl residues in proteins [73] we computed the ratios (R_f) between the median amino acid frequency of the most reactive aminoacyl residues and the means of the median frequencies of the other aminoacyl residues in the group for AI and AT bacteria. We then plotted the ratios $R_f(AT)/R_f(AI)$ as function of $\log_{10}$ of the differences between the solvent accessibility-weighted •OH reactivity of the amino acid in the numerator of R_f and the mean of those in the denominator. In panels B, C the gray symbols indicate the ratios for the replacement groups involving Lys, either considering its reactivity with •OH (closed circles) or an effective reactivity similar to His (circumferences). Mean amino acid accessibility was estimated as described in Methods. Lines are least squares regression lines of $R_f(AT)/R_f(AI)$ vs. $\log_{10}(\Delta(\text{accessibility}\times k_{\bullet OH}))$ for the ratios represented by closed black circles (black), by all closed circles (solid gray), and by the closed black circles plus the gray circumferences (dashed gray). Similar plots for $\Delta k_{\bullet OH}$ are presented in *Figure 3.4* of the main text. Spearman rank correlation coefficients are: (A) -0.61 (0.047), (B) all circles, -0.088 ($p\approx0.78$), black circles -0.25 ($p\approx0.52$), (C) black circles plus gray circumferences -0.73 ($p\approx 0.0050$).

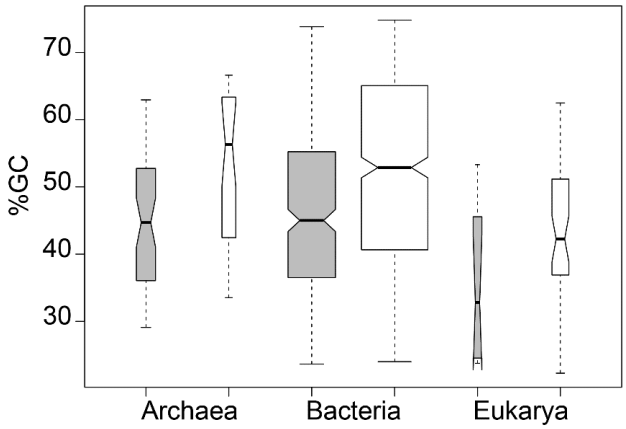

Supplementary Figure 3.12 – Genomic G+C content in AI (gray) and AT (white) organisms of the three phylogenetic domains.

Supplementary Table 3.6 – Number of AI and AT organisms per thermophily class. Note the higher numbers of AI bacteria at higher thermophily.

	Psychrophiles		**Mesophiles**		**Thermophiles**		**Hyperthermophiles**	
Domain	**AI**	**AT**	**AI**	**AT**	**AI**	**AT**	**AI**	**AT**
Archaea	0	1	18	9	6	8	29	10
Bacteria	3	23	259	576	59	40	4	1
Eukarya	0	1	11	40	0	1	0	0

3. Proteome composition and aerotolerance

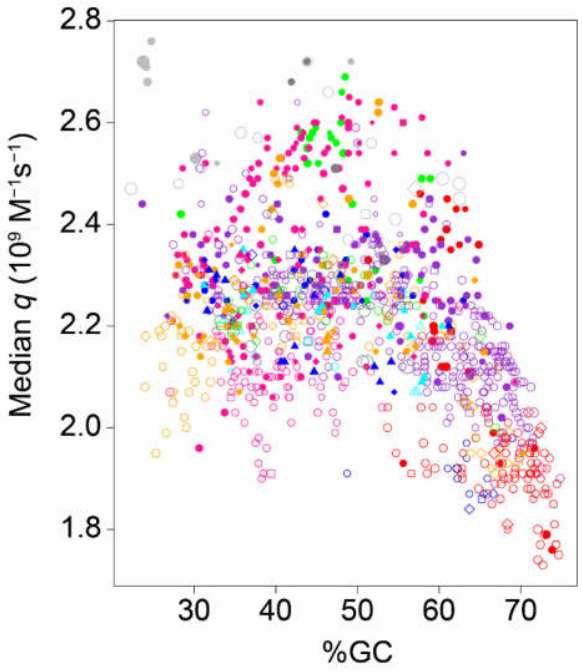

Supplementary Figure 3.13 – Median proteome oxidability q *as function of genomic G+C content in AI (empty symbols) and AT (filled symbols). Thermophily as follows: psychrophiles (squares), mesophiles (circles), thermophiles (diamonds), and hyperthermophiles (triangles). Phyla as follows: Euryarchaeota (blue), Other archaea (cyan), Actinobacteria (red), Chlorobi (green), Firmicutes (pink), Proteobacteria (purple), Other bacteria (orange), Protists (light gray), Opisthokonta (dark gray). Symbol size is proportional to median size of primary sequence.*

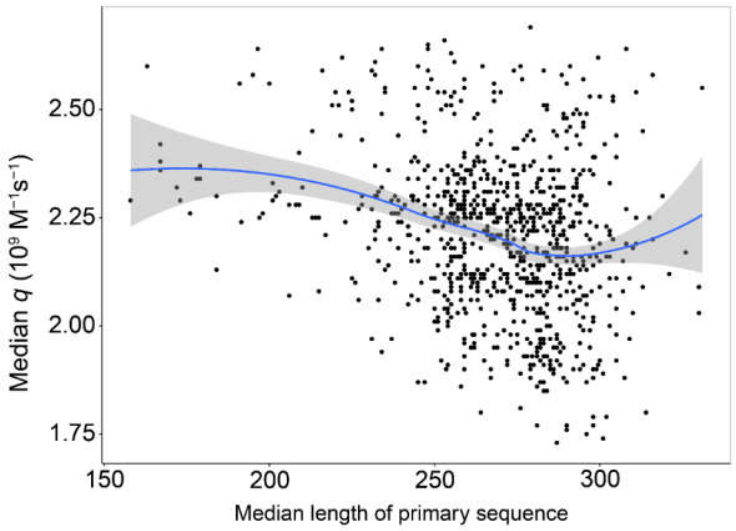

Supplementary Figure 3.14 – Median proteome oxidability q *displays a non-linear relationship with the median length of primary sequence in proteomes. Line represents the LOESS regression line and shaded area the 95% confidence intervals of the fit.*

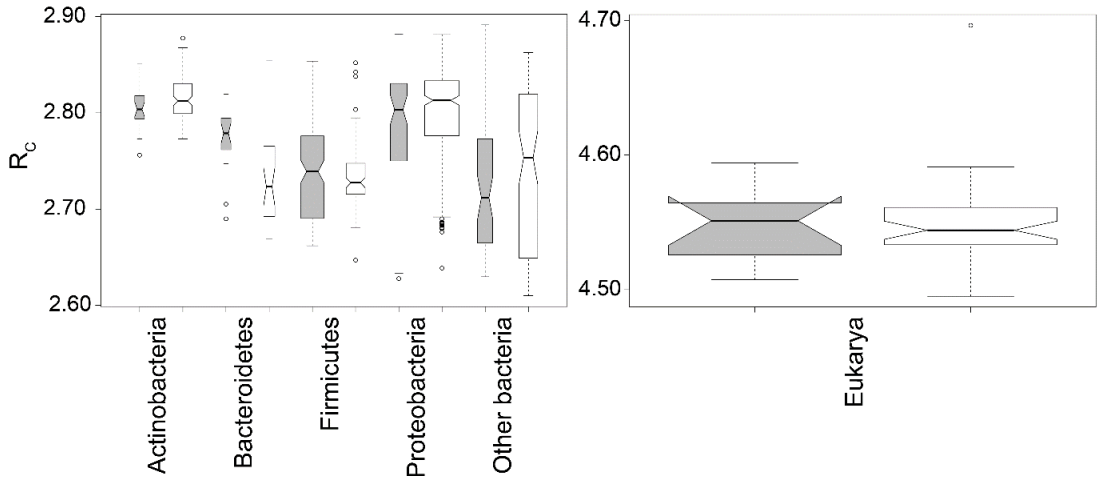

Supplementary Figure 3.15 – Median ratios between the sum of the biosynthetic cost of all the proteins under fermentation and the sum of the costs under respiratory metabolism (R_C) in Bacteria (left) and Eukarya (right). Amino acid biosynthesis costs under respiration and fermentation were determined as indicated in Supporting Information 3.8.2.

3.8.5 Analysis of the interplay among aerotolerance, coding sequence G+C content, phylogeny, thermophily and protein size in determining $\tilde{q}$ values

For the reasons explained in the main text, we used several different statistical models to analyze the interplay among factors determining $\tilde{q}$ values. Here we explain the approach taken and the details of each model. The first model applied to the 862 mesophilic Archaea and Bacteria (Set M) and focused on the interplay between aerotolerance, %GC, phylogeny and median protein size. Inclusion of quadratic %GC and protein size terms was necessary to account for the non-monotonic relationship between $\tilde{q}$ and these variables. The large sample size allowed treating aerotolerance and phylum as factors and considering all possible interactions among all independent variables (maximal model MMM, 49 degrees of freedom) as starting point. In order to evaluate the contribution of variable *x* to the explained variance in $\tilde{q}$ we constructed models MMM-*x* by removing from MMM all terms including *x*. We then computed the adjusted coefficient of determination for each model, the F statistic for the increase in residual variance in replacing MMM by MMM-*x*, and the corresponding p value (Supplementary Table 3.7).

Supplementary Table 3.7 - Comparison of explained variance by models omitting each variable in turn from the maximal multilinear model (MMM), the minimal adequate models for mesophilic Archaea and Bacteria (MMA), for mesophilic, thermophilic and hyperthermophilic Archaea (MMB), and mesophilic and thermophilic Bacteria. df – degrees of freedom.

Model	Adjusted R^2	F statistic for increase in residual variance	df	p-value *
MMM	0.71	-	50	-
MMM-Aerotolerance	0.49	27.8	-24	6×10^{-88}
MMM-%GC	0.59	14.6	-25	7×10^{-49}
MMM-phylum	0.56	11.9	-40	3×10^{-56}
MMM-protein size	0.69	3.10	-25	8×10^{-6}
MMA	0.75	-	12	-
MMA-Aerotolerance	0.57	14.1	-4	2×10^{-7}
MMA-%GC	0.58	11.0	-5	1×10^{-6}
MMA-GTemperature	0.64	9.04	-4	8×10^{-5}
MMA-protein size	0.73	2.56	-4	n.s.
MMB	0.56	-	18	-
MMB-Aerotolerance	0.42	37.8	-8	5×10^{-51}
MMB-%GC	0.32	57.7	-9	3×10^{-82}
MMB-GTemperature	0.53	9.83	-9	4×10^{-12}
MMB-protein size	0.54	5.53	-8	2×10^{-6}

* Includes Bonferroni correction for 12 hypotheses. n.s., non-significant

In order to evaluate the influence of aerotolerance on $\tilde{q}$ while controlling for the other variables we fitted a minimal adequate model (mAMM) to the data for Set M. This model was generated by iteratively deleting unnecessary terms from MMM in two steps. First we deleted all terms such that the Akaike information criterion [126] of simpler model was no higher than that of the model including them. The model obtained after this initial round of simplification still contained terms that did not contribute significantly (i.e. p>0.05 in ANOVA comparisons of successive models) to the explained variance. So, in a second round we deleted these terms until a minimal adequate model was achieved. The latter model (mAMM) has the form:

$$\tilde{q} \sim atol + p\ \ ylum + \ gc + gc^2 + psize + psize^2 + p\ \ ylum{:}\, atol + \\ + p\ \ ylum{:}\, psize + p\ \ ylum{:}\, atol{:}\, gc\ + p\ \ ylum{:}\, atol{:}\, psize$$

in R notation, where *atol*, *gc* and *psize* stand for aerotolerance, %GC and scaled median protein size, respectively. Scaled median protein sizes represent the relative deviation of each organism's median protein size from the grand mean for Set M. The

symbol ":" indicates interaction. The phyla under consideration were as indicated in Table 3.1 of the main text. This model achieved an adjusted R^2= 0.71. Then, for each phylum and aerotolerance we computed fitted values for $\tilde{q}$ at *gc*=0, *psize*=0 or at phylum mean values of *gc* and *psize* and determined the relative differences in fitted values between AT and AI organisms and the respective p values.

In order to analyze the interplay among temperature, aerotolerance, %GC and median protein size we considered two additional sets of organisms: mesophilic and thermophilic Bacteria (Set B, 934 organisms), and mesophilic, thermophilic and hyperthermophilic Archaea (Set A, 80 organisms). In the former case, we used as starting point a maximal model (MMB) similar to MMM but neglecting phylogenetic distribution and considering instead optimal growth temperature, treated as an ordered factor with two levels: Mesophile and Thermophile. We evaluated the influence of aerotolerance on $\tilde{q}$ while controlling for the other variables based on a minimal adequate model (mAMB) generated in the same way as described for mAMM. mAMB has the form:

$$\tilde{q} \sim atol + temp + gc + gc^2 + psize + psize^2 + atol{:}temp + \\ + atol{:}psize + gc{:}psize + atol{:}gc{:}psize$$

where *temp* stands for optimal growth temperature, treated as a two-level factor.

In turn, the relatively low number of organisms in Set A did not allow consideration of higher than two-way interactions and required treating optimal growth temperature as a quantitative variable, which was coded as 1, mesophile, 2, thermophile, 3, hyperthermophile. The maximal model would otherwise be over-parameterized. A gc^2 term was included in order to account for the non-linear dependence of $\tilde{q}$ on %GC. From this model we proceeded as described above to obtain the following minimal adequate model:

$$\tilde{q} \sim atol + temp + gc + gc^2 + atol{:}temp + psize{:}temp$$

Despite the above limitations this model achieves an adjusted R^2= 0.73.

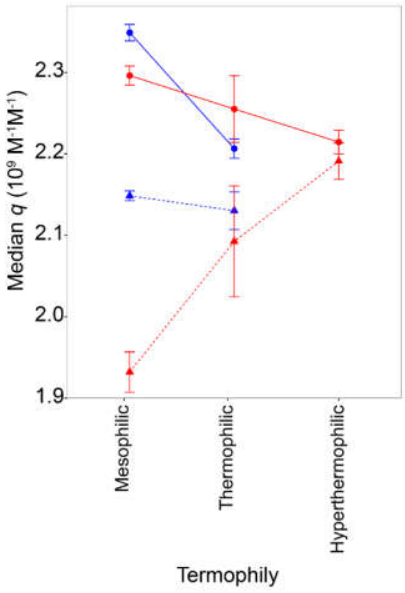

Supplementary Figure 3.16 – Median proteome oxidability q *displays different trends as function of thermophily in AI (circles) vs AT (triangles) Archaea (red) and Bacteria (blue). The number of psychrophilic Archaea and hyperthermophilic Bacteria is insufficient for a statistically robust analysis and was disregarded.*

3.8.6 Modeling protein oxidability and AAC as function of possible sources of compositional bias using first order multilinear regression models

We have modeled median proteome AAC, *q*, and *r* as function of the following control variables: aerotolerance (Aerotol), thermophily (Therm), coding sequence G+C content (%GC), logarithm of the median protein size (PSize), maximum specific growth rate (Growth), total number of proteins in the proteome (nProts), and total number of amino acids in the proteome (nAA).

The estimated adjusted coefficients of determination for each model variant in Bacteria were compared to that of a model considering all [m_{comp}(Full)] (Supplementary Figure 3.18). The number of organisms in Archaea and Eukarya with known growth rates does not permit a statistically robust analysis (25 Archaea and 9 Eukarya with known growth rates, Supplementary Table 3.1). Growth rate was disregarded in these clades. Further, because in Eukarya all but 2 organisms are mesophiles we also disregarded thermophily in this clade.

3. Proteome composition and aerotolerance

The comparison of adjusted R^2s between models shows that %GC and thermophily are the variables that explain most of the observed variability, in Bacteria (and to a certain extent in Archaea and Eukarya), followed by aerotolerance and protein size (Supplementary Figure 3.18 and 19). Disregarding control variables cell growth rate, number of proteins in the proteome, and number of amino acids per proteome leads to models with adjusted R^2s that are similar to those of m_{comp}(Full) (Supplementary Figure 3.18 and 19), indicating that these variables explain a very small fraction of the variance in AAC. Therefore, in subsequent analyses we neglected these three control variables. Accordingly, hereafter and in the main text we consider m_{comp}(All) as the model that combines control variables aerotolerance, thermophily, GC content, and logarithm of protein size (Supplementary Table 3.8 and Supplementary Table 3.9).

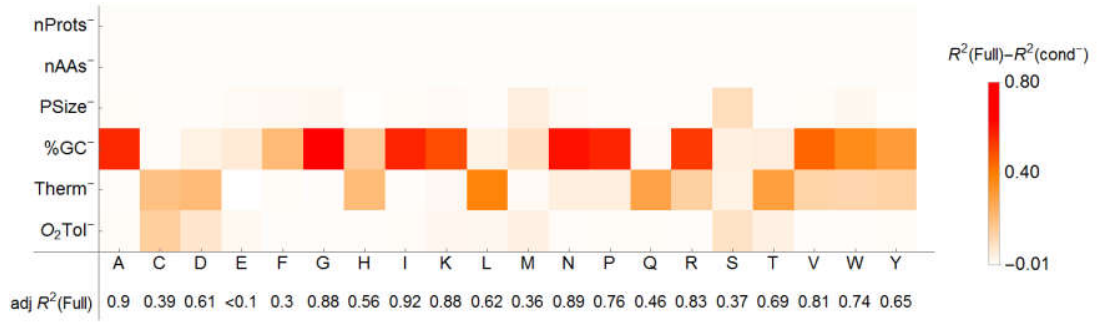

Supplementary Figure 3.17 - Relative change in adjusted coefficients of determination (adj R^2) estimated for Archaea with a multilinear regression model disregarding one of the control variables (Aerotol⁻, Therm⁻, %GC⁻, PSize⁻, nAAs⁻ or nProts⁻) vs a model considering all of these [m_{comp}(Full)]. Differences of adj R^2 for each model variant vs adj R^2 [m_{comp}(All)], presented at the bottom, are indicated according to the scale on the right.

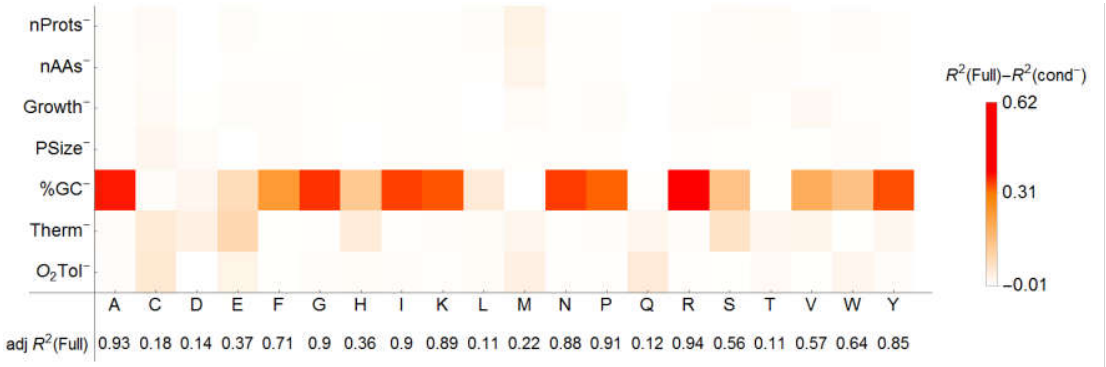

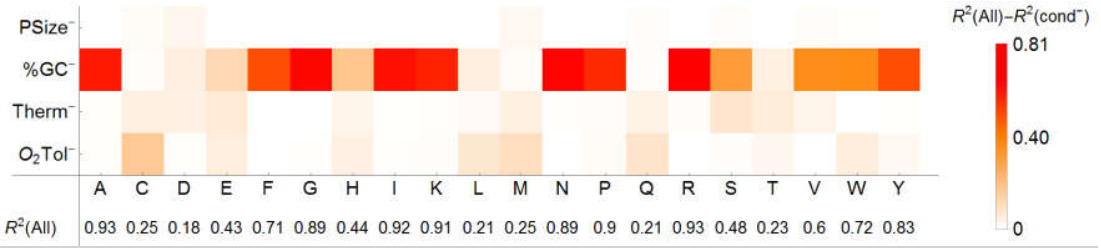

Supplementary Figure 3.18 – Relative change in adjusted coefficients of determination (adj R^2) estimated for Bacteria with a multilinear regression model disregarding one of the control variables (Aerotol$^-$, Therm$^-$, %GC$^-$, PSize$^-$, Growth rate$^-$, nAAs$^-$ or nProts$^-$) vs a model considering all of these [m_{comp}(Full)]. Differences of adj R^2 for each model variant vs adj R^2 [m_{comp}(All)], presented at the bottom, are indicated according to the scale on the right.

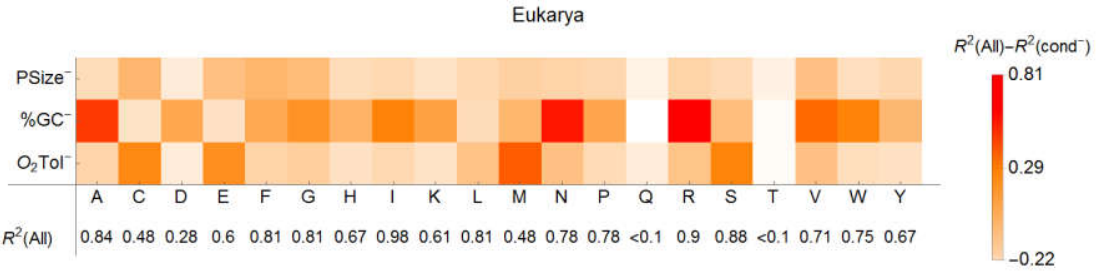

Supplementary Figure 3.19 – Aerotol is one of the main variables explaining AAC in eukaryotes. Multilinear regression models were used to fit AAC as function of Aerotol, %GC and protein size in this domain, and differences between the full model [m_{comp}(All)] and those where one of the control variables was disregarded [m_{comp}(cond$^-$)] were then computed.

The significance of the differences between coefficients of determination for the various model variants [m_{comp}(cond$^-$)] *vs*. m_{comp}(All) or m_{comp}(Full) were performed as follows. For each domain we randomly selected a set of 20×*m* organisms 1000 times, where *m* is the number of control variables in the multilinear regression models [=20×4 and 20×7 for m_{comp}(All) and m_{comp}(Full), respectively]. For each amino acid, the coefficients of determination for each model variant under all bootstrapped datasets were then compared with those for the m_{comp}(All) or m_{comp}(Full) models (Supplementary Figure 3.20). The comparison between model variants and m_{comp}(Full) is only possible in Bacteria because only this domain has sufficient organisms to allow statistically robust comparisons for the 7 control variables.

3. Proteome composition and aerotolerance

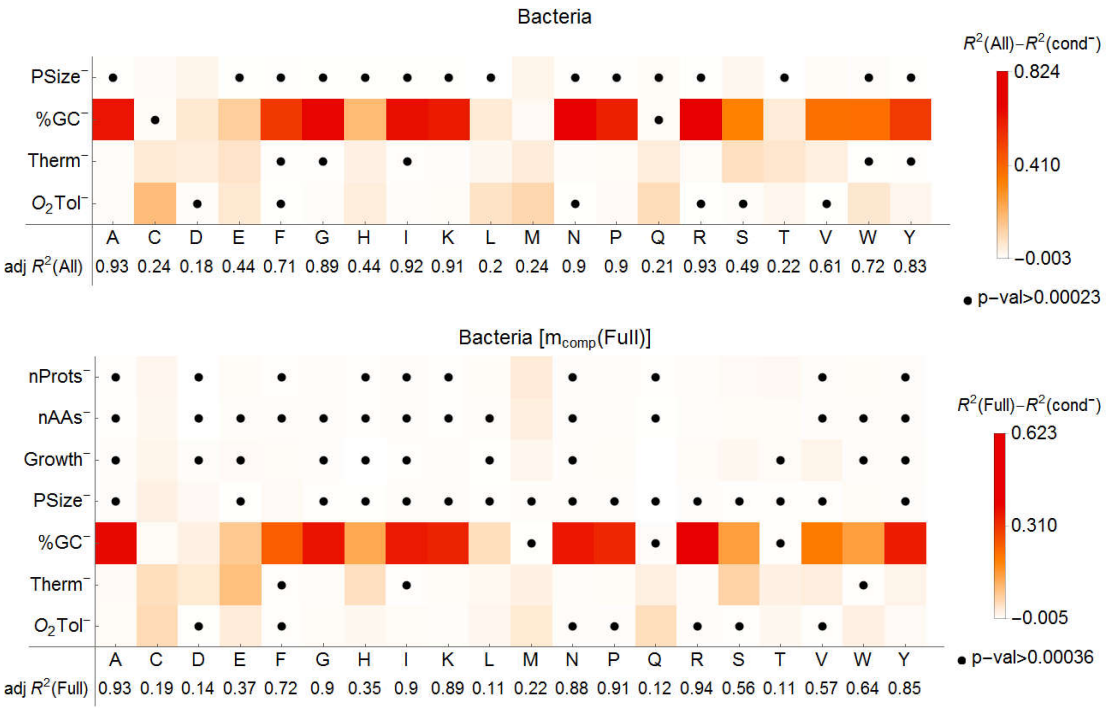

Supplementary Figure 3.20 – Comparison of bootstrapped coefficients of determination in Bacteria using m_{comp}(All) or m_{comp}(Full) as indicated in each row. Means of adjusted R^2 for m_{comp}(cond⁻) vs m_{comp}(All / Full) were tested using Mann-Whitney's test (p-values indicated on the right). Points indicate statistically equal medians under the indicated significance. See text above for details.

Using model m_{comp}(All), we then analyzed how amino acid frequency changes as function of Aerotol in Archaea (Supplementary Table 3.8), Bacteria (Supplementary Table 3.9) and Eukarya (Supplementary Table 3.10). Overall, there is a general trend towards AI organisms displaying higher frequencies of highly •OH-reactive amino acids than AT organisms.

Our observations also indicate that aerotolerance (Supplementary Table 3.11) is one of the main explanatory variables for the observed *q* and *r*.

Supplementary Table 3.8 – Scaled fitting parameters of $m_{comp}(All)$ in Archaea controlling for aerotolerance, thermophily, %GC and protein size. Coefficients and standard errors (SE) were rescaled by dividing by the mean AA frequency (AA freq) and multiplying by the mean parameter value (Aerotolerance = 1.3, Thermophily = 3.1, %GC = 47.4, Log_{10} (median protein size) = 2.4). Exception for ε which was scaled by dividing by AA freq. Highlighted values are statistically significant (<6.2×10^{-4} for a Bonferroni correction considering 20×4 tested hypotheses and an individual significance threshold of 0.05, t-statistic).

AA	Adj R^2	AA freq	ε			Aerotolerance			Thermophily			%GC			PSize		
			Value	SE	p	Value	SE	p	Value	SE	p	Value	SE	p	Value	SE	p
G	0.88	0.072	-1.2	0.49	1.45E-02	-0.011	0.013	4.1E-01	-0.0014	0.016	9.3E-01	**0.46**	**0.021**	**3.3E-35**	**1.8**	**0.48**	**4.0E-04**
N	0.89	0.035	-2.0	1.6	2.10E-01	0.062	0.042	1.4E-01	**-0.32**	**0.051**	**2.4E-08**	**-1.5**	**0.065**	**2.2E-36**	4.7	1.5	2.6E-03
A	0.90	0.073	2.6	1.1	1.89E-02	0.058	0.029	4.6E-02	-0.051	0.035	1.5E-01	**1.0**	**0.045**	**2.1E-36**	-2.6	1.0	1.5E-02
D	0.61	0.056	-0.77	1.9	6.93E-01	**0.22**	**0.052**	**4.5E-05**	**-0.46**	**0.063**	**3.4E-10**	0.24	0.081	4.0E-03	1.8	1.9	3.6E-01
E	0.08	0.079	2.9	1.5	5.40E-02	-0.061	0.040	1.3E-01	0.013	0.048	7.9E-01	0.16	0.062	1.0E-02	-2.0	1.4	1.7E-01
S	0.37	0.056	-4.7	1.5	2.51E-03	**0.15**	**0.041**	**4.9E-04**	-0.12	0.049	1.8E-02	-0.17	0.063	8.4E-03	**5.9**	**1.5**	**1.6E-04**
K	0.88	0.062	7.6	1.9	1.54E-04	**-0.21**	**0.051**	**1.5E-04**	0.19	0.062	2.9E-03	**-1.6**	**0.080**	**4.4E-32**	-5.0	1.9	9.2E-03
P	0.76	0.041	0.28	0.85	7.41E-01	-0.036	0.023	1.2E-01	**0.12**	**0.028**	**5.6E-05**	**0.54**	**0.036**	**8.2E-25**	0.093	0.83	9.1E-01
T	0.69	0.048	0.46	1.3	7.23E-01	0.12	0.035	7.5E-04	**-0.41**	**0.042**	**4.4E-15**	**0.21**	**0.054**	**1.7E-04**	0.62	1.3	6.3E-01
Q	0.46	0.019	3.9	2.4	1.13E-01	0.091	0.066	1.7E-01	**-0.57**	**0.080**	**3.8E-10**	0.15	0.102	1.4E-01	-2.6	2.4	2.8E-01
V	0.81	0.079	1.7	0.83	3.84E-02	0.010	0.022	6.5E-01	**0.22**	**0.027**	**6.6E-12**	**0.52**	**0.035**	**2.7E-24**	-1.5	0.81	6.9E-02
L	0.62	0.094	1.3	0.73	8.76E-02	-0.042	0.020	3.5E-02	**0.24**	**0.024**	**2.4E-15**	0.092	0.030	3.3E-03	-0.54	0.71	4.5E-01
I	0.92	0.075	-0.89	1.1	4.06E-01	-0.069	0.029	1.8E-02	0.057	0.035	1.1E-01	**-1.1**	**0.045**	**3.7E-39**	3.1	1.0	4.6E-03
R	0.83	0.055	-1.9	1.4	1.58E-01	0.0062	0.037	8.7E-01	**0.40**	**0.045**	**1.7E-13**	**0.99**	**0.057**	**4.1E-28**	1.6	1.3	2.5E-01
H	0.56	0.015	0.24	1.4	8.63E-01	-0.036	0.038	3.5E-01	**-0.31**	**0.046**	**2.3E-09**	**0.34**	**0.059**	**1.2E-07**	0.76	1.4	5.8E-01
F	0.30	0.036	3.8	1.5	1.48E-02	-0.038	0.041	3.7E-01	-0.066	0.050	1.9E-01	**-0.35**	**0.064**	**5.2E-07**	-2.4	1.5	1.2E-01
M	0.36	0.023	-3.3	1.8	6.95E-02	-0.12	0.048	1.4E-02	-0.093	0.059	1.2E-01	**-0.28**	**0.075**	**3.6E-04**	4.8	1.8	7.8E-03
W	0.74	0.0085	3.9	1.7	2.31E-02	0.046	0.045	3.1E-01	**0.37**	**0.054**	**2.3E-09**	**0.80**	**0.070**	**2.9E-18**	-4.1	1.6	1.4E-02
Y	0.65	0.036	1.1	1.5	4.60E-01	0.058	0.039	1.4E-01	**0.29**	**0.048**	**3.6E-08**	**-0.56**	**0.061**	**4.8E-14**	0.13	1.4	9.3E-01
C	0.39	0.0070	7.2	4.3	9.89E-02	**-0.57**	**0.12**	**4.6E-06**	**-0.78**	**0.14**	**4.1E-07**	-0.19	0.18	2.9E-01	-4.6	4.2	2.7E-01

Supplementary Table 3.9 – Scaled fitting parameters of $m_{comp}(All)$ in Bacteria controlling for aerotolerance, thermophily, %GC and protein size. Coefficients and standard errors (SE) were rescaled by dividing by the mean AA frequency (AA freq) and multiplying by the mean parameter value (Aerotolerance = 1.7, Thermophily = 2.1, %GC = 50.1, Log_{10} (median protein size) = 2.4). Exception for ε which was scaled by dividing by AA freq. Highlighted values are statistically significant (<6.2×10^{-4} for a Bonferroni correction considering 20×4 tested hypotheses and an individual significance threshold of 0.05, t-statistic).

AA	Adj R^2	AA freq	ε			Aerotolerance			Thermophily			%GC			Protein Size		
			Value	SE	p	Value	SE	p	Value	SE	p	Value	SE	p	Value	SE	p
G	0.89	0.071	0.16	0.10	1.2E-01	**-0.051**	**0.0065**	**2.3E-14**	**0.036**	**0.010**	**3.2E-04**	**0.60**	**0.007**	**<1E-250**	0.25	0.10	1.6E-02
N	0.89	0.037	1.9	0.24	4.3E-15	0.029	0.015	5.2E-02	**-0.19**	**0.023**	**1.2E-15**	**-1.4**	**0.017**	**<1E-250**	0.70	0.24	3.9E-03
A	0.93	0.089	-0.44	0.15	5.0E-03	**0.092**	**0.0099**	**5.4E-20**	**-0.12**	**0.015**	**5.2E-14**	**1.1**	**0.011**	**<1E-250**	0.37	0.16	1.9E-02
D	0.18	0.054	-0.10	0.17	5.6E-01	-0.033	0.011	3.2E-03	**-0.13**	**0.017**	**2.0E-14**	**0.11**	**0.012**	**1.3E-17**	**1.2**	**0.18**	**9.4E-11**
E	0.43	0.064	1.3	0.21	2.7E-10	**-0.14**	**0.013**	**1.4E-24**	**0.24**	**0.021**	**9.8E-30**	**-0.24**	**0.015**	**1.4E-50**	-0.21	0.21	3.3E-01
S	0.48	0.057	0.65	0.16	8.7E-05	**0.041**	**0.010**	**9.0E-05**	**-0.22**	**0.016**	**1.6E-38**	**-0.31**	**0.012**	**5.4E-119**	**0.84**	**0.17**	**5.6E-07**
K	0.91	0.054	3.0	0.27	5.4E-28	**-0.18**	**0.017**	**1.9E-25**	**0.18**	**0.026**	**2.7E-12**	**-1.7**	**0.019**	**<1E-250**	-0.34	0.27	2.1E-01
P	0.90	0.041	-0.49	0.14	5.8E-04	**0.11**	**0.0090**	**7.9E-33**	**0.14**	**0.014**	**6.6E-24**	**0.83**	**0.010**	**<1E-250**	0.40	0.14	5.4E-03
T	0.23	0.051	0.85	0.16	3.5E-07	**0.062**	**0.011**	**4.6E-09**	**-0.16**	**0.016**	**3.3E-21**	**0.10**	**0.012**	**4.5E-17**	0.15	0.17	3.8E-01
Q	0.21	0.034	2.4	0.38	2.8E-10	**0.27**	**0.024**	**1.3E-27**	**-0.29**	**0.037**	**9.3E-15**	-0.09	0.027	8.6E-04	-1.3	0.39	6.6E-04
V	0.60	0.070	-0.31	0.15	4.2E-02	-0.0074	0.0098	4.5E-01	**0.15**	**0.015**	**3.1E-23**	**0.36**	**0.011**	**3.0E-160**	**0.81**	**0.16**	**2.5E-07**
L	0.21	0.099	0.84	0.13	4.2E-11	**0.085**	**0.0081**	**7.7E-25**	**0.062**	**0.012**	**6.1E-07**	**0.08**	**0.009**	**3.1E-18**	-0.07	0.13	5.8E-01
I	0.92	0.064	1.8	0.16	6.5E-28	**-0.085**	**0.010**	**3.0E-16**	**0.083**	**0.016**	**1.3E-07**	**-1.1**	**0.011**	**<1E-250**	0.29	0.16	7.2E-02
R	0.93	0.054	-0.18	0.16	2.4E-01	0.011	0.0099	2.5E-01	**0.17**	**0.015**	**1.5E-27**	**1.2**	**0.011**	**<1E-250**	-0.15	0.16	3.4E-01
H	0.44	0.019	0.95	0.25	1.2E-04	**0.15**	**0.016**	**3.0E-21**	**-0.20**	**0.024**	**6.5E-16**	**0.34**	**0.017**	**3.1E-71**	-0.24	0.25	3.4E-01
F	0.71	0.039	1.3	0.18	1.7E-12	-0.0033	0.012	7.8E-01	0.027	0.018	1.4E-01	**-0.58**	**0.013**	**4.4E-239**	0.25	0.19	1.9E-01
M	0.25	0.024	3.1	0.26	5.4E-30	**-0.21**	**0.017**	**4.7E-34**	**-0.22**	**0.025**	**3.3E-17**	**-0.082**	**0.018**	**9.2E-06**	**-1.6**	**0.26**	**6.1E-09**
W	0.72	0.010	-0.88	0.29	2.6E-03	**0.29**	**0.019**	**6.2E-48**	-0.028	0.029	3.3E-01	**0.81**	**0.021**	**8.1E-202**	0.81	0.30	6.4E-03
Y	0.83	0.030	2.1	0.21	1.1E-23	**-0.16**	**0.013**	**2.3E-31**	**0.087**	**0.020**	**1.6E-05**	-0.85	0.015	<1E-250	-0.21	0.21	3.3E-01
C	0.25	0.0087	4.7	0.58	3.0E-15	**-0.61**	**0.037**	**6.7E-53**	**-0.51**	**0.057**	**2.1E-18**	**0.16**	**0.041**	**1.5E-04**	**-2.7**	**0.59**	**5.1E-06**

Supplementary Table 3.10 – Scaled fitting parameters of m_{comp}(All) in Eukarya controlling for aerotolerance, %GC and protein size. Coefficients and standard errors (SE) were rescaled by dividing by the mean AA frequency (AA freq) and multiplying by the mean parameter value (Aerotolerance = 1.8, %GC = 42.2, Log_{10} (median protein size) = 2.6). Exception for ε which was scaled by dividing by AA freq. Highlighted values are statistically significant (<8.3×10^{-4} for a Bonferroni correction considering 20×3 tested hypotheses and an individual significance threshold of 0.05, t-statistic).

AA	Adj R^2	AA freq	ε			Aerotolerance			%GC			Protein Size		
			Value	SE	p	Value	SE	p	Value	SE	p	Value	SE	p
G	0.73	0.053	0.28	0.58	6.3E-01	0.085	0.080	2.9E-01	**0.67**	**0.063**	**1.9E-14**	-0.041	0.63	9.5E-01
N	0.78	0.052	-0.18	1.0	8.6E-01	-0.34	0.14	1.6E-02	**-1.3**	**0.11**	**1.0E-16**	2.9	1.1	1.2E-02
A	0.86	0.061	-1.6	0.87	6.3E-02	0.10	0.12	3.8E-01	**1.5**	**0.093**	**6.8E-21**	1.1	0.94	2.6E-01
D	<0.1	0.055	1.2	0.44	7.9E-03	0.10	0.061	1.1E-01	-0.071	0.048	1.4E-01	-0.26	0.48	5.9E-01
E	0.22	0.064	1.8	0.45	2.2E-04	-0.10	0.062	1.0E-01	-0.078	0.048	1.2E-01	-0.61	0.49	2.2E-01
S	0.08	0.080	0.067	0.50	8.9E-01	0.030	0.069	6.6E-01	0.036	0.054	5.1E-01	0.87	0.55	1.2E-01
K	0.83	0.065	2.3	0.67	1.1E-03	-0.16	0.092	8.5E-02	**-1.0**	**0.072**	**4.7E-19**	-0.14	0.73	8.5E-01
P	0.70	0.042	-0.62	0.70	3.8E-01	0.17	0.096	8.1E-02	**0.68**	**0.075**	**5.9E-12**	0.77	0.76	3.2E-01
T	0.32	0.054	0.90	0.48	6.8E-02	0.20	0.066	4.2E-03	0.15	0.052	6.5E-03	-0.24	0.52	6.4E-01
Q	0.10	0.038	0.28	1.5	8.6E-01	0.41	0.21	5.8E-02	-0.35	0.17	4.1E-02	0.66	1.7	7.0E-01
V	0.71	0.059	1.9	0.45	1.2E-04	0.17	0.062	8.2E-03	**0.51**	**0.049**	**4.6E-14**	-1.6	0.49	2.4E-03
L	0.10	0.092	1.2	0.27	3.8E-05	0.098	0.038	1.2E-02	0.027	0.029	3.7E-01	-0.37	0.30	2.2E-01
I	0.88	0.061	2.5	0.58	8.7E-05	**-0.31**	**0.080**	**2.8E-04**	**-1.0**	**0.063**	**1.7E-21**	-0.16	0.63	8.1E-01
R	0.79	0.050	0.23	0.72	7.5E-01	-0.037	0.099	7.1E-01	**1.0**	**0.078**	**5.2E-18**	-0.23	0.79	7.7E-01
H	0.62	0.021	-0.41	0.52	4.3E-01	-0.067	0.071	3.5E-01	**0.46**	**0.056**	**9.4E-11**	1.0	0.56	7.6E-02
F	0.75	0.041	2.5	0.41	1.4E-07	0.026	0.056	6.5E-01	**-0.47**	**0.044**	**2.0E-14**	-1.1	0.44	2.0E-02
M	0.39	0.021	2.9	0.56	5.6E-06	-0.15	0.077	5.1E-02	**0.25**	**0.061**	**1.4E-04**	-2.0	0.61	2.3E-03
W	0.61	0.0090	-0.16	0.84	8.5E-01	0.30	0.11	1.3E-02	**0.62**	**0.090**	**9.1E-09**	0.24	0.91	7.9E-01
Y	0.71	0.032	2.3	0.69	1.9E-03	-0.19	0.094	4.9E-02	**-0.70**	**0.074**	**1.4E-12**	-0.38	0.75	6.1E-01
C	0.23	0.014	2.4	1.3	6.3E-02	-0.50	0.17	6.0E-03	0.32	0.14	2.4E-02	-1.2	1.4	3.7E-01

Supplementary Table 3.11 – Scaled fitting parameters of models $m_{q/r}$(All) in Archaea (A, top), Bacteria (B, middle) and Eukarya (E, bottom). Fitting coefficients and standard errors (SE) were scaled by dividing by the mean q *or* r *and multiplying by each mean variable (indicated on the left).*

	Variable		*q*				*r*			
		Mean	**Value**	**SE**	**p**	**Adj R^2**	**Value**	**SE**	**p**	**Adj R^2**
Archaea	**O_2 tol**	1.3	-0.078	0.015	1.8E-06	0.54	-0.041	0.013	2.8E-03	0.41
	Therm	3.1	0.0080	0.018	6.7E-01		0.067	0.016	7.9E-05	
	%GC	47.4	-0.14	0.024	1.3E-07		-0.022	0.021	3.0E-01	
	PSize	2.4	-0.42	0.55	4.5E-01		-1.4	0.48	4.7E-03	
Bacteria	**O_2 tol**	1.7	-0.12	0.0073	5.5E-52	0.40	-0.060	0.0053	7.7E-29	0.44
	Therm	2.1	-0.061	0.011	5.1E-08		-0.023	0.0080	4.4E-03	
	%GC	50.1	-0.094	0.0081	4.3E-29		0.0035	0.0058	5.4E-01	
	PSize	2.4	-0.71	0.12	1.5E-09		-2.0	0.084	2.0E-96	
Eukarya	**O_2 tol**	1.8	-0.16	0.046	1.1E-03	0.40	-0.17	0.042	2.2E-04	0.61
	%GC	42.2	0.0032	0.036	9.3E-01		0.058	0.033	8.3E-02	
	PSize	2.6	-0.69	0.37	6.6E-02		-1.5	0.33	4.0E-05	

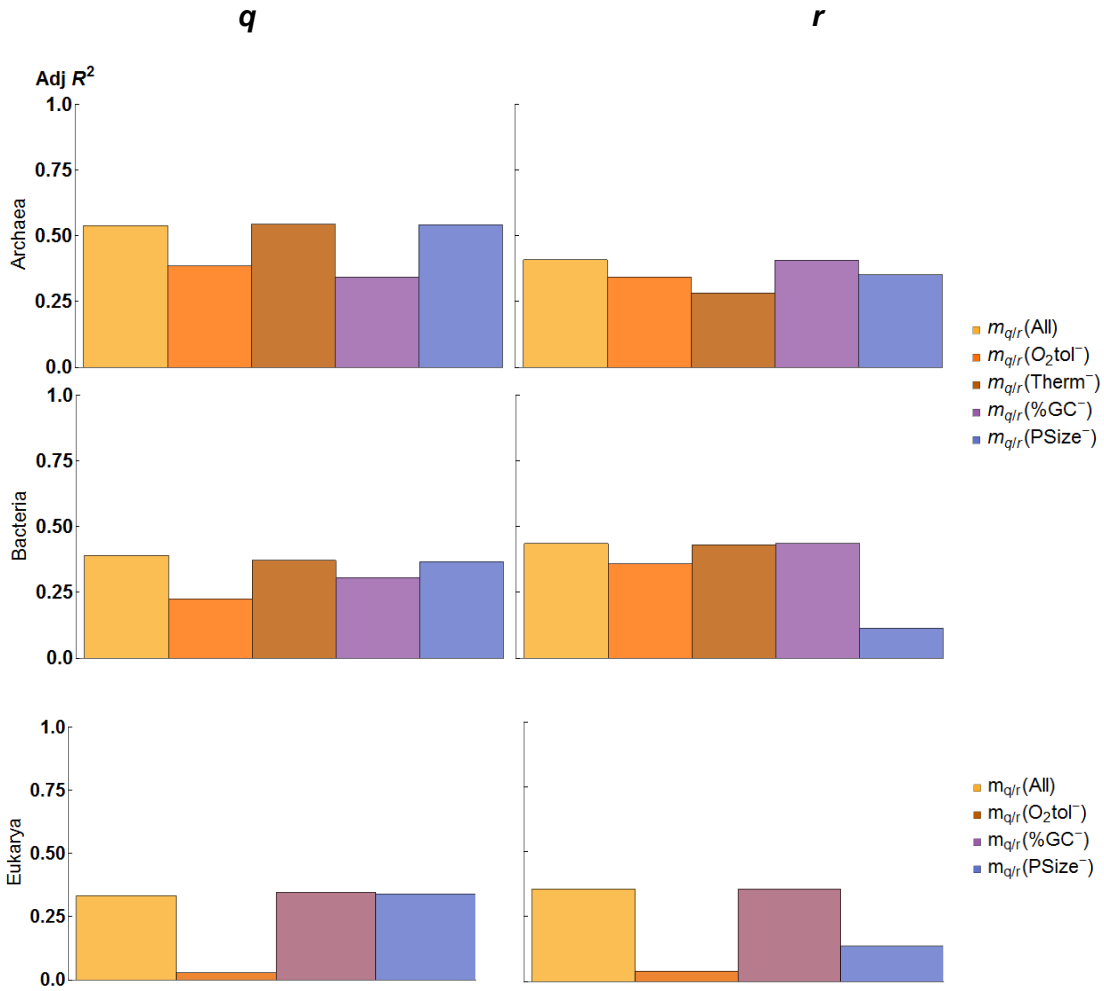

Supplementary Figure 3.21 – Coefficients of determination of models fitting median protein oxidability q *(left) or* r *(right) as function of aerotolerance, thermophily, %GC and protein size or ignoring one of the variables, in Archaea (top), Bacteria (middle) or Eukarya (bottom).*

3.9 References

1. Hinkle, P. C., M. A. Kumar, A. Resetar and D. L. Harris (1991). "Mechanistic stoichiometry of mitochondrial oxidative phosphorylation." Biochemistry **30**(14): 3576-3582.

2. Berg, J. M., J. L. Tymoczko, L. Stryer and L. Stryer (2002). Biochemistry. New York, W.H. Freeman.

3. Akashi, H. and T. Gojobori (2002). "Metabolic efficiency and amino acid composition in the proteomes of Escherichia coli and Bacillus subtilis." Proceedings Of The National Academy Of Sciences Of The United States Of America **99**(6): 3695-3700.

4. Akashi, H. (2003). "Translational selection and yeast proteome evolution." Genetics **164**(4): 1291-1303.

5. Heizer, E. M., D. W. Raiford, M. L. Raymer, T. E. Doom, R. V. Miller and D. E. Krane (2006). "Amino acid cost and codon-usage biases in 6 prokaryotic genomes: A whole-genome analysis." Molecular Biology and Evolution **23**(9): 1670-1680.

6. Vilaprinyo, E., R. Alves and A. Sorribas (2010). "Minimization of Biosynthetic Costs in Adaptive Gene Expression Responses of Yeast to Environmental Changes." Plos Computational Biology **6**(2).

7. Smith, W. L. and R. C. Murphy (2008). "Oxidized lipids formed non-enzymatically by reactive oxygen species." Journal of Biological Chemistry **283**: 15513-15514.

8. Cooke, M. S., M. D. Evans, M. Dizdaroglu and J. Lunec (2003). "Oxidative DNA damage: mechanisms, mutation, and disease." The FASEB journal : official publication of the Federation of American Societies for Experimental Biology **17**: 1195-1214.

9. Cabiscol, E., J. Tamarit and J. Ros (2000). "Oxidative stress in bacteria and protein damage by reactive oxygen species." International Microbiology **3**: 3-8.

10. Höhn, A., J. König and T. Grune (2013). "Protein oxidation in aging and the removal of oxidized proteins." Journal of Proteomics **92**: 132-159.

11. Garrison, W. M. (1987). "Reaction-mechanisms in the radiolysis of peptides, polypeptides, and proteins." Chemical Reviews **87**(2): 381-398.

12. Ross, A. B., W. G. Mallard, W. P. Helman, G. V. Buxton, R. E. Huie and P. Neta (1998). NDRL-NIST solution kinetics database - ver. 3, Notre Dame Radiation Laboratory, Notre Dame, IN and NIST Standard Reference Data, Gaithesburg, MD.

13. Yang, Y. F. and W. W. Wells (1991). "Identification and characterization of the functional amino acids at the active center of pig liver thioltransferase by site-directed mutagenesis." J Biol Chem **266**(19): 12759-12765.

14. Creighton, T. E. (1993). Proteins: structures and molecular properties, Macmillan.

15. Kortemme, T. and T. E. Creighton (1995). "Ionisation of cysteine residues at the termini of model alpha-helical peptides. Relevance to unusual thiol pKa values in proteins of the thioredoxin family." J Mol Biol **253**(5): 799-812.

16. Niimura, Y., L. B. Poole and V. Massey (1995). "Amphibacillus xylanus NADH oxidase and Salmonella typhimurium alkyl-hydroperoxide reductase flavoprotein components show extremely high scavenging activity for both alkyl hydroperoxide and hydrogen peroxide in the presence of S. typhimuri." J Biol Chem **270**: 25645-25650.

17. Obinger, C., M. Maj, P. Nicholls and P. Loewen (1997). "Activity, peroxide compound formation, and heme d synthesis in Escherichia coli HPII catalase." Archives of biochemistry and biophysics **342**: 58-67.

18. Forman, H. J. and I. Fridovich (1973). "Superoxide dismutase: a comparison of rate constants." Archives Of Biochemistry And Biophysics **158**(1): 396-400.

19. Hillar, A., B. Peters, R. Pauls, A. Loboda, H. Zhang, a. G. Mauk and P. C. Loewen (2000). "Modulation of the activities of catalase-peroxidase HPI of Escherichia coli by site-directed mutagenesis." Biochemistry **39**: 5868-5875.

20. Von Sonntag, C. (1987). The chemical basis of radiation biology, Taylor & Francis.

21. Davies, K. J. A. (2000). "Oxidative stress, antioxidant defenses, and damage removal, repair, and replacement systems." Iubmb Life **50**(4-5): 279-289.

22. Davies, K. J. (1987). "Protein damage and degradation by oxygen radicals. I. general aspects." Journal Of Biological Chemistry **262**(20): 9895-9901.

23. Davies, K. J. and M. E. Delsignore (1987). "Protein damage and degradation by oxygen radicals. III. Modification of secondary and tertiary structure." Journal Of Biological Chemistry **262**(20): 9908-9913.

24. Moller, I. M., A. Rogowska-Wrzesinska and R. S. P. Rao (2011). "Protein carbonylation and metal-catalyzed protein oxidation in a cellular perspective." Journal of Proteomics **74**(11): 2228-2242.

25. Vieira-Silva, S. and E. P. C. Rocha (2008). "An assessment of the impacts of molecular oxygen on the evolution of proteomes." Molecular Biology and Evolution **25**(9): 1931-1942.

26. Lobry, J. R. (1997). "Influence of genomic G+C content on average amino-acid composition of proteins from 59 bacterial species." Gene **205**(1-2): 309-316.

27. Kreil, D. P. and C. A. Ouzounis (2001). "Identification of thermophilic species by the amino acid compositions deduced from their genomes." Nucleic Acids Res **29**(7): 1608-1615.

28. Tekaia, F., E. Yeramian and B. Dujon (2002). "Amino acid composition of genomes, lifestyles of organisms, and evolutionary trends: A global picture with correspondence analysis." Gene **297**: 51-60.

29. Zeldovich, K. B., I. N. Berezovsky and E. I. Shakhnovich (2007). "Protein and DNA sequence determinants of thermophilic adaptation." PLoS Computational Biology **3**: 0062-0072.

30. Brbic, M., T. Warnecke, a. Kri ko and F. Supek (2015). "Global shifts in genome and proteome composition are very tightly coupled." Genome Biology and Evolution **7**: 1519-1532.

31. Tekaia, F. and E. Yeramian (2006). "Evolution of proteomes: fundamental signatures and global trends in amino acid compositions." BMC genomics **7**: 307.

32. Baldwin, E. P. and B. W. Matthews (1994). "Core-packing constraints, hydrophobicity and protein design." Current Opinion in Biotechnology **5**: 396-402.

33. Pace, C. N., B. A. Shirley, M. Macnutt and K. Gajiwala (1996). "Forces contributing to the conformational stability of proteins." Faseb: 75-83.

34. Jaenicke, R. and G. Böhm (1998). "The stability of proteins in extreme environments." Current Opinion in Structural Biology **8**: 738-748.

35. Smith, D. R. and M. R. Chapman (2010). "Economical evolution: Microbes reduce the synthetic cost of extracellular proteins." mBio **1**: 28-32.

36. White, S., F. E. Tuttle, D. Blankenhorn, D. C. Dosch and J. L. Slonczewski (1992). "pH dependence and gene structure of inaA in Escherichia coli." J Bacteriol **174**(5): 1537-1543.

37. Sandelin, E. (2004). "On hydrophobicity and conformational specificity in proteins." Biophysical journal **86**: 23-30.

38. Bastolla, U. and L. Demetrius (2005). "Stability constraints and protein evolution: the role of chain length, composition and disulfide bonds." Protein Engineering Design and Selection **18**(9): 405-415.

39. Carugo, O. (2008). "Amino acid composition and protein dimension." Protein Science **17**: 2187-2191.

40. Shirota, M., T. Ishida and K. Kinoshita (2008). "Effects of surface-to-volume ratio of proteins on hydrophilic residues: decrease in occurrence and increase in buried fraction." Protein science : a publication of the Protein Society **17**: 1596-1602.

41. Tatusova, T., S. Ciufo, B. Fedorov, K. O'Neill and I. Tolstoy (2014). "RefSeq microbial genomes database: new representation and annotation strategy." Nucleic Acids Res **42**(Database issue): D553-559.

42. Benson, D. a., M. Cavanaugh, K. Clark, I. Karsch-Mizrachi, D. J. Lipman, J. Ostell and E. W. Sayers (2013). "GenBank." Nucleic Acids Research **41**: 36-42.

43. Milo, R. (2009). "What governs the reaction center excitation wavelength of photosystems I and II?" Photosynthesis Research **101**(1): 59-67.

44. Couturier, E. and E. P. C. Rocha (2006). "Replication-associated gene dosage effects shape the genomes of fast-growing bacteria but only for transcription and translation genes." Molecular Microbiology **59**: 1506-1518.

45. Cruz, J., Y. Liu, Y. Liang, Y. Zhou, M. Wilson, J. J. Dennis, P. Stothard, G. Van Domselaar and D. S. Wishart (2011). "BacMap: an up-to-date electronic atlas of annotated bacterial genomes." Nucleic acids research: gkr1105.

46. Schomburg, I., A. Chang, S. Placzek, C. Sohngen, M. Rother, M. Lang, C. Munaretto, S. Ulas, M. Stelzer, A. Grote, M. Scheer and D. Schomburg (2013). "BRENDA in 2013: integrated reactions, kinetic data, enzyme function data, improved disease classification: new options and contents in BRENDA." Nucleic Acids Res **41**(Database issue): D764-772.

47. Petersen, B., T. N. Petersen, P. Andersen, M. Nielsen and C. Lundegaard (2009). "A generic method for assignment of reliability scores applied to solvent accessibility predictions." BMC structural biology **9**: 51.

48. Mucchielli-Giorgi, M. H., S. Hazout and P. Tuffery (1999). "PredAcc: prediction of solvent accessibility." Bioinformatics **15**(2): 176-177.

49. Pollastri, G., A. J. M. Martin, C. Mooney and A. Vullo (2007). "Accurate prediction of protein secondary structure and solvent accessibility by consensus combiners of sequence and structure information." BMC bioinformatics **8**: 201.

50. Gifford, L. K., L. G. Carter, M. J. Gabanyi, H. M. Berman and P. D. Adams (2012). "The Protein Structure Initiative Structural Biology Knowledgebase Technology Portal: a structural biology web resource." J Struct Funct Genomics **13**(2): 57-62.

51. Berman, H. M., J. Westbrook, Z. Feng, G. Gilliland, T. N. Bhat, H. Weissig, I. N. Shindyalov and P. E. Bourne (2000). "The Protein Data Bank." Nucleic Acids Res **28**(1): 235-242.

52. Neidhardt, F. C., J. L. Ingraham and M. Schaechter (1990). Biosynthesis and fueling. Physiology of the bacterial cell. Sunderland, Mass., Sinauer Associates**:** 133-173.

53. Craig, C. L. and R. S. Weber (1998). "Selection costs of amino acid substitutions in ColE1 and ColIa gene clusters harbored by Escherichia coli." Molecular biology and evolution **15**: 774-776.

54. Wagner, A. (2005). "Energy constraints on the evolution of gene expression." Mol Biol Evol **22**(6): 1365-1374.

55. Raiford, D. W., E. M. Heizer, Jr., R. V. Miller, H. Akashi, M. L. Raymer and D. E. Krane (2008). "Do amino acid biosynthetic costs constrain protein evolution in Saccharomyces cerevisiae?" J Mol Evol **67**(6): 621-630.

56. Heizer, E. M., Jr., M. L. Raymer and D. E. Krane (2011). "Amino acid biosynthetic cost and protein conservation." J Mol Evol **72**(5-6): 466-473.

57. Keseler, I. M., A. Mackie, M. Peralta-Gil, A. Santos-Zavaleta, S. Gama-Castro, C. Bonavides-Martínez, C. Fulcher, A. M. Huerta, A. Kothari, M. Krummenacker, M. Latendresse, L. Muñiz-Rascado, Q. Ong, S. Paley, I. Schröder, A. G. Shearer, P. Subhraveti, M. Travers, D. Weerasinghe, V. Weiss, J. Collado-Vides, R. P. Gunsalus, I. Paulsen and P. D. Karp (2013). "EcoCyc: Fusing model organism databases with systems biology." Nucleic Acids Research **41**: 605-612.

58. Cherry, J. M., E. L. Hong, C. Amundsen, R. Balakrishnan, G. Binkley, E. T. Chan, K. R. Christie, M. C. Costanzo, S. S. Dwight, S. R. Engel, D. G. Fisk, J. E. Hirschman, B. C. Hitz, K. Karra, C. J. Krieger, S. R. Miyasato, R. S. Nash, J. Park, M. S. Skrzypek, M. Simison, S. Weng and E. D. Wong (2012). "Saccharomyces Genome Database: The genomics resource of budding yeast." Nucleic Acids Research **40**: 700-705.

59. Ogata, H., S. Goto, K. Sato, W. Fujibuchi, H. Bono and M. Kanehisa (1999). "KEGG: Kyoto Encyclopedia of Genes and Genomes." Nucleic Acids Research **27**(1): 29 - 34.

60. Nosek, J. and H. Fukuhara (1994). "NADH dehydrogenase subunit genes in the mitochondrial DNA of yeasts." Journal Of Bacteriology **176**(18): 5622-5630.

61. de Vries, S. and L. A. Grivell (1988). "Purification and characterization of a rotenone-insensitive NADH:Q6 oxidoreductase from mitochondria of Saccharomyces cerevisiae." European Journal Of Biochemistry **176**(2): 377-384.

62. Marres, C. A., S. de Vries and L. A. Grivell (1991). "Isolation and inactivation of the nuclear gene encoding the rotenone-insensitive internal NADH: ubiquinone oxidoreductase of mitochondria from Saccharomyces cerevisiae [published erratum appears in Eur J Biochem 1991 Sep 15;200(3):812]." European Journal Of Biochemistry **195**(3): 857-862.

63. de Vries, S. and C. A. Marres (1987). "The mitochondrial respiratory chain of yeast. Structure and biosynthesis and the role in cellular metabolism." Biochimica Et Biophysica Acta **895**(3): 205-239.

64. Verduyn, C., A. H. Stouthamer, W. A. Scheffers and J. P. Vandijken (1991). "A theoretical evaluation of growth yields of yeasts." Antonie Van Leeuwenhoek International Journal of General and Molecular Microbiology **59**(1): 49-63.

65. Priestley, M. B. (1988). Non-linear and non-stationary time series analysis. London San Diego, Academic Press.

66. Wolfram Research, I. (2014). Mathematica. Champaign, Illinois, Wolfram Research, Inc.

67. Team, R. C. (2016). R: A language and environment for statistical computing. R Foundation for Statistical Computing. Vienna, Austria, ISBN 3-900051-07-0.

68. Glass, G. V. and K. D. Hopkins (1996). Statistical methods in education and psychology. Boston, Allyn and Bacon.

69. Muller, J. (1964). "The relation of recombination to mutational advance." Mutation Research **1**(1): 2-9.

70. Ford, E. (1975). Ecological genetics 4th edn, Chapman and Hall, London.

71. Berezovsky, I. N., G. T. Kilosanidze, V. G. Tumanyan and L. L. Kisselev (1999). "Amino acid composition of protein termini are biased in different manners." Protein Eng **12**(1): 23-30.

72. Dayhoff, M. (1979). Atlas of protein sequence and structure. Issue Suppl. Washington, DC, National Biomedical Research Foundation. **5**.

73. Bordo, D. and P. Argos (1991). "Suggestions for "safe" residue substitutions in site-directed mutagenesis." J Mol Biol **217**(4): 721-729.

74. French, S. and B. Robson (1983). "What is a conservative substitution?" Journal of molecular Evolution **19**(2): 171-175.

75. Taylor, W. R. (1986). "The classification of amino acid conservation." Journal of theoretical Biology **119**(2): 205-218.

76. Boguta, G. and A. M. Dancewicz (1981). "Radiation-induced dimerization of tyrosine and glycyltyrosine in aqueous solutions." International Journal of Radiation Biology **39**(2): 163-174.

77. Porter, N. A., S. E. Caldwell and K. A. Mills (1995). "Mechanisms of free radical oxidation of unsaturated lipids." Lipids **30**(4): 277-290.

78. Sultana, R., M. Perluigi and D. A. Butterfield (2006). "Protein oxidation and lipid peroxidation in brain of subjects with Alzheimer's disease: insights into mechanism of neurodegeneration from redox proteomics." Antioxidants & redox signaling **8**(11-12): 2021-2037.

79. Fritz, K. S. and D. R. Petersen (2011). "Exploring the biology of lipid peroxidation-derived protein carbonylation." Chem Res Toxicol **24**(9): 1411-1419.

80. Vidovic, A., F. Supek, A. Nikolic and A. Krisko (2014). "Signatures of conformational stability and oxidation resistance in proteomes of pathogenic bacteria." Cell Reports **7**: 1393-1400.

81. Andersson, S. G. and C. G. Kurland (1998). "Reductive evolution of resident genomes." Trends in microbiology **6**(7): 263-268.

82. Koncarevic, S., P. Rohrbach, M. Deponte, G. Krohne, J. Helena Prieto, J. Yates, S. Rahlfs and K. Becker (2009). "The malarial parasite Plasmodium falciparum imports the human protein peroxiredoxin 2 for peroxide detoxification." Proceedings of the National Academy of Sciences: -.

83. Benfeitas, R., G. Selvaggio, F. Antunes, P. M. B. M. Coelho and A. Salvador (2014). "Hydrogen peroxide metabolism and sensing in human erythrocytes: A validated kinetic model and reappraisal of the role of peroxiredoxin II." Free Radical Biology and Medicine **74**: 35-49.

84. Moura, A., M. a. Savageau and R. Alves (2013). "Relative Amino Acid Composition Signatures of Organisms and Environments." PLoS ONE **8**.

85. Mudd, S. H. and G. L. Cantoni (1964). Biological transmethylation, methyl-group neogenesis and other "one-carbon" metabolic reactions dependent upon tetrahydrofolic acid. Comprehensive biochemistry. M. Florkin and E. H. Stotz. Amsterdam, Elsevier Biomedical Press. **15:** 1 - 47.

86. Plamann, M. D., W. D. Rapp and G. V. Stauffer (1983). "Escherichia coli K12 mutants defective in the glycine cleavage enzyme system." Mol Gen Genet **192**(1-2): 15-20.

87. Perlin, D. S., M. J. San Francisco, C. W. Slayman and B. P. Rosen (1986). "H+/ATP stoichiometry of proton pumps from Neurospora crassa and Escherichia coli." Archives of biochemistry and biophysics **248**: 53-61.

88. Serrano, R., M. C. Kielland-Brandt and G. R. Fink (1986). "Yeast plasma membrane ATPase is essential for growth and has homology with (Na+ + K+), K+- and Ca2+-ATPases." Nature **319**(6055): 689-693.

89. Baccarini Melandri, a., R. Casadio and B. a. Melandri (1977). "Thermodynamics and kinetics of photophosphorylation in bacterial chromatophores and their relation with the transmembrane electrochemical potential difference of protons." European journal of biochemistry / FEBS **78**: 389-402.

90. Steigmiller, S., P. Turina and P. Gräber (2008). "The thermodynamic H+/ATP ratios of the H+-ATPsynthases from chloroplasts and Escherichia coli." Proceedings of the National Academy of Sciences of the United States of America **105**: 3745-3750.

91. Venema, K. and M. G. Palmgren (1995). Metabolic modulation of transport coupling ratio in yeast plasma membrane H+-ATPase. Journal of Biological Chemistry. **270:** 19659-19667.

92. Hryniewicz, M., a. Sirko, a. Pałucha, a. Böck and D. Hulanicka (1990). "Sulfate and thiosulfate transport in Escherichia coli K-12: identification of a gene encoding a novel protein involved in thiosulfate binding." Journal of bacteriology **172**: 3358-3366.

93. Sirko, a., M. Zatyka, E. Sadowy and D. Hulanicka (1995). "Sulfate and thiosulfate transport in Escherichia coli K-12 : evidence for a functional overlapping of sulfate- and thiosulfate-binding proteins . Sulfate and Thiosulfate Transport in Escherichia coli K-12 : Evidence for a Functional Overlapping of Sulfate." **177**: 4134-4136.

94. Valgepea, K., K. Adamberg, R. Nahku, P•-J. Lahtvee, L. Arike and R. Vilu (2010). "Systems biology approach reveals that overflow metabolism of acetate in Escherichia coli is triggered by carbon catabolite repression of acetyl-CoA synthetase." BMC systems biology **4**: 166.

95. Arike, L., K. Valgepea, L. Peil, R. Nahku, K. Adamberg and R. Vilu (2012). "Comparison and applications of label-free absolute proteome quantification methods on Escherichia coli." Journal of Proteomics **75**: 5437-5448.

96. Krug, K., A. Carpy, G. Behrends, K. Matic, N. C. Soares and B. Macek (2013). "Deep coverage of the Escherichia coli proteome enables the assessment of false discovery rates in simple proteogenomic experiments." Molecular & cellular proteomics : MCP **12**: 3420-3430.

97. Breton, A. and Y. Surdinkerjan (1977). "Sulfate Uptake in Saccharomyces-Cerevisiae - Biochemical and Genetic Study." Journal of Bacteriology **132**: 224-232.

98. Cherest, H., J. C. Davidian, D. Thomas, V. Benes, W. Ansorge and Y. SurdinKerjan (1997). "Molecular characterization of two high affinity sulfate transporters in Saccharomyces cerevisiae." Genetics **145**(3): 627-635.

99. Roomans, G. M. (1979). "Biochimica et Biophysica Acta, 551 (1979) 197--206 ©." **551**: 197-206.

100. Cronk, J. D., J. a. Endrizzi, M. R. Cronk and J. W. O. Neill (2001). "Crystal structure of E. coli □-carbonic anhydrase, anenzyme with an unusual pH-dependent activity." Protein Science (2001), 10: **10**: 911-922.

101. Amoroso, G., L. Morell-Avrahov, D. Muller, K. Klug and D. Sultemeyer (2005). "The gene NCE103 (YNL036w) from Saccharomyces cerevisiae encodes a functional carbonic anhydrase and its transcription is regulated by the concentration of inorganic carbon in the medium." Molecular Microbiology **56**(2): 549-558.

3. Proteome composition and aerotolerance

102. Clark, D., R. S. Rowlett, J. R. Coleman and D. F. Klessig (2004). "Complementation of the yeast deletion mutant Delta NCE103 by members of the beta class of carbonic anhydrases is dependent on carbonic anhydrase activity rather than on antioxidant activity." Biochemical Journal **379**: 609-615.

103. Babu, M., J. F. Greenblatt, A. Emili, N. C. J. Strynadka, R. a. F. Reithmeier and T. F. Moraes (2010). "Structure of a SLC26 Anion Transporter STAS Domain in Complex with Acyl Carrier Protein: Implications for E. coli YchM in Fatty Acid Metabolism." Structure **18**: 1450-1462.

104. Zhao, R. M. and R. A. F. Reithmeier (2001). "Expression and characterization of the anion transporter homologue YNL275w in Saccharomyces cerevisiae." American Journal of Physiology-Cell Physiology **281**(1): C33-C45.

105. Wagner, A. (2007). "Energy costs constrain the evolution of gene expression." Journal of Experimental Zoology Part B: Molecular and Developmental Evolution **308B**(3): 322-324.

106. Ghaemmaghami, S., W. K. Huh, K. Bower, R. W. Howson, A. Belle, N. Dephoure, E. K. O'Shea and J. S. Weissman (2003). "Global analysis of protein expression in yeast." Nature **425** 737-741.

107. Newman, J. R. S., S. Ghaemmaghami, J. Ihmels, D. K. Breslow, M. Noble, J. L. DeRisi and J. S. Weissman (2006). "Single-cell proteomic analysis of S. cerevisiae reveals the architecture of biological noise." Nature **441**(7095): 840-846.

108. Lu, P., C. Vogel, R. Wang, X. Yao and E. M. Marcotte (2007). "Absolute protein expression profiling estimates the relative contributions of transcriptional and translational regulation." Nature Biotechnology **25**(1): 117-124.

109. Valgepea, K., K. Adamberg, A. Seiman and R. Vilu (2013). "Escherichia coli achieves faster growth by increasing catalytic and translation rates of proteins." Molecular Biosystems.

110. Hui, S., J. M. Silverman, S. S. Chen, D. W. Erickson, M. Basan, J. Wang, T. Hwa and J. R. Williamson (2015). "Quantitative proteomic analysis reveals a simple strategy of global resource allocation in bacteria." 1-15.

111. Stouthamer, A. (1979). "The search for correlation between theoretical and experimental growth yields." Int. Rev. Biochem **21**(1): 1-47.

112. Calhoun, M. W., K. L. Oden, R. B. Gennis, M. J. de Mattos and O. M. Neijssel (1993). "Energetic efficiency of Escherichia coli: effects of mutations in components of the aerobic respiratory chain." Journal of bacteriology **175**: 3020-3025.

113. Stouthamer, a. H. and C. W. Bettenhaussen (1977). "A continuous culture study of an ATPase-negative mutant of Escherichia coli." Archives of microbiology **113**: 185-189.

114. Bogachev, a. V., R. a. Murtazina and V. P. Skulachev (1996). "H + /e - stoichiometry for NADH dehydrogenase I and dimethyl sulfoxide reductase in anaerobically grown Escherichia coli cells." J. Bacteriol. **178**: 6233-6237.

115. Matsushita, K., T. Ohnishi and H. R. Kaback (1987). "NADH-ubiquinone oxidoreductases of the Escherichia coli aerobic respiratory chain." Biochemistry **26**: 7732-7737.

116. Puustinen, a., M. Finel, T. Haltia, R. B. Gennis and M. Wikström (1991). "Properties of the two terminal oxidases of Escherichia coli." Biochemistry **30**: 3936-3942.

117. Jasaitis, a., V. B. Borisov, N. P. Belevich, J. E. Morgan, a. a. Konstantinov and M. I. Verkhovsky (2000). "Electrogenic reactions of cytochrome bd." Biochemistry **39**: 13800-13809.

118. Belevich, I., V. B. Borisov, J. Zhang, K. Yang, A. a. Konstantinov, R. B. Gennis and M. I. Verkhovsky (2005). "Time-resolved electrometric and optical studies on cytochrome bd suggest a mechanism of electron-proton coupling in the di-heme active site." Proceedings of the National Academy of Sciences of the United States of America **102**: 3657-3662.

119. Belevich, I., V. B. Borisov and M. I. Verkhovsky (2007). "Discovery of the true peroxy intermediate in the catalytic cycle of terminal oxidases by real-time measurement." Journal of Biological Chemistry **282**: 28514-28519.

120. Borisov, V. B., I. Belevich, D. a. Bloch, T. Mogi and M. I. Verkhovsky (2008). "Glutamate 107 in subunit I of cytochrome bd from Escherichia coli is part of a transmembrane intraprotein pathway conducting protons from the cytoplasm to the heme b595/heme d active site." Biochemistry **47**: 7907-7914.

121. Fu, H. a., S. Iuchi and E. C. C. Lin (1991). "The requirement of ArcA and Fnr for peak expression of the cyd operon in Escherichia coli under microaerobic conditions." MGG Molecular & General Genetics **226**: 209-213.

122. Pirt, S. J. (1982). "Maintenance energy: a general model for energy-limited and energy-sufficient growth." Archives of microbiology **133**: 300-302.

123. Pirt, S. J. (1987). "The energetics of microbes at slow growth rates: maintenance energies and dormant organisms." Journal of fermentation technology **65**: 173-177.

124. Bakker, B. M., K. M. Overkamp, A. J. A. van Maris, P. Kotter, M. A. H. Luttik, J. P. van Dijken and J. T. Pronk (2001). "Stoichiometry and compartmentation of NADH metabolism in Saccharomyces cerevisiae." FEMS Microbiology Reviews **25**(1): 15-37.

125. Clark, D. P. (1989). "The fermentation pathways of Escherichia coli." FEMS microbiology reviews **5**: 223-234.

126. Akaike, H. (1998). Information theory and an extension of the maximum likelihood principle. Selected Papers of Hirotugu Akaike, Springer**:** 199-213.

CHAPTER 4 – GENERAL CONCLUSIONS

4. General Conclusions

Reactive oxygen species are potentially toxic for organisms. Cells rely on various levels of defense against them including *active* defense mechanisms. For instance, antioxidant defenses that decompose ROS into non-toxic species are *active* defenses. On the other hand, evolutionary acquired protein structural features that reduce the exposure of more reactive amino acyl residues to ROS is a form of *passive* protection. Here we studied two questions regarding *active* and *passive* defense mechanisms against oxidative stress.

4.1 Study of an *active* defense against oxidative stress: the role of Peroxiredoxin 2 in H_2O_2 metabolism in human erythrocytes

4.1.1 Prx2's *effective* peroxidase activity *in vivo* is much lower than implied by the kinetic parameters for the purified protein

In Chapter 2 we setup a mathematical model of H_2O_2 metabolism in human erythrocytes. This model achieves a remarkable agreement with multiple phenomena observed in intact cells. However, such agreement was only attained by considering a much lower *effective* peroxidase activity for Prx2 than what would be attained should we have considered the parameters from the purified antioxidant defenses. We estimate that >99% of H_2O_2 would be consumed by Prx2 if one considered the intracellular concentrations and H_2O_2-reactivities determined *in vitro*. This goes against various independent experiments with intact erythrocytes that indicate that Prx2's contribution is at most comparable Cat's under low H_2O_2 concentrations. These observations indicate that Prx2's *effective* peroxidase activity *in vivo* is much lower than implied by the cellular concentrations and H_2O_2-reactivities of the purified proteins. They are in line with recent observations in other human cells and in yeast, they cast doubts on whether peroxiredoxins' main function is to remove H_2O_2 [1].

Among the alternative mechanistic hypotheses to explain the lower *effective* Prx2 peroxidase activity *in vivo*, the body of evidence favors a strong (>99%) but reversible non-covalent inhibition. A model encompassing such inhibition

achieves remarkable agreement with various experiments with intact cells in the literature.

Which compound is sufficiently abundant to titrate Prx2, one of the most abundant proteins in the cell? In human erythrocytes, only hemoglobin and carbonic anhydrase 1 are sufficiently abundant proteins [2, 3] to titrate Prx2. Interestingly, Prx2 binds [4, 5] and protects hemoglobin against oxidation [4], raising the possibility that the association of hemoglobin with Prx2 may affect its peroxidase activity. However, it is still unclear what fraction of Prx2 is hemoglobin-bound, and whether this severely inhibits Prx2's peroxidase activity. The observation that hemoglobin controls the circadian oscillations observed in Prx2 sulfinylation independently of sulfiredoxin activity [6] suggests so, but our estimates indicate that only a minor fraction of the protein is sulfinylated. The complexation between Prx2 and carbonic anhydrase 1 was not observed [5]. Other less abundant proteins associate with Prx2 and are discussed below in the context of possible redox signaling partners.

A few low molecular weight compounds such as glutathione [7], lactate [8] and 2,3-diphosphoglycerate [9, 10] are also sufficiently abundant to titrate Prx2. A recent study observed that stable mixed disulfides are formed between Prx2 and glutathione [11], but <10% Prx2 is glutathionylated in mice erythrocytes exposed to 0.5 mM H_2O_2, far from the 99% required to achieve consistency with the experiments in intact cells. 2,3-diphosphoglycerate is important due to its allosteric effect of oxygen binding by hemoglobin [12]. The cytoplasmic concentrations of both lactate and 2,3-diphosphoglycerate are kept in mM ranges in most conditions [8, 13]. Whether any of these two low-molecular weight compounds reversibly binds Prx2 remains to be determined. Experiments are being carried out to determine the source of Prx2's inhibition by our colleagues at Winterbourn's lab in the University of Otago, New Zealand.

Our study also raises some other questions related with the design of Prx/Trx systems and its evolutionary conservation. Namely, should it be experimentally confirmed that Prx2 is inhibited in human erythrocytes, would Prxs in other cells also be subjected to a strong but reversible inhibition? Should the inhibitor be hemoglobin or carbonic anhydrase, future studies could test whether globins or

carbonic anhydrases, proteins widespread in nature [14, 15][19], are inhibitors of Prxs in other human cells. A crucial question is also if they are sufficiently abundant to do so. Alternatively, should Prx2 be inhibited by a low molecular weight compound, lactate or glutathione would be the most likely inhibitors in other cells. Glutathione is abundant in many cells and could be envisaged as a potential Prx inhibitor. Prx2 glutathionylation likely does not explain the Prx2 inhibition because such a post-translational modification should be kept by the purified protein. However, it cannot be excluded that glutathione inhibits the peroxidatic activity of Prx2 through non-covalent binding. Lactate is sometimes very abundant in fermentative cells, and lactate dehydrogenases (EC 1.1.1.27) are ubiquitously found in all three domains of life: ldh-1/ldh-2 are found in 85/24 archaeal, 1295/367 bacterial and 404/171 eukaryotic non-redundant species deposited at PFam as off 28th April 2016 [16]. However, one may wonder if this is also the case in cells where pyruvate is mostly used for oxidative phosphorylation. Lastly, one could discard 2,3-diphosphoglycerate as possible inhibitor in other cells because it only is abundant in human erythrocytes.

The proposal that Prx2's peroxidase activity is strongly inhibited *in vivo* does not imply that Prx2 is not essential for H_2O_2 metabolism. $Prx2^{-/-}$ knockout mice are phenotypically normal but accumulate erythrocyte abnormalities such as Heinz body formation (denaturated forms of oxidized hemoglobin), oxidative hemolytic anemia and higher intracellular ROS levels [17]. $Prx2^{-/-}$ cells display no higher fractions of methemoglobin on the short term [18] but tend to accumulate them with time [17]. It is unclear whether these abnormalities are due to the missing peroxidase activity or to some other protective role of Prx2 [4].

A strongly inhibited Prx2 peroxidase activity raises questions about Prx2's role in defense against H_2O_2 in the absence of other antioxidant defenses. Catalase- and glutathione peroxidase-deficient mice exhibit no significant increase in hemoglobin oxidation or hemolysis compared with wild type cells [19, 20] except when exposed to high H_2O_2 concentrations [18]. These observations suggest that

[19] As of 28th of April of 2016, 51 archaeal, 993 bacterial and 296 eukarotic species had been identified as having carbonic anhydrases on PFam [16]. Globins were identified in 420 bacterial and 300 eukaryotic species.

4. General conclusions

Prx2 is nevertheless capable of protecting against endogenously-generated H_2O_2. Our results here presented indicate that Prx2 would become the erythrocyte's main defense against H_2O_2 should catalase be knocked-down or inhibited. It is unclear whether this protection against hemoglobin oxidation is due to Prx2's peroxidase activity, or Prx2's protective binding of hemoglobin [4]. However, Prx2 knock-out mice do not exhibit significantly higher hemoglobin oxidation under basal and moderate H_2O_2 concentrations [18, 21], raising questions about the importance of Prx2's protective hemoglobin binding. However, one must acknowledge that the non-significant difference in hemoglobin oxidation in Prx2 knockouts may have several explanations besides a low Prx2's cytoplasmic peroxidase activity: First, hemoglobin is oxidized by H_2O_2 very slowly: the pseudo-first order rate constant for hemoglobin oxidation by H_2O_2 is $k \approx 10^{-8}$ s^{-1} considering hemoglobin's reactivity with H_2O_2 100 $M^{-1}s^{-1}$ [22], and 0.4 nM cytoplasmic H_2O_2 (estimated based on Model B without Cat activity in erythrocytes under basal oxidative conditions). This translates into a half-life of many months, therefore indicating that hemoglobin's oxidation by H_2O_2 is negligible. Second, cells still rely on catalase and GPx1 for defense against H_2O_2 in Prx2-knock outs. Third, oxidized hemoglobin is reduced through catalyzed and non-catalyzed processes [23, 24]. This may explain why Prx2-knockouts show no increased fractions of oxidized hemoglobin under low/moderate H_2O_2 concentrations. Future studies should disentangle the protective effect of Prx2-hemoglobin binding from Prx2's cytoplasmic peroxidase activity.

The readily reversible Prx2 inhibition would permit the *regulated recruitment* of Prx2's peroxidase activity. Under normal conditions, the inhibitor is associated with Prx2, and the protein is not peroxidatically active. However, upon an external signal, the inhibitory complex would dissociate and fully activate the protein. This would permit the deployment of Prx2's peroxidase activity only where and when such an activity is necessary. This could also imply that H_2O_2 or potential redox signaling readouts (see below) could accumulate in cell locations where the inhibitor-Prx2 complex would not dissociate - an alternative to the floodgate hypothesis whereby localized H_2O_2 accumulation occurs in regions where Prx is inactivated by sulfinylation [25].

4.1.2 A low *effective* Prx2 peroxidase activity saves on NADPH cost of H_2O_2 defense and shows desirable signaling properties

A low effective Prx2 peroxidase activity indicates that the main role of this protein in erythrocytes is not to minimize H_2O_2 concentrations, and raises the question of what functional advantages could a strong quickly reversible inhibition have. A lower Prx2 peroxidase activity saves on NADPH costs of activity, leaving these reducing equivalents available to be utilized by other processes such as the GSH/GPx1/GSSGR system to scavenge organic peroxides for instance. Additionally, the inhibition endows this system with desirable signaling properties under the various patho-physiological conditions that erythrocytes face while in circulation. These signaling properties are indicated by changes of H_2O_2 supply yielding directly proportional changes in the concentrations of the potential redox signaling molecules: H_2O_2, sulfenic acid and disulfide Prx2 and thioredoxin 1. And also that there is a sharp transition between this proportionality regime and one where the concentrations of these potential signaling outputs are at their maximum, which may be potentially important under high oxidative stress for triggering an emergency response. These hypothetical signaling properties come in line with numerous observations in the literature where those redox species are involved in redox signaling [26-30]. Recent observations also indicate that very abundant and H_2O_2-reactive Prxs in yeast and human cells are not designed to minimize H_2O_2 concentrations under high oxidative loads, conditions in which H_2O_2 is instead mostly scavenged by other defenses [1]. The accumulation of sulfinylated Prx at high oxidative loads led the authors to hypothesize that Prxs are instead required due to their activity in regulation of H_2O_2-induced gene expression and oxidative resistance signaling [1, 31].

Which possible signaling partners could be interacting with Prx2 and Trx in human erythrocytes? No H_2O_2- or Prx2-dependent signaling pathways were clearly identified in these cells to this point. However, Prx2 heterocomplexes with alcohol dehydrogenase, flavin reductase, catalase, selenium-binding protein 1, and peroxiredoxin 6 were identified experimentally [5]. The *in vivo* functional role of these complexes is still unknown. Alcohol dehydrogenase (ADH) has four thiol groups of which two are at the active site [32] and are prone to inactivation by

4. General conclusions

H_2O_2-mediated oxidation as observed in yeast [33]. The binding of Prx2 to ADH may be regulating ADH's activity, and/or have a protective role similar to that observed in hemoglobin-bound Prx2 [4]. This is potentially important for controlling sugar metabolism, given ADH's role in glucose metabolism, the polyol pathway and in diabetes [34]. The Prx2-flavin reductase complex may also be involved in the protection of hemoglobin against oxidative stress, considering that flavin reductase reduces methemoglobin [35] – it is currently unknown whether its two cysteines are significantly H_2O_2-reactive and whether this affects the methemoglobin reductase activity. Prx2-selenium-binding protein 1 (SBP1) complexes in turn may regulate GPx1 activity. SBP1 interacts and decreases the peroxidase activity of GPx1 [36]. Prx2-catalase complexes relocate to the erythrocyte membrane and only some of those complexes maintain Prx2's peroxidase activity [37], suggesting that Prx2-catalase complexes may be important for deploying and regulating Prx2's peroxidase activity and redox status. Finally, the formation of Prx2-Prx6 complexes comes as an interesting and potentially important signaling interaction. Prx6 is a 1-Cys Prx that uses GSH [38] but not Trx [39] as electron donor. Prx6 displays Ca^{2+}-independent phospholipase A_2 activity [40] and enhances superoxide production by NADPH oxidase [41]. The Prx2-Prx6 complexes may regulate these activities, or alternatively the co-localization of Prx2 near Prx6 and active NADPH oxidase may be important to regulate the redox state of Prx2.

Any potential signaling properties of the Prx2/Trx/TrxR system also raise questions about the roles of less abundant peroxiredoxins which may act as signaling mediators themselves. Erythrocytes also possess Prx1, Prx4, and Prx6 though at much lower abundances than Prx2 [42, 43][20]. Erythrocyte Prx1

[20] Prx6's concentration has been reported as <1% of Prx2's [42]. To estimate Prx6's abundance we proceed as follows. The concentrations C_P of each protein in the author's sample in Table 2 of ref. [64] may be converted from their mass fractions M_F and molecular weights M_W through equation

$$C_P = M_F \times P_T \times A_{MW} \times M_W^{-1}$$

where A_{MW} is an average protein molecular weight of 44 kDa [65], P_T is the total erythrocyte protein concentration = 8 mM estimated from 7 mM Hb [66] and assuming that Hb accounts for 90% of the total protein contents in this cell. Applying this approach, we estimate that Prx6's abundance may actually be in the range of that of Prx2 according to proteomic data [3]. Future studies could clarify Prx6's concentration in human erythrocytes.

deficiency leads to hemoglobin oxidation, higher ROS, hemolytic anemia and overall lower erythrocyte lifespan [44]. This indicates that Prx1 is important for redox metabolism but its role remains unclear. *In vitro* studies show that Prx1 is more easily sulfinylated than Prx2 [45], and led the authors to suggest that the two peroxiredoxins are not duplicate proteins where Prx1 is more important due to its chaperone activity and Prx2 due to its peroxidase activity. Our results indicate that while Prx2's peroxidase activity is important for removing low levels of H_2O_2 it additionally may display potentially important signaling properties. However, one cannot rule out the possibility that sulfinylated Prx2, the redox state typically associated with its oligomerization and chaperone activity [46-48], may also be important in the human erythrocyte: because Prx2 is so abundant, even a small fraction of sulfinylated Prx2 after a H_2O_2 bolus could amount to 10 nM – 1 μM. Additionally, the high Prx2 concentration may also be important due to its signaling properties, as exhibited by a design with abundant Prx2 (designs B and D, Chapter 2), but not one with lower Prx2 concentration (design C) that accumulates in sulfinylated form at lower oxidative loads.

Future studies should address the importance of Prx2's peroxidase activity and the role of this defense system in the context of the Prx2-Prx6 interaction, together with whether/how it outcompetes less abundant H_2O_2 sensors such as Prxs 1, 4, 5 and 6. A modeling approach to address this could start by assessing the design features (relative concentrations, kinetics of reaction with H_2O_2 and between Prxs, response to redox stimuli, etc.) necessary for a highly abundant defense to represent a redox relay for less abundant proteins using the mathematical model that we presented.

Prx2 also reacts with various other proteins in other cells. For instance, Prx2 regulates Src-related tyrosine kinase (Syk) activation in mice erythrocytes [21]. Prx2 also forms disulfides with DJ-1 [49], an atypical peroxiredoxin [50] that is present in mature erythrocytes where it is associated with the response to oxidative stress [51, 52]. Whether Prx2 reacts with DJ-1 and Syk in human erythrocytes, and how important is this association, is still unclear. A number of other interactions involving Prx2 and Trx were also identified in human cells (Figure 4.1) and may be studied by adapting our mathematical model in the future.

4. General conclusions

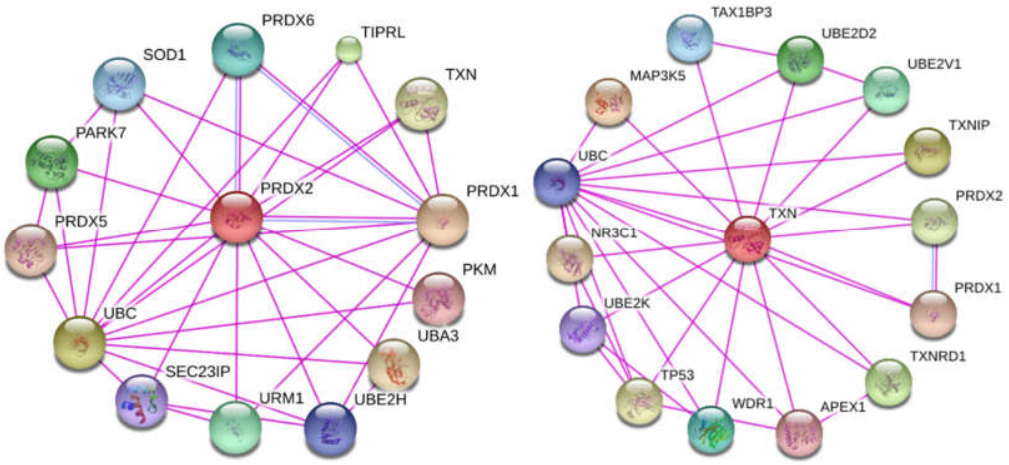

Figure 4.1 – Protein interactions of Prx2 (Prdx2, top in center) and Trx1 (Txn, bottom in center) as indicated by experimental evidence in human cells. Images obtained from STRING v10.0 [53] on 28th April 2016 (confidence score was set to high). Abbreviations stand for gene names. Edge color stands for evidence from experimental observation (pink) or homology (blue). See [53] for details.

The accurate mathematical description of the Catalase/Prx2/Trx 1/TrxR system has several important implications for redox biology in human and other cells. First, it permits having a quantitative perspective of these redox mechanisms that have been widely implicated in various processes in human cells and disease [54-57]. Having a valid mathematical description that can be transposed to other cells will help planning and interpreting experimental studies, and possibly permits a mechanistically understanding of observed phenotypes. For instance, what are the features of Prx1/Prx2 and coupled reactions system that make them important in neurodegenerative diseases [58]? Is it their interaction with various signaling molecules [28, 59], and/or chaperone activity [46-48], and/or peroxidase activity? Our mathematical model could be adapted to help answering such questions.

Second, given the widespread presence of Prxs/Trxs in nature, a sound mathematical description of Prx/Trx systems may help understand how these proteins participate in redox signaling in many cells. Which hypothetical redox signaling mechanisms are consistent with the kinetic properties and cellular abundances of these proteins? What design principles warrant reliable signaling and antioxidant protection? These questions are currently being analyzed in our group.

One other question that is raised by our observations is why Prxs are so abundant in human erythrocytes and other cells [60]. For instance, *E. coli* and *S. cerevisae* also have peroxiredoxins that are much more abundant than catalases or other cellular H_2O_2 defenses [61-64] and display very high Prx reactivity with H_2O_2 ($k \geq 10^7$ $M^{-1}s^{-1}$ [65]). However, the Prxs in those cells only contribute for the protection against low H_2O_2 concentrations [65]. Considering the observation that Prx2's role in human erythrocytes is not to minimize H_2O_2 concentrations (Chapter 2), one wonders whether the high Prx abundances in human erythrocytes and other cells are associated with chaperone activities of Prxs or ability to buffer ROS against ROS pulses. These proteins protect against thermal protein aggregation and denaturation in yeast [46]. This protection is associated with high molecular weight Prxs that are formed upon sulfinylation [46, 47]. The chaperone activity of the Prx Tsa1 in yeast requires the interaction with heat-shock protein 70 [66]. In *L. infantum*, mitochondrial Prxs bind unfolded proteins until the thermal stress conditions pass, after which the client proteins are refolded by other chaperones [67]. Further, observations in mice and human erythrocytes indicate that Prx2 is important for protecting against hemoglobin aggregation [4], though it is unclear whether this is might be due to the peroxidase activity of Prx2. Nevertheless, these observations show that Prxs or Prx-mediated interactions are important to prevent protein denaturation and aggregation.

It is unclear what fraction of the cell's proteins become client proteins for chaperone Prxs [4, 47, 68]. Considering that sulfinylated Prxs exhibit the highest chaperone activity, our estimates that <6 μM Prx2 is sulfinylated is compatible with a substantial erythrocyte protein content being targeted by Prx2's chaperone activity, should all sulfinylated Prx2 display such function. This could either occur by direct catalysis by sulfinylated Prx2 or through reactions with heat-shock proteins in the cell – and human erythrocytes display various proteins of the HSP70 family [5]. Though the interaction between Prx2 and any of these heat shock proteins was not observed experimentally, the formation of such aggregates was not tested under conditions of high oxidative stress [5] where sulfinylated Prx2 could accumulate. Nevertheless, one must also bear in mind that lower-molecular weight forms of Prx2, abundant under low oxidative stress, also show substantial chaperone activity [4, 47, 68]. Future work is required to

understand whether Prxs are abundant in human erythrocytes and other cells due to their chaperone activities and/or important redox signaling properties.

Overall, our work in human erythrocytes permitted establishing an accurate mathematical description of the Cat/Prx2/Trx system that may be expanded to study the design principles of these proteins in other cells. This work has important implications for human health and for the biochemistry of redox metabolism in human and other cells.

4.2 Study of a *passive* defense against oxidative stress: proteome composition bias by aerotolerance

4.2.1 Organism's aerotolerance is an important determinant of proteome oxidability and amino acid composition

Overall we observe that aerotolerant organisms display significantly lower median proteome oxidabilities than aerointolerant organisms whether oxidability is weighted by solvent-exposure or not. This is consistently observed in all domains and most lower taxonomic clades tested. These trends are explained by differences in the frequencies of highly- vs. lowly-oxidizable amino acids Phe, Tyr, Cys and Met. These residues are among the most •OH-reactive ($k_{\bullet OH}$ 10^{10} $M^{-1}s^{-1}$) and together contribute to 60-70% of median protein oxidability in most lineages. However, some residues such as Trp, His and Arg are more abundant in aerotolerant than aerointolerant organisms despite being among the most oxidizable ($k_{\bullet OH}$ 10^{9} $M^{-1}s^{-1}$). This is explained by the physico-chemical similarity to the rarefied residues Tyr, Met and Lys. Further, even within groups of physico-chemical similar residues we observed a general trend towards minimizing the utilization of highly oxidizable residues.

The above differences between aerotolerant and aerointolerant organisms could also be explained by other extrinsic and intrinsic sources of composition bias such as genomic G+C content [69-72], thermophily [70, 71, 73], protein size [74-77], phylogeny [78], amino acid biosynthesis costs [79, 80], or pathogenicity [81]. However, even after controlling for these and other sources of compositional bias,

aerotolerance emerges as one of the main explanatory variables for proteome oxidability and amino acid composition. Aerotolerance is the variable that explains most of variability in proteome oxidability, the main variable to explain the variance in Cys frequency and one of the main variables to explain other residue's frequencies. In turn, the biosynthetic costs of proteomes of aerotolerant and aerointolerant organisms are not significantly different. Additionally, we observe that intracellular organisms (parasites, symbionts, and commensals) display significantly higher protein oxidabilities than free-living organisms. Altogether, the observations above highlight the pivotal importance of aerotolerance in shaping proteome composition and oxidability, independently of other sources of composition bias.

To our knowledge, our study here addresses for the first time how aerotolerance biases proteome composition while controlling for all known intrinsic and extrinsic sources of compositional bias. It also considers the largest number of fully sequenced organisms to date. Not only is this work important because it provides a new understanding of the biology of living cells, it also has important implications for health and biotechnology. The frequent substitutions among groups of physico-chemical similar amino acids were here considered for the first time in the context of proteome composition assessment. We also introduce a new proxy for oxidative damage to proteins (•OH-reactivity) and updated costs of biosynthesis of residues for bacteria and eukaryotes. These costs also consider the utilization of nutrients and energetic compounds that were previously not considered [79, 82, 83] and thus present a more accurate approximation to amino acid biosynthetic costs. This has potentially important implications for cell resource management, and engineering of individual proteins to improve their redox stability. They provide a rational justification for utilizing Cys, Tyr, and Met at lower abundances in highly oxidative environments. Additionally, the lower contribution of some *chemically similar* amino acids for protein oxidability presents alternatives for protein engineering. Further, the costs here presented introduce biosynthetic costs for growth under two conditions: aerobiosis and anaerobiosis. This work also has important implications for immunology and microbiology, due to the observation that intracellular organisms display significantly higher protein oxidabilities than free-living organisms. This suggests

that general mechanisms of pathogenicity of organisms are not carried by fighting the immune response but rather by evading it, and/or that the pathogens are shielded from extracellularly-generated oxidative stress by inhabiting the intracellular environment.

We will now briefly discuss some of the questions that remain unanswered or were raised by our work.

Could a better oxidability predictor be found? The method that we employed where the protein •OH-oxidability is approximated by considering the solvent-exposure of individual amino acids was the best possible predictor that we could use considering accuracy and speed of current bioinformatic methods. Finding a better oxidability predictor would imply determining more accurate solvent-exposures. Recent methods use motif similarity to achieve a good degree of accuracy in their predictions [84, 85]. For instance, 90% prediction accuracy is determined for buried (<5% accessible) residues using these methods [85]. However, these tools would be too slow for the size of our dataset (4 million protein sequences). Nevertheless, these accurate bioinformatic tools for predicting protein accessibility may be used together with our predictor of protein oxidability in smaller scale studies, for instance to study differential protein usage under anaerobiosis vs aerobiosis in a single organism (see below).

One question that remains unanswered is how protein abundance relates with oxidability. Do highly expressed proteins exhibit significantly different oxidabilities with respect to the full proteome and to lowly expressed proteins, and if so, why? Highly expressed proteins display some residues at higher frequencies (Asp, Glu and Lys) [86], have significantly more conserved motifs [87, 88] and are encoded preferentially by some codons [89-91]. This indicates that amino acid composition is biased with respect to protein abundance, which should also be reflected in the oxidabilities of those proteins. Significant information about protein abundances is deposited in proteomics databases (e.g. PaxDB [92] or SPINE 2 [86, 93]) that could allow for a small scale study in a single organism for instance. Should it be aimed for a larger scale study, an important challenge to addressing how protein expression levels relate with oxidability would come from predicting protein

abundances for many organisms. Various bioinformatic predictors based on codon utilization bias have been widely used to predict gene or protein expression [94-99]. But they have known pitfalls [99, 100] such as relying on *a priory* identification of highly expressed genes, low signal-to-noise ratios, or low correlations (<0.65) between predicted and observed expressions. However, it is currently not possible to find better predictors of protein abundance, so focusing on a few well studied organisms is probably a more accurate initial approach.

And how does the subcellular protein distribution relate with oxidability? Presumably, proteins with lower oxidabilities would be observed in compartments with high ROS production (e.g. peroxysomes and mitochondria), or with abundant iron pools which could in turn promote Fenton production of •OH. To our knowledge, protein carbonylation has not been extensively quantified across cell compartments, but observations in cultured mouse neurons under oxidative stress indicate that cytoplasmic proteins may display up to 15-fold higher carbonylation levels than membrane or nuclear proteins [101]. This suggests that cytoplasmic proteins are significantly more oxidizable than membrane/nuclear proteins, or they are exposed to significantly higher levels of oxidative stress. Future work could partition proteins across compartments using predictors of subcellular localization [102-104] and then compare the subcellular proteomes.

One should also distinguish between cytoplasmic/extracellular proteins vs integral membrane proteins. Integral membrane proteins display biased compositions and are rich in hydrophobic residues [105]. Future work could distinguish membrane proteins from non-membrane proteins, and if possible it could also compare whether extracellularly-facing motifs are significantly less oxidizable than intracellularly-facing sequences. This could be done using predictors of membrane sequences. However, care should be taken because such predictions is reliant on motif- and domain-similarity-based predictions. This is prone to substantial errors or is very slow for large sequences numbers [106]. Recent approaches to predict membrane sequences or solvent exposure have employed neural networks and related methodologies with promising results [84, 85, 107-109]. Of course, smaller scale analyses could already be performed on model organisms such as *E. coli*, *M. tuberculosis* or *S. cerevisae*. Studies using our oxidability predictor, and Gene Ontology information may easily identify

subcellular distribution and molecular functions of highly/lowly oxidizable proteins in each proteome using available tools (e.g. PANTHER [110]).

It would also be interesting to test whether proteins expressed under aerobic growth are significantly less oxidizable than those expressed under anaerobic growth. Bacteria respond to oxygen availability by changing the expression of antioxidant response genes (e.g. SoxR and OxyR [111, 112]) and enzymes involved in fermentative and respiratory metabolism. Considering that the proteins expressed under aerobic growth are potentially exposed to oxidative stress it is possible that those proteins also show decreased •OH-oxidabilities compared with proteins expressed under anaerobic growth – especially considering that the added oxidative stress may pose an evolutionary constraint on aerobic protein composition that is not present in proteins expressed under anaerobic growth. To study these hypotheses future work could use gene expression datasets [113-115] to determine which proteins are mostly expressed under both growth conditions in a few well-characterized facultative organisms. Using this information one could then find the *aerobic* and *anaerobic* proteome datasets and compare them in terms of their oxidabilities. Similarly, it remains to test in higher organisms whether the proteome of oxygen-rich tissues (e.g. lungs) is significantly less oxidizable than those of tissues usually under lower oxygen pressures.

And how do protein oxidabilities relate with their folding speed? Amino acids are encoded by 2-6 synonymous codons, but some codons are preferred over others in most genomes [89, 91] affecting gene expression levels [90], translation speed and co-translational folding [116]. This suggests that protein folding speed is biased by amino acid composition. Because slowly folding proteins have their protein cores more accessible to solvent for longer periods, it is possible that they are also exposed to higher oxidative stress than fast-folding proteins. Curiously, protein translation speed decreases under oxidative stress [117, 118], possibly to improve translation efficiency, but a slower translation speed may also expose unfolded protein sequence to ROS in the solvent. Could slowly folding proteins display significantly lower protein oxidabilities? To give some insights into these questions initial approaches could use primary sequence information to predict protein folding rates [119, 120]. Folding rates could then be compared with protein

oxidability and function in an aerobe. Protein folding speed, oxidability and function could also be studied in *E. coli*, a facultative organism, both under aerobic and anaerobic growth, to understand how these properties relate with the growth environment.

Additionally, it would be interesting to identify oxidability signatures. For instance, it is possible that the nascent protein sequence is biased to exhibit lower oxidability: because it is the protein sequence that emerges before higher level protein structures is acquired it may not be able to shield residues from ROS in the solvent. It is also possible that chaperone or ribosome-assisted folding of the nascent sequence [121] is efficient enough to achieve a native conformation that protects it from oxidants in the solvent, or ribosomes may even shield the nascent chain from ROS.

Other potentially important motifs to study are Lys-(Xaa)-Met/Cys. Our observations in aerotolerant organisms indicate that Lys is substantially more depleted than would be predicted from its •OH-reactivity. One of the possible explanations for this is that Lys is avoided in aerotolerant organisms because it increases the H_2O_2-reactivity of Met and Cys [122-124]. Future work could look into the prevalence of Lys-(Xaa)-Met/Cys motifs in aerotolerant organisms in comparison to aerointolerant organisms.

Overall, the work that we here presented highlighted previously unknown features of active and passive mechanisms of protection against oxidative stress. Gaining a deeper understanding of the evolutionary advantages of these mechanisms has potentially important implications for human health, microbiology and biotechnology. And maybe even more important, to our understanding of biology.

This is a work of sheer joy to understand Nature. One of the things that has always pushed me forward has been how creative the work of a scientist is. Isn't this motivating?

"Art is I; science is we." – Claude Bernard [125]

4.3 References

1. Tomalin, L. E., A. M. Day, Z. E. Underwood, G. R. Smith, P. Dalle Pezze, C. Rallis, W. Patel, B. C. Dickinson, J. Bähler and T. F. Brewer (2016). "Increasing extracellular H 2 O 2 produces a bi-phasic response in intracellular H 2 O 2, with peroxiredoxin hyperoxidation only triggered once the cellular H 2 O 2-buffering capacity is overwhelmed." Free Radical Biology and Medicine.

2. Low, F. M., M. B. Hampton, A. V. Peskin and C. C. Winterbourn (2007). "Peroxiredoxin 2 functions as a noncatalytic scavenger of low-level hydrogen peroxide in the erythrocyte." Blood **109**(6): 2611-2617.

3. Zaccaria, A., F. Roux-Dalvai, A. Bouamrani, A. Mombrun, P. Mossuz, B. Monsarrat and F. Berger (2015). "Accessing to the minor proteome of red blood cells through the influence of the nanoparticle surface properties on the corona composition." International journal of nanomedicine **10**: 1869.

4. Han, Y•-H., S•-U. Kim, T•-H. Kwon, D•-S. Lee, H•-L. Ha, D•-S. Park, E•-J. Woo, S•-H. Lee, J•-M. Kim, H•-B. Chae, S. Y. Lee, B. Y. Kim, D. Y. Yoon, S. G. Rhee, E. Fibach and D•-Y. Yu (2012). "Peroxiredoxin II is essential for preventing hemolytic anemia from oxidative stress through maintaining hemoglobin stability." Biochem. Biophys. Res. Commun. **426**(3): 427-432.

5. Pallotta, V., A. D'Alessandro, S. Rinalducci and L. Zolla (2013). "Native protein complexes in the cytoplasm of red blood cells." Journal of proteome research **12**(7): 3529-3546.

6. Cho, C•-S., H. J. Yoon, J. Y. Kim, H. A. Woo and S. G. Rhee (2014). "Circadian rhythm of hyperoxidized peroxiredoxin II is determined by hemoglobin autoxidation and the 20S proteasome in red blood cells." Proceedings of the National Academy of Sciences **111**(33): 12043-12048.

7. Thorburn, D. R. and P. W. Kuchel (1985). "Regulation of the human-erythrocyte hexose-monophosphate shunt under conditions of oxidative stress. A study using NMR spectroscopy, a kinetic isotope effect, a reconstituted system and computer simulation." European Journal Of Biochemistry **150**(2): 371-386.

8. Smith, E. W., M. S. Skelton, D. E. Kremer, D. D. Pascoe and L. B. Gladden (1998). "Lactate distribution in the blood during steady-state exercise." Medicine and science in sports and exercise **30**(9): 1424-1429.

9. Mulquiney, P. J. and P. W. Kuchel (1999). "Model of 2,3-bisphosphoglycerate metabolism in the human erythrocyte based on detailed enzyme kinetic equations: computer simulation and metabolic control analysis." Biochemical Journal **342 Pt 3**: 597-604.

10. Markuszewski, M. J., M. Szczykowska, D. Siluk and R. Kaliszan (2005). "Human red blood cells targeted metabolome analysis of glycolysis cycle metabolites by capillary electrophoresis using an indirect photometric detection method." Journal of pharmaceutical and biomedical analysis **39**(3): 636-642.

11. Peskin, A. V., P. E. Pace, J. B. Behring, L. N. Paton, M. Soethoudt, M. M. Bachschmid and C. C. Winterbourn (2016). "Glutathionylation of the Active Site Cysteines of Peroxiredoxin 2 and Recycling by Glutaredoxin." Journal of Biological Chemistry: jbc. M115. 692798.

12. Benesch, R., R. Benesch, R. Renthal and W. Gratzer (1971). "Cofactor binding and oxygen equilibria in haemoglobin." Nature: New biology **234**(49): 174-176.

13. Spodaryk, K. and J. A. Zoladz (1998). "The 2,3-DPG levels of human red blood cells during an incremental exercise test: Relationship to the blood acid-base balance." Physiological Research **47**(1): 17-22.

14. Smith, K. S., C. Jakubzick, T. S. Whittam and J. G. Ferry (1999). "Carbonic anhydrase is an ancient enzyme widespread in prokaryotes." Proceedings of the National Academy of Sciences **96**(26): 15184-15189.

15. Vinogradov, S. N., D. Hoogewijs, X. Bailly, R. Arredondo-Peter, J. Gough, S. Dewilde, L. Moens and J. R. Vanfleteren (2006). "A phylogenomic profile of globins." BMC Evolutionary Biology **6**(1): 31.

16. Finn, R., P. Coggill, R. Eberhardt, S. Eddy, J. Mistry, A. Mitchell, S. Potter, M. Punta, M. Qureshi and A. Sangrador-Vegas (2016). "The Pfam protein families database: towards a more sustainable future." Nucleic acids research **44**(D1): D279-285.

17. Lee, T$^{\bullet-}$H., S$^{\bullet-}$U. Kim, S$^{\bullet-}$L. Yu, S. H. Kim, D. S. Park, H$^{\bullet-}$B. Moon, S. H. Dho, K$^{\bullet-}$S. Kwon, H. J. Kwon, Y$^{\bullet-}$H. Han, S. Jeong, S. W. Kang, H$^{\bullet-}$S. Shin, K$^{\bullet-}$K. Lee, S. G. Rhee and D$^{\bullet-}$Y. Yu (2003). "Peroxiredoxin II is essential for sustaining life span of erythrocytes in mice." Blood **101**(12): 5033-5038.

18. Johnson, R. M., Y$^{\bullet-}$S. Ho, D$^{\bullet-}$Y. Yu, F. A. Kuypers, Y. Ravindranath and G. W. Goyette (2010). "The effects of disruption of genes for peroxiredoxin-2, glutathione peroxidase-1, and catalase on erythrocyte oxidative metabolism." Free Radical Biology And Medicine **48**(4): 519-525.

19. Johnson, R. M., G. Goyette, Jr., Y. Ravindranath and Y. S. Ho (2000). "Red cells from glutathione peroxidase-1-deficient mice have nearly normal defenses against exogenous peroxides." Blood **96**(5): 1985-1988.

20. Ho, Y$^{\bullet-}$S., Y. Xiong, W. Ma, A. Spector and D. S. Ho (2004). "Mice Lacking Catalase Develop Normally but Show Differential Sensitivity to Oxidant Tissue Injury." Journal Of Biological Chemistry **279**(31): 32804-32812.

21. Matté, A., A. Pantaleo, E. Ferru, F. Turrini, M. Bertoldi, F. Lupo, A. Siciliano, C. H. Zoon and L. De Franceschi (2014). "The novel role of peroxiredoxin-2 in red cell membrane protein homeostasis and senescence." Free Radical Biology and Medicine **76**: 80-88.

22. Giulivi, C. and K. J. Davies (1990). "A novel antioxidant role for hemoglobin. The comproportionation of ferrylhemoglobin with oxyhemoglobin." Journal Of Biological Chemistry **265**(32): 19453-19460.

23. Huennekens, F., R. W. Caffrey, R. Basford and B. W. Gabrio (1957). "Erythrocyte metabolism IV. Isolation and properties of methemoglobin reductase." Journal of Biological Chemistry **227**(1): 261-272.

24. Sutton, H. C., P. B. Roberts and C. C. Winterbourn (1976). "The rate of reaction of superoxide radical ion with oxyhaemoglobin and methaemoglobin." Biochemical Journal **155**(3): 503-510.

25. Perkins, A., L. B. Poole and P. A. Karplus (2014). "Tuning of peroxiredoxin catalysis for various physiological roles." Biochemistry **53**(49): 7693-7705.

26. Saitoh, M., H. Nishitoh, M. Fujii, K. Takeda, K. Tobiume, Y. Sawada, M. Kawabata, K. Miyazono and H. Ichijo (1998). "Mammalian thioredoxin is a direct inhibitor of apoptosis signal-regulating kinase (ASK) 1." The EMBO journal **17**(9): 2596-2606.

27. Zhang, R., R. Al-Lamki, L. Bai, J. W. Streb, J. M. Miano, J. Bradley and W. Min (2004). "Thioredoxin-2 inhibits mitochondria-located ASK1-mediated apoptosis in a JNK-independent manner." Circulation research **94**(11): 1483-1491.

28. Choi, M. H., I. K. Lee, G. W. Kim, B. U. Kim, Y•-H. Han, D•-Y. Yu, H. S. Park, K. Y. Kim, J. S. Lee, C. Choi, Y. S. Bae, B. I. Lee, S. G. Rhee and S. W. Kang (2005). "Regulation of PDGF signalling and vascular remodelling by peroxiredoxin II." Nature **435**(7040): 347-353.

29. Pace, P. E., A. V. Peskin, M•-H. Han, M. B. Hampton and C. C. Winterbourn (2013). "Hyperoxidized peroxiredoxin 2 interacts with the protein disulphide isomerase ERp46." Biochem. J.

30. Sobotta, M. C., W. Liou, S. Stöcker, D. Talwar, M. Oehler, T. Ruppert, A. N. Scharf and T. P. Dick (2015). "Peroxiredoxin-2 and STAT3 form a redox relay for H2O2 signaling." Nature chemical biology **11**(1): 64-70.

31. Brown, J. D., A. M. Day, S. R. Taylor, L. E. Tomalin, B. A. Morgan and E. A. Veal (2013). "A peroxiredoxin promotes H2O2 signaling and oxidative stress resistance by oxidizing a thioredoxin family protein." Cell Rep **5**(5): 1425-1435.

32. Kowalczyk, A., M. Puchała, K. Wesołowska and E. Serafin (2007). "Inactivation of alcohol dehydrogenase (ADH) by ferryl derivatives of human hemoglobin." Biochimica et Biophysica Acta (BBA)-Proteins and Proteomics **1774**(1): 86-92.

33. Men, L. and Y. Wang (2007). "The oxidation of yeast alcohol dehydrogenase-1 by hydrogen peroxide in vitro." Journal of proteome research **6**(1): 216-225.

34. Das, B. and S. K. Srivastava (1985). "Purification and properties of aldose reductase and aldehyde reductase II from human erythrocyte." Archives Of Biochemistry And Biophysics **238**(2): 670-679.

35. Yubisui, T., M. Takeshita and Y. Yoneyama (1980). "Reduction of methemoglobin through flavin at the physiological concentration by NADPH-flavin reductase of human erythrocytes." Journal of Biochemistry (Tokyo) **87**(6): 1715-1720.

36. Fang, W., M. L. Goldberg, N. M. Pohl, X. Bi, C. Tong, B. Xiong, T. J. Koh, A. M. Diamond and W. Yang (2010). "Functional and physical interaction between the selenium-binding protein 1 (SBP1) and the glutathione peroxidase 1 selenoprotein." Carcinogenesis **31**(8): 1360-1366.

37. Rinalducci, S., G. M. D'Amici, B. Blasi and L. Zolla (2011). "Oxidative stress-dependent oligomeric status of erythrocyte peroxiredoxin II (PrxII) during storage under standard blood banking conditions." Biochimie **93**(5): 845-853.

38. Manevich, Y., S. Feinstein and A. Fisher (2004). "Activation of the antioxidant enzyme 1-CYS peroxiredoxin requires glutathionylation mediated by

heterodimerization with πGST." Proceedings of the National Academy of Sciences of the United States of America **101**(11): 3780-3785.

39. Kang, S. W., I. C. Baines and S. G. Rhee (1998). "Characterization of a mammalian peroxiredoxin that contains one conserved cysteine." Journal of Biological Chemistry **273**(11): 6303-6311.

40. Leavey, P. J., C. Gonzalez-Aller, G. Thurman, M. Kleinberg, L. Rinckel, D. W. Ambruso, S. Freeman, F. A. Kuypers and D. R. Ambruso (2002). "A 29-kDa Protein Associated with p67 phox Expresses Both Peroxiredoxin and Phospholipase A2 Activity and Enhances Superoxide Anion Production by a Cell-free System of NADPH Oxidase Activity." Journal of Biological Chemistry **277**(47): 45181-45187.

41. Ambruso, D. R., M. A. Ellison, G. W. Thurman and T. L. Leto (2012). "Peroxiredoxin 6 translocates to the plasma membrane during neutrophil activation and is required for optimal NADPH oxidase activity." Biochimica et Biophysica Acta (BBA)-Molecular Cell Research **1823**(2): 306-315.

42. Cho, C•-S., G. J. Kato, S. H. Yang, S. W. Bae, J. S. Lee, M. T. Gladwin and S. G. Rhee (2010). "Hydroxyurea-induced expression of glutathione peroxidase 1 in red blood cells of individuals with sickle cell anemia." Antioxid. Redox Signal. **13**(1): 1-11.

43. O'Neill, J. S. and A. B. Reddy (2011). "Circadian clocks in human red blood cells." Nature **469**(7331): 498-U470.

44. Neumann, C. A., D. S. Krause, C. V. Carman, S. Das, D. P. Dubey, J. L. Abraham, R. T. Bronson, Y. Fujiwara, S. H. Orkin and E. Van (2003). "Essential role for the peroxiredoxin Prdx1 in erythrocyte antioxidant defence and tumour suppression." Nature **424**(6948): 561-565.

45. Lee, W. S., K. S. Choi, J. Riddell, C. Ip, D. Ghosh, J. H. Park and Y. M. Park (2007). "Human peroxiredoxin 1 and 2 are not duplicate proteins - The unique presence of Cys(83) in Prx1 underscores the structural and functional differences between Prx1 and Prx2." Journal of Biological Chemistry **282**(30): 22011-22022.

46. Jang, H. H., K. O. Lee, Y. H. Chi, B. G. Jung, S. K. Park, J. H. Park, J. R. Lee, S. S. Lee, J. C. Moon, J. W. Yun, Y. O. Choi, W. Y. Kim, J. S. Kang, G•-W. Cheong, D•-J. Yun, S. G. Rhee, M. J. Cho and S. Y. Lee (2004). "Two enzymes in one; two yeast peroxiredoxins display oxidative stress-dependent switching from a peroxidase to a molecular chaperone function." Cell **117**(5): 625-635.

47. Moon, J. C., Y•-S. Hah, W. Y. Kim, B. G. Jung, H. H. Jang, J. R. Lee, S. Y. Kim, Y. M. Lee, M. G. Jeon and C. W. Kim (2005). "Oxidative stress-dependent structural and functional switching of a human 2-Cys peroxiredoxin isotype II that enhances HeLa cell resistance to H2O2-induced cell death." Journal of Biological Chemistry **280**(31): 28775-28784.

48. Saccoccia, F., P. Di Micco, G. Boumis, M. Brunori, I. Koutris, A. E. Miele, V. Morea, P. Sriratana, D. L. Williams and A. Bellelli (2012). "Moonlighting by different stressors: crystal structure of the chaperone species of a 2-Cys peroxiredoxin." Structure **20**(3): 429-439.

49. Fernandez-Caggiano, M., E. Schroder, H. J. Cho, J. Burgoyne, J. Barallobre-Barreiro, M. Mayr and P. Eaton (2016). "Oxidant-induced interprotein

disulfide formation in cardiac DJ-1 occurs via an interaction with peroxiredoxin 2." J Biol Chem(1083-351X).

50. Andres-Mateos, E., C. Perier, L. Zhang, B. Blanchard-Fillion, T. M. Greco, B. Thomas, H. S. Ko, M. Sasaki, H. Ischiropoulos and S. Przedborski (2007). "DJ-1 gene deletion reveals that DJ-1 is an atypical peroxiredoxin-like peroxidase." Proceedings of the National Academy of Sciences **104**(37): 14807-14812.

51. Xu, X., F. Martin and J. S. Friedman (2010). "The familial Parkinson's disease gene DJ-1 (PARK7) is expressed in red cells and plays a role in protection against oxidative damage." Blood Cells, Molecules, and Diseases **45**(3): 227-232.

52. Ma, J., R. Wu, Q. Zhang, J•-b. Wu, J. Lou, Z. Zheng, J•-q. Ding and Z. Yuan (2014). "DJ-1 interacts with RACK1 and protects neurons from oxidative-stress-induced apoptosis." Biochemical Journal **462**(3): 489-497.

53. Jensen, L. J., M. Kuhn, M. Stark, S. Chaffron, C. Creevey, J. Muller, T. Doerks, P. Julien, A. Roth and M. Simonovic (2009). "STRING 8—a global view on proteins and their functional interactions in 630 organisms." Nucleic acids research **37**(suppl 1): D412-D416.

54. Berndt, C., C. H. Lillig and A. Holmgren (2007). "Thiol-based mechanisms of the thioredoxin and glutaredoxin systems: implications for diseases in the cardiovascular system." American Journal Of Physiology-Heart And Circulatory Physiology **292**(3): H1227-H1236.

55. Sarsour, E. H., M. G. Kumar, L. Chaudhuri, A. L. Kalen and P. C. Goswami (2009). "Redox control of the cell cycle in health and disease." Antioxidants & redox signaling **11**(12): 2985-3011.

56. Bell, K. F. and G. E. Hardingham (2011). "CNS peroxiredoxins and their regulation in health and disease." Antioxidants & redox signaling **14**(8): 1467-1477.

57. Hanschmann, E•-M., J. R. Godoy, C. Berndt, C. Hudemann and C. H. Lillig (2013). "Thioredoxins, glutaredoxins, and peroxiredoxins—molecular mechanisms and health significance: from cofactors to antioxidants to redox signaling." Antioxidants & redox signaling **19**(13): 1539-1605.

58. Fang, J., T. Nakamura, D•-H. Cho, Z. Gu and S. A. Lipton (2007). "S-nitrosylation of peroxiredoxin 2 promotes oxidative stress-induced neuronal cell death in Parkinson's disease." Proceedings of the National Academy of Sciences **104**(47): 18742-18747.

59. Egler, R. A., E. Fernandes, K. Rothermund, S. Sereika, N. de Souza-Pinto, P. Jaruga, M. Dizdaroglu and E. V. Prochownik (2005). "Regulation of reactive oxygen species, DNA damage, and c-Myc function by peroxiredoxin 1." Oncogene **24**(54): 8038-8050.

60. Halliwell, B. and J. M. Gutteridge (1999). Free radicals in biology and medicine, Oxford university press Oxford.

61. Link, A. J., K. Robison and G. M. Church (1997). "Comparing the predicted and observed properties of proteins encoded in the genome of Escherichia coli K-12." Electrophoresis **18**(8): 1259-1313.

62. Taoka, M., Y. Yamauchi, T. Shinkawa, H. Kaji, W. Motohashi, H. Nakayama, N. Takahashi and T. Isobe (2004). "Only a small subset of the horizontally transferred chromosomal genes in Escherichia coli are translated into proteins." Molecular & Cellular Proteomics **3**(8): 780-787.

63. Lopez-Campistrous, A., P. Semchuk, L. Burke, T. Palmer-Stone, S. J. Brokx, G. Broderick, D. Bottorff, S. Bolch, J. H. Weiner and M. J. Ellison (2005). "Localization, annotation, and comparison of the Escherichia coli K-12 proteome under two states of growth." Molecular & Cellular Proteomics **4**(8): 1205-1209.

64. Ghaemmaghami, S., W. K. Huh, K. Bower, R. W. Howson, A. Belle, N. Dephoure, E. K. O'Shea and J. S. Weissman (2003). "Global analysis of protein expression in yeast." Nature **425** 737-741.

65. Seaver, L. C. and J. A. Imlay (2001). "Alkyl hydroperoxide reductase is the primary scavenger of endogenous hydrogen peroxide in Escherichia coli." Journal of Bacteriology **183**(24): 7173-7181.

66. Hanzen, S., K. Vielfort, J. Yang, F. Roger, V. Andersson, S. Zamarbide-Fores, R. Andersson, L. Malm, G. Palais, B. Biteau, B. Liu, M. B. Toledano, M. Molin and T. Nystrom (2016). "Lifespan Control by Redox-Dependent Recruitment of Chaperones to Misfolded Proteins." Cell.

67. Teixeira, F., H. Castro, T. Cruz, E. Tse, P. Koldewey, D. R. Southworth, A. M. Tomas and U. Jakob (2015). "Mitochondrial peroxiredoxin functions as crucial chaperone reservoir in Leishmania infantum." Proc Natl Acad Sci U S A **112**(7): E616-624.

68. Ogasawara, Y., T. Ohminato, Y. Nakamura and K. Ishii (2012). "Structural and functional analysis of native peroxiredoxin 2 in human red blood cells." International Journal of Biochemistry & Cell Biology **44**(7): 1072-1077.

69. Lobry, J. R. (1997). "Influence of genomic G+C content on average amino-acid composition of proteins from 59 bacterial species." Gene **205**(1-2): 309-316.

70. Kreil, D. P. and C. A. Ouzounis (2001). "Identification of thermophilic species by the amino acid compositions deduced from their genomes." Nucleic Acids Res **29**(7): 1608-1615.

71. Tekaia, F., E. Yeramian and B. Dujon (2002). "Amino acid composition of genomes, lifestyles of organisms, and evolutionary trends: A global picture with correspondence analysis." Gene **297**: 51-60.

72. Zeldovich, K. B., I. N. Berezovsky and E. I. Shakhnovich (2007). "Protein and DNA sequence determinants of thermophilic adaptation." PLoS Computational Biology **3**: 0062-0072.

73. Tekaia, F. and E. Yeramian (2006). "Evolution of proteomes: fundamental signatures and global trends in amino acid compositions." BMC genomics **7**: 307.

74. White, S., F. E. Tuttle, D. Blankenhorn, D. C. Dosch and J. L. Slonczewski (1992). "pH dependence and gene structure of inaA in Escherichia coli." J Bacteriol **174**(5): 1537-1543.

75. Sandelin, E. (2004). "On hydrophobicity and conformational specificity in proteins." Biophysical journal **86**: 23-30.

76. Bastolla, U. and L. Demetrius (2005). "Stability constraints and protein evolution: the role of chain length, composition and disulfide bonds." Protein Engineering Design and Selection **18**(9): 405-415.

77. Carugo, O. (2008). "Amino acid composition and protein dimension." Protein Science **17**: 2187-2191.

78. Brbic, M., T. Warnecke, a. Kri ko and F. Supek (2015). "Global shifts in genome and proteome composition are very tightly coupled." Genome Biology and Evolution **7**: 1519-1532.

79. Akashi, H. and T. Gojobori (2002). "Metabolic efficiency and amino acid composition in the proteomes of Escherichia coli and Bacillus subtilis." Proceedings Of The National Academy Of Sciences Of The United States Of America **99**(6): 3695-3700.

80. Smith, D. R. and M. R. Chapman (2010). "Economical evolution: Microbes reduce the synthetic cost of extracellular proteins." mBio **1**: 28-32.

81. Vidovic, A., F. Supek, A. Nikolic and A. Krisko (2014). "Signatures of conformational stability and oxidation resistance in proteomes of pathogenic bacteria." Cell Reports **7**: 1393-1400.

82. Akashi, H. (2003). "Translational selection and yeast proteome evolution." Genetics **164**(4): 1291-1303.

83. Heizer, E. M., D. W. Raiford, M. L. Raymer, T. E. Doom, R. V. Miller and D. E. Krane (2006). "Amino acid cost and codon-usage biases in 6 prokaryotic genomes: A whole-genome analysis." Molecular Biology and Evolution **23**(9): 1670-1680.

84. Yachdav, G., E. Kloppmann, L. Kajan, M. Hecht, T. Goldberg, T. Hamp, P. Honigschmid, A. Schafferhans, M. Roos, M. Bernhofer, L. Richter, H. Ashkenazy, M. Punta, A. Schlessinger, Y. Bromberg, R. Schneider, G. Vriend, C. Sander, N. Ben-Tal and B. Rost (2014). "PredictProtein--an open resource for online prediction of protein structural and functional features." Nucleic Acids Res **42**(Web Server issue): W337-343.

85. Drozdetskiy, A., C. Cole, J. Procter and G. J. Barton (2015). "JPred4: a protein secondary structure prediction server." Nucleic Acids Res **43**(W1): W389-394.

86. Price, W. N., 2nd, S. K. Handelman, J. K. Everett, S. N. Tong, A. Bracic, J. D. Luff, V. Naumov, T. Acton, P. Manor, R. Xiao, B. Rost, G. T. Montelione and J. F. Hunt (2011). "Large-scale experimental studies show unexpected amino acid effects on protein expression and solubility in vivo in E. coli." Microb Inform Exp **1**(1): 6.

87. Pal, C., B. Papp and L. D. Hurst (2001). "Highly expressed genes in yeast evolve slowly." Genetics **158**(2): 927-931.

88. Wolf, M. Y., Y. I. Wolf and E. V. Koonin (2008). "Comparable contributions of structural-functional constraints and expression level to the rate of protein sequence evolution." Biology Direct **3**.

89. Ikemura, T. (1985). "Codon usage and tRNA content in unicellular and multicellular organisms." Mol Biol Evol **2**(1): 13-34.

90. Sharp, P. M., T. M. Tuohy and K. R. Mosurski (1986). "Codon usage in yeast: cluster analysis clearly differentiates highly and lowly expressed genes." Nucleic Acids Res **14**(13): 5125-5143.

91. Plotkin, J. B. and G. Kudla (2011). "Synonymous but not the same: the causes and consequences of codon bias." Nature Reviews Genetics **12**(1): 32-42.

92. Wang, M., M. Weiss, M. Simonovic, G. Haertinger, S. P. Schrimpf, M. O. Hengartner and C. von Mering (2012). "PaxDb, a database of protein abundance averages across all three domains of life." Molecular & Cellular Proteomics **11**(8): 492-500.

93. Goh, C. S., N. Lan, N. Echols, S. M. Douglas, D. Milburn, P. Bertone, R. Xiao, L. C. Ma, D. Zheng and Z. Wunderlich (2003). "SPINE 2: a system for collaborative structural proteomics within a federated database framework." Nucleic acids research **31**(11): 2833-2838.

94. Sharp, P. M. and W. H. Li (1987). "The codon Adaptation Index--a measure of directional synonymous codon usage bias, and its potential applications." Nucleic Acids Research **15**(3): 1281-1295.

95. Karlin, S., J. Mrazek and A. M. Campbell (1998). "Codon usages in different gene classes of the Escherichia coli genome." Molecular Microbiology **29**(6): 1341-1355.

96. Carbone, A., A. Zinovyev and F. Képès (2003). "Codon adaptation index as a measure of dominating codon bias." Bioinformatics **19**(16): 2005-2015.

97. Jansen, R., H. J. Bussemaker and M. Gerstein (2003). "Revisiting the codon adaptation index from a whole-genome perspective: analyzing the relationship between gene expression and codon occurrence in yeast using a variety of models." Nucleic Acids Research **31**(8): 2242-2251.

98. Fox, J. M. and I. Erill (2010). "Relative codon adaptation: a generic codon bias index for prediction of gene expression." DNA Res **17**(3): 185-196.

99. Lee, S., S. Weon, S. Lee and C. Kang (2010). "Relative codon adaptation index, a sensitive measure of codon usage bias." Evolutionary Bioinformatics **6**: 47.

100. Friberg, M., P. von Rohr and G. Gonnet (2004). "Limitations of codon adaptation index and other coding DNA-based features for prediction of protein expression in Saccharomyces cerevisiae." Yeast **21**(13): 1083-1093.

101. Jung, T., M. Engels, B. Kaiser, D. Poppek and T. Grune (2006). "Intracellular distribution of oxidized proteins and proteasome in HT22 cells during oxidative stress." Free Radic Biol Med **40**(8): 1303-1312.

102. Rey, S., J. L. Gardy and F. S. Brinkman (2005). "Assessing the precision of high-throughput computational and laboratory approaches for the genome-wide identification of protein subcellular localization in bacteria." BMC genomics **6**(1): 1.

103. Su, E., H•-S. Chiu, A. Lo, J•-K. Hwang, T•-Y. Sung and W•-L. Hsu (2007). "Protein subcellular localization prediction based on compartment-specific features and structure conservation." BMC bioinformatics **8**(1): 1.

104. Chou, K•-C. and H•-B. Shen (2008). "Cell-PLoc: a package of Web servers for predicting subcellular localization of proteins in various organisms." Nature protocols **3**(2): 153-162.

105. Ulmschneider, M. B. and M. S. Sansom (2001). "Amino acid distributions in integral membrane protein structures." Biochim Biophys Acta **1512**(1): 1-14.

106. Rost, B. (2005). "Prediction of protein structure in 1D—secondary structure, membrane regions, and solvent accessibility." Struct Bioinform **44**: 559-587.

107. Zhang, H., T. Zhang, K. Chen, K. D. Kedarisetti, M. J. Mizianty, Q. Bao, W. Stach and L. Kurgan (2011). "Critical assessment of high-throughput standalone methods for secondary structure prediction." Briefings in bioinformatics **12**(6): 672-688.

108. Kurgan, L. and F. M. Disfani (2011). "Structural protein descriptors in 1-dimension and their sequence-based predictions." Curr Protein Pept Sci **12**(6): 470-489.

109. Faraggi, E., Y. Zhou and A. Kloczkowski (2014). "Accurate single-sequence prediction of solvent accessible surface area using local and global features." Proteins: Structure, Function, and Bioinformatics **82**(11): 3170-3176.

110. Mi, H., S. Poudel, A. Muruganujan, J. T. Casagrande and P. D. Thomas (2016). "PANTHER version 10: expanded protein families and functions, and analysis tools." Nucleic acids research **44**(D1): D336-D342.

111. Nunoshiba, T., E. Hidalgo, C. F. Am bile Cuevas and B. Demple (1992). "Two-stage control of an oxidative stress regulon: the Escherichia coli SoxR protein triggers redox-inducible expression of the soxS regulatory gene." J Bacteriol **174**(19): 6054-6060.

112. Zheng, M., F. Aslund and G. Storz (1998). "Activation of the OxyR Transcription Factor by Reversible Disulfide Bond Formation." Science **279**(5357): 1718-1722.

113. Starck, J., G. Kallenius, B. I. Marklund, D. I. Andersson and T. Akerlund (2004). "Comparative proteome analysis of Mycobacterium tuberculosis grown under aerobic and anaerobic conditions." Microbiology **150**(Pt 11): 3821-3829.

114. Weber, A., S. A. Kögl and K. Jung (2006). "Time-dependent proteome alterations under osmotic stress during aerobic and anaerobic growth in Escherichia coli." Journal of bacteriology **188**(20): 7165-7175.

115. Bruckmann, A., P. J. Hensbergen, C. I. Balog, A. M. Deelder, R. Brandt, I. S. Snoek, H. Y. Steensma and G. P. van Heusden (2009). "Proteome analysis of aerobically and anaerobically grown Saccharomyces cerevisiae cells." J Proteomics **71**(6): 662-669.

116. Yu, C. H., Y. Dang, Z. Zhou, C. Wu, F. Zhao, M. S. Sachs and Y. Liu (2015). "Codon Usage Influences the Local Rate of Translation Elongation to Regulate Co-translational Protein Folding." Mol Cell **59**(5): 744-754.

117. Shenton, D., J. B. Smirnova, J. N. Selley, K. Carroll, S. J. Hubbard, G. D. Pavitt, M. P. Ashe and C. M. Grant (2006). "Global translational responses to oxidative stress impact upon multiple levels of protein synthesis." J Biol Chem **281**(39): 29011-29021.

118. Zhong, J., C. Xiao, W. Gu, G. Du, X. Sun, Q. Y. He and G. Zhang (2015). "Transfer RNAs Mediate the Rapid Adaptation of Escherichia coli to Oxidative Stress." PLoS Genet **11**(6): e1005302.

119. Ouyang, Z. and J. Liang (2008). "Predicting protein folding rates from geometric contact and amino acid sequence." Protein Sci **17**(7): 1256-1263.

120. Dill, K. A., K. Ghosh and J. D. Schmit (2011). "Physical limits of cells and proteomes." Proceedings of the National Academy of Sciences.

121. Kaiser, C. M., D. H. Goldman, J. D. Chodera, I. Tinoco, Jr. and C. Bustamante (2011). "The ribosome modulates nascent protein folding." Science **334**(6063): 1723-1727.

122. Yang, Y. F. and W. W. Wells (1991). "Identification and characterization of the functional amino acids at the active center of pig liver thioltransferase by site-directed mutagenesis." J Biol Chem **266**(19): 12759-12765.

123. Creighton, T. E. (1993). Proteins: structures and molecular properties, Macmillan.

124. Kortemme, T. and T. E. Creighton (1995). "Ionisation of cysteine residues at the termini of model alpha-helical peptides. Relevance to unusual thiol pKa values in proteins of the thioredoxin family." J Mol Biol **253**(5): 799-812.

125. Garrison, F. H. (1928). "Medical Proverbs, Aphorisms and Epigrams." Bull N Y Acad Med **4**(10): 979-1005.